

**WOOD STRESSED-SKIN PANELS:  
AN INVESTIGATION INTO THEIR  
BEHAVIOUR, LOAD DISTRIBUTION AND  
COMPOSITE PROPERTIES**

**Part 1: Review, modelling and design**

**Christophe Daniel Gerber**

**Doctor of Philosophy**

**2007**

**University of Technology Sydney**

Faculty of Engineering

## CERTIFICATE OF AUTHORSHIP

I certify that the work in this thesis has not been previously submitted for a degree nor has it been submitted as part of requirements for a degree except as fully acknowledged within the text.

I also certify that the thesis has been written by me. Any help that I have received in my research work and the preparation of the thesis itself has been acknowledged. In addition, I certify that all information sources and literature used are indicated in the thesis.

Sydney, 28 March 2007

Production Note:  
Signature removed prior to publication.



Christophe D. Gerber

## ACKNOWLEDGEMENT

"Entre l'incroyance et la foi il n'y a qu'un souffle;  
Entre l'état de doute et celui de certitude il n'y a qu'un souffle;  
Sache chérir ce souffle si précieux car  
C'est lui l'unique fruit de notre existence."

Khayyam Naishapuri,  
astronome, mathématicien et poète persan (1048-1131)

Between 2002 and 2006, I have been undertaking my PhD project at the University of Technology, Sydney. Its completion would not have been possible without the contribution and expertise of many, whom I would like to thank here:

I would like to start with addressing many thanks to Prof. Keith Crews, my principal supervisor, for his support and expertise. With his experience and knowledge Keith's involvement has been valuable to my research. Many thanks also to Prof. Christophe Sigrist, my external co-supervisor and former fellow at SWOOD, who has been involved since the very concept of this project and contributed greatly to its concretisation, and to Prof. Bijan Samali, my internal co-supervisor.

During this research, the support and assistance from the laboratory staff have been fantastic. I want to thank them all for their contribution and for coping with me; especially when frustration took the better off me and my temper was getting short. While some of you have been on board for a short while, others have seen the whole research program through. So, I would like to thank Mario, David, Warwick, Ian, Rami, young Peter, and... I wish to dearly thank Setu, Laurence and Greg for getting the acquisition system of the test data working and for responding quickly and positively to interferences and breakdowns ...there is magic that science cannot explain! Last but surely not least and certainly not short of contribution and support: viele herzliche Danke Wolf für Deinen wunderbaren Einsatz, Deine Stimmung und Deine Freundschaft! Es hat mir echt Spass gegeben, mit Dir zusammenzuarbeiten aber auch mit Dir zu schwatzen. I am not certain the list is exhaustive so may the ones I have forgotten receive my sincerest apologies.

This research would not have been possible either without the financial support of the research commission "Académie suisse des sciences techniques" and the Faculty of Engineering at UTS and without the outstanding participation, support and contributions from industry, that is, Trus Joist<sup>TM</sup>, a Weyerhaeuser Business, Purbond AG (Collano Ebnöther AG), Kronoply AG, Paslode Australia Ltd. and CADWORK. In particular, I would especially like to thank Mr Matt Stafford from Trus Joist<sup>TM</sup> and Mr Florian Stoffel from Purbond AG. TrusJoist<sup>TM</sup> supplied all the I-joists needed for the construction of the specimens and Purbond AG supplied custom-made polyurethane adhesive.

To my friends and/or colleagues at UTS and elsewhere I express my gratitude. I would like to acknowledge Joko for sharing his expertise with me. Un merci special à Laurent, de l'ENSAM à Cluny (France), pour son accompagnement lors de mes premier pas en éléments finis. Of course, there has been CFC ...thanks buddy for your companionship and great "in- and out-of-research" chitchats! Good luck with your own research ...and with your future endeavour! A vous tous mes amis au pays – en particulier Lisa, Willy et les petites – and to all of you ...wherever you are ...MERCI! ...THANK YOU! ...QUE DIEU VOUS GARDE!!! ...GOD BLESS YOU!!!

Pour terminer j'aimerais remercier ceux qui dans mon cœur occupe une place privilégiée. Mes plus reconnaissants et affectueux remerciements sont pour ma famille, tout spécialement mes parents. Vous m'avez témoigné un soutien infaillible et une confiance infinie, non seulement pour ce doctorat mais pour les entreprises qui ont jalonné mon parcours professionnel. Mes chers parents, je vous remercie de m'avoir laissé le libre choix ...et même si un sourire peut se dessiner parce que je n'ai pas choisi la ligne la plus droite pour arriver où je suis ...le voyage accompli m'a enrichi de rencontres et expériences merveilleuses! Vos encouragements m'ont été et me sont encore précieux et, votre affection et votre amour sont sans valeur. Je vous aime! ...j'ai encore une pensée toute spéciale et une gratitude énorme pour mon "chargé d'affaire" pour son application et efficacité. Il se reconnaîtra!

My last thought and lots of love go to the person who has suffered the most from the extreme dedication that completing this thesis has demanded. It has been hard to be my girlfriend ...I thank you for your support and love! I love you too!

## CONTENT SUMMARY: PART 1

<b>CERTIFICATE OF AUTHORSHIP .....</b>	<b>II</b>
<b>ACKNOWLEDGEMENT .....</b>	<b>III</b>
<b>CONTENT SUMMARY: PART 1 .....</b>	<b>V</b>
<b>EXTENDED CONTENT: PART 1 .....</b>	<b>VI</b>
<b>LIST OF FIGURES AND TABLES .....</b>	<b>X</b>
<b>LIST OF PUBLICATIONS.....</b>	<b>XIV</b>
<b>ABBREVIATION AND KEY-TERM DEFINITIONS .....</b>	<b>XVI</b>
<b>ABSTRACT .....</b>	<b>XVII</b>
<b>FOREWORD.....</b>	<b>XIX</b>
<b>1 INTRODUCTION.....</b>	<b>2</b>
<b>2 REVIEW OF THE LITERATURE.....</b>	<b>10</b>
<b>3 WOOD JOIST FLOOR SYSTEMS .....</b>	<b>40</b>
<b>4 STRESSED-SKIN PANEL PROPERTIES AND DESIGN .....</b>	<b>56</b>
<b>5 GRILLAGE MODEL .....</b>	<b>103</b>
<b>6 FINITE ELEMENT MODEL AND ANALYSIS .....</b>	<b>156</b>
<b>7 DESIGN PROCEDURE AND RECOMMENDATIONS .....</b>	<b>198</b>
<b>8 CONCLUSIONS .....</b>	<b>216</b>

# EXTENDED CONTENT: PART 1

<b>CERTIFICATE OF AUTHORSHIP .....</b>	<b>II</b>
<b>ACKNOWLEDGEMENT .....</b>	<b>III</b>
<b>CONTENT SUMMARY: PART 1 .....</b>	<b>V</b>
<b>EXTENDED CONTENT: PART 1 .....</b>	<b>VI</b>
<b>LIST OF FIGURES AND TABLES .....</b>	<b>X</b>
<b>LIST OF PUBLICATIONS.....</b>	<b>XIV</b>
<b>ABBREVIATION AND KEY-TERM DEFINITIONS .....</b>	<b>XVI</b>
<b>ABSTRACT .....</b>	<b>XVII</b>
<b>FOREWORD .....</b>	<b>XIX</b>
<b>1 INTRODUCTION.....</b>	<b>2</b>
<b>1.1 Objectives.....</b>	<b>3</b>
<b>1.2 Research methodology .....</b>	<b>4</b>
<b>1.3 Scope.....</b>	<b>5</b>
<b>1.4 Significance .....</b>	<b>6</b>
<b>1.5 Organisation of thesis .....</b>	<b>6</b>
1.5.1 Organisation of Part 1 of the thesis .....	7
<b>2 REVIEW OF THE LITERATURE.....</b>	<b>10</b>
<b>2.1 Lightweight wood floor systems.....</b>	<b>11</b>
<b>2.2 On the interlayers: construction and behaviour .....</b>	<b>14</b>
2.2.1 Mechanical fasteners .....	15
2.2.2 Screw- and nail-gluing .....	16
<b>2.3 Interaction in wood joist floors .....</b>	<b>18</b>
2.3.1 Composite action.....	21
2.3.2 Two-way action.....	23
<b>2.4 Investigations into wood joist floors .....</b>	<b>27</b>
<b>2.5 Modelling of wood joist floors.....</b>	<b>29</b>
2.5.1 Model for multi-layer composites .....	29

2.5.2	Models for wood joist floors .....	30
2.5.2.1	Finite element analysis for floors (FEAFLO and NONFLO) .....	30
2.5.2.2	Floor analysis program (FAP).....	32
2.5.2.3	Spring model .....	33
2.5.2.4	Partial composite action (PCA).....	33
2.5.2.5	Construction factor method.....	35
<b>2.6</b>	<b>Reliability design for wood joist floors.....</b>	<b>36</b>
<b>3</b>	<b>WOOD JOIST FLOOR SYSTEMS .....</b>	<b>40</b>
<b>3.1</b>	<b>Conventional wood joist floor technology.....</b>	<b>40</b>
<b>3.2</b>	<b>Stressed-skin panel technology .....</b>	<b>42</b>
<b>3.3</b>	<b>Floor structure as horizontal diaphragm.....</b>	<b>46</b>
<b>3.4</b>	<b>Comparing conventional wood joist floor and SSP technologies .....</b>	<b>47</b>
3.4.1	Construction and architectural aspects.....	47
3.4.2	Design and structural aspects .....	49
<b>4</b>	<b>STRESSED-SKIN PANEL PROPERTIES AND DESIGN .....</b>	<b>56</b>
<b>4.1</b>	<b>Section properties of SSP Systems.....</b>	<b>57</b>
<b>4.2</b>	<b>Theory of the tributary width of the skin(s) .....</b>	<b>61</b>
4.2.1	Stress distribution in SSP skin(s) .....	61
4.2.2	Estimating the tributary width of the skin(s) .....	64
4.2.3	Codified approaches for approximating the tributary width of the skin(s) .....	66
4.2.3.1	Australia – AS 1720.1–1997.....	67
4.2.3.2	Europe – EC5 .....	68
4.2.3.3	Switzerland – SIA 164 .....	70
4.2.3.4	USA – the APA method.....	73
4.2.4	Effectiveness ratios of the panel contribution.....	82
4.2.5	Concluding summary on the tributary width .....	87
<b>4.3</b>	<b>Capacity under gravity load.....</b>	<b>89</b>
<b>4.4</b>	<b>Splicing requirements .....</b>	<b>92</b>
<b>4.5</b>	<b>Verification of buckling capacity .....</b>	<b>94</b>
<b>4.6</b>	<b>Verification of the serviceability – deflection .....</b>	<b>96</b>
<b>4.7</b>	<b>Verification of the serviceability – vibration .....</b>	<b>100</b>
<b>5</b>	<b>GRILLAGE MODEL .....</b>	<b>103</b>
<b>5.1</b>	<b>Development and construction of the grillage model .....</b>	<b>104</b>
5.1.1	Model concept.....	104
5.1.2	Simulation principle.....	106
5.1.3	Construction principle of the grillage model .....	106
5.1.4	Beam elements .....	107
5.1.5	Derivation of the stiffness matrix of the girders and crossbeams .....	108
5.1.6	Static condensation of the stiffness matrix of the girders and crossbeams.....	110
5.1.7	Boundary condition of the grillage members.....	112

5.1.8	Superposition technique – stiffness matrix of the grillage structure.....	114
<b>5.2</b>	<b>Definition of the attributes of the grillage model .....</b>	<b>115</b>
5.2.1	Apparent stiffness of the girders .....	115
5.2.2	Apparent stiffness of the crossbeams.....	116
<b>5.3</b>	<b>Load introduction .....</b>	<b>119</b>
<b>5.4</b>	<b>Solution of the grillage model .....</b>	<b>120</b>
<b>5.5</b>	<b>Application of the grillage model to the specimens of the subject research .....</b>	<b>121</b>
5.5.1	Modelling principle – application to the specimens of the subject research.....	121
5.5.2	Material properties of the members of the grillage model .....	123
<b>5.6</b>	<b>Computer solution routine .....</b>	<b>124</b>
5.6.1	Concept .....	124
5.6.2	Working with the routine .....	124
<b>5.7</b>	<b>Parameterisation of the grillage model .....</b>	<b>125</b>
5.7.1	Concept of the parameterisation .....	125
5.7.2	Benchmarks of the parameterisation .....	125
5.7.3	Key outcomes of the parameterisation.....	126
5.7.3.1	Distribution of uniformly distributed line loads .....	126
5.7.3.2	Attribute of the crossbeam .....	127
<b>5.8</b>	<b>Evaluation of the capability of the grillage model.....</b>	<b>130</b>
<b>5.9</b>	<b>Introducing skin discontinuity(ies) in the grillage model.....</b>	<b>145</b>
<b>5.10</b>	<b>Concluding summary.....</b>	<b>152</b>
<b>6</b>	<b>FINITE ELEMENT MODEL AND ANALYSIS.....</b>	<b>156</b>
<b>6.1</b>	<b>Construction platform and fundamentals of the finite element model.....</b>	<b>157</b>
<b>6.2</b>	<b>Concept and development of the finite element model.....</b>	<b>159</b>
6.2.1	Schematic plan of the finite element analysis .....	160
6.2.2	Assisting tools .....	162
6.2.3	First prototype of the finite element model.....	163
6.2.4	The finite element model (FEM).....	165
6.2.5	Element types of the finite element model.....	165
6.2.6	Real constants of the finite element model .....	169
6.2.7	Material properties of the members of the finite element model .....	170
6.2.8	Characterising the I-joists .....	173
<b>6.3</b>	<b>Parameterisation of THE finite element model.....</b>	<b>175</b>
6.3.1	Concept of the parameterisation .....	175
6.3.2	Benchmarks of the parameterisation.....	176
6.3.3	Findings/outcomes of the parameterisation .....	176
<b>6.4</b>	<b>Evaluation of the finite element model’s capability .....</b>	<b>179</b>
<b>6.5</b>	<b>Introducing skin discontinuity(ies) in the grillage model.....</b>	<b>188</b>
<b>6.6</b>	<b>Concluding summary.....</b>	<b>194</b>
<b>7</b>	<b>DESIGN PROCEDURE AND RECOMMENDATIONS .....</b>	<b>198</b>



- 7.1 Background summary ..... 199**
- 7.2 Recapitulation of the key outcomes ..... 200**
- 7.3 Design recommendations..... 200**
  - 7.3.1 Introduction and concept of the design recommendations..... 200
  - 7.3.2 Outline of the design procedure of stressed-skin panels..... 202
- 7.4 Concluding summary ..... 212**
  
- 8 CONCLUSIONS ..... 216**
- 8.1 Literature review ..... 216**
- 8.2 Modelling of SSP systems ..... 217**
  - 8.2.1 Numerical (grillage) model ..... 218
  - 8.2.2 Finite element model ..... 218
- 8.3 Design recommendations ..... 219**
- 8.4 Final comments ..... 220**

## LIST OF FIGURES AND TABLES

### FIGURES

Figure 2–1: Two-layer floor system (Breyer et al. 2003) .....	12
Figure 2–2: Construction model for light wood floor (Gerber & Sigrist 2002).....	13
Figure 2–3: Strong and weak strength axis of plywood (Breyer et al. 2003) .....	21
Figure 2–4: Effect of sheathing stiffness on the two-way action (Sherwood & Moody 1989).....	24
Figure 3–1: Typical SSP floor constructions .....	45
Figure 3–2: Strain and stress distribution across the floor section – free slip in the interlayers.....	51
Figure 3–3: Strain and stress distribution across the floor section – no slip in the interlayers.....	52
Figure 4–1: Location of the neutral axes.....	58
Figure 4–2: Stress distribution in the skin(s) of SSP deck.....	62
Figure 4–3: Symbols for stressed-skin panels used in the subject research.....	63
Figure 4–4: Depiction of the tributary width of the skin(s) .....	67
Figure 4–5: Basic spacing, $b_{basic}$ , chart for plywood and OSB panel.....	75
Figure 4–6: Correction coefficient $K_c$ , (Baird & Ozelton 1984; Foschi 1969b).....	76
Figure 4–7: Stress reduction factor (APA – The Engineered Wood Association 1990; Desler 2002; McLain 1999) .....	77
Figure 4–8: Effective contribution of the skins of 200-mm I-joist specimens (EC5 vs. Möhler) .....	84
Figure 4–9: Effective contribution of the skins of 356-mm I-joist specimens (EC5 vs. Möhler) .....	85
Figure 4–10: Effective contribution of the skins of 200-mm I-joist specimens – plywood.....	86
Figure 4–11: Effective contribution of the skins of 356-mm I-joist specimen – plywood.....	87
Figure 4–12: Stress verifications of SSP system (specimen of the subject research).....	90
Figure 5–1: Longitudinal girder about an interior joist (I-profile).....	105
Figure 5–2: Crossbeam – slice of the floor system.....	105
Figure 5–3: Finite flexural elements (beam elements) with end node conditions .....	107
Figure 5–4: Merging of adjacent beam element → superposition of the node DOFs ..	109
Figure 5–5: Condensation of DOF → node merging of girder members .....	109
Figure 5–6: Boundary conditions of the girders .....	113

Figure 5–7: Boundary conditions of the crossbeams .....	113
Figure 5–8: Merging the shared nodes of the girders and crossbeams → superposition of the node DOF .....	114
Figure 5–9: Shear area of box-section SSP specimen.....	116
Figure 5–10: Anticipated pattern of the load distribution.....	117
Figure 5–11: Geometric characteristics of the anticipated load distribution pattern ....	118
Figure 5–12: 200-mm I-joist grillage model.....	122
Figure 5–13: 356-mm I-joist grillage model.....	123
Figure 5–14: Locations of the nodal loads – 200-mm grillage model .....	131
Figure 5–15: Comparison of the calculated – grillage model – and measured – test results – deflection per unit load (all load positions).....	138
Figure 5–16: Histogram of the calculated – grillage model – and measured – test results – deflection per unit load .....	140
Figure 5–17: Grillage model computations – C05-series perpendicular profiles of deflection at mid-span (continuous skin).....	142
Figure 5–18: Grillage model computations – C08-series perpendicular profiles of deflection at mid-span (continuous skins) .....	143
Figure 5–19: Grillage model computations – C09-series perpendicular profiles of deflection at mid-span (continuous skins) .....	144
Figure 5–20: Comparison of the calculated – grillage model – and measured – test results – deflection per unit load (discontinuous skin(s)) .....	148
Figure 5–21: Histogram of the calculated – grillage model – and measured – test results – deflection per unit load (discontinuous skin(s)) .....	149
Figure 5–22: Grillage model computations – C08-01 perpendicular profiles of deflection at mid-span (discontinuous skins).....	151
Figure 6–1: Schematic plan of the FEA protocol.....	162
Figure 6–2: Element attributes of Alpha-FEM <sup>l</sup> .....	164
Figure 6–3: Element attributes of the FEM.....	166
Figure 6–4: SOLID185 geometry (ANSYS Inc. 2005) .....	167
Figure 6–5: SOLSH190 geometry (ANSYS Inc. 2005) .....	167
Figure 6–6: SHELL43 geometry (ANSYS Inc. 2005).....	168
Figure 6–7: CONTA173 geometry (ANSYS Inc. 2005) .....	168
Figure 6–8: TARGE170 geometry (ANSYS Inc. 2005).....	169
Figure 6–9: Calibration coefficient of the I-joist .....	175
Figure 6–10: Comparison of the calculated – finite element model – and measured – test results – deflection per unit load .....	182
Figure 6–11: Histogram of the calculated – finite element model – and measured – test results – deflection per unit load .....	183
Figure 6–12: Finite element simulations – C03&04-family perpendicular profiles of deflection at mid-span.....	185
Figure 6–13: Finite element simulations – C13-series perpendicular profiles of deflection at mid-span.....	186
Figure 6–14: Finite element simulations – C12-series perpendicular profiles of deflection at mid-span.....	187

Figure 6–15: Comparison of the simulated – finite element model – and measured – test results – deflection per unit load (discontinuous skin(s)).....	190
Figure 6–16: Histogram of the simulated – finite element model – and measured – test results – deflection per unit load (discontinuous skin(s)).....	192
Figure 6–17: Finite element simulations – C13-01 perpendicular profiles of deflection at mid-span (discontinuous skin(s)) .....	193
Figure 7-1: Construction of stressed-skin panels.....	203
Figure 7-2: Stress distribution and tributary width of the skin under flexural action ...	203
Figure 7-3: Tributary width of the skins under flexural action (two-sided stressed-skin panel) <sup>1)</sup> .....	204
Figure 7-4: Critical stresses of the stressed-skin panel under flexural action (two-sided stressed-skin panel).....	206
Figure 7-5: Point load location – interior girder .....	210
Figure 7-6: Point load location – interior girder .....	211

## TABLES

Table 2–1: Terminology of floor model .....	14
Table 2–2: Magnitude of lateral load distribution.....	26
Table 3–1: Comparison of the construction and architectural characteristics of wood floor systems .....	49
Table 3–2: Comparison of the design characteristics of wood floor systems.....	54
Table 4–1: Möhler – shear lag estimates according to the specimen parameters (panel materials and dimensions) of the subject research.....	66
Table 4–2: Coefficients for the estimate of the tributary width – shear lag and plate buckling.....	68
Table 4–3: EC5 – shear lag estimates according to the specimen parameters (panel materials and dimensions) of the subject research .....	70
Table 4–4: SIA 164 – shear lag estimates according to the specimen parameters (panel materials and dimensions) of the subject research .....	73
Table 4–5: Basic spacing, $b_{basic}$ , plywood and OSB panels used in the subject research .....	78
Table 4–6: Correction coefficient ( $K_c$ ) and ratio of allowable stress ( $K_s$ ) for the subject research .....	79
Table 4–7: APA method – shear lag and plate buckling obtained under the specimen parameters (panel materials and dimensions) of the subject research ....	82
Table 4–8: Summary of the tributary widths according to the specimen parameters (materials and physical dimensions) of the subject research .....	88
Table 4–9: Stress verifications of SSP system.....	91
Table 4–10: Stress verifications of I-joist cross-section .....	92
Table 4–11: Length of splicing plate (APA – The Engineered Wood Association 1997) .....	94
Table 5–1: Material properties of the grillage components .....	124

Table 5–2: Comparison between the calculated – grillage model – and the measured – test results – deflections .....	133
Table 5–3: Reduction factors (loss of global stiffness).....	145
Table 5–4: Comparison between the calculated – grillage model – and the measured – test results – deflections (discontinuous skin(s)) .....	147
Table 6–1: Material properties of the I-joist flange (SOLID185) and web (SOLSH190) .....	171
Table 6–2: Material properties of the sheathing (SHELL43) .....	172
Table 6–3 : Calibration coefficients of the I-joist (awfac).....	177
Table 6–4 : Calibration coefficients of the sheathing (epfac).....	178
Table 6–5 : Comparison between the simulated – finite element model – and the measured – test results – deflections .....	180
Table 6–6 : Comparison between the simulated – finite element model – and the measured – test results – deflections (discontinuous skin(s)) .....	189
Table 7–1: Maximum effective contribution of the skins due to the effects of shear lag and plate buckling' .....	204

## LIST OF PUBLICATIONS

- Gerber, C., Crews, K. & Sigrist, C. 2004, 'Investigation on Load/Stress Distribution in SSP and Composite Characteristics of SSP', in *Proceedings of 'The 18<sup>th</sup> Australasian Conference on the Mechanics of Structures & Materials'*, vol. 1, eds A.J. Deeks & H. Hao, A.A. Balkema Publishers, Perth (WA), Australia, pp. 77-83.
- Gerber, C., Crews, K. & Sigrist, C. 2004, 'Wood Stressed-Skin Floor Systems — Investigation on Stress and Load Distribution', in *Proceedings of 'The 8<sup>th</sup> World Conference on Timber Engineering'*, Finnish Association of Civil Engineers RIL, Lahti, Finland.
- Gerber, C., Crews, K. & Sigrist, C. 2004, 'Wood Stressed-Skin Floor Systems: Investigation on Load/Stress Distribution in SSP and Composite Characteristics of SSP', in *Proceedings of 'Inaugural Research Showcase'*, University of Technology Sydney, Faculty of Engineering, Sydney (NSW), Australia, pp. 8-10.
- Gerber, C., Crews, K. & Sigrist, C. 2005, 'Investigation of the Ultimate Behaviours and FEA of Wood Stressed-Skin Panels', in *Proceedings of 'The 3rd International Structural Engineering and Construction Conference: Collaboration and Harmonization in Creative Systems'*, ed. T. Hara, A.A. Balkema Publishers, Shunan, Japan.
- Gerber, C., Crews, K. & Sigrist, C. 2005, 'Stressed-Skin Panels — Analysis of the Strain/Stress Distribution and Experimental Behaviours', in *Proceedings of 'The Australasian Structural Engineering Conference 2005'*, Newcastle (NSW), Australia.
- Gerber, C., Crews, K. & Sigrist, C. 2005, 'WOOD STRESSED-SKIN FLOOR SYSTEMS — Investigation on Load/Stress Distribution in SSP and on Ultimate Responses', in *Proceedings of 'The 4<sup>th</sup> Australasian Congress on Applied Mechanics'*, eds Y.M. Xie, A.P. Mouritz, A. Afaghi Khatabi, C. Gardiner & W.K. Chiu, Institute of Materials Engineering Australasia Ltd, Melbourne (VIC), Australia, pp. 323-329.

- Gerber, C., Crews, K. & Sigrist, C. 2006, 'Assessment of the Composite Action of Wood Stressed-Skin Panels', in *Proceedings of the '10<sup>th</sup> East Asia-Pacific Conference on Structural Engineering and Construction*', Bangkok, Thailand.
- Gerber, C., Crews, K. & Sigrist, C. 2006, 'Design Review of Wood Stressed-Skin Panels', in *Proceedings of the '10<sup>th</sup> East Asia-Pacific Conference on Structural Engineering and Construction*', Bangkok, Thailand.
- Gerber, C., Crews, K. & Sigrist, C. 2006, 'Numerical Analysis for Predicting the Load Distribution in Wood Stressed-Skin Panels', in *Proceedings of the '6<sup>th</sup> International PhD Symposium in Civil Engineering*', Zurich, Switzerland.
- Gerber, C., Crews, K. & Sigrist, C. 2006, 'Simulating the Serviceability of Stressed-Skin Panels with Changing Boundary Conditions – Finite Element Approach', in *Proceedings of 'The 9<sup>th</sup> World Conference on Timber Engineering*', Portland (OR), USA.
- Gerber, C., Crews, K. & Sigrist, C. 2006, 'On the Service Responses and Failure Mechanisms of Stressed-Skin Panels – Experimental Approach', in *Proceedings of 'The 9<sup>th</sup> World Conference on Timber Engineering*', Portland (OR), USA.
- Gerber, C., Crews, K. & Sigrist, C. 2006, 'Accessible and Reliable Design of Stressed-Skin Panels – an Australian Perspective', in *Proceedings of 'The 19<sup>th</sup> Australasian Conference on the Mechanics of Structures & Materials*', A.A. Balkema Publishers, Christchurch, New Zealand, *in print*.
- Gerber, C., Crews, K. & Sigrist, C. 2006, 'Screw- and Nail-Gluing Techniques for Wood Composite Structures', in *Proceedings of 'The 19<sup>th</sup> Australasian Conference on the Mechanics of Structures & Materials*', A.A. Balkema Publishers, Christchurch, New Zealand, *in print*.

## ABBREVIATION AND KEY-TERM DEFINITIONS

AS	Australian Standard™
AS/NZS	Australian/New Zealand Standard™
CV	coefficient of variation
DOF	degree of freedom
EMC	equilibrium moisture content
FEA	finite element analysis
FEM	finite element model
LVDT	Linear Variable Differential Transducer
MOE	modulus of elasticity (Young's modulus)
MOR	modulus of rupture
PUR	one-component polyurethane
OSB	oriented strand board
RBA	rubber-based adhesive
SBT	simple beam theory
SLS	serviceability limit state
SSP	stressed-skin panel
ULS	ultimate limit state
UTS	University of Technology, Sydney, Australia

Strength axis: in an orthotropic panel, the axis showing the strongest strength



## ABSTRACT

Stressed skin panels (SSPs) offer enhanced reliability and load-bearing capacity, potentially generating new opportunities for the use of timber in multi-storey residential, industrial, commercial and public buildings. However, in Australia, the design code for timber structures, AS 1720.1–1997 (Australian Standard<sup>TM</sup> 1997), does not make the most of the structural capabilities of this technology. In order to address this shortcoming, a major research project commenced in 2002 at the University of Technology, Sydney to investigate and quantify the structural performance of SSPs. This thesis details the research processes and outcomes from investigating the structural behaviours of SSP constructions. The project, which has emphasised that the sheathing and joists of SSP assemblies act compositely together, provides design recommendations that will ensure the safe and efficient design of SSP structures.

This PhD project focuses on the short-term behaviour of SSP structures subjected to quasi-static loading of serviceability and ultimate regime. The full-scale specimens are subjected to third-point loading (two uniformly distributed line loads) and centre-point loading (single uniformly distributed line load and concentrated point load). Effects of changing the physical integrity (skin discontinuities) and the boundary conditions (buckling restraint at the support) of the specimen are investigated. On the other hand, the long-term behaviour and specimen responses to and effects of in-plane loading, dynamic excitation, cyclic loading and loading history are outside the scope of this PhD research. Investigating multiple-span SSP systems and installing blockings inside the span are also excluded.

The experimental work involves full-scale testing of 27 simply supported single-span specimens, constructed in a variety of configurations and subjected to a series of non-destructive and destructive tests. This testing program enables the identification of the serviceability and ultimate responses, quantification of the two-way action, and characterising of the composite properties of SSP systems. It also permits quantification of the effects of discontinuing the skin and restraining buckling at the supports.

Two numerical models are developed within the framework of this project, that is, a mathematical procedure is derived from grillage theory and a finite element model is assembled using ANSYS software. Both models are capable of accurately predicting the serviceability responses of SSP structures.

This project puts forward design recommendations, culminating in the outline of a proposal to amend the Australian code for the design of timber structures (AS 1720). The current edition of this code, AS 1720.1–1997 (Australian Standard™ 1997), provides incomplete guidelines for the design of SSP systems. The recommendations offer Australian engineers a thorough and reliable design procedure for SSP systems.

## FOREWORD

The author acknowledges the comments of the examiners. In general, only minor clarification and textual amendments have been required. Therefore, the thesis content, including the design recommendations and substantive conclusions, has not been affected by this editorial work.

The final thesis has been organised into two parts – Part 1: Review, modelling and design, and Part 2: Experimental work – in order to facilitate the legibility and accessibility of its content. Part 1 presents the literature and SSP technology review, the development and validation of two numerical models, and the design recommendations. Part 2 focuses on the laboratory investigation, introducing the testing program and presenting/discussing the test results. This organisational change required accommodating the introduction and conclusions of both parts.

A number of the examiners' comments address aspects/issues which are outside of the scope of the PhD project. The author, while appreciating the value of these comments, has been aware of most of these aspects/issues and, in the thesis, has proposed future work to address them.

<b>1</b>	<b>INTRODUCTION.....</b>	<b>2</b>
<b>1.1</b>	<b>Objectives.....</b>	<b>3</b>
<b>1.2</b>	<b>Research methodology.....</b>	<b>4</b>
<b>1.3</b>	<b>Scope.....</b>	<b>5</b>
<b>1.4</b>	<b>Significance.....</b>	<b>6</b>
<b>1.5</b>	<b>Organisation of thesis.....</b>	<b>6</b>
1.5.1	Organisation of Part 1 of the thesis.....	7

# 1 INTRODUCTION

In the late 1940s Whittemore remarked: “There appears to be a great need for application of sound engineering principles to the development of new construction having just the necessary strength with which to use material efficiently.” (in: National Bureau of Standards 1948). About 30 years later, Vanderbilt et al. (1974) stated that wood design did not benefit from the state-of-the-art design methods available for other building materials, such as steel and reinforced concrete.

Where are we about 30 years later? The introduction of Eurocode 5 (European Committee for Standardisation 1995) in Europe – to which many European countries have adapted their national code – arguably constitutes respectable progress. On the other side of the Atlantic, the availability of the “Standard for Load and Resistance Factor Design (American Society of Civil Engineers 1996) represents another step toward more efficient and economic design of wood construction. However, the emergence of new grading techniques and engineered wood products, and the progress in adhesive technology – all of which provide greater reliability and load-bearing capability – demand an evolution in design practices. This is particularly the case for complex structures, such as stressed-skin panels (SSPs) and other composite constructions.

The focus of this PhD research, which commenced at the University of Technology, Sydney in 2002, is the load responses of SSP systems. This project is a logical continuation of a previous investigation performed by the author (Gerber & Sigrist 2002), which involved characterising and categorising the performances of floor systems according to Swiss practices. In the course of this Swiss investigation, research

needs were identified in areas such the reliability of the design model, the load/stress distribution and the long-term behaviour of SSP structures. It also highlighted the need for thorough and user-friendly design aids for engineers and builders alike. This PhD research attempts to address some of these.

Timber is a very versatile and competitive building material and, in Australia, it plays a major role in building, mostly in individual housing. Therefore, SSP systems have a sound potential and/or can create new opportunities for the use of timber in multi-storey residential, industrial, commercial and public buildings. This perspective has resulted in several Australian industries from the timber sector supplying wood products and materials for the laboratory study. Favouring the implementation of SSP system in Australia is also essential to this PhD project. In order to achieve this, comprehensive and reliable design guidelines need to be outlined for SSP systems considering the Australian context.

The PhD project involves full-scale testing of 27 specimens, constructed in a variety of configurations and subjected to a comprehensive range of static non-destructive and destructive load situations, which have enabled identification of the SSP specimens' serviceability and ultimate responses. Numerical procedures capable of predicting/simulating the behaviours of SSP systems are also developed, including a mathematical procedure and a finite element model. The first, which is derived from grillage theory, provides the basis for a protocol using MATLAB software (The MathWorks Inc. 2005). The second is developed using ANSYS software (ANSYS Inc. 2005).

## 1.1 OBJECTIVES

The principal objective of this project is to investigate the structural behaviour of SSP systems, with a view to developing and validating a practical design procedure for Australia.

The specific objectives are to:

1. Characterise the construction parameters of SSP systems such as the interlayers – skin-to-joist connections – and skin splicing. This includes quantifying the strength and slip modulus of bonded interfaces manufactured in a variety of configurations (refer to Chapter 2 in Part 2).

2. Investigate the structural behaviour of “full-scale” SSP elements. This experimental work consists of subjecting test specimens to a comprehensive range of quasi-static non-destructive loadings, and in some instances to quasi-static ultimate loading. The research program of this laboratory investigation is presented in Chapter 3 in Part 2.

3. Analyse and interpret the structural behaviour of the specimens. This comprises the quantification and characterisation of the effects of changing the specimen state, such as discontinuing the skin(s) (damage state) and/or restraining buckling at the support (restrained state). The following behavioural phenomena are examined:

- Linear-elastic properties, including the definition of the limit of linear-elasticity – load versus displacement and load versus strain characteristics (in Chapter 4 in Part 2);
- Characteristics of the two-way action – lateral load distribution (in Chapter 5 in Part 2);
- Properties of the composite action – characteristics of the strain distribution over the depth of the section (in Chapter 6 in Part 2);
- Characteristics of the strain distribution in the skins at mid-span and the supports (in Chapter 6 in Part 2).

4. Develop and verify predictive models for simply-supported SSP systems using mathematical (refer to Chapter 5 in Part 1) and finite element (refer to Chapter 6 in Part 1) approaches. These models also accommodate changes to the specimen state, such as discontinuing the skin(s) (damage state) and/or restraining buckling at the support (restrained state).

5. Formulate design recommendations for SSP technology in the form of a proposal for a design procedure in Australia (refer to Chapter 7 in Part 1).

## 1.2 RESEARCH METHODOLOGY

In order to develop a thorough understanding of SSP technology, this project adopts the following research methodology.

A **literature review** summarises the development of SSP systems, and analyses existing modelling techniques for wood joist floors and/or SSP systems. In addition, a

comparative analysis between conventional wood joist floors and SSP constructions is conducted and the benefits of SSP structures over conventional wood joist systems are detailed. The literature review also examines design procedures for SSP systems, particularly techniques for estimating the tributary width of the skin(s).

The **characterisation of SSP parameters**, such as the interlayers and the skin splicing, is conducted, because of the lack of directives for the design – fabrication and structural properties – in the literature. These two investigations permit the identification of the structural responses and characterisation of both assemblies. Furthermore, the performance of two adhesives – a rubber-based adhesive and a one-component polyurethane – with Australian softwood (*Pinus Radiata*) are assessed.

The **experimental work** investigates the responses of 27 full-scale specimens to a comprehensive range of static non-destructive loadings, and in some instances to static ultimate loading. The outcomes of this testing program permit the quantification and qualification of serviceability behaviour, load distribution and the composite properties of SSP structures.

Two **numerical procedures** are developed. A mathematical model, derived from the grillage theory, is based on small displacement theory for linear structural systems, in which the principle of superposition holds. A second model, based on finite element analysis, is developed using ANSYS software. Both models are calibrated/verified with the data acquired from the experimental work.

A set of **design recommendations** synthesises the outcomes of the project, outlining a design procedure for Australian engineers.

*NOTE: the literature review (reviews of SSP technology and design), the numerical procedures (grillage and finite element models) and the design recommendations are presented in Part 1 of the thesis, while the experimental work, including the investigation of SSP parameters and of full-scale SSP specimens, is presented in Part 2 of the thesis.*

### 1.3 SCOPE

This PhD research focuses on the short-term behaviour of SSP structures to quasi-static loading, including the serviceability and ultimate loading regimes. Full-scale specimens, which are simply supported and single-span, are subjected to third-point loading and centre-point loading. Construction parameters, in particular the interlayers and skin



splicing, are characterised. Effects of changing the physical integrity – inflicting discontinuity on the skin(s) near mid-span – and the boundary conditions of the specimen – restraining buckling at the supports – are also investigated.

On the other hand, the long-term behaviour and specimen responses to and effects of in-plane loading, dynamic excitation, cyclic loading and loading history are outside the scope of this PhD research. Investigating multiple-span SSP systems and installing blockings inside the span are also excluded.

## **1.4 SIGNIFICANCE**

The benefits of composite structures – enhanced reliability and load-bearing capacity – make them attractive to engineers. For this reason, SSP systems have the potential to generate new opportunities for the use of timber in multi-storey residential, industrial, commercial and public buildings. In Australia, the design code for timber structures, AS 1720.1–1997 (Australian Standard™ 1997), provides incomplete design guidelines that may curb the potential of SSP constructions. This PhD research, which contributes towards a better understanding of the responses of SSP to working loading, will develop a thorough design procedure and propose an amendment for future editions of AS 1720.

Two analytical models are also proposed. Both models compute/simulate the behavioural responses of SSP systems to service loading. They therefore offer efficient simulative aids for developing SSP solutions, whilst minimising the need for costly experiments.

## **1.5 ORGANISATION OF THESIS**

Because of the magnitude of the project – laboratory investigation and modelling work – and in order to facilitate the accessibility to the two main thematic of the research, this thesis is organised into two parts. The first part of the thesis – Part 1: Review, modelling and design – treats the aspects of the literature and technology reviews of SSP technology, the developments of a mathematical procedure derived from grillage theory and a finite element model assembled using ANSYS software, and the outline of design recommendations proposed for the Australian design code of timber structures (AS 1720). The second part of the thesis – Part 2: Experimental work – deals with the aspects of the laboratory experiments and the analysis of the test data of SSP full-scale specimens, enabling the identification of the serviceability and ultimate responses,

quantification of the two-way action, and characterisation of the composite properties of SSP systems.

### 1.5.1 Organisation of Part 1 of the thesis

The organisation of part one of the thesis – Part 1: Review, modelling and design – is as follows:

**Chapter 2** reviews the construction of lightweight wood floor systems. Composite and two-way actions exhibited in these systems are also discussed. This chapter also addresses the interlayers between the joists and the panels directly attached to them. The chapter finishes with a review of existing techniques to model wood floor systems.

**Chapter 3** compares conventional wood joist floor and SSP technology, with a view to positioning SSP constructions within the family of lightweight wood floor systems. The benefits of SSP systems are also discussed in detail.

**Chapter 4** presents a design procedure for estimating section properties of SSP decks, based on a review of existing standards and codes from outside Australia. In particular, the different techniques for approximating the tributary width of the skin(s) are discussed. Ultimate and serviceability limit state requirements are also detailed.

**Chapter 5** presents a mathematical model to predict the deflection of the SSP specimens based on grillage theory, for which an automated solution protocol is assembled using MATLAB software (The MathWorks Inc. 2005). Measurements from the experimental work are used as benchmark solutions for the parameterisation and verification of the model.

**Chapter 6** introduces a finite element model (FEM), which simulates the behaviour of the full-scale specimens using ANSYS software (ANSYS Inc. 2003, 2004, 2005). Measurements from the experimental work are used as benchmark solutions for the parameterisation and verification of the FEM.

**Chapter 7** synthesises the key outcomes of the PhD project into design recommendations. It outlines an amendment proposal for the current edition of the Australian design code for timber structures, AS 1720.1–1997 (Australian Standard™ 1997).

The list of references and bibliography, and the appendices are located at the end of Part 2 of the thesis.

The list of references and bibliography, and the appendices are located at the end of Part 2 of the thesis.

<b>2</b>	<b>REVIEW OF THE LITERATURE.....</b>	<b>10</b>
<b>2.1</b>	<b>Lightweight wood floor systems.....</b>	<b>11</b>
<b>2.2</b>	<b>On the interlayers: construction and behaviour .....</b>	<b>14</b>
2.2.1	Mechanical fasteners.....	15
2.2.2	Screw- and nail-gluing.....	16
<b>2.3</b>	<b>Interaction in wood joist floors .....</b>	<b>18</b>
2.3.1	Composite action.....	21
2.3.2	Two-way action.....	23
<b>2.4</b>	<b>Investigations into wood joist floors .....</b>	<b>27</b>
<b>2.5</b>	<b>Modelling of wood joist floors.....</b>	<b>29</b>
2.5.1	Model for multi-layer composites.....	29
2.5.2	Models for wood joist floors.....	30
2.5.2.1	Finite element analysis for floors (FEAFLO and NONFLO).....	30
2.5.2.2	Floor analysis program (FAP).....	32
2.5.2.3	Spring model .....	33
2.5.2.4	Partial composite action (PCA).....	33
2.5.2.5	Construction factor method.....	35
<b>2.6</b>	<b>Reliability design for wood joist floors.....</b>	<b>36</b>

## 2 REVIEW OF THE LITERATURE

Wood is a very versatile and competitive building material and is frequently used in floor systems. Among them, wood joist floors are a prominent technique and are used worldwide. This type of floor construction corresponds to a light frame structure, which comprises joists and superimposed layers. The latter have structural and/or functional (insulating, acoustic, aesthetic, etc.) roles. Wood joist floor systems can have a broad range of constructions and meet a large variety of requirements; for example, from Spartan constructions – joists associated with a single layer – to intricate assemblages – series of layers and/or fixtures arranged on one or both sides of the joists. However, each floor construction must fulfil a range of well-defined duties. The NAHB Research Center Inc. (2000) described that the tasks or purposes of floor systems are to support dead and live loads, to resist lateral loads and transfer them to the bearing walls, to offer suitable subsurface(s) for floor and/or ceiling finishes, to satisfy the users' expectancies (serviceability), to have adequate thermal insulation level, and to provide a fire barrier with sufficient resistance.

Wood joist floor systems may a priori look simple and straightforward. However, they are very complex and highly redundant, and interactions should be expected. Floor design differs from the simple beam theory (SBT) because of the occurrence of composite action between the joists and the panelling (also referred to in this thesis as sheathing) and the load distribution ability of the latter. Current practice for wood joist floor design does not always reflect this complexity. Furthermore, floors can also be expensive to test and/or require complicated analysis, which may make them expensive to simulate (Bulleit & Vacca 1988).

The review presented in this chapter aims to discuss works undertaken in connection with wood joist floor systems. It starts with fundamentals about wood joist floors and discusses ways of representing/approaching the construction of the floor systems. A section of this chapter focuses on the interfaces (also referred to in this thesis as interlayer) between the joists and the panels (directly) attached to them. This connection corresponds to a key parameter in wood joist floor constructions. The composite and two-way actions are then introduced and discussed. Next, researches on and models of wood joist floors are reviewed. This chapter finishes with a reliability consideration of wood joist floor systems.

## **2.1 LIGHTWEIGHT WOOD FLOOR SYSTEMS**

Light-frame wood constructions including joist floor systems are generally built with multiple parallel framing members to which superimposed layers (sheathing) may be attached (Moody & McCutcheon 1984). Wood joist floors may also be described as horizontal structural systems composed primarily of sheathing, joists and girders (NAHB Research Center Inc. 2000). The concept of lightweight floors may appear simplistic. Actually they are extremely complex, redundant, that is, repetitive members, multi-layer and load-sharing structures, and are highly anisotropic/orthotropic and statically indeterminate constructions (Gerber, Crews & Sigrist 2006a; Liu & Bulleit 1995). In addition to this, the floor members show variable, orthotropic, viscoelastic and non-linear properties, and are affected by natural defects, while the interlayers have non-linear behaviour. Therefore, Goodman et al. (1974b) stated that wood joist floor systems are best described as multi-layered constructions whereby each layer has orthotropic features and some variability of mechanical properties, and each interlayer has slip of sufficient magnitude to significantly affect the structural performance of the deck.

The number, nature and organisation of the layers define the properties and characteristics of the floor. Multi-layer floor constructions are well established and the layer can have structural and/or functional (insulating, acoustic, aesthetic, etc.) roles. Focusing on the “structural” sheathing – the sheathing which is immediately superimposed to the joists (refer to Figure 2–2 and Table 2–1), McLain (1999), Baker (2002), Breyer (1993) and Breyer et al. (2003) distinguished between single and two-

and more-layer floor systems (Figure 2–1). The following terminology has been agreed upon and is used to differentiate the type of sheathing (Breyer et al. 2003):

- combined subfloor-underlayment – a single-layer floor system.
- subfloor – the bottom layer in a two-layer floor system.
- underlayment – the top layer in a two-layer floor system.

Single-layer systems are economical, but ensuring the continuity between the panels of the sheathing is recommended. In two-layer constructions, the underlayment provides a plane and even surface. Figure 2–1 depicts the arrangement of the subfloor and underlayment of a two-layer floor construction.

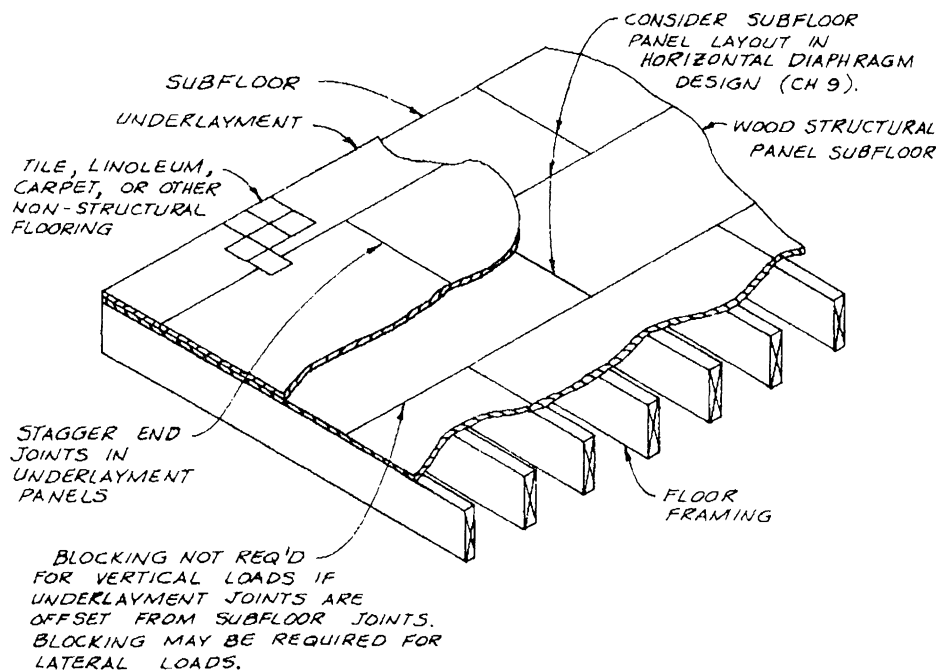


**Figure 2–1: Two-layer floor system (Breyer et al. 2003)**

Sigrist et al. (2000), Sigrist and Gerber (2002) and Gerber and Sigrist (2002) proposed a standard model for a lightweight floor that considered the complete floor construction and broke it down into individual floor components (Figure 2–2). This model incorporated all components of a floor construction; the joists and the structural and non-structural superimposed layers are included in the model. From this model a step-by-step conception and design schema for light wood floors was developed and design charts were proposed (Gerber & Sigrist 2002; Sigrist & Gerber 2002, 2004).

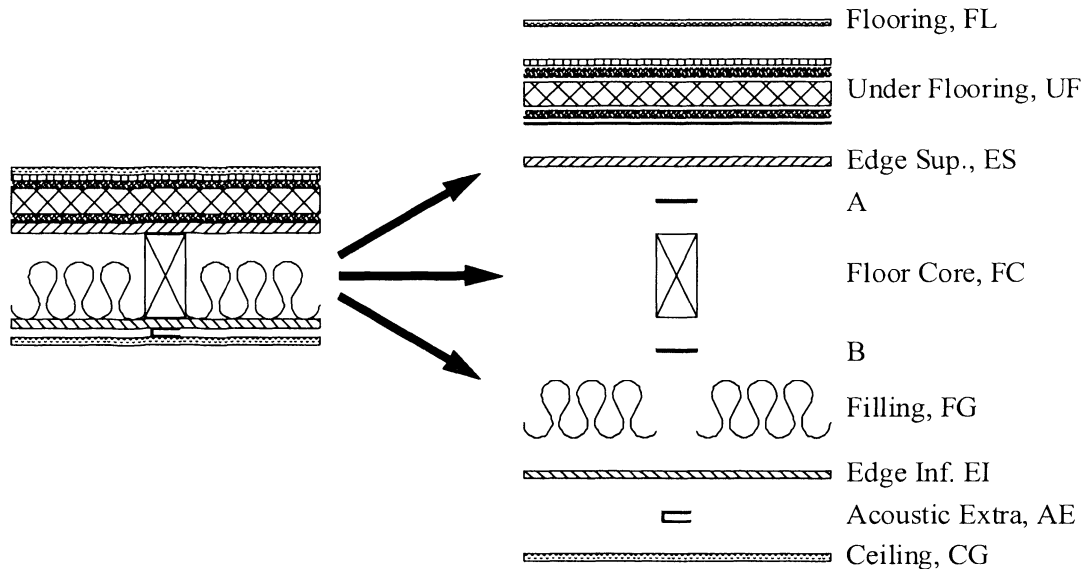


**Figure 2–2: Construction model for light wood floor (Gerber & Sigrist 2002)**

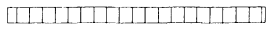
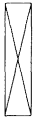
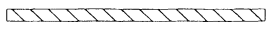
In the model of Gerber and Sigrist (Figure 2–2), the structural strength and serviceability of the floor construction is governed by the Edge Sup (ES), the Floor Core (FC) and the Edge Inf (EI), whereby the degree of composite action between these components is determined by the structural properties of the interlayers A and/or B. The use of additional layers – Flooring (FL), Under Flooring (UF), Filling (FG), Acoustic Extra (AE) and Ceiling (CG), which have no structural role, contribute to achieve the service/utility requirements of the deck.

Elsewhere, Kilpeläinen and Ukonmaanaho (2001) proposed a system with three degrees of prefabrication: (1) construction on-site, (2) open elements, and (3) closed elements. The first one (1) is comparable to a “stick-by-stick” technique, while the others (2) and (3) correspond to two prefabricating extents of completion. This system also aims to remain open/flexible. Because of this, it is left to the builders to choose the strategy with regard to the degree of prefabrication, and to some extent the materials and the suppliers.

This PhD project focuses on the structural elements of the floor, that is, the joists and the panels directly superimposed and connected to them. These are presented in Table 2–1, in which the analogies to the concepts of McLain (1999), Baker (2002) and Breyer et al. (2003) and the model of Gerber and Sigrist (2002) have been drawn.



**Table 2–1: Terminology of floor model**

Floor structure	Model and terminology		
	Model of PhD thesis	Model 1 <sup>*</sup>	Model 2 <sup>†</sup>
	Upper skin	Subfloor/ Combined subfloor- underlayment	Edge sup, ES
	Joist	Joist	Floor core, FC
	Lower skin	–	Edge inf, EI

<sup>\*</sup>model of McLain (1999), Baker (2002) and Breyer et al. (2003), <sup>†</sup>model of Gerber and Sigrist (2002).

## 2.2 ON THE INTERLAYERS: CONSTRUCTION AND BEHAVIOUR

In light-frame construction, wood floor systems are generally built with joists to which sheathing is attached on one or two sides. The structural performance of the assemblies depends on the mechanical properties of the wood members and connections between them. Therefore, the interlayers have an important role because they affect the strength and stiffness of the floor unit (Corder & Jordan 1975; Foschi 1982; Vanderbilt, Goodman & Criswell 1974). In practice, the nature and construction of these interfaces – connections between the joists and the superimposed panels – can have different forms; from mechanical only (nail, screws, etc.) to fully bonded. For Moody and McCutcheon (1984), the use of improved fastening techniques produces much gain. Respectively, higher shear strength and slip modulus of the interlayers would increase the load-bearing performance, reduce the deflection and increase the diaphragm capability of the floor assembly.

Studying the interlayers is on the periphery of the scope of the subject research. However, considering the significance of this parameter for floor systems, particularly stressed-skin panels (SSP), a non-exhaustive review of works on wood connections is presented henceforth. Furthermore, in the early stages of the subject research, a laboratory investigation was conducted in order to quantify the performance of bonded connections. This research is presented in detail in Chapter 2 in Part 2.

The scope of the review on wood connections is limited in two ways. First, it focuses on the techniques of mechanical fasteners and of screw- and nail-gluing, because both interface techniques are used for conventional floor systems and SSP decks respectively. Second, the relevance of the works to the subject research defines the magnitude of the review, that is, results of some researches were used in model development. For example, a nail-gluing technique was implemented to assemble the full-scale decks of the subject research.

### **2.2.1 Mechanical fasteners**

In conventional floors, nominal mechanical fasteners (with about 300-mm spacing) are generally used to attach the sheathing to the joists. A complex interaction exists between a mechanical fastener and the surrounding wood members, that is, the contact areas between a nail and the wood fibres. In floor systems, only the general mechanism is considered, that is, the overall slip modulus is characterised so that the deformations of the fastener and the wood member are included.

A considerable amount of work has been carried out on the topic of wood members connected with mechanical fasteners. Indeed, wood connections with connectors such as nails, screws or bolts have been comprehensively studied in order to identify the behaviour and properties of such assemblies and to develop theoretical methods of design analysis. Most works focused on the performance of connectors submitted to lateral load. However, several researchers suggested that in some cases, especially with nails and screws, combined lateral and withdrawal solicitations might be induced. As such, Vanderbilt, Goodman and Criswell (1974) proposed that, in nailed floor systems under concentrated point loads, the nails experience both axial and lateral loads.

Some researchers presented theoretical analysis to describe the load-slip response of nailed or bolted joints under lateral load (Kuenzi 1955; Patterson 1973; Wilkinson 1971, 1972). Stluka (1960) demonstrated that the Kuenzi (1955) theory was accurate for pre-drilled nailed joints. For the purpose of defining that same behaviour, further studies followed a more pragmatic orientation and empirical equations were employed (Foschi 1974; Vanderbilt, Goodman & Criswell 1974; Wilkinson 1972). Other researchers focused their efforts on investigating the effect of combined axial and lateral forces in nailed connections (DeBonis & Bodig 1975). To date, most codes present design methods for assessing the structural performance – strength – of wood-to-wood or

wood-to-steel connections with mechanical fasteners (Australian Standard<sup>TM</sup> 1997; British Standard 2004; Société Suisse des Ingénieurs et Architectes 2003).

Under lateral load, non-rigid fasteners such as nails experienced a non-linear load to deformation relationship. It is common, though, to assume linearity for modelling. Amana and Booth (1967; 1968) proposed to approximate the slip modulus, considering the quasi-linear portion of the load-slip curves of nailed connections, because it completely embraces the range of the working loads. McLain (1975; 1976) proposed a logarithmic function that estimates the load-slip relationship of two-member nailed connections. Later, Stone (1980) developed a technique for the prediction of the curve parameters of McLain's function. Elsewhere, Wheat (1980) proposed an iterative procedure to approximate the non-linear slip of the interlayers. As for the strength, the design code also proposed methods for the assessment of the deformation/distortion of wood-to-wood or wood-to-steel connections with mechanical fasteners (Australian Standard<sup>TM</sup> 1997; British Standard 2004; Société Suisse des Ingénieurs et Architectes 2003).

### **2.2.2 Screw- and nail-gluing**

Pioneered in the 1960s by APA – The Engineered Wood Association, the use of elastomeric adhesives in wood joist floor composites was first documented by Rose (1970). This development followed innovations in elastomeric adhesives that made screw- and nail-gluing more practical, and consequently enabled assembling composite floor systems on-site (Rose 1970). The adhesive plays a major role in screw- and nail-gluing techniques. Corder and Jordan (1975) proposed that wood-joist floors manufactured with a nail-gluing technique experienced a large increase of stiffness in comparison to nailing alone. In addition to this, the shear transfer between the joists and the sheathing is improved (Liu & Bulleit 1995).

For the manufacturing of glued interfaces, one should aim for an adhesive layer as thin and uniform as possible. In order to achieve this, the viscosity and spread of the glue must be adapted to the conditions of the wood substrates and climatic conditions of the environment (Vick 1999), and the technique used for generating pressure. This last aspect is critical to screw- and nail-gluing, because both fasteners have the inconvenience of generating irregular and significantly less pressure (0.0–0.2MPa) in the glue line than hydraulic and pneumatic infrastructures (Kairi et al. 1999). In any

case, the level of the (compressive) pressure should be adequate in order to achieve proper curing of the adhesive, that is, thin glue line – 0.076 to 0.152 mm (Vick 1999) – free of entrapped air and without starving the interface or causing any damage to the substrates. As a final recommendation, the assemblies should remain undisturbed until complete curing of the adhesive (Vick 1999), or be handled with care in order to avoid any damage in the glue line (Kairi et al. 1999).

In order to achieve composite mechanism in the assemblies, structural adhesives should be preferred. Such glues are generally stronger than wood substrates and maintain strength and rigidity under long-term load (Vick 1999). Choosing the right adhesive is paramount and should be governed by the anticipated loading life (nature, direction, level, duration, etc.) and the climatic exposure (temperature, humidity, etc.). Technical and practical aspects such as availability, applicability, working properties – especially pressure requirements – and cost should also receive some consideration.

In recent years, the adhesive industry has developed products that require lower pressure and need a shorter setting time. This new generation of adhesives is particularly adapted for screw- and nail-gluing techniques whereby a reasonable number of mechanical fasteners is required. Investigating the suitability of low pressure and screw-gluing techniques of assemblies constructed with mono-component polyurethane (PUR) adhesives, Kairi et al. (1999) identified the parameters affecting the performance and quality of the bond; also published elsewhere (Nokelainen 2000). Kairi et al. (1999) found that PUR responded well with low pressure (0.03 to 0.1 MPa), that is, glue spread and shear strength of the specimens built under low pressure matched those of the specimens assembled under normal pressure (0.6 to 0.8 MPa). Under a lower pressure range (0.01 MPa and less), Kairi et al. (1999) reported a significant reduction of shear strength. However, in any pressure regimes, exceeding the 0.3-mm threshold of the glue line thickness, as recommended by FMPA certification (FMPA – Forschungs- und Materialprüfungsanstalt Baden-Württemberg Otto-Graf-Institut 2000), was never observed (Kairi et al. 1999). Kairi et al. (1999) concluded that the screw-gluing technique produced assemblies of similar strength to uniformly pressed specimens and that the performance of PUR assemblies are equal to resorcinol-phenol glued specimens. In order to achieve such results, Kairi et al. (1999) recommended clean and smooth substrate surfaces, a spread of 250 g/m<sup>2</sup>, and adequate screw spacing. Jung (2002) proposed similar recommendations.

Elsewhere, a study on screw-gluing techniques with phenol resorcinol formaldehyde glue and solid wood and plywood substrates (Kurt 2003) showed that enough pressure was provided in the glue line in order to achieve proper curing of the assemblies. Interestingly, Kurt (2003) removed the screws prior to the tests.

Screw- and nail-gluing offer economical alternatives to expensive press infrastructures and enable the construction of customised and large(r) composite structures (Kairi 2001). Both techniques can also be applied for on-site manufacturing with minimum inspection and supervision. Between the two techniques, nails produce lower compressive pressure than screws but are more economical. Screw- and nail-gluing techniques are economical production processes because the assemblies can be moved off the manufacturing rack before the complete curing of the glue, provided that the mechanical fasteners provide enough strength and stiffness (Kairi et al. 1999).

Simulating and predicting the strength and slip modulus of screw- or nail-glued assemblies is highly complex, because each connector has non-linear behaviour and works with areas of the wood members, which show heterogeneous properties. Expressed in another way, the nails are influenced by the wood properties around them locally, while the glue interacts with the wood properties of or very near to the glue line (Pellicane 1992a, 1992b, 1994). Despite this highly non-linear status of screw- or nail-glued joints, Pellicane (1992a; 1992b; 1994) proposed a model based on the concept of the superposition of both connector strengths and stiffnesses. In this model, the strength and slip modulus are governed by the adhesive unless/until it fails; subsequently the connection properties are determined by the mechanical fasteners. Using the superposition technique, accurate estimates were achieved for both the strength and stiffness of connections within the range of service loading. For loading beyond the range of service, the predictor remained accurate for approximating the strength (including the ultimate strength), but lacked such accuracy for the load-slip modulus, that is, the connection stiffness is consistently underestimated.

### **2.3 INTERACTION IN WOOD JOIST FLOORS**

In joist floor systems, some interaction should be expected between the ribs and sheathing. Expressed in another way: “in joist floor systems, joists and sheathing interact both by composite action of the joist and sheathing and by load sharing between joists resulting from the distribution of load by the sheathing” (Vanderbilt et al. 1974).

Therefore, the sheathing does more than simply transfer loads to the nearest joist. It takes the function of flanges in the composite beams about the joists and acts as a continuous beam crossing the joists (Criswell 1981), and its mechanical properties determine the potential contribution to the composite beams and two-way action. Wolfe (1990) proposed that the composite action affects the load-bearing capacity more significantly than the load sharing effect because it modifies properties of the floor section, that is, both the first and second moment of area increase. On the other hand, load-sharing may also depend on the boundary conditions of the floor (Wolfe 1990).

Floors cannot be accurately and optimally designed solely on the mechanical properties of the joists and sheathing considered as series of independent single or bare element. Williston and Abner (1962) proposed that the structural performance is significantly affected by the construction features of the floor and some load-sharing should be considered. The effect of the construction features was also identified by Wheat, Gromola and Moody (1986) who measured that the moduli of elasticity of the joists would increase by 8–10% when end-nailed to headers. They also suggested that partial composite and two-way actions should be accounted for in design. In floor systems, other parameters of the floor such as the variability of the joist stiffness, the sheathing construction (un-spliced, spliced, gaps) and the aspect ratio (depth to span, joist depth to sheathing thickness) may also play a role in the floor features (Wheat, Gromola & Moody 1986).

Parametric studies on the composite and two-way actions (Goodman et al. 1974b; Vanderbilt, Goodman & Criswell 1974) showed that the composite action affects the stiffness and strength performance of floor assemblies. McCutcheon (1986) reported significant stiffness increases for T- and box-section floor assemblies in comparison to the joists acting alone. Goodman et al. (1974b) assessed that the joist on which a concentrated point load is applied carries only about a third of that load; the adjacent load carrying most of the load remainder.

Observed separately, the composite action primarily reduces the deflections of the joists, that is, the average floor deflection becomes smaller and the two-way action reduces the variation between the deflections of the joists, that is, the perpendicular deflection profile of the floor becomes smoother (Criswell 1983). Optimising the composite and two-way actions demands contradictory action (Sherwood & Moody 1989). The composite action is maximised when the joist orientation and the strength axis of the sheathing concur, whereas the optimum two-action is obtained when the joist

longitudinal axis and the strength axis of the sheathing are orthogonally arranged. Elsewhere, Goodman et al. (1974b) reported that thicker sheathing positively affects both the composite and two-way actions.

Typically, in conventional floor construction, the longitudinal axis of the joists and strength axis of the panels are perpendicular to each other. With such an arrangement of the floor members, larger joist spacing can be bridged (Raadschelders & Blass 1995), and the two-way action is reinforced. On the other hand, in prefabricated floors, such as stressed-skin panels, both the longitudinal axis of the joists and strength axis of the panels coincide (Baker 2002), which incidentally strengthens the composite action. Depending on the arrangement of the axes, that is, the way the panel works with joists, Breyer et al. (2003) described the orthogonal and concomitant arrangements respectively as strong and weak orientation of the strength axis of the panel.

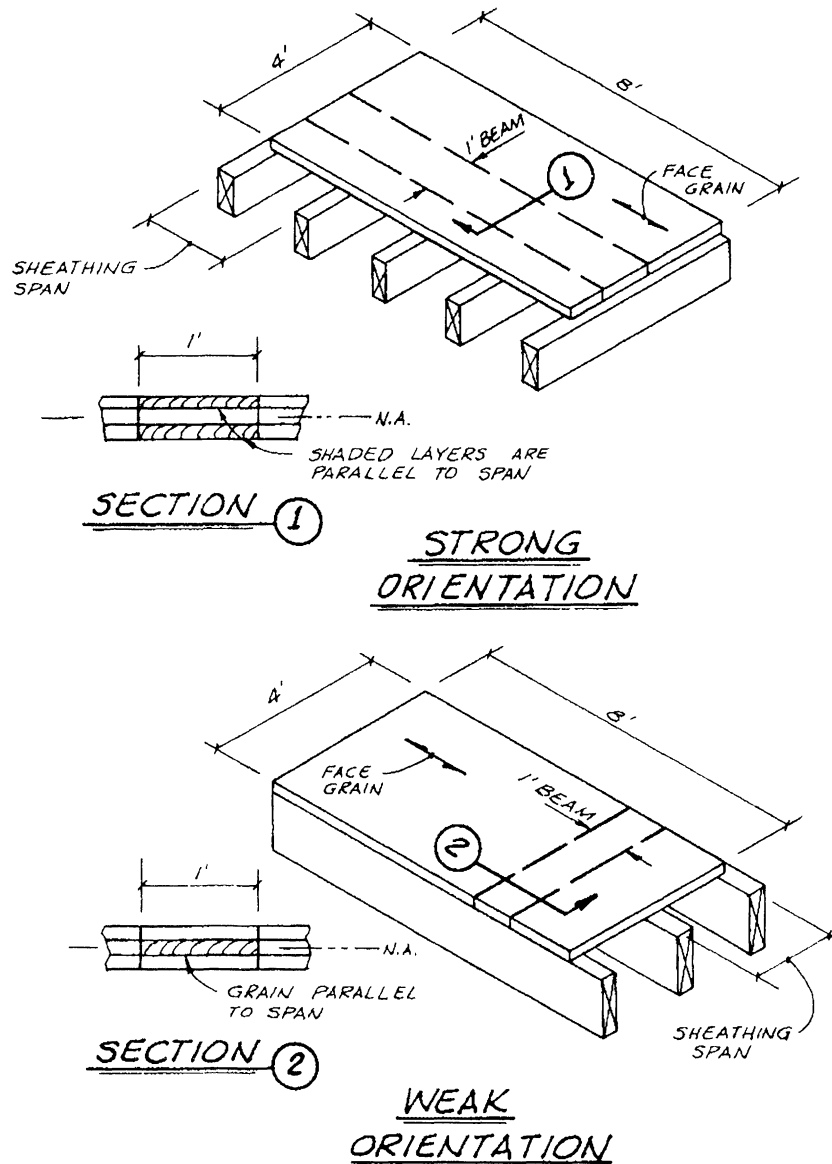


Figure 2-3: Strong and weak strength axis of plywood (Breyer et al. 2003)

### 2.3.1 Composite action

Composite action occurs whenever the interaction between two components infers a shift in their neutral axis for flexural stress, that is, this mechanism moves the neutral axes of the components toward one another. Under full composite action conditions, the neutral axes of the section members coincide. The first and second moduli of the section area increase, thus reducing the stress in the section members and increasing the stiffness of the section respectively. Expressed in another way, improvement provided by partly or fully composite action should lead to longer span and/or to shallower wood



joist assemblies (Onysko 1970), thus providing economic and architecturally suitable floor systems.

Criswell (1981) observed that the amount of composite action depends on the relative size and stiffness of the sheathing and the joist, the efficiency (stiffness provided) of the interlayer connection, and the continuity of the sheathing. The negative effects of gaps in the sheathing was also identified by other researchers (Dawson 1974; Dawson & Goodman 1976). Elsewhere, the damaging effects of gaps in the sheathing were also identified and reported as disrupting the continuity of the sheathing and thus curtailing its strength and stiffness severely (Dawson 1974; Dawson & Goodman 1976; McCutcheon 1986). Sherwood and Moody (1989) reported that a single gap at mid-span caused a factor four loss of connector stiffness, but did not quantify its effect on the overall responses of the deck.

Admitting that the composite action is a parameter of the floor structures, the extent of the increase of strength and stiffness needs to be identified. After Sherwood and Moody (1989), the effect of the composite action relies on the material properties (Young's modulus) and construction (stiffness of the skin-to-joist connection and splicing of the plates) of the sheathing in co-axial direction to the joists. Vick's work (1999) indicated that, in structural applications, the adhesive contributes to the strength and stiffness of the composite assemblies. In principle, three cases can be encountered, depending on the properties of the connection between the joists and the sheathing:

1. no connection → no composite action: the floor members act independently/individually.
2. mechanical fastenings → limited/incomplete composite action: limited interaction between the floor members.
3. bonded connection → complete composite action: the floor structure acts as a fully composite section.

Nokelainen (2000) reported that glued floor constructions have higher stiffness and bending strength, and no interlayer slip. In an attempt to quantify the stiffness improvement inferred by bonded interface, Nokelainen (2000) proposed a relative comparison in which 100% corresponds to fully composite constructions; floor systems without connection (friction resistance between the floor members) and with mechanical fasteners reach about 25% and 45% respectively. Elsewhere, a comparison of the stiffness of "bare" joist to partial (second situation) and fully (third situation) composite

joist floor assemblies, stiffness increases of about 15% (Folz & Foschi 1989; National Association of Home Builders 1973) and about 40% (National Association of Home Builders 1973; Williston & Abner 1962) were reported respectively.

In building practice, the second situation – incomplete composite action – is most common. It also exhibits a highly variable degree of composite action, depending on the stiffness and arrangement of the fasteners. From a design perspective, this situation presents great mathematical complexity because of the non-linear behaviour of the connection. However, in the range of design load, it is reasonable to assume linearity (Sherwood & Moody 1989). Stressed-skin panels belong to the third group – complete composite action. Under these conditions, linear strain distribution can be assumed over the depth of deck section (Raadschelders & Blass 1995) and simple beam theory can be applied (Amana & Booth 1967).

### **2.3.2 Two-way action**

In addition to forming the flanges of the longitudinal composite girders, as mentioned previously, the sheathing also works as a continuous multiple span beam, which runs to the joists orthogonally. The sheathing therefore carries the imposed loads to the nearest joists. It also distributes the load among the joists, performing the so-called “two-way” action, also described as the lateral load distribution. Consequently, the sheathing must be sized in order to resist the loads, for example pad loads, applied placed between the joists (Criswell 1983). Respectively, such design consideration is required by most design codes.

Sherwood and Moody (1989) reported that with increased stiffness of the sheathing in the direction perpendicular to the joists, the two-way action accentuates and the joist deflections become more uniform, that is, increased stiffness of the sheathing perpendicular to the joists reduces the variability of the joist deflections (Figure 2–4). Therefore, the orientation of the strength axis of the panels to the joists also affects the two-way action. Seemingly, this was also reported elsewhere (Criswell 1983). On the other hand, gaps in the sheathing were identified to reduce the effectiveness of the two-way action (Dawson 1974; Dawson & Goodman 1976).

Figure 2–4 depicts the smoothing capability – levelling the variations between the joist deflections – of the sheathing considering different stiffness intensities. It indicates that sheathings generally used in floor systems, that is, with “common” thickness and

mechanical properties, is insufficiently stiff to manage a significant smoothing action. This also suggest that the sheathing achieves limited load (re)distribution (Criswell 1979b). For situations without sheathing, or sheathing showing very low stiffness, the system interactions are limited. Therefore, no system feature should be assumed, that is, each floor member acts independently/individually and the single/bare joist approach is recommended. On the other hand, increasing the sheathing stiffness toward infinity in the direction perpendicular to the joists produces uniformed deflections among the joists of the floor system. Thus, sheathing with infinite stiffness forces the joists to work in unison, that is, for a uniformly distributed load, the effect of joist property variability is evened, and for a concentrated point load each joist receives an equal share of load.

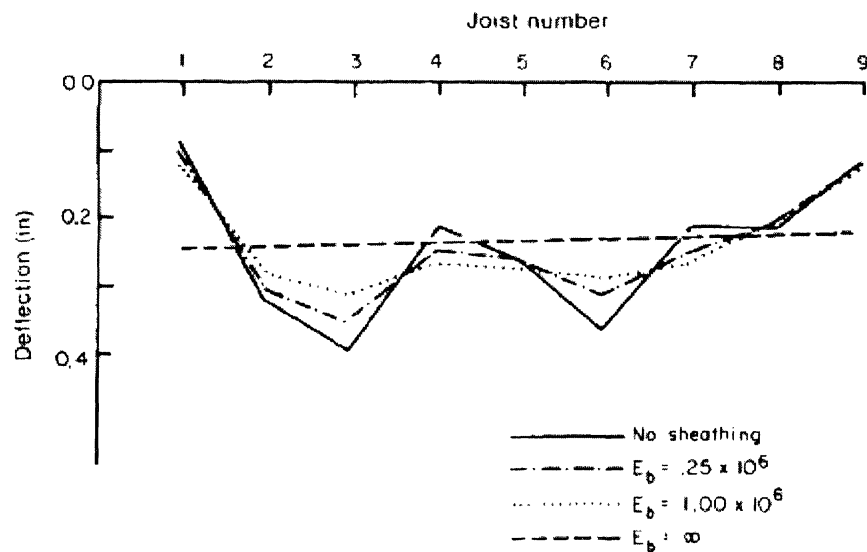


**Figure 2-4: Effect of sheathing stiffness on the two-way action (Sherwood & Moody 1989)**

Other studies related to the two-way action also pointed to a smoothing effect on the deflections of the joists – less variation between the joists – in floor systems (Criswell 1979b; Vanderbilt, Goodman & Criswell 1974). Expressed in another way, the sheathing reduces the differences in deflection among the joists (Criswell 1983), thus the deflections of the joists become more uniform (Fridley, Hong & Rosowsky 1997). This smoothing mechanism was reported in studies on floor systems under uniformly distributed load (Polensek et al. 1972; Vanderbilt, Goodman & Criswell 1974; Vanderbilt et al. 1974). Elsewhere, McCutcheon (1977) proposed that the two-way action scales down the effects of the stiffness variability of the joists. This

phenomenon was observed in floor assemblies in which the joists show significant differences of stiffness (Criswell 1979a; McCutcheon 1984). Two-way action and smoothing effect on the deflections of the joists were also reported by Philpot and Rosowsky (1996)

Load sharing or lateral load distribution corresponds to a phenomenon that is similar/assimilable to the two-way action. It is an important feature of wood joist floors (Polensek 1971) and corresponds to the ability found in repetitive parallel member systems, thus include wood joist floor systems, to transfer load away from the member/joist, onto which the load is applied, toward the adjacent/neighbouring members through the flexural stiffness of the sheathing (Tucker & Fridley 1999). Under this assumption, the sheathing forms a series of continuous beams in the direction perpendicular to the joists (Rosowsky & Ellingwood 1991). With panellised sheathing, Wilfred (2003) proposed that the effective width of the cross-beams should be equal to 1.4 to 2.0 times the joist spacing. The load sharing capacity greatly depends on the bending stiffness of the sheathing, that is, the stiffer the sheathing, the greater the load (re)distribution. To some extent, the joist properties, especially the mechanical variability of the latter, are also influential. Elsewhere, Tucker and Fridley (1999) studied load-sharing in wood joist floors without identifying the contributors.

Wolfe (1990) proposed that the load-sharing calls upon several features of assembly interactions such as the size effect (size and number of the members), mutual restraint (higher stress in stiffer member), and bridging (load redistribution around a local weak zone). Therefore, increasing joist spacing degrades load-sharing, whereas increasing sheathing thickness enhances load-sharing. Zahn (1970) also reported that the mutual restraint would produce an increase of about 12% load-sharing and Liu and Bulleit (1995) that thicker sheathing increased the first-member yield load. Elsewhere, Wheat, Gromola and Moody (1986) proposed that bridging effects could explain the fact that the load capacity of floors was not always governed by the weakest members and that in some situations load capacity increased beyond initial failure. Considering uniformly distributed loadings, some load is presumably moved away from the weak members. Thus, “strong” neighbouring members may accept more loads and give higher strength to the floor system overall. As a consequence of this, Sliker (1972) proposed that the phenomenon of load-sharing allows for optimising the design of floor systems, for example, by alternating joist grades and/or dimensions assuming that “weak” joists would carry a reduced share of load.

In order to account for floor features on load distribution, a multiple regression (Equation 2-1) was proposed by Wolfe (1990). Equation 2-1 indicates that stiffness of common residential floor systems may be increased by about 15%, provided that the sheathing material has a strong positive correlation between stiffness and strength.

$$LSI = 2.75JS^{-1} + 0.010114D^{-1} + 0.1223t + 0.887 \quad (\text{Eq. 2-1})$$

where  $JS$  is the joist spacing [in],  $D$  is the joist depth [in], and  $t$  is the thickness of the sheathing [in].

Aiming to predict the load distribution, Crews (2002) developed a lateral load distribution model based on a Fourier cumulative polynomial series, in which the deflection coefficient is approximated by equating a joist individual deflection over the sum of the joist deflections as per laboratory experiments. Elsewhere, several complex models were developed to predict load distribution in the linear range (Cramer & Wolfe 1989; DeBonis & Bodig 1980; Folz & Foschi 1989; Foschi 1982; Thompson, Vanderbilt & Goodman 1977).

**Table 2–2: Magnitude of lateral load distribution**

Number of spacing(s) from loaded joist	*Load distribution factor [%]		
	†(I)	†(II)	†(III)
0	32.0	33.5	36.0
‡1	24.0	28.9	28.3
‡2	8.0	–	–
‡3	2.0	–	–

\*distribution is tributary of sheathing properties and joist stiffness, †sources: (I) Polensek (1971), (II) Criswell (1983) and (III) Hong (1994) Fridley, Hong and Rosowsky (1997) and Tucker and Fridley (1999), ‡distribution symmetry, that is, adjacent joists on both side of the joist under load take similar intensity of loads (indicated values).

NOTE: sum of the load intensity – distribution factor – is equal to 100%; in (II) and (III) the load residuals on subsequent joists, 2 and 3 spacings away from the load introduction, are not available.

Criswell (1983) investigated the load-sharing with numerical simulations, while the other researchers assessed the load distribution by laboratory experiments (Fridley, Hong & Rosowsky 1997; Hong 1994; Kloot & Schuster 1963; Polensek 1971; Tucker & Fridley 1998, 1999).

Blocking and/or rim plates are not necessities (Kairi et al. 1999; Nokelainen 2000). However, an increase of the magnitude of the two-way action was identified by the presence of bridging and/or solid blocking (Onysko & Jessome 1973). Onysko and Jessome (1973) observed that the perpendicular stiffness of the floor increased, and that the overall deflection was reduced and the relative deflection under concentrated point load was improved.

## **2.4 INVESTIGATIONS INTO WOOD JOIST FLOORS**

Polensek et al. (1972) investigated floors constructed with solid wood joists on which plywood sheathing was nailed. Nominal blocking was placed and rim boards/headers were fastened at the ends of the joists. The specimens were simply supported at joist ends. Polensek et al.'s (1972) research comprised tests with uniformly distributed (entire area of the deck and localised areas) and concentrated point loads. The research aimed at understanding the “true” deck stiffness and strength and the load-sharing factor.

Wheat et al. (1986) investigated floors constructed with solid wood joists on which plywood tongue and groove sheathing was nailed. The ends of the joists were connected to rim boards. The entire perimeter of the deck was simply supported. Wheat et al.'s (1986) research focused on the behaviours of floors under design load (40 psf about 1.95 kPa), the first joist rupture and the failure to sustain uniform load.

Corder and Jordan (1975) investigated floors constructed with solid wood joists on which plywood or particleboard tongue and groove sheathing (subfloor + underlayment) was nailed or glued. With glued specimens, the panels of the sheathing were glued on the edge, that is, glued tongue and groove. In addition to this, the subfloor and underlayment were glued together. Headers were fastened at the ends of the joists. Corder and Jordan's (1975) research focused on the behaviour of floors under line load at mid-span (200 lbs about 0.9 kN) and the free vibration and impact load responses. The sheathing was also studied with regard to concentrated load. The specimen was simply supported at joist ends, except for the concentrated load investigation whereby the side/exterior joists sat on continuous support.

Elsewhere, a study using Monte Carlo simulations focused on the effects of the joist, sheathing and interlayer stiffnesses and their effects on the responses of floor assemblies under uniformly distributed and concentrated loads. Fezio (1976) reported

that increased joist variability has significant effects such as increased average floor deflection, higher maximum joist deflection and stress, and increased maximum nail force. Therefore, Fezio (1976) identified that the joist stiffness had a significant effect, whereas the sheathing and connector stiffness had a minor effect on the behaviour of the floor systems.

In Australia, the finite element technique and T-beam analogue were used to study the composite action in floor systems, considering parameters such as the contribution of the sheathing, the stiffness of the interface, and the gaps in the sheathing (Yang, Pham & Leicester 1994). Yang, Pham and Leicester (1994) proposed that between 62 and 83% of the floor decking acted compositely with the joists, that is, for typical spacing from 450 to 600 mm, tributary width ranges from 70 to 75%. The contribution of the sheathing is less than 100%, because of shear effects in decking under compression. Considering nominal nailing and gluing for the interlayers, Yang, Pham and Leicester reported that these interfaces create respectively limited and quasi full composite action. The gaps in the sheathing were identified to increase the deflection by 16 to 34% and reduce the strength by 14 to 30%. Yang, Pham and Leicester also reported that the ceiling increases the stiffness of the floor system. Experimental data from elsewhere (Bier, Britton & McLellan 1993a, 1993b; Bier & Taylor 1992) were used to validate this model. Based on their findings, Yang, Pham and Leicester (1994) concluded that design floor systems by the bare-joist procedure may be maintained. However, they proposed that a modification factor should be introduced in order to account for the interaction between the joists and the sheathing. This design enables increases of 2 to 6% in strength and 5 to 15% in stiffness.

Multiple-span floor systems were also investigated. The continuity of the floor — particularly the sheathing — had a noticeable effect on the deflections in the spans (National Association of Home Builders 1961). Working back the benefit of the continuity into the stiffness, increases of about 40% were observed, compared with single-span predictions.

In studies on the failure mechanism of wood joist floors, a post-failure behaviour was accommodated in numerical models, that is, a failed joist would retain 0 to 10% of its initial stiffness. Bulleit and Vacca (1988; 1989) and Criswell (1979b) reported that the failure of two neighbouring members infers the collapse of most floor assemblies. However, experimental work showed that the collapse of floor systems was consecutive to the failure of at least four adjacent components (Wheat, Gromola & Moody 1986).

Elsewhere, Wheat (1980) reported that the floor assembly retained substantial, potentially higher, strength after the first joist failure, and explained this phenomenon by the bridging effect of the sheathing. Other investigators reported similar behaviours (Bufano 1980; Criswell 1979b; Schaefer 1981; Vanderbilt et al. 1980).

## **2.5 MODELLING OF WOOD JOIST FLOORS**

### **2.5.1 Model for multi-layer composites**

Wood joist floors consist of multi-layer composite sections in which the joists form the centre part – web – and the sheathing(s) correspond(s) to the flange(s). The intensity of the composite action is determined by the properties of the interface(s) between the joists and the sheathing(s), depending on the interlayer properties. In several models, layered T-beam analogues were used to model composite girder of the floor systems (Foschi 1982; McCutcheon 1986; Thompson, Vanderbilt & Goodman 1977). There are therefore number similarities between by layered beams and wood joist floors (T-beams). Because of this common ground/basis, some works on the layered beams have been included in this review.

Theoretical and/or experimental works on layered composites can be traced as far back as the late 1940s. Works from Granholm (1949) and Pleshkov (1952) are often cited in the literature. Granholm (1949) proposed a theory for doubly symmetric cross-sections, which included the effect of interlayer slip, while Pleshkov (1952), generalising Granholm's work, developed a theory for multi-layer systems. The effect of incomplete interaction was also studied by Newmark, Siess and Viest (1951). Elsewhere, a theory proposed by Clark (1954) considered layered systems connected by discrete rigid connections. Interestingly, although these early works were conducted independently, Goodman (1967) demonstrated that they shared similar assumptions.

During the 1960s and 1970s, accounting for the effects of the composite action on the strength and the stiffness, a T-beam model was proposed by Kuenzi and Wilkinson (1971). Teams lead by Goodman (Goodman 1967, 1969; Goodman, Henghold & Rassam 1972; Goodman & Popov 1968; Ko 1972; Rassam & Goodman 1970, 1971), and by Amana (Amana 1967; Amana & Booth 1967, 1968) proposed further analysis procedures. Aiming to obtain a complete analysis of layered beams, Goodman's model was expanded in order to accommodate non-linear connector properties (Tremblay 1974; Tremblay, Goodman & Criswell 1976). Further works on the non-linear aspect of



layered wood beams were also published elsewhere (Henghold 1972; Henghold & Goodman 1972; Kamiya 1985; Ko 1972; Kuo 1974; Schelling 1982; Thompson, Goodman & Vanderbilt 1975; Wheat & Calixto 1994).

The T-beam model by Kuenzi and Wilkinson (1971) was later simplified by McCutcheon (1986), who proposed an approximation that allowed the treating of composite T-beams with a single centroid. Elsewhere, Itani and Brito (1978) expanded the theory of partial composite action to T-beams with discontinuous flanges (gaps in the sheathing) and proposed a close-form approach to estimate mid-span deflections and stresses. McGee and Hoyle (1974) used the contributions of Newmark, Siess and Viest (1951) for deriving design equations for two-layer systems glued with elastomeric adhesive. Expansion of this design procedure to three-layer beams was carried out by Anderson (Anderson 1975).

## **2.5.2 Models for wood joist floors**

### **2.5.2.1 Finite element analysis for floors (FEAFLO and NONFLO)**

In the 1970s, a group of researchers at Colorado State University expanded the theory of layered composite beams to wood joist floors (Goodman et al. 1974b; Vanderbilt, Goodman & Criswell 1974). The various stages of and contributions to the development of this model, Finite Element Analysis for Floors (FEAFLO), have been comprehensively reported and published (Thompson, Goodman & Vanderbilt 1975; Thompson, Vanderbilt & Goodman 1977; Vanderbilt et al. 1973, 1974). FEAFLO was also extensively verified with laboratory data (Ko 1972; Kuo 1974; Liu 1974; Vanderbilt et al. 1974), and, on occasion, expanded (Dawson & Goodman 1976; Vanderbilt et al. 1983; Wheat, Vanderbilt & Goodman 1983).

In FEAFLO, floor assemblies are idealised as series of multi-layered crossing beams, that is, girders and crossbeams, and the partial composite and two-way actions are accounted for. The composite girders consist of T-beams whereby the joist forms the rib and the sheathing the flange. Commonly, the flange is equal to the joist spacing (Liu 1974) but may be reduced in particular situations (Liu 1974; Vanderbilt et al. 1974). The phenomenon of shear lag may deteriorate the accuracy of FEAFLO for floors with relatively short span or wide joist spacing. The crossbeams correspond to strips of sheathing with arbitrary width. Generally, they span across several joists continuously and may have single or multiple layers, depending on the construction of the flooring.

FEAFLO calls upon the large displacement theory and assumes that all materials are linear-elastic. It accounts for the effects of interlayer slip, variable material properties, and sheathing discontinuities (gaps) were included (Thompson, Goodman & Vanderbilt 1975; Thompson, Vanderbilt & Goodman 1977; Vanderbilt et al. 1973, 1974). At the nodes, where the girders and crossbeams intercept, their flexural stiffnesses are summed; thus defining the stiffness of the floor assembly. The model idealisation ignores the contribution of the torsional stiffness of the sheathing and T-beams. Thompson, Goodman and Vanderbilt (1975) proposed that this assumption generated minimal error only because the ratio of the modulus of elasticity to the shear modulus is small. However, Foschi (1982) argued that even though lateral bending deflections and torsional deformations are small, they cannot be neglected because of the joist bridging phenomenon on the floor deflection. In a model developed later by Foschi (1982), those parameters were included. In addition to this, FEAFLO assumption restricts some degrees of freedom and the model may be stiffer than the actual floor structures. In fact, laboratory investigation showed that the experimental deflections were consistently larger than the model predictions (Thompson, Goodman & Vanderbilt 1975).

Further information and results of parametric studies carried out with FEAFLO were reported in theses at the Colorado State University (Antonides 1979; Cunningham 1982; Dawson 1974; DeBonis 1978; Fezio 1976; Jizba 1978; McCormick 1980; Penner 1972; Sazinski 1978), and/or were also published elsewhere (Fezio & Criswell 1976; Goodman et al. 1974a; McCutcheon et al. 1981; Sazinski & Vanderbilt 1979; Schaefer & Vanderbilt 1983; Vanderbilt et al. 1980, 1983; Wheat & Moody 1984).

Later, FEAFLO was expanded in order to account for non-linearity and an analysis procedure was proposed: Non-linear Floor Analysis (NONFLO) (Wheat 1980; Wheat, Vanderbilt & Goodman 1983). NONFLO, which is based on the same mathematical model as FEAFLO, that is, floors are treated as orthogonal networks of T-beams and sheathing crossbeams, aims to accommodate the non-linearity phenomenon that happens in conventional floor systems in which mechanical fasteners are used. Respectively, this parameter was reported to be the main contributor to the non-linearity mechanism (Wheat 1980; Wheat, Vanderbilt & Goodman 1983). It is actually related to the decay of the connector stiffness. To the floor assembly, this infers a loss of composite action and incidentally lower stiffness and strength. On the other hand, minor phenomena such as closed gaps in the sheathing in compression and dominantly linear-

elastic characteristic of the joists may curb the occurrence of non-linearity. In NONFLO, the force-slip relationship of the connection is characterised with a non-linear function proposed by McLain (1975) and later refined by Stone (1980). For the wood members, constant and linear material properties are considered.

NONFLO may be complex and need expensive computation, using an iterative non-linear solution analysis. It can predict the responses of floor assemblies reasonably well under overload and ultimate load, that is, load ranges where non-linear behaviour of the connectors can be expected and has significant effect (Liu & Bulleit 1995). In such situations, NONFLO would predict deflections about 10% higher than those obtained with FEAFLO (Bufano 1980; Bufano, Criswell & Vanderbilt 1980; Criswell 1981; Schaefer 1981; Wheat 1980).

### **2.5.2.2 Floor analysis program (FAP)**

The Floor Analysis Program (FAP), was developed by Foschi (1982). This program combined Fourier series and finite element analysis, and included lateral and torsional joist deformations and plate action in the sheathing. FAP (1982) is rather complex and calls upon the strain energy method. It treats the joist with simple beam theory and assumes that the sheathing is an orthotropic plate with small deflections (Timoshenko & Woinowsky-Krieger 1959). FAP considers gaps in the sheathing that are only perpendicular to the joists and always remain in an open state, that is, the phenomenon of gap closing is ignored. Each joist is expressed in terms of displacements that includes the axial deformations, the vertical and lateral flexures, and the torsional rotations. The behaviour of the connectors is approximated considering lateral deformation (slip) and the discrete pattern of nailing, but nail withdrawal is ignored. In principle, FAP does not consider any non-linearity in the connectors and of the joists or sheathing. However, Foschi (1982) suggested that non-linear fasteners could be accommodated by the model. FAP can also account for lateral reinforcement such as blocking, bridging, etc., assuming that the out-of-plane rotation of the joists is fully restrained. This assumption may lead to overestimating the contribution of the lateral reinforcements significantly. By the principle of virtual work, the system of equations is defined; thus, the governing equations result from the minimisation of the total potential energy in the structure. A semi-analytical approach is followed to solve the equation systems, taking Fourier series

for the functions along the longitudinal direction, and finite element approximations in the perpendicular direction.

### **2.5.2.3 Spring model**

First presented by Zahn (1970) and Sliker (1972) and later refined by McCutcheon (1984), the spring analog is a simple analytical procedure accounting for the interactions of wood joist floors. In this model, the sheathing is simulated as a beam element supported by springs. Because the springs symbolise/simulate the joists, their stiffness is estimated considering the deflection of the joist at mid-span under uniformly distributed load. In order to account for material variability of the joists, the spring stiffness is unequal, that is, presents sound variation (McCutcheon 1984). Sliker (1972) proposed that the rotational resistance of the fasteners should also be considered in the stiffness of the springs.

### **2.5.2.4 Partial composite action (PCA)**

McCutcheon (1986) proposed to estimate the effective moment of inertia by dividing the effective stiffness of the composite by a weighted modulus of elasticity. First proposed in 1977 (McCutcheon 1977), it was later refined (McCutcheon 1986). This procedure, Partial Composite Action (PCA), was developed aiming to offer a solution with moderate complexity to the designers and builders. PCA is based on the T-Beam model (Kuenzi & Wilkinson 1971) and accounts for the effects of partial composite action for the strength and stiffness. The materials are assumed to have linear properties, connectors included, and the interlayer stiffness is much lower than that of the wood members. PCA treats the floor structure as a series of composite T-beams or I-beams in which the axial stiffness (direction parallel to the joists) of the sheathing is modified in order to account for non-linearity caused by interlayer slip and gaps in the sheathing. Expressed in another way, McCutcheon (1986) proposed that accounting for interlayer slip and gaps in the sheathing only requires manipulating the axial stiffness of composite beams. Equation 2-2 presents this manipulation.

Axial stiffness of the flanges:

$$\overline{EA}_{f,n} = \frac{EA_{f,n}}{1 + 10 \frac{EA_{f,n}}{SL_{f,n}^2}} \quad (\text{Eq. 2-2})$$

where  $\overline{EA}_f$  is the transformed axial stiffness of the flange (width of panel acting compositely to the joist) [N],  $EA_f$  is the actual axial stiffness of the flange [N],  $S$  is the interlayer stiffness [N/m<sup>2</sup>], and  $L_f$  is the distance between gaps in the flange [m].

In order to estimate the section properties, the composite girder is treated as a transformed-section, in which McCutcheon (1986) proposed introducing the weighted modulus of elasticity (Equation 2-3a, b and c).

Weighted stiffness for T-beam composite:

$$EI = EI_u + \frac{(\overline{EA}_f)(EA_w)}{EA_f + EA_w} h^2 \quad (\text{Eq. 2-3a})$$

Weighted stiffness for I-beam composite:

$$EI = EI_u + EA_w \bar{y}^2 + \overline{EA}_{f,1} (h_1 - \bar{y})^2 + \overline{EA}_{f,2} (h_2 + \bar{y})^2 \quad (\text{Eq. 2-3b})$$

$$EI = EI_u + EA_w \bar{y}^2 + \overline{EA}_{f,1} (h_1 + \bar{y})^2 + \overline{EA}_{f,2} (h_2 - \bar{y})^2 \quad (\text{Eq. 2-3c})$$

where  $EI$  is the flexural stiffness of the composite [Nm<sup>2</sup>],  $EI_u$  is the flexural stiffness if the joist and flange are fully unconnected [Nm<sup>2</sup>],  $EA_w$  is the axial stiffness of the joist [N],  $h$  is the distance between centroids of the joist and flange [m], and  $\bar{y}$  is the distance of the neutral axis of the composite above (Equation 2-3b) or below (Equation 2-3c) the centroid of the joist.

In the 1990s, Kliger and Pellicane (1997a; 1998) proposed a similar method to PCA. Both models by McCutcheon (1986) and Kliger and Pellicane (1997a; 1998), produce good estimates of the stiffness of the composite beams but lack the same accuracy in predicting the interlayer slips and/or the strains.

### 2.5.2.5 Construction factor method

In order to account for the notable increase of flexural stiffness in glued wood joist floor systems, a construction coefficient was proposed (APA – The Engineered Wood Association 1990; Rose 1970). The value of this construction factor (C-factor), which is later applied upon the flexural stiffness of the composite and the joist in order to obtain that of the floor assembly (Equation 2-4), is determined with experimental data and corresponds to an interpolation between no composite action (C-factor = 0) and complete composite action (C-factor = 1.0). As presented hereafter, Equations 2-4 and 2-5 relate to a deck as a whole system; thus using the sum symbol with the flexural stiffness of the joists. On the other hand, the design procedure with construction factor disregards/ignores any beneficial effect on the strength of floor assemblies.

$$EI_{\text{apparent}} = C EI_{\text{composite}} + (1-C) \sum_{i=1}^n EI_{\text{joist},i} \quad (\text{Eq. 2-4})$$

in which:

$$C = \frac{\text{actual \% increase of stiffness}}{\text{\% increase if fully composite}} = \frac{\frac{EI_{\text{apparent}}}{\sum_{i=1}^n EI_{\text{joist},i}} - 1}{\frac{EI_{\text{composite}}}{\sum_{i=1}^n EI_{\text{joist},i}} - 1} \quad (\text{Eq. 2-5})$$

where  $EI_{\text{apparent}}$  is the apparent flexural stiffness of the deck [ $\text{Nm}^2$ ],  $EI_{\text{composite}}$  is the flexural stiffness of the fully composite deck [ $\text{Nm}^2$ ],  $EI_{\text{joist}}$  is the axial stiffness of the joist [ $\text{Nm}^2$ ].

For floor assemblies constructed with nail-gluing or screw-gluing techniques C-factors of 0.45 and 0.90 are recommended with butt contact and spliced (glued tongue and groove, scarfed, spliced) sheathing respectively (APA – The Engineered Wood Association 1990; Rose 1970). In APA – The Engineered Wood Association's (2005) latest guide for engineered wood construction, precise recommendations are given for the construction of glued floor systems and the benefit of the composite action is integrated into the design span tables. Trus Joist™ (Trus Joist™ a Weyerhaeuser Business 2002a), recommended the same approach with equivalent recommendations.

Stafford (2003a), senior engineer with Trus Joist<sup>TM</sup> noted that a C-factor equal to 0.25 is also acceptable for nailed-only floor assemblies.

## **2.6 RELIABILITY DESIGN FOR WOOD JOIST FLOORS**

When designed using the load and resistance factor design (LRFD), the structures are examined from the perspective of their reliability. This design procedure aims to consider service variables (loading, climate, etc.) with some random patterns in order to determine the lifetime behaviour of the structure. In LRFD, the stiffness and strength of the members of the floor assemblies are modified with factors in order to account for parameters such as interlayer slip, plate action of the sheathing and variability of the mechanical properties of the wood members (Folz & Foschi 1989). The modification factors are calibrated so that full use of the favourable effects associated to complex systems is achieved. However, contrary to some widespread beliefs, reliability-based design does not necessarily lead to more economical wood structures (Foschi, Folz & Yao 1993). In LRFD, the system factors are applied in order to design complex systems with a single bare member procedure without losing the benefits conferred by the whole structure (Philpot, Rosowsky & Fridley 1995). But for Foschi (1984), the assessment of the reliability of light frame systems should rather focus on the entire structural system than on the individual members, and consider the ultimate and service limit states (Foschi 1984).

Applied to complex redundant assemblies such as wood joist floors (conventional and stressed-skin panels), reliability-based design relies on the probability that the weakest joist has a reduced chance of occupying the most critical position in the system, and that the plate action of the sheathing enables load-sharing and a bridging effect. Bulleit and Vacca (1988) proposed that most floor systems would only collapse after the failure of two members. This hypothesis is supported by Criswell (1979a; 1979b).

For wood assemblies, the reliability relies mostly on the behaviour of the components and the load-sharing capability (Foschi 2000). Folz and Foschi (1989) carried out a parametric study that included 14 parameters and performed a sensitivity analysis of the system modification factor. It exposed that the latter was quasi insensitive to the support conditions, size of the joists, ratio of dead to live load, but was sensitive to variations of the remaining parameters such as the stiffness of the joists and sheathing, the variability of the joists, the gaps in the sheathing, etc. Further, Folz and

Foschi also reported that the strength of the members of floor systems could be increased by some 15%. Elsewhere, Bulleit and Vacca (1989) proposed that the reliability analysis of wood joist floors should consider three aspects: (1) the structural model must include composite and two-way actions, (2) the loading must consider duration effect and random regimes, and (3) the redundancy of the floor system must be accounted for.

Considering the ultimate limit state, scenarios of overload (Bulleit & Vacca 1989) and failure of the structure are accounted for. For system failure, the reliability of the floor structure may be set at different levels. The system reliability can be governed by the less reliable individual members (Foschi 2000) or to the failure of any members of the system (Bulleit 1985; Folz & Foschi 1989; Foschi 1982, 1984, 2000). Elsewhere, several investigators proposed that the system failure occurs when two adjacent members fail (Bulleit 1987; Criswell 1979b; Philpot, Rosowsky & Fridley 1995), that is, occurring of progressive failure (Foschi 2000). While the first failure mechanism is arguable because it neglects the load redistribution (Rosowsky & Ellingwood 1990, 1991), investigations into the behaviours of wood joist floors (Criswell 1979b; Vanderbilt, Goodman & Criswell 1974) and stud wall frames (Polensek 1976) indicated that the second failure mechanism represents/qualifies the ultimate resistance of both structures well. This indicates that the load is redistributed to the population of undamaged floor members. With rather flexible sheathing, as used commonly, Rosowsky and Ellingwood (1990; 1991) proposed that the load is transferred to the adjacent members only or to all undamaged members in a linear degressive manner (starting from the failed member). Elsewhere, a linear degressive redistribution was also proposed (Cramer & Wolfe 1989).

In addition to failure considerations, time-dependent loads – static, cyclic and/or stochastic loading patterns – should also be accounted for in LRFD. Under long-term loading regimes, a structure could fail after some time, because the long-term strength of structural timber and wood-based materials is lower than the short-term strength (Bulleit & Liu 1995). Respectively cumulative damages could be inflicted to a structure by repetitive loads and eventually cause its failure (Bulleit & Liu 1995; Foschi 1984, 2000; Foschi, Folz & Yao 1989, 1993; Rosowsky & Ellingwood 1990, 1991; Yao 1987). Under lifetime service loadings, Philpot and Rosowsky (1996) proposed that most floor assemblies might experience gradual failure caused by load duration.



Therefore, the reliability analysis of wood structures must consider the effect of load duration in order to avoid overestimating the reliability of floor systems.

In Chapter 3 in Part 1, a specific review of the concept and development of wood joist floors will be presented. This will help to position SSP constructions within the family of lightweight floors. Chapter 3 also presents the advantages/benefits that constructing with SSP systems bring.

<b>3</b>	<b>WOOD JOIST FLOOR SYSTEMS .....</b>	<b>40</b>
<b>3.1</b>	<b>Conventional wood joist floor technology.....</b>	<b>40</b>
<b>3.2</b>	<b>Stressed-skin panel technology .....</b>	<b>42</b>
<b>3.3</b>	<b>Floor structure as horizontal diaphragm.....</b>	<b>46</b>
<b>3.4</b>	<b>Comparing conventional wood joist floor and SSP technologies .....</b>	<b>47</b>
3.4.1	Construction and architectural aspects.....	47
3.4.2	Design and structural aspects.....	49

## 3 WOOD JOIST FLOOR SYSTEMS

Wood products now available on the market enable strong and reliable floor structures whereby the lightness is preserved. In addition, new-generation adhesives facilitate short processing times (particularly curing time) and high bonding strength. Associating both aspects together in stressed-skin panels (SSP) produces composite structures with enhanced performance, reliability, lightweight and dimensional stability. Thus, this can generate new opportunities for the use of wood in multi-storey residential, industrial, commercial and public buildings. In addition, floor systems built with SSP technology, on-site or prefabricated, can work as diaphragms and thus can provide excellent horizontal bracing to the construction. Other benefits of SSP include prefabrication suitability and architectural aspects.

The purpose of this chapter is to present a state-of-the-art of wood joist floor systems and to position stressed-skin panels (SSP) within the family of lightweight floors. This chapter starts with the concepts of conventional floors and stressed-skin panels (SSP). Afterwards, the requirements for the diaphragm are discussed, before the chapter finishes with an analytical comparison between the two techniques.

### 3.1 CONVENTIONAL WOOD JOIST FLOOR TECHNOLOGY

A summary description from Boyd (1964) proposed that conventional deck constructions invariably comprise two to three integrated, horizontally arranged layers (in top-down order): 1) the flooring (boards or sheets), 2) the joists at about 450-mm centre, 3) the ceiling (boards or sheets). The joists and the panels are connected with mechanical fasteners at nominal – about 300 mm – spacing. Such connections have low

stiffness and limited shear strength. Consequently, slip occurs between the joists and the panels, and the contribution of the superimposed layers to resisting loads is limited (McCutcheon 1977) and the simple beam theory (SBT) cannot be applied (Amana & Booth 1967). After Amana & Booth (1967), the concept of a contribution from the sheathing should not be considered when interlayer slip is not impeded. In any case, the occurrence of interlayer slip prevents using the material strength properties of the panels efficiently.

From a design point of view, it is very common to assume that each structural member acts without interaction, that is, the joists and superimposed panels do not act compositely and the two-way action is ignored (McCutcheon 1977, 1986). Each floor member acting independently, it is confined to the distinct role for which it is specifically designed. For example, the sheathing transfers the load to the nearest joists, and the joists act independently in bridging the span (McCutcheon et al. 1979; Schaefer & Vanderbilt 1983; Sherwood & Moody 1989; Vanderbilt et al. 1974) and the joists only carry the load **within their tributary area** (Criswell 1981; Tucker & Fridley 1999).

In the 1950s, this **piece-by-piece assumption** or **bare joist** was assessed as “sound” (Russel 1954) and justified because of the **lack of reliable method for structural analysis**. It was still identified as being adequate some 20 years later (Onysko 1970). However, the legitimacy of this practice had also been questioned (Goodman & Gutkowski 1979; Moody & McCutcheon 1984; Schaefer & Vanderbilt 1983; Vanderbilt, Goodman & Criswell 1974). It was identified as being very conservative (Dawson & Goodman 1976; McCutcheon et al. 1981; Williston & Abner 1962) or as being a grossly simplified assumption (Criswell 1983; Goodman et al. 1974a; Goodman et al. 1974b; Vanderbilt, Goodman & Criswell 1974; Vanderbilt et al. 1974), because it neglected that interactions occur between the joists and the sheathing (McCutcheon 1977). Although recognising the limitation imposed by interlayer slip, Möhler (1963) proposed that with nailed connections some composite actions can be achieved, provided that the joist spacing does not exceed the tributary capacity<sup>a)</sup> (USDA report 1957, in Möhler 1963). Foschi (1982) claimed that disregarding any composite action and assuming that the joists carry the load entirely is too simplistic and is only justified when the nailing is minimal and the sheathing stiffness is negligible in comparison with that of the joists.

---

<sup>a)</sup> later defined as the basic spacing (Desler 2002).

Current/normal practice for joist floor design, which is inherent in many codes, still ignores any interaction between the structural wood members (British Standard 2004; Société Suisse des Ingénieurs et Architectes 2003). Other codes or practices account for the floor acting as a unit of repetitive parallel members, especially the bridging effect of the sheathing, that is, some load is moved away from the weak members. Therefore, the strength of the sawn/solid wood joists may be increased up to 24% in Australia (Australian Standard<sup>TM</sup> 1997) or 15% in the USA (American Forest & Paper Association 1997, 2004; American Institute of Timber Construction 2005), depending on the geometry and construction of the floor. With engineered wood products (Laminated Veneer Lumber (LVL), I-joist, etc.), whose mechanical properties show reduced variability – lower coefficient of variation (CV), inferior sharing strength coefficients are recommended (American Forest & Paper Association 1996). This factor can only be applied for uniformly distributed loadings; there is no factor available for concentrated point load situations. Therefore, as such these codes and practices do not consider that the panels contribute to the structural performances of the joists. Also to date, design of the members of floor assemblies can be carried out using readily available aids (American Forest & Paper Association 1997, 2004; State Forest N.S.W. 1994).

### **3.2 STRESSED-SKIN PANEL TECHNOLOGY**

Panels longitudinally and/or orthogonally reinforced with stiffeners/ribs combine lightweight with high strength. The versatility of this technology is recognised in many fields. For example, this technology was considered for ship construction (Pietzker 1914; Schade 1940, 1951; Schnadel 1924), in aeronautics (Blumrich 1942; Borsari & Yu 1948; Thielemann 1950; Winter 1940), vehicles, that is, cars, trucks, trains, etc., furniture (Kotas 1956) and civil engineering. Interestingly, some of these early research projects were related to wood because plywood was also used in fields other than building. With regard to buildings, it was in the 1940s that, because of the shortage of building materials during World War 2, a design method was developed for wood floors (Baird & Ozelton 1984). Other composites, that is, assemblies combining steel beams and superimposed concrete slabs were also developed (Newmark, Siess & Viest 1951; Sabnis & Rao 1979; Salmon & Fisher 1979) to become common applications in structural engineering today.

From the perspective of lightweight construction, floor structures where the superimposed structural panels (skins) are glued to the joists, that is, the skin(s) and the joists are firmly bonded with structural adhesives (Carradine, Woeste & Kent 2001), form a composite unit (Ozelton & Baird 2002) called a stressed-skin panel (SSP) (Moody, Hernandez & Liu 1999). Elsewhere, a more restrictive description proposed that SSP should meet four conditions (Timber Engineering Company): (1) sheathing must be glued on both sides of the joists, (2) sheathing and joists must be continuous or adequately spliced, (3) headers are required with thin, deep framing members, and (4) any clear distance between the joist must not exceed twice the basic spacing. The latter aspect relates to a design method from North America (APA – The Engineered Wood Association 1990; Desler 2002; McLain 1999) and is presented elsewhere in Chapter 4 in Part 1.

The structural performances of SSP decks depend upon the composite action (Plywood Association of Australia LTD 1998), whose efficiency relies on the strength of connection between the joists and the panel(s) (Carradine, Woeste & Kent 2001). In an SSP system, the shear strength of the adhesive should be greater than that of the wood substrate (Timber Research and Development Association), that is, the wood members should govern the strength of the connections. On many occasions, the interlayers are built combining mechanical fasteners and adhesives, that is, techniques described as nail-gluing or screw-gluing (Gerber 2003; Jung 2002; Kairi 2001; Kairi et al. 1999). Carradine et al. (2001) postulated that, with these hybrid techniques, damaged SSP structures may retain sufficient strength to carry a large percentage of the design load in the case of bond failure. Finally, making use of adhesive in the connection affects the comfort of service of SSP decks by reducing squeaking (Collins 2001; McLain 1999) and nail popping (McLain 1999). The nail-gluing technique was implemented to built the full-scale specimens of the subject research (refer to Chapter 3 in Part 2).

In order to minimise the risk of bond failure, structural adhesives, such as those defined in AS/NZS 4364:1996 (Australian/New Zealand Standard<sup>TM</sup> 1996), must be favoured. Adhesives that meet the directives of that code will have known and reliable/tested properties. Therefore, they comply with the short and long term requirements of SSP composites because they are capable of generating bonds with strong shear resistance and high rigidity. Raadschelders and Blass (1995) proposed that gluing results in skin-to-joist connections of infinite stiffness. As a result of this, a linear

strain distribution may be assumed over the depth of SSP (Raadschelders & Blass 1995) and SBT can be applied (Amana & Booth 1967).

Because of the high stiffness property of the interlayers, the joists and the sheathing(s) of SSP composites work together efficiently and function as open (T-beam) or box sections (McLain 1999). Amana and Booth (1967) proposed that SSP behaves as interlinked parallel T- or I-beams, and Möhler et al. (1963) assumed that the joists and the portions of skin(s) that act compositely with them correspond to fictive composite beams. Desler (2002) described SSP elements as series of built-up T- or I-beams, in which the panel(s) or skin(s) take the greatest portion of the bending stress and the joists take shear stress. The fact that in SSP the skin(s) – flange(s) – provide(s) the bending moment resistance and the joists – webs – resist shear forces is also accepted by others (APA – The Engineered Wood Association 1990; McLain 1999; Moody, Hernandez & Liu 1999). Figure 3–1 depicts typical SSP elements; open-section (one-sided or T-section SSP systems), box-section (two-sided SSP systems) and T-flange SSP systems respectively. T-flange SSP construction is a variation of open-section SSP system wherein the lower edges of the joists are reinforced with narrow flanges, for example, strips of Laminated Veneer Lumber (LVL) (Desler 2002; McLain 1999).

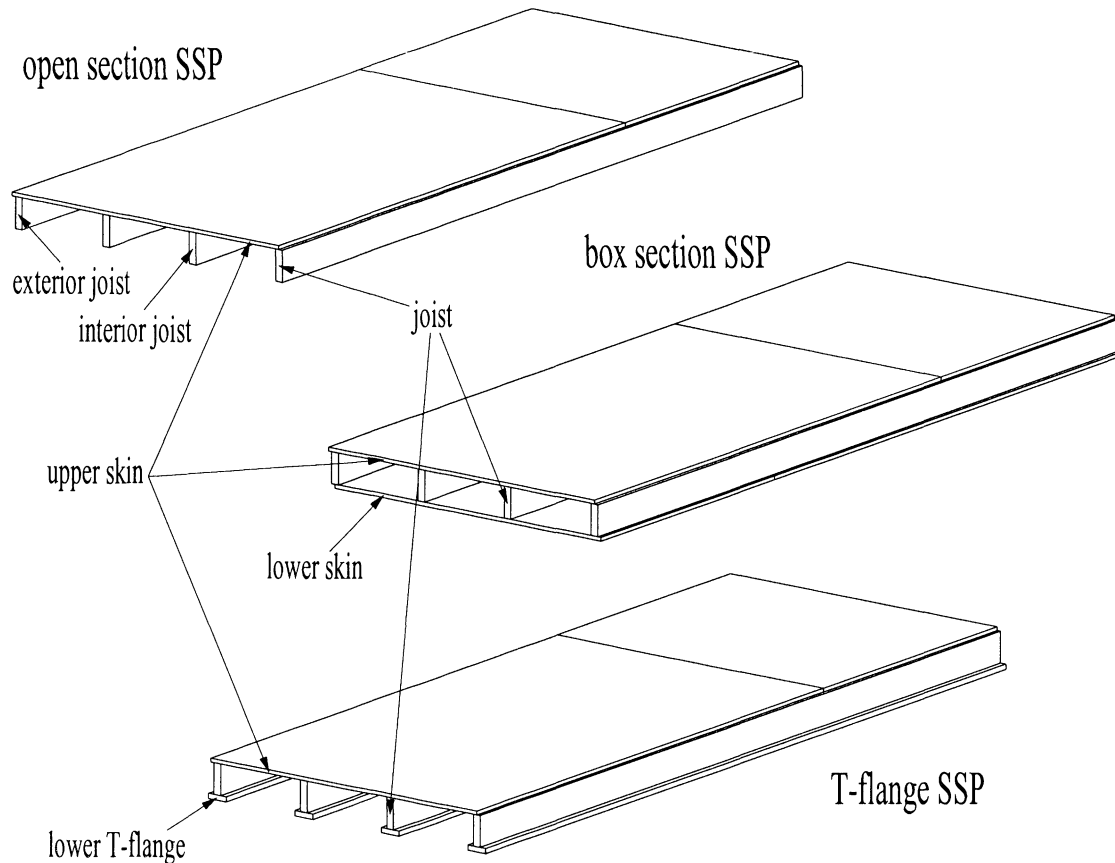


**Figure 3–1: Typical SSP floor constructions**

To generate skin continuity, splicing of the panels between the stringers may be desirable. For economic reasons, splice plates are preferred to finger and scarf joints (McLain 1999). Generally, the splice plates are made with the same material as that of the skin and orientated to the skin concordantly. In the subject research, splicing with plates has been implemented; therefore, hereafter splicing indicates this system exclusively (refer to Chapters 2 and 3 in Part 2). With today's technology, panel suppliers are able to produce engineered wood panels of “unlimited” length and increased width; restrictions being, however, imposed by transport regulations. For SSP, it signifies that large elements can be built without splicing (Merz 1996); thus reducing the manufacturing cost.

Most of the early researches were focused on plywood skin, but after oriented strand board (OSB) gained more popularity, studies investigating the performance of SSP with OSB skins were carried out (Bach & Cheng 1990; Bach, Wong & Cheng 1988; Thomas 2000a, 2000b). Bach and Cheng (1990) reported that the predictions estimated with conventional design agree fairly well with the experimental values of SSP specimens. Elsewhere, Kliger's research (1993; 1995) focused on chipboard



materials for the compression skin(s). Interestingly, Kliger (1997a) also investigated SSP built with a concrete slab on the compression side and steel sheet on the tensile side.

Today, because of innovations in areas such as wood materials, adhesives, analytical tools and constructions methods, SSP composites have improved in efficiency and reliability and allow constructing a wide variety of wood “only” systems (Gerber & Sigrist 2002) or combining wood products with non-wood materials, but connections may prove problematic (Kliger 1993, 1995; Kliger & Pellicane 1997a). Using various types of materials in composites does not only aim to increase the structural performance but to enhance other aspects of the structures, such as the fire resistance, the sound insulation, vibration response, etc. (Kliger 1993; Kliger & Pellicane 1997a).

### **3.3 FLOOR STRUCTURE AS HORIZONTAL DIAPHRAGM**

Wood joist floor can be used as a horizontal diaphragm (Alsmarker 1995; Moody & McCutcheon 1984). This type of solicitation on floor structures is very different from those “commonly” applied. Diaphragms are out of the scope of the subject research. Hereafter, the author present some fundamentals without details on design. That aspect and further details can be found in the literature (Alsmarker 1995; European Committee for Standardisation 1995).

Under the diaphragm approach, the floor assemblies are solicited by in-plane forces, and are assumed to behave similarly to deep I-beams (Alsmarker 1995). For Alsmarker (1995), the sheathing acts as the web and resists shear forces, while the joists act as flanges and resist flexural moments. Therefore, the connections between the sheathing and the joists must be shear resistant, so that the assembly forms a unit. Thus, this solicitation in the interlayer must be accounted for in conjunction to the shear stress induced by the flexural moment of the floor system under load normal to its plane. This mechanism of superposition should be accounted for in designing SSP structures. Furthermore, the floor elements have to be strongly attached to the bearing walls or bracing structure with the connectors designed to resist and transfer the horizontal forces. In prefabricated floor systems, the shear forces must also be transferred between the elements. Breyer et al. (2003) proposed examples for the constructions of these connections.

The design of diaphragms is as complex as that of floor systems, that is, diaphragms are designed as composite structures consisting of several layers connected by means of connectors that resist shear. The efficiency of diaphragm elements relies on the loss of stiffness inferred by interlayer slip and sheathing discontinuities. Thus, thorough design analysis relies on a set of differential equations. However, as for floor constructions, system factors can be implemented in order to simplify the design procedure and make it more accessible to designers. Studies on and analysis of the composite action in diaphragms were published by several researchers (Hiremath 1979; Itani & Hiremath 1980; Itani, Morshed & Hoyle 1981), while works on diaphragms respectively on light-frame walls were also published elsewhere (Criswell 1983; Foschi 1977; McCutcheon 1985; Polensek 1976; Tuomi & McCutcheon 1978; Yu 2003). Design guidelines are also available in the literature (American Institute of Timber Construction 2005; Breyer et al. 2003; Diekmann 1999; Ozelton & Baird 2002; Skaggs & Martin 2002).

### **3.4 COMPARING CONVENTIONAL WOOD JOIST FLOOR AND SSP TECHNOLOGIES**

#### **3.4.1 Construction and architectural aspects**

With the implementation of SSP systems, substantial savings can be achieved in comparison to conventional floors. This is rendered possible because SSP systems consume less material, that is, use of optimised member dimensions, weigh less and have higher quality (Nokelainen 2000). SSP constructions also allow various degrees of prefabrication, which leads to less on-site work (Gerber & Sigrist 2002; Kilpeläinen & Ukonmaanaho 2001; Sigrist & Gerber 1999, 2002; Sigrist et al. 2000); indirectly reducing spending for the rolling interest of the home loan. Furthermore, SSP elements provide a ready-to-use platform for the subsequent stages of the building construction. Prefabricated systems offer additional benefits such as a quicker and easier design for the building framework and the elements (Kilpeläinen & Ukonmaanaho 2001). As for manufacturing, assembling the SSP elements in workshop conditions enables enhancing the reliability and quality of the products and a system of quality control can be implemented with ease. In addition to this, using seasoned wood materials to build SSP systems enhances the dimensional stability of the structure (Mårtensson 2003); thus

undesirable effects caused by drying of the floor components, that is, shrinkage, deformation, cracking, etc. are avoided.

From architectural perspectives, SSP decks offer structures with shallower depths and/or that are capable of bridging longer spans than conventional floor constructions. In multi-storey buildings, this allows increasing the flexibility of the layout arrangement/reshaping of the storeys, and in some renovation cases to optimise the use of the volume of the existing building (Falk, Engström & Samuelsson 2001). SSP systems also permit quality finish – visual aspect – of the ceiling and/or flooring (depending on the material elected for the respective sheathing).

The interfaces between the joists and the sheathing(s) can contribute to generating noise in a floor. In SSP, by using adhesives squeaking can be reduced (Collins 2001; McLain 1999). In addition to this, nail popping can be avoided (McLain 1999). Consequently, the comfort of the users – at least the perception by them – and hence the serviceability of the floor are improved. On the other hand, because SSP decks are lightweight structures with the capability of bridging long spans, undesirable floor vibrations may be generated and cause discomfort for the users. Furthermore, full composite action as in SSP may increase the natural frequency of the decks and reduce the damping capacity of the deck (Wolfe 1990). In any case, damping in floors is very complex and depends only partly on the materials and construction details of the floor (Hu 2002), that is, elastic skin-to-joist connections help in decaying the energy. However, vibration problems in SSP may be avoided by proper concept and design.

In Table 3–1, the comparison of the construction and architectural aspects is presented and rated. The first section summarises the constructions parameters. The second part focuses on the architectural aspects. Finally, some general parameters are presented.

**Table 3–1: Comparison of the construction and architectural characteristics of wood floor systems**

SSP parameter		Conventional floor system	Stressed-skin panel (SSP)
Construction parameters	Prefabrication	Very low	*High
	On-site work & erection time	High	Low
	†Material saving	No	Yes
Architectural parameters	Floor depth/gauge	High	Low
	Span & free volume	Low	High
	Layout flexibility	Low	High
General parameters	‡Economy potential	Low	High
	§Structure reliability	Medium	High
	Quality control	Low/medium	High
	**Dimensional stability	Low/medium	High
	User “comfort”/serviceability	Low/medium	High
	††Experience of vibration by the users	Low	High

\* multiple levels of prefabrication (Kilpeläinen & Ukonmaanaho 2001), † optimised member sizes, that is, mainly joist dimensions, ‡ aspects of saving: running loan interest, material (floor & walls), optimised volume use, § implementation of fully tested floor system and engineered wood products (Plywood Association of Australia LTD 1998), \*\* use of seasoned wood materials, †† subjective perception of floor vibrations.

### 3.4.2 Design and structural aspects

The quality of the connection between the joist and the skin differentiates conventional floors and SSP systems. As a result, conventional structures have none to few composite properties, while SSPs work as full composites. This major difference affects the structural performances of the floor systems; the bending capacity and stiffness of SSP exceed the values of conventional structures. Corder and Jordan (1975) reported that SSP structures experience a large increase of stiffness in comparison to conventional floor systems. Further, in SSP, shear transfer between the joists and the sheathing is improved (Liu & Bulleit 1995). The Canadian Wood Council (2005) suggested that floor structures built conventionally or with an SSP technique achieve the same

performances, span from five to seven metres, but with higher span-to-depth ratios for SSP structures. It is expected that structures built with I-joists for the stringers, like the full-scale specimens of the subject research, can span further and compete with floors constructed with I-joists in a conventional manner, which can bridge distances from six to ten metres (Boughton & Crews 1998; Canadian Wood Council 2005). The American Institute of Timber Construction (2005) indicated economical span ranges for a series of wood structures; for sawn solid joists, 6–20 ft (1.8–6.1 m); for I-joist 12–30 ft (3.7–9.1 m); and for SSP with solid joists, 10–24 ft (3–7.3 m). Once again, it is reasonable to assume that SSP decks built with I-joists can economically compete with conventional I-joist floors and that their economical span range can to some extent be expanded. Because of the performances achieved by SSP composites, this type of structure offers attractive and reliable solutions in modern construction in Europe and North America, where it is becoming increasingly popular (Kliger & Pellicane 1997b).

Being built with mechanical fasteners only, the skin-to-joist connection of conventional structures has low stiffness and high slip; whereas in SSP the adhesive gives high stiffness to the connection and inhibits slip. Goodman and Popov (1968) and Goodman and Gutkowski (1979) proposed that assuming a high rigidity in glued interconnections is legitimate but affirmed that such assumption is improper for mechanical assemblies or when elastomeric adhesives are used.

The occurrence or the absence of slip in the interconnection affects the performances of a composite structure immensely. Interlayer slip increases the complexity of the behaviour of wood composites and requires a thorough analysis. The simple beam theory (SBT) cannot be applied (Amana & Booth 1967). Because of the slip impediment in SSP, the members of the assembly work efficiently together; thus, optimum uses of the material properties of all structural members is achieved. In addition to this, the strain distribution over the depth of the cross-section is linear. Thus, fundamental static principles such as SBT (Amana & Booth 1967) and the transformed-section (Gere & Timoshenko 1999) can be applied.

Figures 3–2 and 3–3 demonstrate the effect that slip in the connections of a three-member composite has on the strain and stress distribution over the depth of the section. In this three-member model, every member has different material properties. Therefore the relationship between the modulus of elasticity is as follows:

- $E_1 < E_2$  and  $E_3 < E_2$ .

CASE I: free slip in the connections (conventional floor), thus assuming non-linear strain distribution along the depth of the floor section (Amana & Booth 1967).

CASE I: free slip in the interlayers

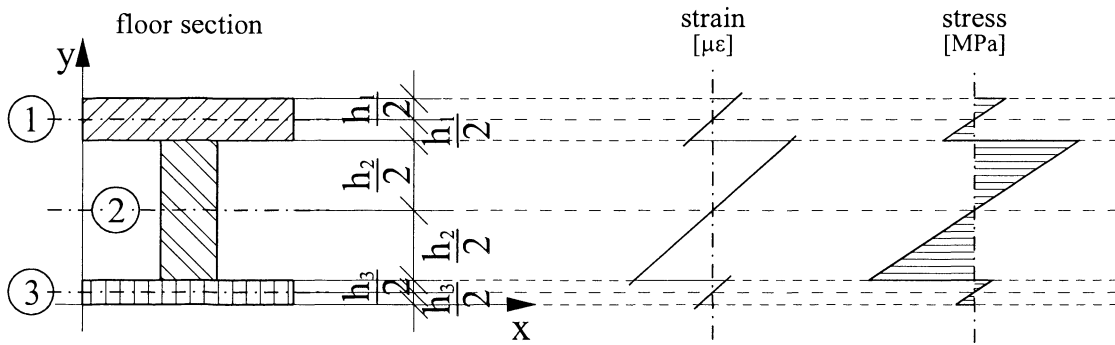
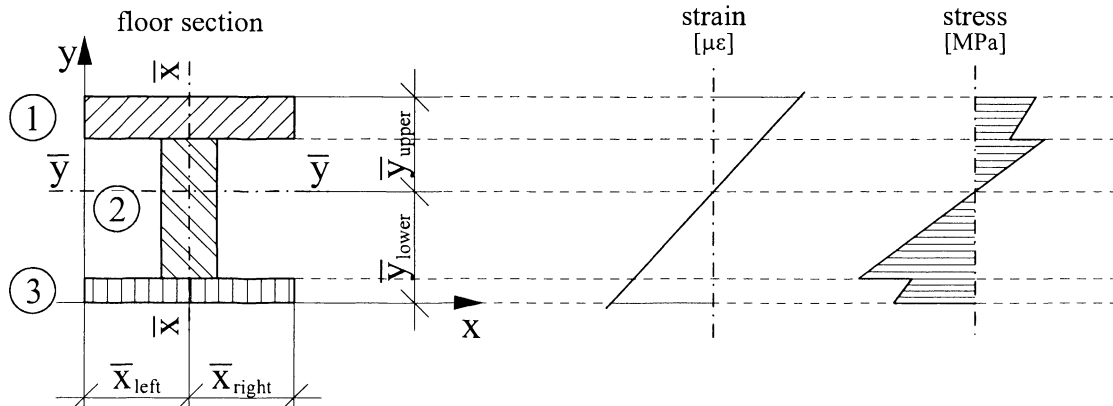


Figure 3–2: Strain and stress distribution across the floor section – free slip in the interlayers

CASE II: impeded slip in the connections (stressed-skin panel), thus assuming a linear strain distribution along the depth of the floor section (Amana & Booth 1967; Raadschelders & Blass 1995).

CASE II: no slip in the interlayers



**Figure 3–3: Strain and stress distribution across the floor section – no slip in the interlayers**

To estimate the section properties of cross-sections built with mechanical fasteners (Figure 3–2), guidelines are presented, for example, in Blass et al. (2004), in BS EN 1995-1-1:2004 (British Standard 2004) and in “Kommentar DIN 1052 (DIN Deutsches Institut für Normung e. V. 1988) Teil 1”. (Beuth-Kommentar 1989). For case II (Figure 3–3), because of the impediment of slip and the linearly elastic property of wood materials, the transformed-section method is applicable. This method is well-known and described in numerous literature, for example, Beer and Johnston (1992), Gere (2004), and Gere and Timoshenko (1999). This method has been also applied in the subject research to estimate the section properties of the specimens.

The nature of the skin-to-joist connections of SSP composites allows structural constructions of high efficiency (Moody, Hernandez & Liu 1999) and significant increase of stiffness and bearing capacity compared to conventional floors. SSPs are versatile systems in which a wide range of wood and non-wood products can be associated (Gerber & Sigrist 2002; Klinger 1993, 1995). The material properties of SSP components affect the performances of the structures. Therefore, to meet the specific requirements of a building, materials must be selected accordingly. Gerber and Sigrist (2002) proposed different material mixes for floors in family homes and for multi-storey, industrial, commercial, office and/or public buildings. Implementing stress-graded and seasoned solid wood materials and/or engineered wood products gives floor

structures highly reliable structural characteristics; thus SSPs have the reliability of fully engineered systems (Gerber, Crews & Sigrist 2004a, 2004b, 2005b; Plywood Association of Australia LTD 1998).

In contrast to floors built using conventional techniques, floors built with SSP elements can work as very effective diaphragms and provide an excellent horizontal bracing to the construction (Alsmarker 1995; Gerber, Crews & Sigrist 2004a, 2004b, 2005b; Merz 1996; Moody & McCutcheon 1984). To achieve this, the connections between the SSP elements and the connections of the floor to the bearing walls must resist shear. Breyer (1993) and Breyer et al. (2003) proposed guidelines and details for the construction of diaphragm-to-shear wall anchorages. In addition, in SSP decks working as diaphragms, the skin-to-joist connections must resist the result of shear stresses induced by an appropriate combination of loads perpendicular to the SSP surface (shear forces due to gravity load) and in the plane of the skin(s) (shear forces caused by horizontal load).



Table 3–2 summarises the major design differences between conventional floors and SSPs and the successive structural consequences; first the distinct construction parameters, second the effects of them on the structural performances.

**Table 3–2: Comparison of the design characteristics of wood floor systems**

		Conventional floor system CASE I (Figure 3–2)	Stressed-skin panel (SSP) CASE II (Figure 3–3)
Construction parameters	Skin-to-joist connection	*Nominal	†Structural
	Composite action in floor structure	Low	High
Structural responses	Strain distribution in floor cross-section	Non-linear	‡Linear
	Stress distribution in floor structure	Low	High
	Ultimate resistance of floor structure	Low	High
	Stiffness of floor structure	Low	High
	Torsional rigidity of floor structure	Low	§High
	**Diaphragm	No	Yes

\*occurrence of interlayer slip, †impediment of interlayer slip, ‡compatibility with SBT conditions (Amana & Booth 1967), §enhanced load/stress distribution in floor structure, \*\*floor structure capable of resisting in plane – horizontal – loads.

In order to maximise the advantages/benefits of SSP systems, a thorough and reliable design method must be applied. Around the world, several design procedures are available. Aspects of these design procedures are now comprehensively reviewed in Chapter 4 in Part 1.

<b>4</b>	<b>STRESSED-SKIN PANEL PROPERTIES AND DESIGN</b> .....	<b>56</b>
<b>4.1</b>	<b>Section properties of SSP</b> .....	<b>57</b>
<b>4.2</b>	<b>Theory of the tributary width of the skin(s)</b> .....	<b>61</b>
4.2.1	Stress distribution in SSP skin(s).....	61
4.2.2	Estimating the tributary width of the skin(s) .....	64
4.2.3	Codified approaches for approximating the tributary width of the skin(s).....	66
4.2.3.1	Australia – AS 1720.1–1997.....	67
4.2.3.2	Europe – EC5.....	68
4.2.3.3	Switzerland – SIA 164.....	70
4.2.3.4	USA – the APA method.....	73
4.2.4	Effectiveness ratios of the panel contribution.....	82
4.2.5	Concluding summary on the tributary width .....	87
<b>4.3</b>	<b>Capacity under gravity load</b> .....	<b>89</b>
<b>4.4</b>	<b>Splicing requirements</b> .....	<b>92</b>
<b>4.5</b>	<b>Verification of buckling capacity</b> .....	<b>94</b>
<b>4.6</b>	<b>Verification of the serviceability – deflection</b> .....	<b>96</b>
<b>4.7</b>	<b>Verification of the serviceability – vibration</b> .....	<b>100</b>

## 4 STRESSED-SKIN PANEL PROPERTIES AND DESIGN

Estimating the section properties of stressed-skin panels (SSP), on which the strength and serviceability of the floor system depend, forms an important aspect of the design. In SSP sections, the joists are the centre members – webs – with which the skins or portions of them – flanges – act compositely. The shape of the composite section about each joist agrees with those of SSP construction, that is, one- or two-sided, and with the location of the joist, that is, interior or exterior. Thus, composite sections such as L- and T-beams are identifiable in open-section SSP systems, while box-section SSP construction can be broken down into C- and I-beams. In each one of these composite beams, the magnitude of the tributary width and the strength and slip modulus of the interlayers affect the properties of SSP sections. The first one corresponds to the effective contribution of the sheathing – in this situation also denominated skin – and the second one determines the efficiency of the composite action, which is also determined the strain distribution over the depth of the section.

In this chapter, the aspects relevant to the properties of SSP sections are presented and discussed. The chapter starts with presenting a method for estimating the section properties. It discusses the aspect of the tributary width with regard to the stress distribution in the sheathing and the magnitude of the contribution of the panel. Several procedures for estimating the tributary width are studied and an analysis on the effectiveness of each estimate is presented. Finally, this chapter also summarily reviews aspects that are important for the design of SSP systems.

## 4.1 SECTION PROPERTIES OF SSP SYSTEMS

The section properties of the SSP structure are needed to determine its strength and serviceability limit states. The estimate of these section properties refers to theories that have been developed for multi-layer composites built up with members exhibiting different mechanical properties and having an asymmetrical shape. It is performed considering the mechanical properties, especially the moduli of elasticity, of the section members and the characteristics of the interlayers.

Structural timber and wood-based materials are assumed to exhibit linear-elastic behaviour under the range of working or serviceability loads. Such an assumption is sound for wood materials. Elsewhere, Criswell (1979b) even suggested that a linear-elastic behaviour could reasonably be assumed until failure, even though it may not be correct. Furthermore, by using structural adhesive in the connections, the interlayers have stiff slip modulus, that is, slip impediment can be assumed. Therefore, SSP systems have full-composite action. Thus, it can be anticipated that the strain distribution over the depth of the section is linear (Amana 1967; Amana & Booth 1967, 1968) and that the composite assembly satisfies the conditions of the transformed-section method (Gere & Timoshenko 1999). In this method, the neutral axis is determined with Equations 4-1 and 4-2; in the latter the modular ratios (Equation 4-3) have been introduced. The modular ratios express the relationship between the moduli of elasticity of the wood members.

$$E_1 \int y_1 dA_1 + E_2 \int y_2 dA_2 + \dots + E_n \int y_n dA_n = 0 \quad (\text{Eq. 4-1})$$

where: E: modulus of elasticity of a section component [MPa]  
 y: y-axis (vertical) distance [mm]  
 A: area of a section component [mm<sup>2</sup>]

*NOTE: the "initial" location of the y-axis is set arbitrarily inside the cross-section. For the convenience of the calculation, it is, however, recommended to locate this axis at the lower extreme fibre of the composite section.*

$$\int y_1 dA_1 + n_2 \int y_2 dA_2 + \dots + n_n \int y_n dA_n = 0 \quad (\text{Eq. 4-2})$$

where:  $n$ : modular ratio [--]

$$n_1 = \frac{E_1}{E_1} = 1 ; n_2 = \frac{E_2}{E_1} ; \dots ; n_n = \frac{E_n}{E_1} \quad (\text{Eq. 4-3})$$

In Gere and Timoshenko (1999) and Schneider (1994), an alternate procedure to estimate the neutral axis and moment of inertia for plane areas is depicted. Equation 4-4 depicts the estimate of the neutral axis of the composite sections. In replicating the approach of the transformed-section method to this procedure, the modular ratios can be introduced in Equation 4-4 in order to derive Equation 4-5.

The neutral axis of a composite section ( $\bar{y}$ ):

$$\bar{y} = \frac{E_1 \int y_1 dA_1 + E_2 \int y_2 dA_2 + \dots + E_n \int y_n dA_n}{E_1 \int dA_1 + E_2 \int dA_2 + \dots + E_n \int dA_n} \quad (\text{Eq. 4-4})$$

$$\bar{y} = \frac{\int y_1 dA_1 + n_2 \int y_2 dA_2 + \dots + n_n \int y_n dA_n}{\int dA_1 + n_2 \int dA_2 + \dots + n_n \int dA_n} \quad (\text{Eq. 4-5})$$

In order to illustrate the previous equations, Figure 4-1 depicts a composite I-section and the locations of the neutral axes. The shape of this section is symmetric about the  $\bar{x}$ -axis but asymmetric about the  $\bar{y}$ -axis, and it has wood members with different materials properties – characterised by the stripe patterns in Figure 4-1.  $\bar{x}$  may be estimated with Equations 4-4 and 4-5, after some arrangements.

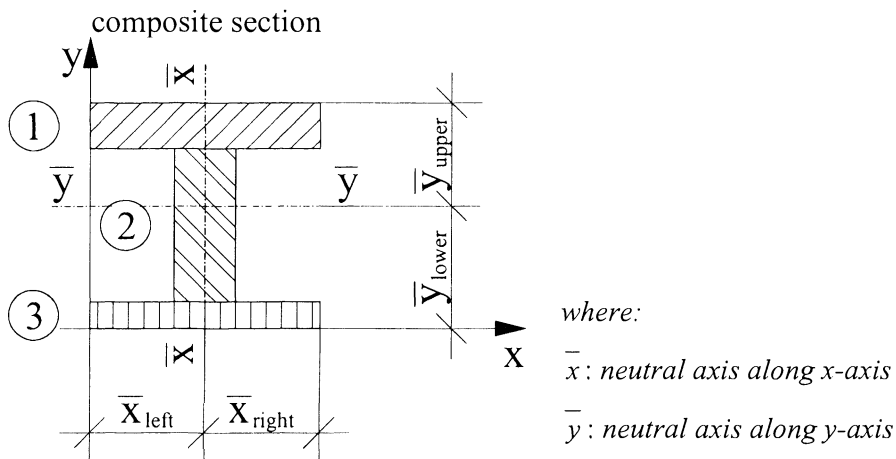


Figure 4-1: Location of the neutral axes

Continuing/developing the method of the transformed-section, the subsequent section properties of the composite section are estimated with Equations 4-6 to 4-9.

The area of a composite section ( $A_T$ ):

$$A_T = \sum_{i=1}^n n_i \int dA_i \quad (\text{Eq. 4-6})$$

The first moment of area of a composite section ( $Q_T$ ):

$$Q_T = \sum_{i=1}^n n_i \int y_i dA_i \quad (\text{Eq. 4-7})$$

The second moment of area of a composite section ( $I_T$ ):

$$I_T = \sum_{i=1}^n n_i \int y_i^2 dA_i \quad (\text{Eq. 4-8})$$

The section moduli of a composite section ( $S_T$ ):

$$S_{T,upper} = \frac{I_T}{y_{upper}} \quad (\text{Eq. 4-9a})$$

$$S_{T,lower} = \frac{I_T}{y_{lower}} \quad (\text{Eq. 4-9b})$$

Gere and Timoshenko (1999) also proposed a simplified procedure to estimate the properties of composite sections. Elsewhere, Schneider (1994) described this method as the Steiner's theorem in reference to the second moment of area. In this procedure, the geometric shape of the section is divided into small finite areas of regular geometric shapes, that is, squares, rectangles, circles, etc., and each area is given an index. Finally, the integrations are replaced by summations. Because of the division of the composite section, this procedure offers a very favourable alternative for estimating the properties of composite sections as long as they comply with simple beam theory (SBT) conditions<sup>a)</sup>. For sections built with member materials that have different mechanical

---

<sup>a)</sup> The simple beam theory corresponds to an approximation of the internal action/reaction conditions in beams. It relates two variables of the beam internal status, that is, the shear force and bending moment, and enunciates that, at points along the span/length of the beam, the stress regime is a function of both forces. Thus, it assumed that wherever the shear stress is equal to zero, the beam experiences pure bending. Under the assumption of the simple beam theory, there is no normal/axial force in the beam.

properties, this aspect can be accounted for with ease by means of the modular ratios of each sub-area. This procedure also allows the introduction of a connection coefficient,  $\gamma$ , which expresses the slip modulus of the interlayers.

Equations 4-10 to 4-13 expressed this procedure, whereby the modular ratio and  $\gamma$ -factor have been introduced directly into the equations for which it is relevant.

The neutral axis of a composite section ( $\bar{y}$ ):

$$\bar{y} = \frac{\sum_{i=1}^n n_i y_i A_i}{\sum_{i=1}^n n_i A_i} \quad \bar{y} = \frac{\sum_{i=1}^n \gamma_i n_i y_i A_i}{\sum_{i=1}^n n_i A_i} \quad (\text{Eq. 4-10})$$

The area of a composite section ( $A_T$ ):

$$A_T = \sum n_i A_i \quad (\text{Eq. 4-11})$$

The first moment of area of a composite section ( $Q_T$ ):

$$Q_T = \sum_{i=1}^n \gamma_i n_i y_i A_i \quad (\text{Eq. 4-12})$$

where:  $\gamma$ : connection coefficient [--]

The second moment of area of a composite section ( $I_T$ ):

$$I_T = \sum (n_i I_i + \gamma_i n_i y_i^2 A_i) \quad (\text{Eq. 4-13})$$

The specimens of the subject research are built with a nail-gluing technique. As a consequence of using this technique for the interfaces, it is accurate to assume that, for the strength or serviceability investigation, slip is fully impeded. Thus, the  $\gamma$ -factor is equal to 1.0.

As mentioned previously, the sheathing, or portions of it, act with the joists compositely. It is therefore required that, in order to perform the estimate of the section properties of SSP structures, it is necessary to assess/quantify the magnitude of the sheathing actually contributing to the joists. The following section addresses the estimate of the contribution of the skin(s), that is, the assessment of the skin tributary width.

## 4.2 THEORY OF THE TRIBUTARY WIDTH OF THE SKIN(S)

The concept of tributary width goes back as early as Pietzker's (1914) work on the buckling resistance of stiffened plates. In SSP systems, the tributary width is an essential aspect of the structural performance. It corresponds to the portions of the skin that act compositely with the joist, that is, the segments of the panels that take stress and contribute to the stiffness of the structure. It is thus a parameter that must be accounted for the estimate of the properties of SSP sections for both the ultimate and service performances of the floor. The magnitude of the tributary width may not be constant along the span. Amana (1967) and Amana and Booth (1967; 1968) reported that the panel is fully contributing only a short distance away from the ends of and gaps in the sheathing.

For Moody and McCutcheon (1984), the effectiveness of the contribution of the sheathing is affected by the axial stiffness of the sheathing, the slip modulus of the interlayers, and the presence of gaps in the sheathing. The buckling propensity of the flanges under compression may also limit the contribution of the sheathing. Raadschelders and Blass (1995) reported that with joist clearances less than twice the tributary width, the buckling of the panel is avoided. However, more thorough analysis can be carried, in which the critical buckling load is assessed (Foschi 1969a, 1969b; Mansour 1976; von Halász & Cziesielski 1966). Elsewhere, König (1989) reported that flanges in compression retain consequent load-bearing capacity, even after having buckled, and Kliger and Pellicane (1997a) observed that curling had very little effect on the performance of SSP decks.

### 4.2.1 Stress distribution in SSP skin(s)

In bending conditions, normal stresses develop in the skin(s) of SSP structures (Foschi 1969b; Ozelton & Baird 2002). Because of shear deformations occurring, the distribution of these normal stresses is not uniform in the section of the cantilevered – unsupported – portion of the skin(s) (Raadschelders & Blass 1995). Foschi (1969b) Ozelton and Baird (2002) proposed that the normal stresses reach a maximum at the junctions between the joists and the panels, and a minimum at equidistance between the joists (Figure 4–2). However, Foschi (1969b) suggested that for common physical dimensions of wood joist floors, the distribution of the normal stress is nearly uniform. Foschi's model used the orthotropic plate theory (Timoshenko & Woinowsky-Krieger



1959) for the sheathing and the simple beam theory for the girders, whereby the solution is obtained by convergence of a series function. Study on this mechanism of stress distribution, depicted as “shear lag”, go back to the 1920s (von Karman 1924) and focused on isotropic materials. Later, works accounted for orthotropic materials with study on stresses in plywood stressed-skin panels (Amana 1967; Amana & Booth 1967, 1968; Smith 1966a, 1966b).

Shear lag describes the phenomenon that occurs when, with constant span but increasing joist spacing, the contribution of the panel(s) decreases and stress peaks become larger; thus reducing the serviceability and load-bearing capacity of an SSP composite. Raadschelders and Blass (1995) proposed that the magnitude of the stress diminution depends on the ratios  $b_f L$  and  $E/G$ . Thus, with the increase of these ratios, the tributary width of the skin(s) decreases, whereby;  $b_f$  is the clearance between the joists (Figure 4–2),  $L$  is the span and  $E$  and  $G$  are respectively the modulus of elasticity and the shear modulus of the skin in the direction of the SSP span.

Figure 4–2 depicts the stress distribution in the upper skin of an SSP element. It is assumed that the deck is in flexural state generated by symmetric/uniformly distributed load conditions. Figure 4–2 shows that the peaks of axial stresses in the skins coincide with the location of the joists, while the lowest intensity of these stresses is situated in cantilevered portions of the skins – equidistant from two adjacent joists.

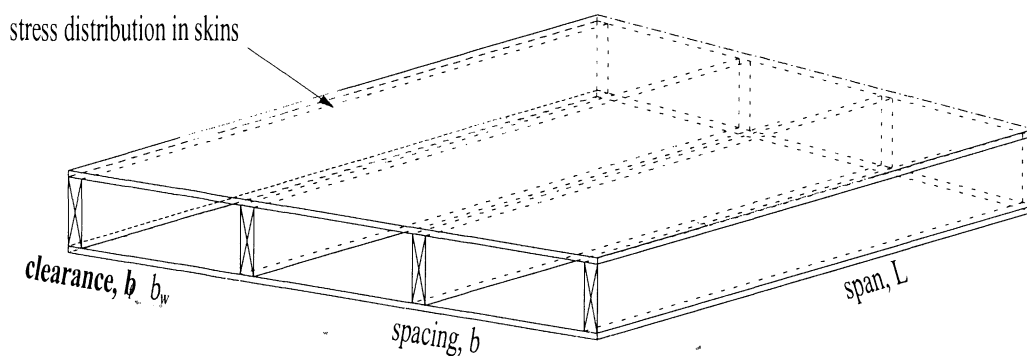


**Figure 4–2: Stress distribution in the skin(s) of SSP deck**

Figure 4–3 depicts an SSP section and the symbols related to it. These symbols and denotations are used hereafter in this thesis. In Figure 4–3, a single-span floor element in flexural state is assumed, that is, the upper skin takes compression stress and the lower tension stress.

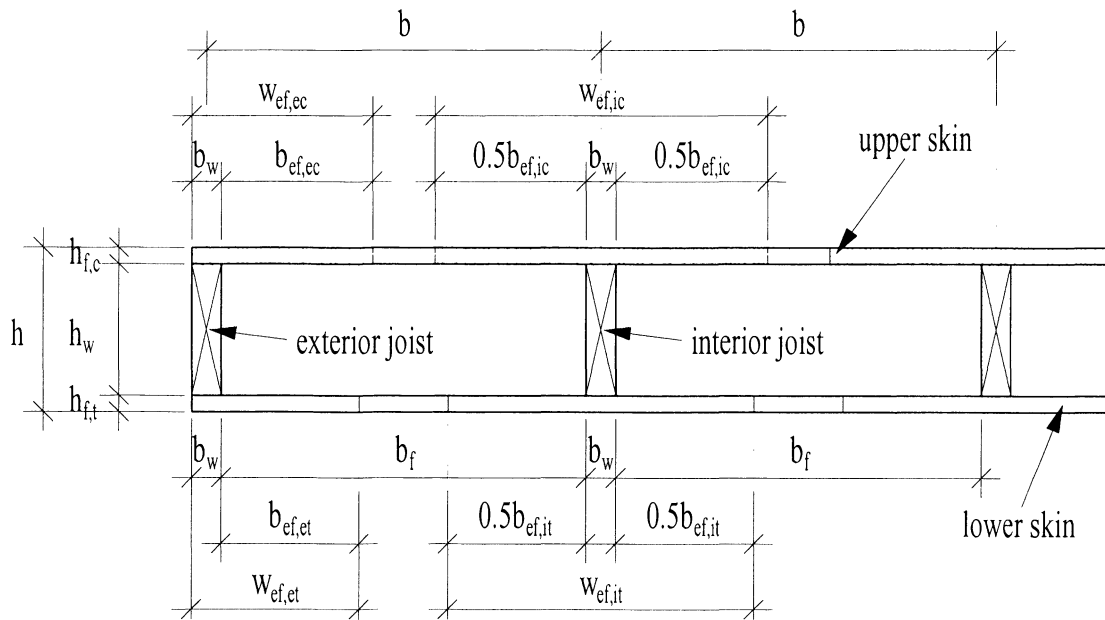


Figure 4–3: Symbols for stressed-skin panels used in the subject research

The symbols in Figure 4–3 and their units are:

w:	tributary width	[mm]
subscripts:	ef: effective	
	ec: compressive panel about an exterior joist	
	et: tensile panel about an exterior joist	
	ic: compressive panel about an interior joist	
	it: tensile panel about an interior joist	
b:	joist spacing	[mm]
b <sub>f</sub> :	joist clearance (clear spacing (Ozelton & Baird 2002))	[mm]
b <sub>ef,--</sub> :	effective contribution of the panel	[mm]
b <sub>w</sub> :	breadth of the joist	[mm]
h:	depth of SSP structure	[mm]
h <sub>f,u</sub> :	thickness of the upper panel	[mm]
h <sub>w</sub> :	depth of the joist	[mm]
h <sub>f,l</sub> :	thickness of the lower panel	[mm]

*NOTE: in Figure 4–3, the magnitude of the tributary width is schematically depicted as per BS EN 1995-1-1:2004 (British Standard 2004) – in this depiction, the magnitude of the tributary width of the upper skin is larger than that of the lower skin. On the other hand, SIA 265 (Société Suisse des Ingénieurs et Architectes 2002) proposes a depiction wherein the magnitude of the tributary width of the lower skin is larger than that of the upper skin.*

#### 4.2.2 Estimating the tributary width of the skin(s)

Quantifying the tributary width depends on the material properties of the skins and is based on the stress distribution in the panels, which is not linear because of shear deformations (Raadschelders & Blass 1995). Because this distribution is non-linear, estimating the tributary width may prove complex (Amana 1967; Amana & Booth 1967, 1968). In addition, it relies on material data, which are not always available, even in specialised literature.

In the 1960s, Möhler (1963) and Möhler, Abdel-Sayed and Ehlbeck (1963) carried out works on the tributary width of plywood skins and derived a geometric function for the shear lag (Equations 4-16a and b) accounting for the elastic orthotropic properties of the sheathing and the geometric dimensions of the floor. Therefore, Equations 4-16a and b are characterised by the moduli of elasticity ( $E$ ), the shear modulus ( $G$ ) and the Poisson's ratio ( $\mu$ ) and by the span of the floor ( $L$ ) and the joist clearance ( $b_f$ ). Furthermore, the buckling propensity of the compression flange is also considered together with the shear deformation in the panel(s). Even though Möhler (1963) and Möhler, Abdel-Sayed and Ehlbeck (1963) gave no clear indication, the consideration of buckling aspect in the formula suggests that the latter applies to compression skin. Hereafter Equations 4-16a and b are referred to as Möhler equations.

Estimates of SSP tributary width about interior joists (T- or I-beams):

$$w_{Möhler.i} = w_{ef.ic} = b_w + b_{ef.ic} \quad (\text{Eq. 4-14})$$

Estimates of SSP tributary width about exterior joists (L- or C-beams):

$$w_{Möhler.e} = w_{ef.ec} = b_w + b_{ef.ec} \quad (\text{Eq. 4-15})$$

whereby the shear lag is (tensile and compressive skin):

- for interior joists:

$$b_{ef.ic} = 2L \frac{(\lambda_1 \tanh \alpha_1 - \lambda_2 \tanh \alpha_2)}{\pi(\lambda_1^2 - \lambda_2^2)} \quad (\text{Eq. 4-16a})$$

- for exterior joists:

$$b_{ef.ec} = L \frac{(\lambda_1 \tanh \alpha_1 - \lambda_2 \tanh \alpha_2)}{\pi(\lambda_1^2 - \lambda_2^2)} \quad (\text{Eq. 4-16a})$$

in which the coefficients are:

$$\alpha_1 = \frac{\lambda_1 \pi b_f}{2L} \quad (\text{Eq. 4-17})$$

$$\alpha_2 = \frac{\lambda_2 \pi b_f}{2L} \quad (\text{Eq. 4-18})$$

$$\lambda_1 = \sqrt{a + \sqrt{a^2 - c}} \quad (\text{Eq. 4-19})$$

$$\lambda_2 = \sqrt{a - \sqrt{a^2 - c}} \quad (\text{Eq. 4-20})$$

$$a = \frac{E_y}{2G} - \nu_{xy} \quad (\text{Eq. 4-21})$$

$$c = \frac{E_y}{E_x} \quad (\text{Eq. 4-22})$$

where: w:	tributary width (Figure 4–3)	[mm]
	subscripts: Möhler: Möhler equation (related to)	
	i: about an interior joist	
	e: about an exterior joist	
L:	span of the SSP structure	[mm]
$\nu_{xy}$ :	Poisson's ratio of the panel	[–]
	subscripts: x: parallel to the joist's longitudinal axis	
	y: perpendicular to the joist's longitudinal axis	
$E_y$ and $E_x$ :	moduli of elasticity of the panel	[MPa]
G:	shear modulus	[MPa]

Table 4–1 summaries the magnitude of the shear lag effects obtained with Möhler equation in which the specimen parameters of the subject research have been considered, that is, the dimensions (joist spacing,  $b = 375$  and  $500$  mm, span,  $L = 3700$  and  $6600$  mm) and the panel materials (15-mm F11 plywood, 22-mm Kronoply OSB and 19-mm AS1859 particleboard<sup>b)</sup>). Table 4–1 shows that an important portion of the unsupported panel area acts compositely with the joists. The ratios of tributary width,  $RTW$ , range from 0.969 to 0.994, 1.0 representing a full contribution of the panel. Elsewhere, investigating the effectiveness of the skin contribution with photoelastic technique, Smith (1966a; 1966b) reported that the panels contribute up to some 96% to the joists.

**Table 4–1: Möhler – shear lag estimates according to the specimen parameters (panel materials and dimensions) of the subject research**

Panel material	<sup>1</sup> $b_r$ [mm]	<sup>2</sup> $L$ [mm]	<sup>3</sup> $h_r$ [mm]	<sup>4</sup> SL [mm]	<sup>A</sup> RTW
	(1)			(2)	(2)/(1)
*F11 plywood	305	<sup>†</sup> 3700	15	295.5	<b>0.969</b>
	410	<sup>‡</sup> 6600		402.6	<b>0.982</b>
*Kronoply OSB	305	3700	22	301.6	<b>0.989</b>
	410	6600		407.4	<b>0.994</b>
AS1859 particleboard	305	3700	19	300.5	<b>0.985</b>

\*panel strength axis parallel to the joists; <sup>†</sup>joist spacing,  $b = 375$  mm; <sup>‡</sup>joist spacing,  $b = 500$  mm.

<sup>1</sup>joist clearance, <sup>2</sup>span, <sup>3</sup>panel thickness, <sup>4</sup>shear lag.

<sup>A</sup>ratio of tributary width, that is, unsupported skin portion acting compositely with the joist, max.: 1.0.

### 4.2.3 Codified approaches for approximating the tributary width of the skin(s)

Estimating the tributary width as accurately as possible is expected for design processes. On the other hand, for design convenience, the engineers should have access to uncomplicated methods. To achieve this, the tributary width is produced by equating the stress distribution under the geometric curve of the non-linear distribution and a fictive uniform rectangular (Figure 4–4). Therefore, the panels take equal amounts of stress and

<sup>b)</sup> The material properties of the panels are presented in Chapter 3 in Part 2.

the real and idealised T- or I-beams have similar ultimate and service performances (Amana & Booth 1967).

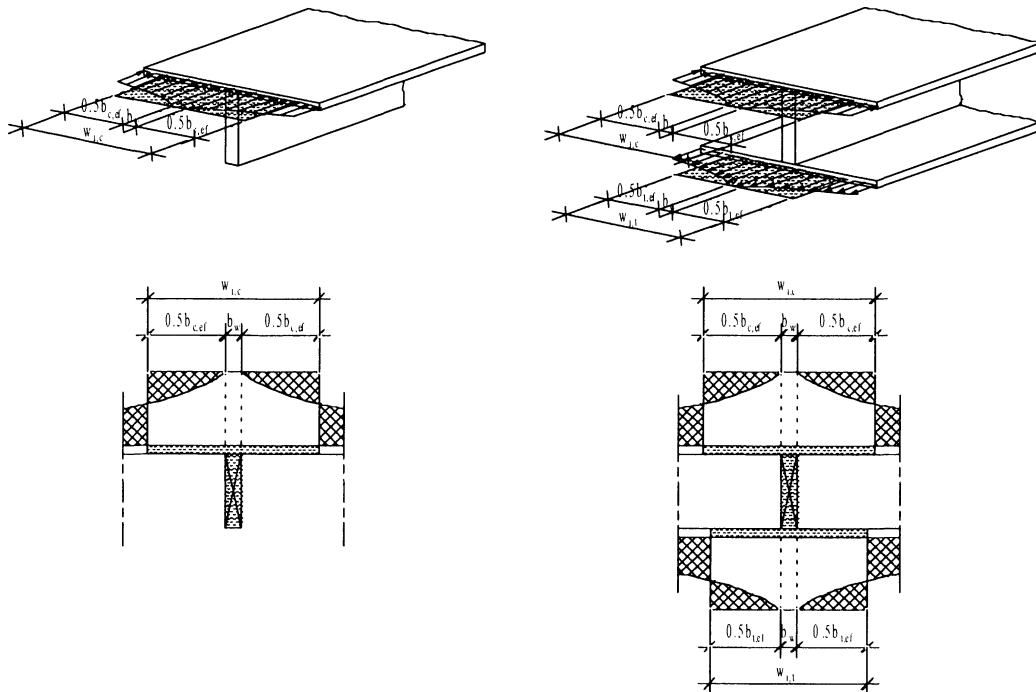


**Figure 4-4: Depiction of the tributary width of the skin(s)**

Different codes around the world have adopted this “idealisation” and provide directives for approximating the portion of the skin(s) that effectively acts compositely with the joists. Hereafter, the design guidelines for SSP systems provided by different codes are analysed. The analysis, which particularly focuses on the estimate of the tributary width, includes AS 1720.1–1997 (Australian Standard<sup>TM</sup> 1997), Eurocode 5 (EC5) (European Committee for Standardisation 1995), former Swiss code SIA 164 (Société Suisse des Ingénieurs et Architectes 1992), and a design procedure used in the USA (APA – The Engineered Wood Association 1990; Desler 2002; McLain 1999).

#### **4.2.3.1 Australia – AS 1720.1–1997**

The current edition of the Australian code for timber design, AS 1720.1–1997 (Australian Standard<sup>TM</sup> 1997), makes only scarce recommendations for SSP design. It provides directives for the design of the skin-to-joist connections. However, it does not provide any guideline about the estimation of the tributary width.

In Australia, further information about SSP constructions may be found in a technical brochure published by the Plywood Association of Australia LTD (1998). This brochure provides construction requirements and span tables for one-sided (T-section) SSP floors built with plywood sheathing. However, it gives no precise indication about the design background, that is, about the way the tributary width is estimated.

#### 4.2.3.2 Europe – EC5

In Europe, Eurocode 5 (EC5) (European Committee for Standardisation 1995) forms the basis of many national codes. Switzerland’s SIA 265 code (Société Suisse des Ingénieurs et Architectes 2003), the United Kingdom’s BS EN 1995-1-1:2004 code (British Standard 2004) and Germany’s DIN 1052 code (DIN Deutsches Institut für Normung e. V. 2004) have been revised and/or adapted recently. With regard to SSP systems, these codes provide very similar guidelines. Therefore, hereafter this design procedure is referred to as “EC5”.

EC5 specifies that the tributary width,  $w$ , is determined by the span of the floor and the material, thickness and compressive buckling propensity of the panel(s). Table 4–2 presents the coefficients to apply to some widely used engineered wood products.

**Table 4–2: Coefficients for the estimate of the tributary width – shear lag and plate buckling**

Skin material	Shear lag $C_{SL}$	Plate buckling $C_{PB}$
Plywood (ref.: face grain direction):		
parallel to the joists	0.1	25
perpendicular to the joists	0.1	20
Oriented strand board (OSB)	0.15	25
Particleboard/fibreboard with random fibre orientation	0.2	30

The shear lag is relevant for tensile and compressive skins, whereby the buckling propensity of the latter is checked. Further, EC5 gives two equations for estimating the tributary width, depending on the position of the joist in SSP structures. The first approximation (Equations 4-23a and b) applies to interior joists (T- or I-beams); whereas the second one (Equations 4-24a and b) relates to the exterior joists (L- or C-beams).

Estimates of SSP tributary width about interior joists (T- or I-beams):

- tensile skin – shear lag:

$$w_{EC5,it} = w_{ef,it} = b_w + \min b_{ef,it} = b_w + \min \left| \begin{array}{l} b_f \\ C_{SL}L \end{array} \right| \quad (\text{Eq. 4-23a})$$

- compressive skin – shear lag and plate buckling:

$$w_{EC5,ic} = w_{ef,ic} = b_w + \min b_{ef,ic} = b_w + \min \left| \begin{array}{l} b_f \\ C_{SL}L \\ C_{PB}h_{f,c} \end{array} \right| \quad (\text{Eq. 4-23b})$$

Estimates of SSP tributary width about exterior joists (L- or C-beams):

- tensile skin – shear lag:

$$w_{EC5,et} = w_{ef,et} = b_w + \min b_{ef,et} = b_w + \min \left| \begin{array}{l} 0.5b_f \\ 0.5C_{SL}L \end{array} \right| \quad (\text{Eq. 4-24a})$$

- compressive skin – shear lag and plate buckling:

$$w_{EC5,ec} = w_{ef,ec} = b_w + \min b_{ef,ec} = b_w + \min \left| \begin{array}{l} 0.5b_f \\ 0.5C_{SL}L \\ 0.5C_{PB}h_{f,c} \end{array} \right| \quad (\text{Eq. 4-24b})$$

where:  $w$ : tributary width (Figure 4–3) [mm]  
subscripts: EC5: EC5 equation  
 $c_{SL}$ : shear lag coefficient [–]  
 $c_{PB}$ : plate buckling coefficient [–]

Table 4–3 summarises the magnitude of the shear lag and plate buckling when the EC5 method is applied to the specimen parameters of the subject PhD research. These parameters were the dimensions such as the joist spacing,  $b = 375$  and  $500$  mm, and the



span,  $L = 3700$  and  $6600$  mm, and the panel materials such as plywood (15-mm F11 plywood), oriented strand board (22-mm Kronoply OSB) and particleboard (19-mm AS1859 particleboard). EC5 estimates allow full contributions of the unsupported portion of the panels to work with the joists compositely, with the exception of one case (Table 4–3). Therefore, only the 356-mm I-joist specimen displays a ratio of tributary width,  $RTW$ , of 0.915, the limit being imposed by the buckling plate condition. For all other specimens,  $RTW$  is equal to 1.0.

**Table 4–3: EC5 – shear lag estimates according to the specimen parameters (panel materials and dimensions) of the subject research**

Panel material	<sup>1</sup> $b_f$ [mm]	<sup>2</sup> $L$ [mm]	<sup>3</sup> $SL$ [mm]	<sup>A</sup> $RTW$	<sup>4</sup> $h_f$ [mm]	<sup>5</sup> $PB$ [mm]	$RTW$
	(1)		(2)	(2)/(1)		(3)	(3)/(1)
*F11 plywood	305	<sup>†</sup> 3700	370	<b>1.000</b>	15	375	<b>1.000</b>
	410	<sup>‡</sup> 6600	660	<b>1.000</b>			<b>0.915</b>
*Kronoply OSB	305	3700	555	<b>1.000</b>	22	550	<b>1.000</b>
	410	6600	990	<b>1.000</b>			<b>1.000</b>
AS1859 particleboard	305	3700	740	<b>1.000</b>	19	570	<b>1.000</b>

\*panel strength axis parallel to the joists; <sup>†</sup>joist spacing,  $b = 375$  mm; <sup>‡</sup>joist spacing,  $b = 500$  mm.

<sup>1</sup>joist clearance, <sup>2</sup>span, <sup>3</sup>shear lag, <sup>4</sup>panel thickness, <sup>5</sup>plate buckling.

<sup>A</sup>ratio of tributary width, that is, unsupported skin portion acting compositely with the joist, max.: 1.0.

#### 4.2.3.3 Switzerland – SIA 164

The former Swiss code, SIA 164<sup>c)</sup> (Société Suisse des Ingénieurs et Architectes 1992), is considered because it presents an alternative approach for approximating the tributary width of the skin(s). In this procedure, the shear lag is governed by the span of the floor and the joist clearance, and the plate buckling is determined by the thickness and material properties (compression strength and modulus of elasticity) of the panel. The shear lag is relevant for both the tensile and compressive skin, whereby the latter must also satisfy the buckling requirement. The joist spacing forms another limitation to the tributary width.

For the sections about interior joists, the shear lag is estimated with Equations 4-25a, b and c, the compliance with the conditional ratio (Equations 4-25a, b and c) of

<sup>c)</sup> SIA 164 is superseded by SIA 265 (Société Suisse des Ingénieurs et Architectes 2003).

the joist clearance to the span defining the equation to use. For most cases, the floor structure complies with Equation 4-25b's conditions. The buckling stability is controlled by Equation 4-25d, in which the modulus of elasticity,  $E_v$ , is given by Equations 4-26a and b.

Estimates of SSP tributary width about interior joists (T- or I-beams):

- shear lag – tensile and compressive skin:

$$w_{i,SIA} = w_{i,ef} = b_w + b_f \quad \text{if} \quad \frac{b_f}{2L} \leq 0.025 \quad (\text{Eq. 4-25a})$$

$$w_{i,SIA} = w_{i,ef} = b_w + \left(1.1 - \frac{2b_f}{L}\right) b_f \quad \text{if} \quad 0.025 < \frac{b_f}{2L} < 0.125 \quad (\text{Eq. 4-25b})$$

$$w_{i,SIA} = w_{i,ef} = b_w + 0.15L \quad \text{if} \quad \frac{b_f}{2L} \geq 0.125 \quad (\text{Eq. 4-25c})$$

- plate buckling – compressive skin:

$$w_{ic,SIA} = w_{ic,ef} \leq b_w + 1.8h_{f,c} \sqrt{\frac{E_v}{n f_{c,x} \text{ resp } c,y}} \leq b_w + b_f \quad (\text{Eq. 4-25d})$$

in which:

for plywood:  $E_v = \sqrt{E_{b,x} E_{b,y}}$  (Eq. 4-26a)

for particleboard and fibreboard:  $E_v = E_b$  (Eq. 4-26b)

*NOTE: for OSB panel, because  $E_{b,x} \neq E_{b,y}$ , Equation 4-26a is applied.*

where: w: tributary width (Figure 4-3) [mm]  
 subscript: SIA: SIA 164 equation  
 $f_c$ : characteristic strength in compression [MPa]  
 n: security factor for stability; general cases, n = 2 [–]

For the sections about exterior joists, Equation 4-27's series is derived from Equation 4-25 series in which a 0.5 coefficient is introduced.

Estimates of SSP tributary width about exterior joists (L- or C-beams):

- shear lag – tensile and compressive skin:

$$w_{SIA,e} = w_{ef,e} = b_w + 0.5b_f \quad \text{if} \quad \frac{b_f}{2L} \leq 0.025 \quad (\text{Eq. 4-27a})$$

$$w_{SIA,e} = w_{ef,e} = b_w + 0.5 \left( 1.1 - \frac{2b_f}{L} \right) b_f \quad \text{if} \quad 0.025 < \frac{b_f}{2L} < 0.125 \quad (\text{Eq. 4-27b})$$

$$w_{SIA,e} = w_{ef,e} = b_w + 0.075L \quad \text{if} \quad \frac{b_f}{2L} \geq 0.125 \quad (\text{Eq. 4-27c})$$

- plate buckling – compressive skin:

$$w_{SIA,ec} = w_{ef,ec} \leq b_w + 0.9h_{f,c} \sqrt{\frac{E_v}{n f_{c \text{ resp } c \perp}}} \leq b_w + 0.5b_f \quad (\text{Eq. 4-27d})$$

*NOTE: modulus of elasticity,  $E_v$ , is estimated with the Equation 4-26 series.*

In some floor structures, the exterior joists are indented, that is, the outer edge of the skin is not supported. SIA 164 gives directives in order to avoid buckling in the unsupported portion of the panel. In such cases the buckling limitation is controlled by Equation 4-28 wherein the joist clearance,  $b_f$ , has been substituted with the cantilevered length of the skin,  $b_f'$ .

Estimates of SSP tributary width about exterior joists (asymmetric T- or I-beams):

- plate buckling – compressive skin:

$$w'_{SIA,ec} = w'_{ef,ec} \leq b_w + 0.5h_{f,c} \sqrt{\frac{E_v}{n f_{c \text{ resp } c \perp}}} \leq b_w + b_f' \quad (\text{Eq. 4-28})$$

*NOTE: modulus of elasticity,  $E_v$ , is estimated with the Equation 4-26 series.*

where:  $b_f'$ : cantilevered length of the panel edge [mm]

In Table 4-4, the values of the shear lag and plate buckling determined with the SIA 164 method are summarised. These approximations considered the specimen characteristics of the subject research relevant to the tributary width of the panels. Such parameters were the joist spacing ( $b = 375$  and  $500$  mm), the span ( $L = 3700$  and  $6600$

mm) and the panel thickness and materials (15-mm F11 plywood, 22-mm Kronoply OSB and 19-mm AS1859 particleboard). For the determination of the buckling propensity, the characteristic strength in compression and the modulus of elasticity of the skin are also taken into consideration. With SIA 164, shear lag estimates demand reducing up to about 7.0% the skin contribution to the deck composite section. Buckling plate conditions affect the skin contribution more heterogeneously. For specimen with OSB and particleboard skins, no decrease is imposed; with plywood the reduction reaches close to 30% in one case. Table 4–4 summarises SIA 164’s ratios of tributary width, *RTW*.

**Table 4–4: SIA 164 – shear lag estimates according to the specimen parameters (panel materials and dimensions) of the subject research**

Panel material	<sup>1</sup> b <sub>r</sub> [mm]	<sup>2</sup> L [mm]	<sup>3</sup> SL [mm]	<sup>4</sup> RTW	<sup>4</sup> h <sub>r</sub> [mm]	<sup>5</sup> PB [mm]	RTW
	(1)		(2)	(2)/(1)		(3)	(3)/(1)
*F11 plywood	305	<sup>†</sup> 3700	285.2	<b>0.935</b>	15	289.6	<b>0.949</b>
	410	<sup>‡</sup> 6600	400.1	<b>0.976</b>			<b>0.706</b>
*Kronoply OSB	305	3700	285.2	<b>0.935</b>	22	472.4	<b>1.000</b>
	410	6600	400.1	<b>0.976</b>			<b>1.000</b>
AS1859 particleboard	305	3700	285.2	<b>0.935</b>	19	404.7	<b>1.000</b>

\*panel strength axis parallel to the joists; <sup>†</sup>joist spacing, b = 375 mm; <sup>‡</sup>joist spacing, b = 500 mm.

<sup>1</sup>joist clearance, <sup>2</sup>span, <sup>3</sup>shear lag, <sup>4</sup>panel thickness, <sup>5</sup>plate buckling.

<sup>4</sup>ratio of tributary width, that is, unsupported skin portion acting compositely with the joist, max.: 1.0.

#### 4.2.3.4 USA – the APA method

From America, a method to approximate the tributary width of the skin(s) of one- and two-sided plywood SSP systems can be found in numerous sources, for instance, in technical brochures by APA – The Engineered Wood Association (1990), in McLain (1999) and in Desler (2002). This approach (hereafter referred to as the APA method) considers SSP elements as composite units rather than series of cross-sections and calls upon the concept of “basic spacing”, which is a coefficient relying on the buckling behaviour of plywood uniformly loaded (in-plane load) in compression (Baird & Ozelton 1984; Newlin 1940). After Desler (2002), the purpose of the basic spacing is to consider the buckling propensity of the panel and define the maximum portion of the

skin that can act compositely with the joists. For Wardle and Peek (1970), whenever the joist spacing is smaller than twice the basic spacing, the longitudinal buckling of the compression plywood panel is avoided.

The basic spacing indicates the upper limit of the tributary width. After Baird and Ozelton (1984), the APA method is only applicable to Douglas Fir plywood. Nevertheless, Desler (2002) proposed that the method can be transposed and applied to OSB panels as well. Notwithstanding the design requirements for the sheathing to span adequately between the joists (strength and serviceability); this governs the thickness of the panels in most cases. The basic spacing is determined by the construction and the depth of SSP elements. The compressive and tensile panels are handled in a similar manner. However, with the APA method, the tributary width may be different for the ultimate limit state and the serviceability limit state. Finally, the tributary width must be consistent with the location of the joist (exterior and interior joist). Equation 4-29 enables the calculation of the basic spacing for plywood panels and Figure 4–5 for plywood and OSB panels.

$$b_{basic} = k_p h_f \sqrt{\frac{h_f}{\sum h_p}} \quad (\text{Eq. 4-29})$$

where:	$b_{basic}$ :	basic spacing	[mm]
	$k_p$ :	n-ply coefficient of the plywood panel [--] for 3-ply panel: $k_p = 31$ ; for 5-ply panel, $k_p = 36$ (Timber Engineering Company; Timber Research and Development Association)	
	$h_f$ :	thickness of the plywood panel	[mm]
	$h_{p  }$ :	ply(ies) parallel to span (plywood face grain to joists)	[mm]

From the literature, tables that indicate the values of the basic spacing according to the type and quality finish of the panel spacing are available (APA – The Engineered Wood Association 1990; Desler 2002; McLain 1999). Built with values from these tables, Figure 4–5 depicts graphically the values of the basic spacing and allows approximation of the basic spacing for both plywood and OSB panels.

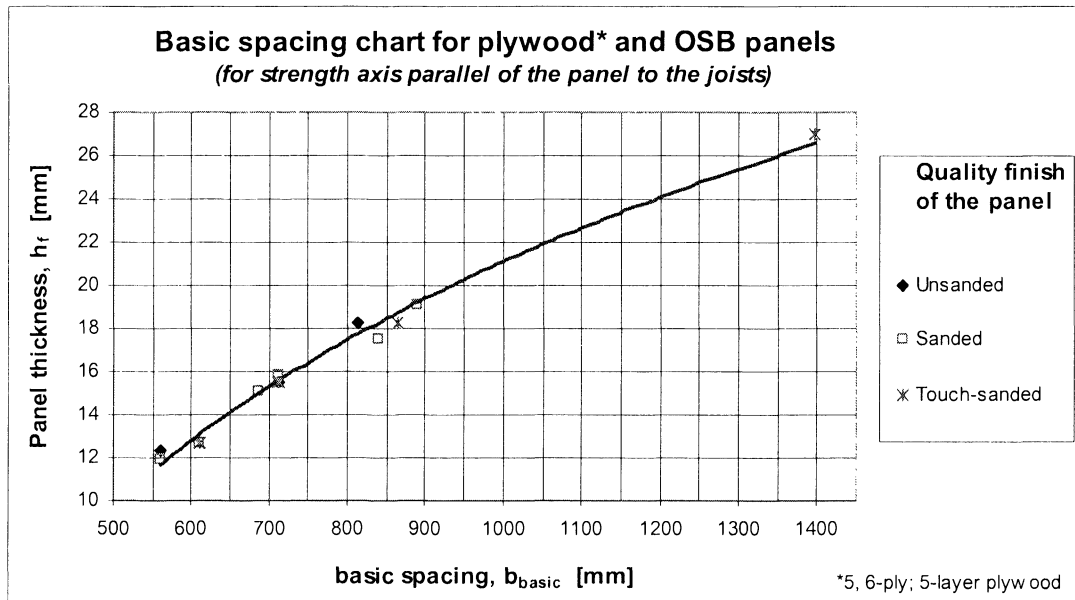


Figure 4–5: Basic spacing,  $b_{basic}$ , chart for plywood and OSB panel

An analysis from Foschi (1969b) identified discrepancies between the shear lag theory and the earlier theory of the basic spacing and claimed that they could not simultaneously produce accurate estimates of stresses and deflections. In order to correct these disagreements and give more consistency to the results of the basic spacing approach, Foschi (1969b) derived a coefficient,  $K_c$ . With the application of  $K_c$ , the bending stress and deflection are increased (Baird & Ozelton 1984).  $K_c$  is determined by the ratio of the span and the joist clearance of the SSP deck (Figure 4–6). Foschi's correction coefficient applies to SSP with plywood skin(s).

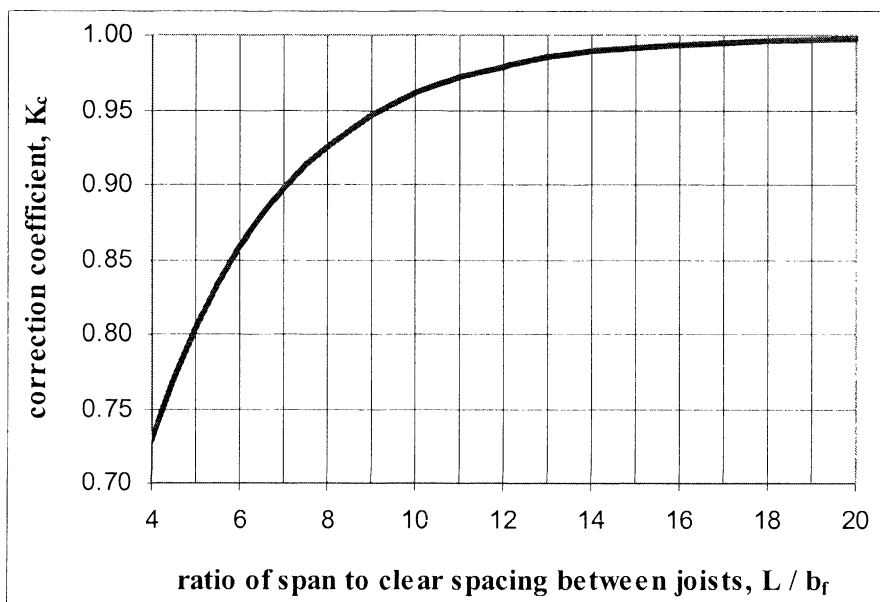


Figure 4–6: Correction coefficient  $K_c$ , (Baird & Ozelton 1984; Foschi 1969b)

Elsewhere, restrictive factors or conditional ratios have also been introduced into the basic spacing design method (1990; Desler 2002; McLain 1999). After Desler (2002) and McLain (1999), the permissible performance of SSP decks is limited in two ways; first the basic spacing and the reduction of the allowable stress (Figure 4–7). Found in APA guidelines (APA – The Engineered Wood Association 1990),  $K_s$  is applied to all stresses except shear and rolling-shear stresses. Furthermore, this additional reduction aims to avoid buckling of the compression skin.

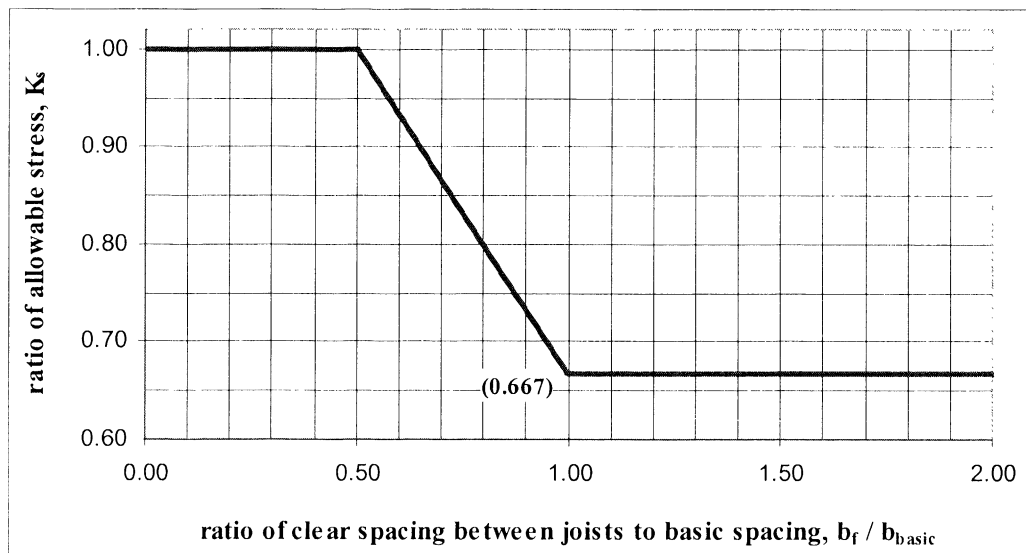


Figure 4–7: Stress reduction factor (APA – The Engineered Wood Association 1990; Desler 2002; McLain 1999)



Considering the panel materials and the specimen construction of the subject research, Table 4–5 indicates the basic spacing of the plywood panel (15-mm F11 plywood) and OSB panel (22-mm Kronoply OSB) estimated with Equation 4-29 and/or approximated with the chart (Figure 4–5). Also in Table 4–5, the estimates of the basic spacing as per the tables of the literature (APA – The Engineered Wood Association 1990; Desler 2002; McLain 1999) are presented. Marginal differences are apparent between the approximations. For the subject research, the values of the chart (Figure 4–5) are used hereafter.

**Table 4–5: Basic spacing,  $b_{\text{basic}}$ , plywood and OSB panels used in the subject research**

Panel material	Panel thickness, $h_f$ [mm]	Basic spacing, $b_{\text{basic}}$ [mm]		
		Equation 4-29	Figure 4–5	*APA
<sup>†</sup> F11 plywood	15	697	695	711*
<sup>†</sup> Kronoply OSB	22	–	1050	~1100
<b>AS1859 particleboard</b>	19	Not addressed by APA method		

\* source: (APA – The Engineered Wood Association 1990; Desler 2002; McLain 1999).

<sup>†</sup> panel strength axis parallel to the joists.

NOTE: quality finish of the panel: touch-sanded.

In Table 4–6 the estimates of the correction coefficient ( $K_c$ ) and of the ratio of allowable stress ( $K_s$ ) with regard to the specimen parameters of the subject research are presented.  $K_c$  imposes a correction a just a few per cent in all cases, whereas  $K_s$  forces a about 5% reduction of allowable stress on a single case only, that is, 356-mm I-joist specimen with a 15-mm F11 plywood compression skin.

**Table 4–6: Correction coefficient ( $K_c$ ) and ratio of allowable stress ( $K_s$ ) for the subject research**

Panel material	<sup>1</sup> L [mm]	<sup>2</sup> b <sub>f</sub> [mm]	<sup>3</sup> b <sub>basic</sub> [mm]	L/b <sub>f</sub>	<sup>4</sup> K <sub>c</sub>	b <sub>f</sub> /b <sub>basic</sub>	<sup>5</sup> K <sub>s</sub>
<b>200-mm I-joist</b>							
*F11 plywood	‡3700	305	695	12.131	0.980	0.439	1.000
*Kronoply OSB			1050			0.290	1.000
AS1859 particleboard			–			–	–
<b>356-mm I-joist</b>							
F11 plywood	‡6600	410	695	16.098	0.994	0.590	0.949
Kronoply OSB			1050			0.390	1.000

\*panel strength axis parallel to the joists; †joist spacing, b = 375 mm ; ‡joist spacing, b = 500 mm.

<sup>1</sup>span, <sup>2</sup>joist clearance, <sup>3</sup>basic spacing (), <sup>4</sup>correction coefficient, <sup>5</sup>ratio of allowable stress.

Remaining consistent with the methodology of the subject PhD research, the approximation of the tributary is expressed with regard to individual joists (Equations 4-30 to 4-33). For one-sided SSP constructions with depths,  $h$ , of 75 mm or less, the contribution of the skin is reduced whenever the joist clearance,  $b_f$ , exceeds the basic spacing,  $b_{basic}$ . Equations 4-30 and 4-32 depict the approximation of the tributary width about interior joists; for resisting bending moment (ULS), Equations 4-31 and 4-33 for serviceability (SLS). As mentioned previously the contribution of the skin must agree with the location of the joist. In order to comply with this, Equations 4-34 to 4-37 are derived from Equations 4-30 to 4-33, in which a reduction factor, 0.5, is introduced. The approximation of the tributary width about exterior joists for resisting bending moment is depicted by Equations 4-34 and 4-36 and for serviceability by Equations 4-35 and 4-37.

Estimates of SSP tributary width about interior joists (T-beams):

- shear lag and plate buckling for  $h < 75 \text{ mm}^*$  one-sided SSP systems (open section):

$$\text{if } b_f \leq b_{basic} \quad \text{for ULS:} \quad w_{APA-ULS,i} = w_{ef,i\_ULS} = b_w + b_f \quad (\text{Eq. 4-30a})$$

$$\text{for SLS:} \quad w_{APA-SLS,i} = w_{ef,i\_SLS} = b_w + b_f \quad (\text{Eq. 4-31a})$$

$$\text{if } b_f > b_{basic} \quad \text{for ULS:} \quad w_{APA-ULS,i} = w_{ef,i\_ULS} = b_w + 0.5b_{basic} \quad (\text{Eq. 4-30b})$$

$$\text{for SLS:} \quad w_{APA-SLS,i} = w_{ef,i\_SLS} = b_w + 0.5b_{basic} \quad (\text{Eq. 4-31b})$$

\*when the joist clearance exceeds the basic spacing,  $b_f > b_{basic}$ , the tributary width experiences a sharp drop; Equation 4-30a versus Equation 4-30b and Equation 4-31a versus Equation 4-31b. Desler (Desler 2002) reported that this sharp change of dimension complies with test results.

---

Estimates of SSP tributary width about interior joists (T- or I-beams):

- shear lag and plate buckling for  $h \geq 75 \text{ mm}$  one-sided SSP systems and  $h =$  all depth two-sided SSP – tensile and compressive skin:

$$\text{for ULS:} \quad w_{APA-ULS,i} = w_{ef,i\_ULS} = b_w + \min b_{ef,i} = b_w + \min \left| \begin{array}{c} b_f \\ b_{basic} \end{array} \right| \quad (\text{Eq. 4-32})$$

$$\text{for SLS:} \quad w_{APA-SLS,i} = w_{ef,i\_SLS} = b_w + b_f \quad (\text{Eq. 4-33})$$

Estimates of SSP tributary width about exterior joists (L-beams):

- shear lag and plate buckling for  $h < 75 \text{ mm}^*$  one-sided SSP systems (open section):

$$\text{if } b_f \leq b_{basic} \quad \text{for ULS:} \quad w_{APA-ULS,e} = w_{ef,e\_ULS} = b_w + 0.5b_f \quad (\text{Eq. 4-34a})$$

$$\text{for SLS:} \quad w_{APA-SLS,e} = w_{ef,e\_SLS} = b_w + 0.5b_f \quad (\text{Eq. 4-34a})$$

$$\text{if } b_f > b_{basic} \quad \text{for ULS:} \quad w_{APA-ULS,e} = w_{ef,e\_ULS} = b_w + 0.25b_{basic} \quad (\text{Eq. 4-35b})$$

$$\text{for SLS:} \quad w_{APA-SLS,e} = w_{ef,e\_SLS} = b_w + 0.25b_{basic} \quad (\text{Eq. 4-35b})$$

\*when the joist clearance exceeds the basic spacing,  $b_f > b_{basic}$ , the tributary width experiences a sharp drop; Equation 4-34a versus Equation 4-34b and Equation 4-35a versus Equation 4-35b. This sharp change of dimension complies with test results (Desler 2002).

---

Estimates of SSP tributary width about exterior joists (L- or C-beams):

- shear lag and plate buckling for  $h \geq 75$  mm one-sided SSP systems and  $h =$  all depth two-sided SSP systems – tensile and compressive skin:

$$\text{for ULS: } w_{APA-ULS,e} = w_{ef,e\_ULS} = b_w + \min b_{ef,e} = b_w + \min \left| \begin{array}{l} 0.5b_f \\ 0.5b_{basic} \end{array} \right| \quad (\text{Eq. 4-36})$$

$$\text{for SLS: } w_{APA-SLS,e} = w_{ef,e\_SLS} = b_w + 0.5b_f \quad (\text{Eq. 4-37})$$

where:  $w$ : tributary width (Figure 4–3) [mm]  
subscripts: APA: APA equation  
                  ULS: for resisting bending stress  
                  SLS: for serviceability (deflection)  
 $b_{basic}$ : basic spacing (Table 4–5) [mm]  
 $h$ : depth of SSP structure (Figure 4–3) [mm]

Table 4–7 summarises the effective contribution of the panels (15-mm F11 plywood and 22-mm Kronoply OSB) of the subject research, using the approximations of the APA method. The tributary width of particleboard panel (AS1859 particleboard) is not addressed by the APA method. Additional specimen parameters of the subject research project, such as the joist spacing ( $b = 375$  and  $500$  mm) and the span ( $L = 3700$  and  $6600$  mm) have also been considered. Before considering any correction, the “basic spacing” estimates give a full contribution of the panels to act compositely with the joists for strength and serviceability limit states; RTW in Table 4–7. From the correction factor,  $K_c$ , as per the findings of Foschi (1969b), a marginal reduction is imposed for the ultimate and services limit states. As for the ratio of allowable stress,  $K_s$ , it imposes a decrease of the permissible stress, about 5.0%, to a 356-mm I-joist element with plywood top panel (APA – The Engineered Wood Association 1990). Interestingly, the modification factors depict contradictory adjustments for decks with plywood skins; for 200-mm I-joist panels,  $K_c$  imposes a higher reduction than  $K_s$  ( $K_c = 0.980$  versus  $K_s = 1.0$ ), whereas for 356-mm I-joist elements  $K_s$  requires a larger decrease than  $K_c$  ( $K_c = 0.994$  versus  $K_s = 0.949$ ).

**Table 4–7: APA method – shear lag and plate buckling obtained under the specimen parameters (panel materials and dimensions) of the subject research**

Panel material	<sup>1</sup> b <sub>f</sub> [mm]	<sup>2</sup> L [mm]	<sup>3</sup> h <sub>f</sub> [mm]	<sup>4</sup> b <sub>basic</sub> [mm]	<sup>A</sup> K <sub>c</sub>	<sup>B</sup> K <sub>s</sub>	<sup>5</sup> TW <sub>ULS</sub> and <sup>6</sup> TW <sub>SLS</sub> [mm]	<sup>C</sup> RTW
	(1)						(2)	<b>(2)/(1)</b>
*F11 plywood	305	<sup>†</sup> 3700	15	695	0.980	1.000	305	<b>1.000</b>
	410	<sup>‡</sup> 6600			0.994	0.949	410	<b>1.000</b>
*Kronoply OSB	305	3700	22	1050	–	1.000	305	<b>1.000</b>
	410	6600			–	1.000	410	<b>1.000</b>
<b>AS1859 particleboard</b>	Not addressed by APA method							

\* panel strength axis parallel to the joists; <sup>†</sup> joist spacing, b = 375 mm; <sup>‡</sup> joist spacing, b = 500 mm.

<sup>1</sup> joist clearance, <sup>2</sup> span, <sup>3</sup> panel thickness, <sup>4</sup> basic spacing (Figure 4–2), <sup>5</sup> skin contribution for bending resistance, <sup>6</sup> skin contribution for deflection.

<sup>A</sup> correction coefficient (Foschi 1969b).

<sup>B</sup> ratio of allowable stress (APA – The Engineered Wood Association 1990).

<sup>C</sup> ratio of tributary width, that is, unsupported skin portion acting compositely with the joist, max.: 1.0.

Note: correction coefficient (K<sub>c</sub>) or ratio of allowable stress (K<sub>s</sub>) may apply (Table 4–6).

#### 4.2.4 Effectiveness ratios of the panel contribution

The effectiveness ratio of the tributary width enables quantification the contribution of the panel – particularly the unsupported portions of the panel – to the composite sections about the joists. It also permits identification the variation between the estimates of the Möhler equation and the approximations of the codes. The depictions allow presentation of the plots of the procedures on single graphs, for example, the Möhler equation versus EC5 approximations. This facilitates the comparison between the methods. For single-span uniformly loaded SSP structures, Möhler, Abdel-Sayed and Ehlbeck (1963) proposed to evaluate the effectiveness ratio by dividing the effective contribution of the panel by the joist clearance (Equation 4-38) and to express this graphically, considering the ratio of the joist clearance and the span ( $b_f/L$ ). Raadschelders and Blass (1995) also employed this graphical display and proposed that in practice, most SSP structures have  $b_f/L$  ratios under 0.3. This value is obtained, for example, with floors that exhibit a 2.0-m span and 600-mm joist clearance. Arguably, ratios between 0.058 (6.0-m span and 350-mm joist clearance) and 0.183 (3.0-m span

and 550-mm joist clearance) encompass most of the situations encountered in domestic housing.

Equation 4-38 depicts the evaluation of the effective contribution of the skin. It applies to interior joists of SSP floors.

$$\frac{w_{Möhler,i} - b_w}{b_f} \quad (\text{Equation 4-38})$$

For this analysis, the estimates of the Möhler equation are used for references and are compared to the approximations of EC5, SIA 164 and APA methods. In order to illustrate the analysis, the EC5 method is presented hereafter (Figures 4–8 and 4–9). In Figures 4–8 and 4–9, the curves with markers correspond to the effectiveness ratios of the Möhler equation and have been obtained with Equation 4-38, whereas the curves without marker express the values of the EC5 method and have been estimated with Equation 4-39.

$$\frac{w_{EC5,ic} - b_w}{b_f} \quad (\text{Eq. 4-39})$$

As mentioned previously, Figures 4–8 and 4–9 enable visualisation and qualification of the differences between both the Möhler equation and EC5 methods. The graphs show that the approaches agree well with low joist clearance to span ratios ( $b_f L \leq 0.1$ ) but diverge significantly with higher  $b_f L$  ratios. Figures 4–8 and 4–9 indicate that the EC5 approximation of the tributary width has a conservative trend compared to the estimate of the Möhler equation. Considering the limit proposed by Raadschelders and Blass (1995), that is,  $b_f L$  ratio equal to 0.3, there are significant deviations between both approaches; for example with plywood, whose effective contribution as per EC5 (ratio of about 0.35) deviates quasi 100% from that of Möhler (ratio of about 0.7). Looking at the upper limit proposed for domestic housing, the deviation between the Möhler equation (ratio of about 0.85) and EC5 approximation (ratio of about 0.55) is still consequent, about 55%. For the other panels, the variations are acceptable, that is, about 12% for oriented strand board and about 5% for particleboard.

With regard to the material parameters of the specimens tested in the subject research, Figure 4–8 shows that the contribution of the compressive panel is firstly governed by the joist spacing (plateaux of the curves) and secondly by the shear lag (asymptotic – exponential decay – portions of the curves). This also indicates that the 100% contribution of the sheathing is initially achieved before decaying severely with increasing  $b_f/L$  ratios. Considering the physical dimensions of the specimens, Figure 4–8 suggests that the full contribution of the skin can be assumed.

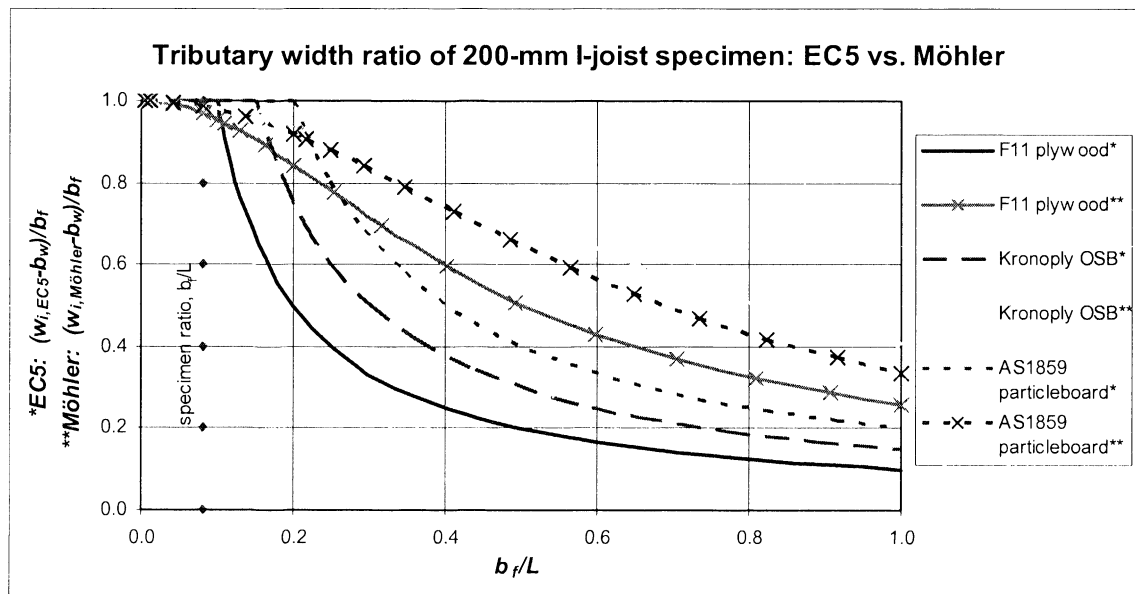


Figure 4–8: Effective contribution of the skins of 200-mm I-joist specimens (EC5 vs. Möhler)

In Figure 4–9, similar patterns to 200-mm I-joist specimens can be observed, whereas for plywood the tributary width is firstly governed by the plate buckling (plateaux of the curve). This indicates that the instability of the plywood panel in compression prevents achievement of 100% contribution of the sheathing. Particleboard was not used to build 356-mm I-joist specimens.

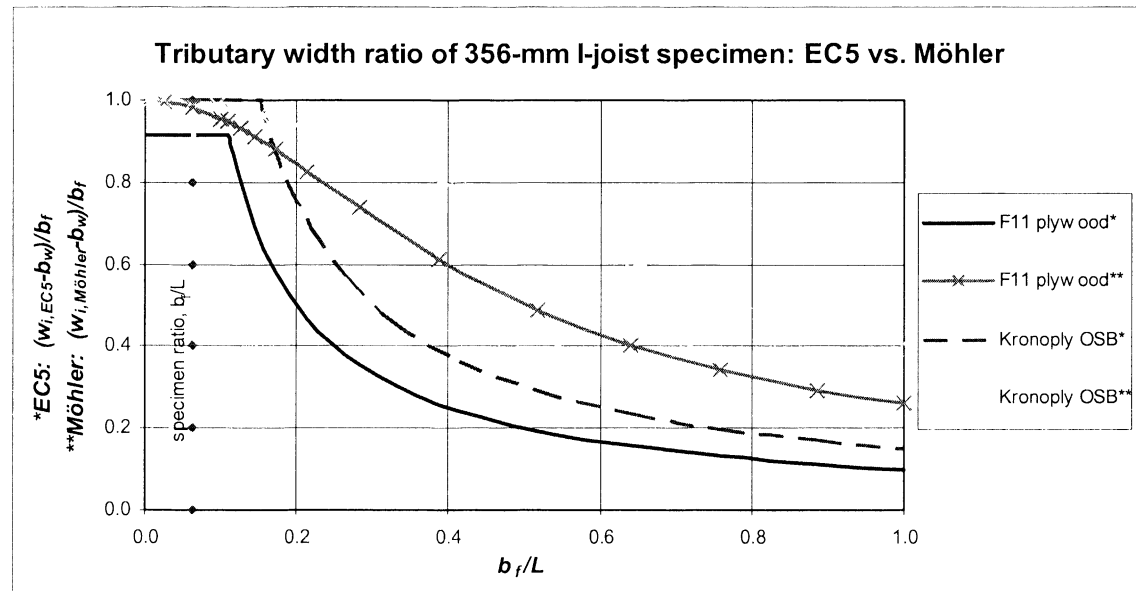


Figure 4–9: Effective contribution of the skins of 356-mm I-joist specimens (EC5 vs. Möhler)

Instead of comparing the estimates of one code versus the Möhler equation, the analysis of the effectiveness ratios can be conducted according to the material of the sheathing. As a means to illustrate this, the analysis presented hereafter focuses on plywood (Figures 4–10 and 4–11). In this analysis, the APA method is not considered, because to determine its effectiveness ratios, the ratio estimates required some adjustments. Looking at the limit indicated by Raadschelders and Blass (1995), that is,  $b_f/L$  ratio of 0.3, the depictions show that the effective contribution as per EC5 and SIA 164 notably disagree with the Möhler equation, the first one (EC5) by about 100% and the second one (SIA 164) by about 40%. Considering the limit proposed for domestic housing ( $b_f/L$  ratio equal to 0.183), the disagreement between the Möhler equation and EC5 estimates corresponds to about 55%, while the variation between the Möhler equation and the SIA 164 approximation reaches about 13%.

For 200-mm I-joist specimens, the graph (Figure 4–10) demonstrates that the approaches disagree marginally at low joist clearance to span ratios ( $b_f/L \leq 0.1$ ), SIA



164 being the most conservative approach. At higher  $b_f/L$  ratios, the disagreement increases and EC5 becomes the most conservative procedure.

Figure 4–10 also illustrates shows that for both code methods, the compressive panel of the specimens is firstly governed by the joist spacing (plateaux of the curves), that is, 100% contribution of the sheathing to the joists, and secondly by the shear lag (asymptotic – exponential decay – portions of the curves), that is, decreasing contribution of the skin(s).

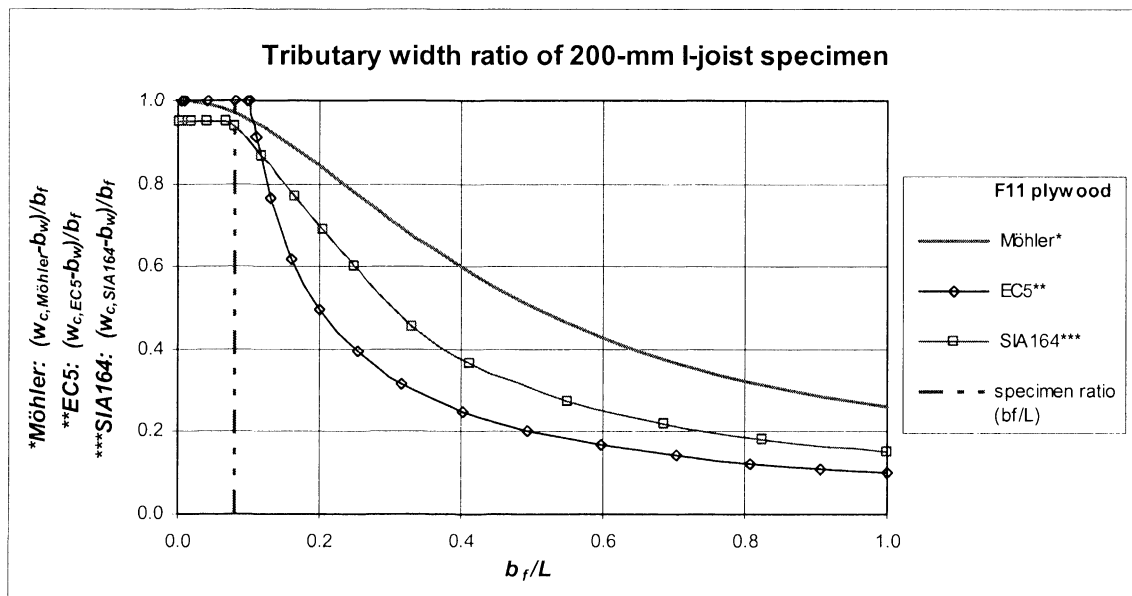


Figure 4–10: Effective contribution of the skins of 200-mm I-joist specimens – plywood

Figure 4–11 demonstrates that the tributary width is firstly governed by the buckling propensity of the plywood panels (plateaux of the curves) with both EC5 and SIA 164 procedures. Furthermore, in Figure 4–11, significant disagreement between the methods is generally identifiable. Only within the range of low joist clearance to span ratios,  $b_f/L \leq 0.1$ , is the deviation between the Möhler equation and EC5 procedure reasonable. Within this similar range, SIA 164 disagrees very significantly and is much more conservative than the Möhler equation. Elsewhere, the contribution of the panels is controlled by the shear lag (asymptotic – exponential decay – portions of the curves) and both code methods are more conservative than the Möhler equation; EC5 becoming more conservative than SIA 164 in the tail of curves.

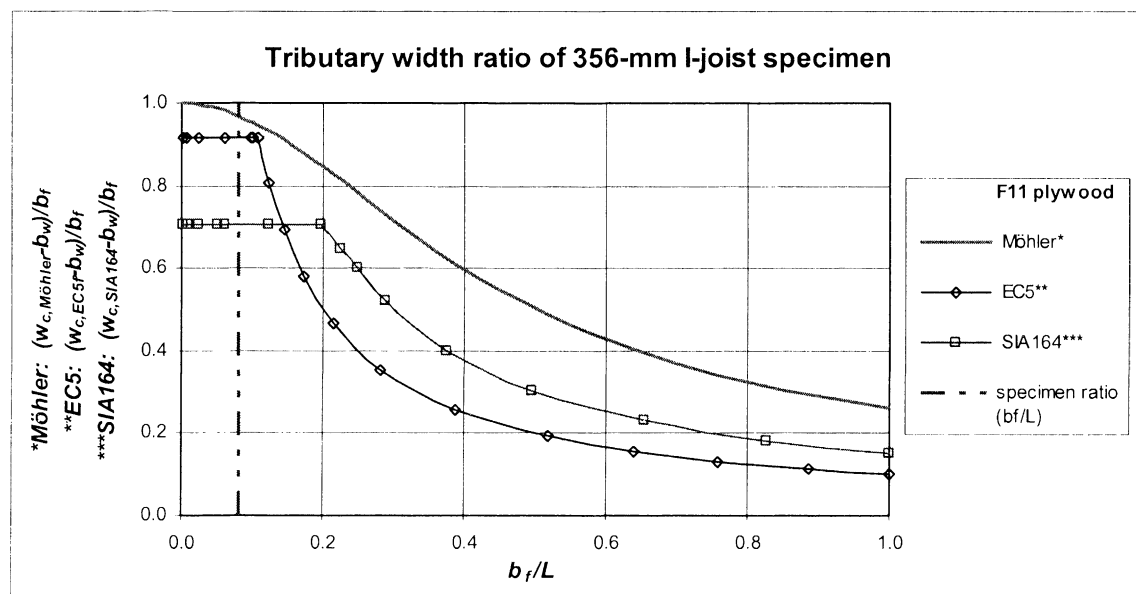


Figure 4–11: Effective contribution of the skins of 356-mm I-joist specimen – plywood

Further depictions of this analysis of the effectiveness ratios are also presented in Appendix 1.

#### 4.2.5 Concluding summary on the tributary width

In SSP, the tributary width is important for the estimate of the section properties of the composite beams in which it forms the flange(s). Accurate assessment of the magnitude may prove expensive in calculation, therefore approximates from the codes are mostly used. Different procedures for the estimates of the tributary width have been considered and analysed under the conditions of the full-scale deck specimens of the subject

research. This analysis has indicated that generally the procedures of the codes (EC5 (European Committee for Standardisation 1995) and SIA 164 (Société Suisse des Ingénieurs et Architectes 1992) methods) or guidelines (APA method (APA – The Engineered Wood Association 1990; Desler 2002; McLain 1999)) permit approximating the tributary width reasonably well; with acceptable accuracy for safe design of SSP floors.

Table 4–8 summarises the magnitude of the sheathing contributions produced by each method, considering the parameters – materials and physical dimensions – of the specimens of the subject research. The values of EC5 are used hereafter in the subject research because of the absence of guidelines in AS 1720.1–1997 (Australian Standard™ 1997).

**Table 4–8: Summary of the tributary widths according to the specimen parameters (materials and physical dimensions) of the subject research**

Panel material	Joist spacing [mm]	Tributary width [mm]						
		Möhler	EC5		SIA 164		APA	
			<sup>A</sup> T	<sup>B</sup> C	T	C	<sup>C</sup> ULS	<sup>D</sup> SLS
* F11 plywood	<sup>†</sup> 375	365.5	375.0	375.0	355.2	355.2	375.0	375.0
	<sup>‡</sup> 500	492.6	500.0	465.0	490.1	379.6	500.0	500.0
* Kronoply OSB	375	371.6	---	375.0	---	355.2	375.0	375.0
	500	497.4	---	500.0	---	490.1	500.0	500.0
AS1859 particleboard	375	370.5	---	375.0	---	355.2	---	---

\* panel strength axis parallel to the joists; joist spacing for <sup>†</sup>200-mm and <sup>‡</sup>356-mm I-joist specimen.

<sup>A</sup>tensile side; <sup>B</sup>compressive side; <sup>C</sup>for design strength; <sup>D</sup>for serviceability design.

Investigating the effectiveness – the latter being measured by the ratio of the tributary width to the joist clearance – has shown that for SSP structures with joist clearance to floor span ratios under about 0.1, the full panel(s) contribute(s) to the joists. For higher ratios, the contribution of the sheathing is less than 100%. This analysis has also indicated that, in situations where the joist clearance to floor span ratio ( $b_{fj}L$ ) is less or equal to about 0.1, the estimates of the Möhler method and code procedures tally well, whereby the results of Möhler equation are assumed as the benchmarks. In other situations, where the ratio exceeds 0.1, the codes generally produce tributary widths of more conservative magnitude than the Möhler method. However, it can be concluded

that the code guidelines permit estimating the tributary width acceptably for SSP structures with common dimensions, that is, for SSP systems whose  $b_f / L$  ratios are comprised between 0.058 and 0.183.

### 4.3 CAPACITY UNDER GRAVITY LOAD

In most situations, SSP decks are in flexural conditions. This generates bending, normal and/or shear stresses in the members of the floor structure. As result, the strength properties of the members, especially the panel(s), are used optimally. Because the joists and sheathing act compositely, the greatest portion of the bending stress is taken by the panel(s), while the joists take the shear stress (Desler 2002). Elsewhere, Foschi (1969b) and Ozelton and Baird (2002) proposed that mostly normal stresses can be found in the sheathing, while Gerber and Sigrist (2002) proposed that considering combined normal and bending stresses at the axial fibre of the skin(s) corresponds to more accurate assumption. Further, normal and rolling shear stresses are particularly significant for the integrity of the interlayers and, incidentally, the composite action. Shear failure may also appear inside the sheathing (Desler 2002; McLain 1999).

The procedure of the stress verification across SSP composite – floor system in flexural conditions – is variedly treated by the design procedures, especially with regard to the skin(s). For example, EC5 (European Committee for Standardisation 1995) imposes that the flanges should satisfy the requirements of axial stresses at the centre fibre of the skin(s). Meanwhile, AS 1720.1–1997 (Australian Standard<sup>TM</sup> 1997), SIA 164<sup>d)</sup> (Société Suisse des Ingénieurs et Architectes 1992) and the APA method (Desler 2002; McLain 1999) require that the (extreme fibre of the) flanges should be designed to resist bending stresses. Elsewhere, Gerber and Sigrist (2002) proposed that, in order to account for the actual action experienced by the skin(s) thoroughly, the latter should be verified considering the combination of axial and bending actions that occur at the centre fibre of the skin(s). However, they also reported that verifying the bending and axial stress at respectively the extreme and centre fibres of skin(s) represents an acceptable approximation.

---

<sup>d)</sup> Indicative only, SIA 164 is superseded by SIA 265 (Société Suisse des Ingénieurs et Architectes 2003).

Figure 4–12 depicts the locations – along the depth of the SSP composite – where the stresses should be verified. This depiction presents a specimen of the subject research, that is, composite about an interior joist. It shows that the use of I-joists for the “webs” in the SSP construction imposes additional stress verifications. More detailed information about the specimens of the subject research is reported in Chapter 3 in Part 2.

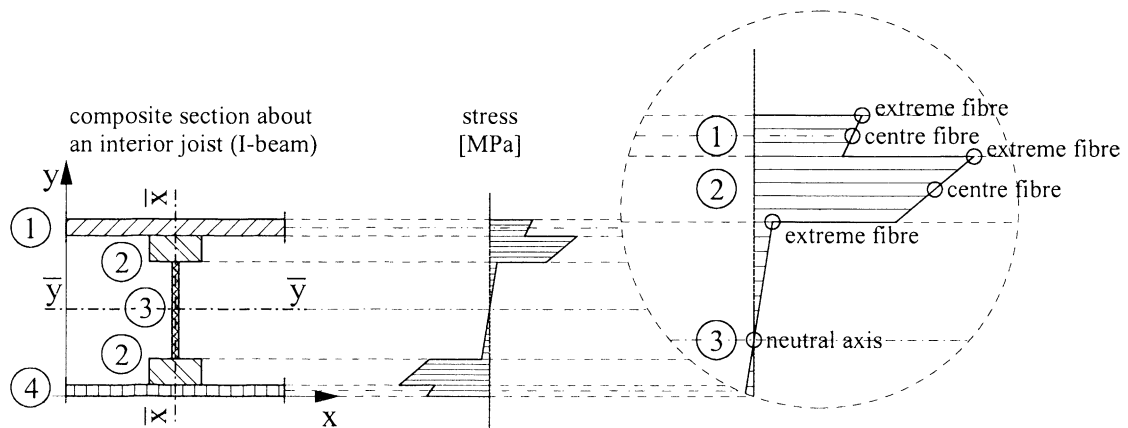


**Figure 4–12: Stress verifications of SSP system (specimen of the subject research)**

Table 4–9 summarises the stresses that should be verified, respectively imposed and/or recommended for the design of SSP systems. It exhibits that the design procedures, as mentioned previously, disagree on the actions – type and/or location – that are critical for SSP floors. In order to preserve the legibility of the table, Table 4–9 focuses on stringers with “rectangular” section. The verifications that may be imposed on more complex/composite stringers, such as I-joists, are treated in Table 4–10.

**Table 4–9: Stress verifications of SSP system**

Location of the stress verification		*Type of stress			
		EC5	AS 1720.1–1997 and SIA 164	†APA method	Gerber and Sigrist (2002)
Upper skin	Extreme fibre		Bending	Bending	Bending
	Centre fibre	Axial			Axial
	‡Plywood 1 <sup>st</sup> glue line			Rolling and planar shear	
Upper interlayer		Fastener load	Rolling shear	Rolling and planar shear	Rolling and planar shear
§Stringer	Upper extreme fibre	Axial	Bending	Bending	Bending
	Neutral axis	Shear	Shear	Shear	Shear
	Lower extreme fibre	Axial	Bending	Bending	Bending
Lower interlayer		Fastener load	Rolling shear	Rolling and planar shear	Rolling and planar shear
Lower skin	‡Plywood 1 <sup>st</sup> glue line			Rolling and planar shear	
	Centre fibre	Axial			Axial
	Extreme fibre		Bending	Bending	Bending

\*for single-span simply supported SSP system in flexural state, †including the necessary panel and/or joist splices (McLain 1999). ‡glue line between the inner face of the first ply and the adjacent ply, §more complex/composite stringer, for example, I-joists, may require further verifications (in Table 4–10).

As mentioned previously, I-joists are used for the stringers of the full-scale specimens of this project. This imposes additional verifications on the stringers than those described in Table 4–9. For I-joists, the design comprises verifying the bending (extreme fibre) and normal (centre fibre) stresses in the flanges, rolling shear in the web-to-flange connections (tongue-and-groove), and bending (both extreme fibres) and shear stresses in the web (neutral axis) (Table 4–10).

**Table 4–10: Stress verifications of I-joist cross-section**

Location of the stress verification in cross-section		*Type of stress
Upper flange	Extreme fibre	Bending
	Centre/axis fibre	Compression
Upper web-to-flange interlayer		Rolling shear
Web	Upper extreme fibre	Bending
	Neutral axis	Shear
	Lower extreme fibre	Bending
Lower web-to-flange interlayer		Rolling shear
Lower flange	Axial fibre (skin axis)	Tension
	Extreme fibre	Bending

\* for single-span simply supported joist in flexural state.

The analysis of the SSP system capacity under gravity loads is completed by comparing the characteristic/permissible stresses to those experienced by the structure. The generic formulae for determination of these characteristic/permissible stresses are provided by the respective codes/and procedures (Australian Standard<sup>TM</sup> 1997; Desler 2002; European Committee for Standardisation 1995; McLain 1999).

#### 4.4 SPLICING REQUIREMENTS

Generating skin continuity may be desirable to achieve structural economies. In order to attain this, skin splicing must be capable of transferring the forces occurring in the skins(s). Splicing techniques are tongue-and-groove, scarf jointing, and butt jointing with splice plate. A well-made splicing of the latter technique can reach up to 90% of the strength of plywood panel (Timber Research and Development Association).

As mentioned previously, a reasonable assumption is that, for SSP under bending conditions, the skin is in pure compression and tension (Ozelton & Baird 2002).

Another sound postulation is that in compression conditions most of the normal forces are transmitted by contact directly between the skin segments.

Splicing may be located randomly in SSP decks. However, Ozelton and Baird (2002) proposed that they must be designed assuming that they are located in the maximum bending zone. Two checks are imposed on skin splicing (McLain 1999; Ozelton & Baird 2002); the cross-section of the splice plate must resist the tensile or compression stress applied (Equations 4-40a and b) and the glue line between the splicing plate and the skin panels should not exceed the permissible shear stress. Alternatively, the dimension of the splicing plate can be estimated with Table 4–11 (APA – The Engineered Wood Association 1997).

Normal stress in splice plate:

$$\frac{\phi N_{t,d}}{A_{t-plate}} = \frac{\phi N_{t,d}}{h_{f,t} b_f} \leq f_{t,k} \quad (\text{Eq. 4-40a})$$

$$\frac{\phi N_{c,d}}{A_{c-plate}} = \frac{\phi N_{c,d}}{h_{f,c} b_f} \leq f_{c,k} \quad (\text{Eq. 4-40b})$$

where:  $\phi$  capacity factor (refer to Clause 2.3 in AS 1720.1–1997 (Australian Standard<sup>TM</sup> 1997))

N: normal force [N]

A: area of the cross-section of the splice plate [m<sup>2</sup>]

h<sub>f</sub>: thickness of the panel [m]

b<sub>f</sub>: joist clearance [m]

f: permissible tension stress [Pa]

subscripts: t: tension

c: compression

||: parallel to grain/strength axis

Shear stress in the interlayer:

$$\frac{\phi N_d}{A_{contact}} = \frac{\phi N_d}{l_s b_f} \leq f_{v,k} \quad (\text{Eq. 4-41})$$

where:  $\tau$ : shear stress [Pa]

l<sub>s</sub>: length of splice [m]

(note: actual length of the splice plate is: l<sub>plate</sub> = 2l<sub>s</sub> )



**Table 4–11: Length of splicing plate (APA – The Engineered Wood Association 1997)**

Plywood thickness [mm]	Note	Length of splice plate, $l_{\text{plate}}$ [mm]
6.4		152.4
7.9		203.2
8.7	<i>sanded</i>	254.0
9.5	<i>sanded</i>	
9.5	<i>unsanded</i>	304.8
11.9		355.6
12.7		
15.1		406.4
15.9		
18.3		
19.1		

#### 4.5 VERIFICATION OF BUCKLING CAPACITY

Under the assumption stated previously: in flexural conditions, normal stresses parallel to the joists are generated in the skin(s) of SSP decks (Foschi 1968, 1969a, 1969b; Ozelton & Baird 2002) and the skin on the compression side of the SSP element may be prone to buckling. Buckling is a complex phenomenon. A multitude of parameters influences the behaviour of elements under compression, that is, section properties, material and boundary conditions. In SSP, the latter might prove difficult to predict. Studying buckling in depth is beyond the scope of the subject research. The present chapter only introduces general principles of buckling theory and presents guidelines and statements valid for SSP decks.

The theory of plates is certainly the most appropriate way to approach buckling that is problematic in SSP composites. Thorough descriptions and development of the theory of plates, buckling of plates and/or stability of structures can be found in many books, for example, by Girkmann (1954), Timoshenko and Woinowsky-Krieger (1959), Timoshenko and Gere (1961), Timoshenko and Goodier (1987), etc. These books present a broad and general approach on plate behaviours. Research reports, journal articles and papers “more wood related” are also available, for example, from Seydel (1930), Blumrich (1942), Thielemann (1950), Möhler, Abdel-Sayed and Ehlbeck (1963), Zahn and Romstad (1965), von Halász and Cziesielski (1966), Foschi (1968; 1969a), Moody, Hernandez and Liu (1999), etc. These valuable contributions allow

better understanding of the behaviour of wood plates, with focus on plywood, and provide tools to perform a detailed analysis of buckling.

In the case of SSP, the buckling propensity of the skin is related to the orientation of the sheathing according to the joists, because it affects the stress distribution in the decking (Foschi 1969a).

However, for SSP elements, simple rules and/or guidelines exist that help to determine the buckling stability. After Ozelton and Baird (2002), tests showed that whenever the members of an SSP deck have “normal” proportions, that is, panel thicknesses and joist spacing, skin buckling is unlikely. Implementing EC5 guidelines, that is, designing in satisfaction of the shear lag and plate buckling conditions, permits avoidance of buckling instability. Furthermore, Raadschelders and Blass (1995) proposed that buckling of the compressive skin is avoided whenever the clear spacing is less than twice the permissible effective flange width.

An alternative to tedious analysis of buckling stability is described by Baird and Ozelton (1984). This analysis calls upon the critical load,  $N_{cr}$ , of the first buckling mode for an ideal elastic skin (Equation 4-42). To some extent, it is related to Euler’s theory of buckling<sup>e)</sup> for an ideal elastic column (Gere & Timoshenko 1997).

$$N_{cr} = \frac{eK_{cr}}{(b_f L)^2} * h_f b_f \quad (\text{Eq. 4-42})$$

\*  $h_f$  of compression skin

in which:

$$e = \frac{2h - h_{f,u} - h_{f,l}}{2} \quad (\text{Eq. 4-43})$$

where: $N_{cr}$ :	critical normal load	[N]
$e$ :	refer to Equation 4-43	[m]
$K_{cr}$ :	buckling coefficient	[Nm]
$b_f$ :	joist clearance (Figure 4-3)	[m]
$L$ :	span	[m]
$h$ :	depth of SSP structure (Figure 4-3)	[m]

<sup>e)</sup> Euler's equation for buckling:

$$P_{cr} = \frac{\pi^2 EI}{L^2} \quad (\text{Eq. 4-44})$$

where:  $P_{cr}$  is the critical normal load [kN],  $EI$ : flexural stiffness of the skin section [kNm<sup>2</sup>],  $L$ : length [m].

$h_{f,u}$ :	thickness of the upper panel (Figure 4–3)	[m]
$h_{f,l}$ :	thickness of the lower panel (Figure 4–3)	[m]

The buckling coefficient,  $K_{cr}$ , varies for each material and thickness, the support conditions and to some extent the load introduction. In a table, Baird and Ozelton (1984) indicated the buckling coefficients for Douglas Fir-faced plywood. Critical buckling loads for Douglas Fir plywood were also published elsewhere (Foschi 1969a). For other panel materials, buckling data are scarce.

In the subject research, the full-scale specimens comply with EC5 guidelines and comments:

- the shear lag and plate buckling conditions are fulfilled (for one case, 356-mm I-joist specimens with 15-mm F11 plywood compression skin, the plate buckling determines the contribution of the compression skin).
- the clear spacing is always less than twice the tributary width of the skin.

#### 4.6 VERIFICATION OF THE SERVICEABILITY – DEFLECTION

Many design codes and guidelines impose maximum deflection at mid-span. Often, the deflection limit is expressed by ratios of the span (Equation 4-45), and some codes may consider instantaneous and/or long-term requirements.

$$u_{\max} = \frac{L}{d_{\lim}} \quad (\text{Eq. 4-45})$$

where:	$u_{\max}$ :	maximum deflection	[m]
	L:	span	[m]
	$d_{\lim}$ :	limitation coefficient of the deflection	[ – ]

In Australia, AS/NZS 1170.0:2002 (Australian/New Zealand Standard™ 2002b) imposes a limitation coefficient of 300 in order to control the sagging of the floor structure. Load cases comprise permanent load and imposed actions (live load).

Differential equations form the basis in the procedure used to analyse the deflection of SSP decks. Equation 4-46 is the generic differential equation for prismatic flexural beams and refers to the bending moment equation. Abundant literature addresses this topic, for example, Beer and Johnston (1992), Gere (2004), Gere and Timoshenko (1999).

$$M = EI \frac{d^2u}{dz^2} = EIu'' \quad (\text{Eq. 4-46})$$

where: M:	bending moment	[Nm]
E:	modulus of elasticity	[Pa]
I:	second moment of area of the section	[m <sup>4</sup> ]
u:	deflection	[m]
z:	longitudinal axis, that is, distance along the span	[m]

Successive integrations of Equation 4-46 enable production of:

- with the first integration, the slope of the deflection curve.
- with the second integration, the magnitude of the deflection curve.

In the subject research, the full-scale specimens are built with I-joists. In order to consider the shear deformation that is inherent to such composite joists, the principle of virtual work was used to estimate the deflection (Equation 4-47). The principle of virtual work is amply presented in the literature, for example Carpinteri, (1997), Ghali and Neville (1989), Schneider (1994), and Timoshenko and Young (1968).

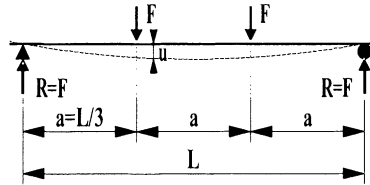
$$u = \int \frac{Mm}{EI} dz + \kappa \int \frac{Vv}{GA} dz \quad (\text{Eq. 4-47})$$

where: u:	deflection	[m]
M:	“real load” bending moment	[Nm]
m:	“virtual load” bending moment	[m]
V:	“real load” shear force	[N]
v:	“virtual load” shear force	[–]
E:	modulus of elasticity	[Pa]
I:	second moment of area of the section	[m <sup>4</sup> ]
G:	shear modulus	[Pa]
A:	area of the section	[m <sup>2</sup> ]
κ:	coefficient of the section – geometry modification factor	[–]
z:	longitudinal axis, that is, distance along the span	[m]

After integration and arrangement of Equation 4-46 and the consideration of the shear deflection (Equation 4-47), it is possible to produce the deflection equations for four-point bending (Equations 4-48a and b) and three-point bending (Equations 4-49a and 4-50a) conditions. These engineering principles have been chosen because they correspond to the set-ups studied during the laboratory investigation on full-scale SSP

elements. With Equations 4-48c, 4-49b and 4-50b, the maximum deflection,  $u_{max}$ , can be estimated.  $u_{max}$  is located at mid-span, thus it coincides with  $u_C$  (mid-span deflection).

Four-point bending (third-point loading):



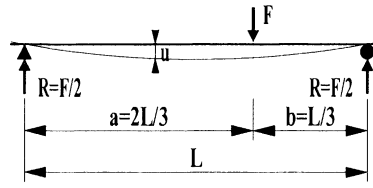
$$u = \frac{Fz}{12EI_T} \left( \frac{2L^2}{3} - z^2 \right) + \kappa \frac{Fz}{2GA_T} \quad 0 \leq z \leq a \quad (\text{Eq. 4-48a})$$

$$u = \frac{FL}{324EI_T} \left( -L^2 + 27Lz - 27z^2 \right) + \kappa \frac{FL}{6GA_T} \quad a \leq z \leq \frac{L}{2} \quad (\text{Eq. 4-48b})$$

$$u_{max} = u_C = \frac{23FL^3}{648EI_T} + \kappa \frac{FL}{6GA_T} \quad z = \frac{L}{2} \quad (\text{Eq. 4-48c})$$

where: u: deflection [m]  
 F: load [N]  
 z: longitudinal axis, that is, distance along the span [m]  
 L: span [m]  
 subscript: T: transformed-section

Three-point bending (third-point loading):



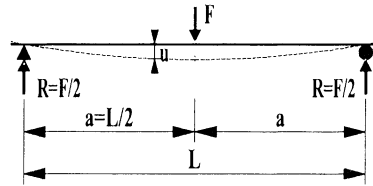
$$u = \frac{Fz}{18EI_T} \left( \frac{8L^2}{9} - z^2 \right) + \kappa \frac{Fz}{3GA_T} \quad 0 \leq z \leq \frac{L}{2} \quad (\text{Eq. 4-49a})$$

$$u_C = \frac{23FL^3}{1296EI_T} + \kappa \frac{FL}{6GA_T} \quad z = \frac{L}{2} \quad (\text{Eq. 4-49b})$$

$$u_{\max} = \frac{F}{27\sqrt{3}EI_T} \left( \frac{8L^2}{9} \right)^{\frac{3}{2}} + \kappa \frac{FL}{6GA_T} \quad z = \left( \frac{8L^2}{27} \right)^{\frac{1}{2}} \quad (\text{Eq. 4-49c})$$

*NOTE: the mirror of this loading arrangement is needed to complete the set of principles investigated in the course of the laboratory tests of the subject research, that is, the load is applied at the third of the span. Thus,  $a = L/3$  and  $b = 2L/3$ .*

Three-point bending (centre-point loading):



$$u = \frac{Fz}{48EI_T} (3L^2 - 4z^2) + \kappa \frac{Fz}{2GA_T} \quad 0 \leq z \leq \frac{L}{2} \quad (\text{Eq. 4-50a})$$

$$u_{\max} = u_C = \frac{FL^3}{48EI_T} + \kappa \frac{FL}{4GA_T} \quad z = \frac{L}{2} \quad (\text{Eq. 4-50b})$$

Because the subject research focuses on the instantaneous deflection, the long-term behaviour has not been studied. However, in practice it forms an important aspect of the design of floors. In order to integrate long-term or creep effect, the codes suggest introducing a modification factor onto the instantaneous deflection. This procedure aims to account for the polymeric nature and/or viscoelastic properties of wood. Therefore,

the value of the modification factor varies according to the duration of the load, the moisture conditions of the wood element and/or the climate conditions of the structure environment.

#### **4.7 VERIFICATION OF THE SERVICEABILITY – VIBRATION**

Vibration of floors appears to be an important criterion of acceptance by the floor users (Sherwood & Moody 1989). Therefore, it may prove a critical and limiting condition for the design of floor systems (Foschi et al. 1999). Studying the dynamic behaviour of SSP systems is beyond the scope of the subject research, which focuses on the static response of SSP specimens. As such and even though vibration could be problematic for SSP decks – gluing may cause a light increase of the natural frequency of the floor, which might consequently vibrate as a diaphragm (Polensek 1971) – the vibration responses of the specimens were not investigated. The present chapter introduces general statements valid for SSP decks and AS/NZS 1170.0:2002 guidelines (Australian/New Zealand Standard™ 2002b) and EC5 (European Committee for Standardisation 1995) recommendations to the designers.

Together with the deflection under point load, the natural frequency is good indicator of the serviceability of floor systems (Chui et al. 2004). However, if the first is fairly straightforward to estimate, approximating the second and successive vibration responses may prove more problematic because of the multitude of parameters that needs to be considered and the uncertainties/unknowns surrounding lightweight timber floors. Furthermore, the perception of vibrations is subjective for the users, therefore hard to interpret (Smith 2003), for example, studies on floor toppings showed that they enhanced static stiffness and modal damping (Hu, Chui & Smith 1998; Taylor & Hua 2000), but sometimes with negative effects on the users' perception (Taylor & Hua 2000). Although damping in wood-based floors is not known, it appears that damping may be attributed to the materials and construction of the floor, including the supports (Hu 2002). Polensek (1971; 1973) proposed that friction between the members of the floor assemblies (between joists and sheathing, between superimposed layers) is the most important source of damping. However, glued connections – presumably rigid – have a minor effect on the damping (Polensek 1971; 1973). Smith (2003) proposed that adequate blocking or cross-bracing enables improvement of the floor sufficiently in order to avoid problems.

In AS/NZS 1170.0:2002 (Australian/New Zealand Standard<sup>TM</sup> 2002b) and EC5 (European Committee for Standardisation 1995), the analysis of the vibration responses of residential floors is part of the serviceability limit state. In Australia, AS/NZS 1170.0:2002 proposes that if the criterion – mid-span deflection between 1.0 to 2.0 mm under a 1.0 kN point load at mid-span – the floor structures should not experience vibration problems. If the criterion is not satisfied, AS/NZS 1170.0:2002 recommends a thorough analysis examination. Elsewhere, EC5 gives a procedure for floors with a fundamental frequency not lower than eight Hertz, and requirements to satisfy. For floors with smaller fundamental frequency, EC5 requires a special investigation. Details about the EC5 procedure can be found in the code.

Based on the review of existing literature (refer to Chapter 2 in Part 1) and design codes for timber structures, as presented in this chapter, there appear to be few recommendations to assist with the design aspects of SSP constructions, such as the interlayers and the skin splicing. Therefore, it is necessary to undertake further research into these assemblies (refer to Chapter 2 in Part 2) prior to developing a testing program for “full-scale” SSP elements (refer to Chapter 3 in Part 2). Investigating full-scale SSP elements is indispensable for understanding the serviceability and ultimate performance of SSP systems. Key outcomes from the analyses of the laboratory testing, such as the deflection response, the lateral load distribution and the composite properties, are presented in Chapters 4 to 6 in Part 2.

The experimental data also provides the benchmarks/controls necessary for the development, parameterisation and validation of the mathematical and finite element models. Descriptions of both models are presented in Chapters 5 and 6 in Part 1 respectively. In addition, these data are used to develop and substantiate the empirically based aspects of the design procedure (refer to Chapter 7 in Part 1).



<b>5</b>	<b>GRILLAGE MODEL .....</b>	<b>103</b>
<b>5.1</b>	<b>Development and construction of the grillage model .....</b>	<b>104</b>
5.1.1	Model concept.....	104
5.1.2	Simulation principle.....	106
5.1.3	Construction principle of the grillage model .....	106
5.1.4	Beam elements .....	107
5.1.5	Derivation of the stiffness matrix of the girders and crossbeams .....	108
5.1.6	Static condensation of the stiffness matrix of the girders and crossbeams ...	110
5.1.7	Boundary condition of the grillage members.....	112
5.1.8	Superposition technique – stiffness matrix of the grillage structure.....	114
<b>5.2</b>	<b>Definition of the attributes of the grillage model .....</b>	<b>115</b>
5.2.1	Apparent stiffness of the girders .....	115
5.2.2	Apparent stiffness of the crossbeams.....	116
<b>5.3</b>	<b>Load introduction .....</b>	<b>119</b>
<b>5.4</b>	<b>Solution of the grillage model .....</b>	<b>120</b>
<b>5.5</b>	<b>Application of the grillage model to the specimens of the subject research .....</b>	<b>121</b>
5.5.1	Modelling principle – application to the specimens of the subject research	121
5.5.2	Material properties of the members of the grillage model.....	123
<b>5.6</b>	<b>Computer solution routine .....</b>	<b>124</b>
5.6.1	Concept .....	124
5.6.2	Working with the routine .....	124
<b>5.7</b>	<b>Parameterisation of the grillage model .....</b>	<b>125</b>
5.7.1	Concept of the parameterisation .....	125
5.7.2	Benchmarks of the parameterisation.....	125
5.7.3	Key outcomes of the parameterisation.....	126
5.7.3.1	Distribution of uniformly distributed line loads .....	126
5.7.3.2	Attribute of the crossbeam .....	127
<b>5.8</b>	<b>Evaluation of the capability of the grillage model.....</b>	<b>130</b>
<b>5.9</b>	<b>Introducing skin discontinuity(ies) in the grillage model.....</b>	<b>145</b>
<b>5.10</b>	<b>Concluding summary.....</b>	<b>152</b>

## 5 GRILLAGE MODEL

Accommodating SSP systems into a numerical model is a multi-dimensional challenge because they are highly complex, orthotropic, statically indeterminate and multi-layer assemblies. Polensek et al. (1972) described wood-joist floors as “complex, statically indeterminate systems”, and proposed that the structural model of a wood-joist floor can be categorised as anisotropic plate-membrane (sheathing) reinforced by a set of equidistant ribs (joists). Elsewhere, Vanderbilt et al. (1974) described wood-joist systems as “multilayered orthotropic planar structures, with interlayer slip, varying material properties, and complicated articulations of joints”. Furthermore, each member/component of the floor system can exhibit viscoelastic and non-linear behaviour under certain conditions. In addition to this, structural timber/solid wood lengths – such as those of the flange of the I-joist used in the subject research – exhibit notable variability because they are randomly affected by natural growth characteristics, which can be described as “defects” in terms of uniform structural performance. The use of I-joists in the specimens of the subject research further increases the complexity of the SSP systems, thus rendering the modelling more difficult.

This chapter describes and discusses the concept, development and capability of a grillage model constituted of orthogonally arranged girders and crossbeams. It aims at simulating/predicting the behaviour of SSP structures for uniformly distributed and concentrated point loadings. It is based on the small displacement theory for linear structural systems, in which the principle of superposition holds. The longitudinal properties of the model are characterised by those of the girders, while orthogonal ones are related to the crossbeam characteristics. The latter, which determine the intensity of

the two-way action – capability of lateral load distribution, can be related to the physical aspects – box/open – of the SSP section. In the model, it is also assumed that the glued interfaces – the connection between the I-joists and the skin(s) – are continuous and exhibit homogeneous strength. Further assumptions are that the girders and crossbeams are fully composite (strain distribution over the depth of the SSP system is linear), and that each layer of the SSP system experiences an identical radius of curvature. The model solution embraces the range of working load, within which SSP structures are anticipated to work linear-elastically.

## **5.1 DEVELOPMENT AND CONSTRUCTION OF THE GRILLAGE MODEL**

### **5.1.1 Model concept**

Grillage models fundamentally correspond to conglomerates of joists/girders and crossbeams. Generally, the grillage members are orthogonally arranged and connected together with mechanical fasteners. With such connections, vertical displacements are constrained, whereas rotations are not blocked. Subsequently, the joists and crossbeams are subdivided into a number of finite elements. Grillage theory is abundantly available in the literature. For the current research, the theoretical background of the model development can be found in Ghali and Neville (1989).

Panellised wood floor systems can be modelled as grillages, in which the joists constitute the longitudinal girders and strips of the sheathing(s) form the crossbeams. For panellised sheathing, Wilfred (2003) proposed that the effective width of the crossbeams should be equal to 1.4 to 2.0 times the joist spacing. Furthermore, in conventional floors, the characteristics of the interlayers between the joists and the sheathing(s) – use of mechanical fasteners – comply with the fundamental grillage principle.

In the subject research, a grillage model is extended in order to accommodate the complexity of SSP systems. In this approach, the cross-section about the joists, for example, in box-section constructions, C- and I-profile (Figure 5–1) about the exterior and interior joists respectively, form the longitudinal girders, while “slices” (perpendicular to the longitudinal axis) of the specimen constitute the crossbeam(s) (Figure 5–2).

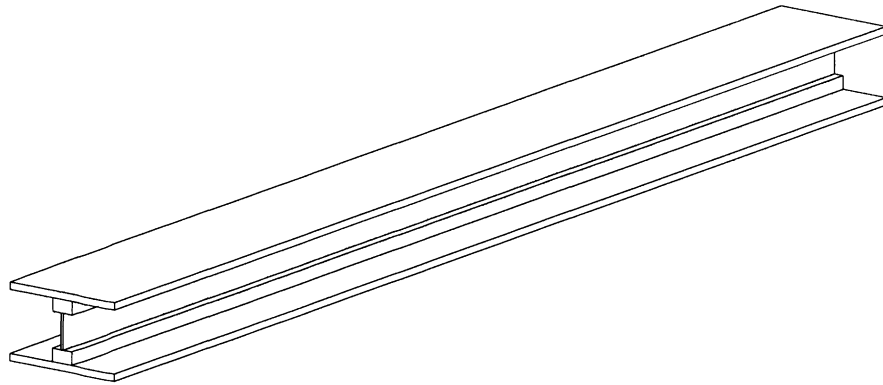


**Figure 5-1: Longitudinal girder about an interior joist (I-profile)**

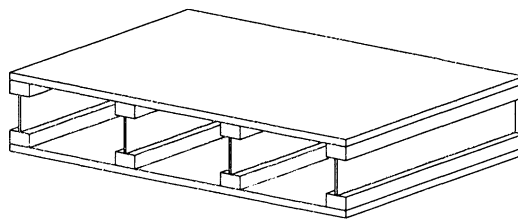


**Figure 5-2: Crossbeam – slice of the floor system**

In SSP assemblies, the joists and sheathing(s) are structurally glued together. This indicates that the interlayers exhibit enhanced mechanical properties, that is, higher stiffness and strength. Consequently, major portions of the torsion propensity between the joists and the sheathing(s) are impeded, resulting in an increase of the section torsional resistance. It is therefore anticipated that this constraint increases the perpendicular stiffness of the floor assembly. The current model attempts to accommodate the rotational restraint.

The effect of the rotational restraint can be significant for box-section SSP systems in particular. Furthermore, considering the specimens of the current research, in which I-joists are used, significant shear deformation occurs. Secondly, the properties of the flange-web connections – web glued in grooves carved in the flanges – exhibit weak torsional restraint.

### 5.1.2 Simulation principle

The grillage simulation of the grillage structure employs the superposition/assembly of three types of finite/beam elements, which are the main contributors to the stiffness matrix of the grillage structure system. Because there is no moment acting on the grillage model, the stiffness matrix considers vertical degrees of freedom (DOFs), whereby the rotational DOFs of the system are statically condensed out. With this technique, the number of DOFs is significantly reduced and the computing time is shortened. Furthermore, this procedure enables optimising the computing phase considerably, that is, the model becomes less demanding in terms of computer resources, that is, machine specifications (processor speed, RAM, etc.) and time.

Following the simulation process for the grillage structure, the deflection of the individual girder is computed by solving the force-deflection relationship of the system using simultaneous algebraic equations. Consequently, the solution renders the computation results using the small displacement method (Ghali & Neville 1989).

### 5.1.3 Construction principle of the grillage model

Constructing the grillage model requires three steps. Each step expresses the model expansion from the fundamental elements to the interacting grillage. The three levels of model construction are described hereafter:

(1) Segment level, whereby element stiffness matrices of the beam/finite elements are defined as commonly found in text books, for example, Ghali and Neville (1989).

(2) Girder and crossbeam level, whereby the stiffness matrices of these grillage members are assembled using the superposition method, that is, vectorially superposing the element stiffness matrices. At this level, the rotational degrees of freedoms are condensed out.

(3) Grillage structure level, whereby the stiffness matrix of the SSP deck is determined using a technique similar to that in (2). However, at the deck level, the stiffness matrices of the girder and cross beam are used. Boundary conditions are at that point applied into the equilibrium equation of the grillage structure.

### 5.1.4 Beam elements

For simulating SSP systems, the construction of the grillage model requires three fundamental beam – finite – elements. As indicated previously, the torsional rigidity of the grillage structure is included in the apparent flexural stiffness of the crossbeam elements (if relevant for the load arrangement under scrutiny). However, the element torsional stiffness may be ignored in the conditions of the end nodes; thus these beam elements become less complex. Figure 5–3 depicts the beam elements used in the grillage model, successively a pin-rigid (a), rigid-rigid (b) and rigid-pin (c) beam element.

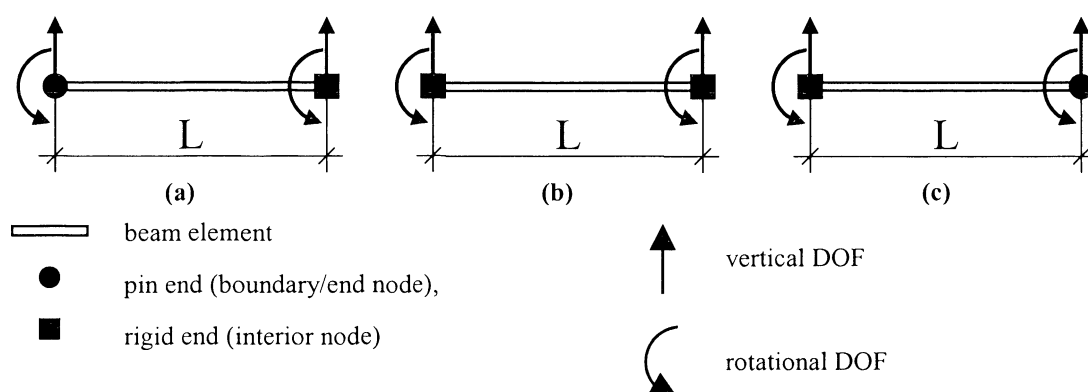


**Figure 5–3: Finite flexural elements (beam elements) with end node conditions**

The stiffness matrix of the beam elements is vectorially represented by the nodal stiffness of the beam ends, that is, according to the DOFs, which are regarded as two different types (vertical and rotational) at each beam end. This simplification is rendered possible by the end conditions applied to the beam elements, that is, inclusion of torsional rigidity in the flexural rigidity for relevant cases. Applying the stiffness matrix for the beam elements (Ghali & Neville 1989), the stiffness matrices for the beam elements (a), (b) and (c) of the model (Figure 5–3) can be expressed by Equations 5-1a, b and c respectively; whereby:

(a) in Equation 5-1a, the pin end is on the left-hand side and the rigid end is on the right-hand side.

(b) in Equation 5-1b, both the left-hand side and the right-hand side have rigid ends.

(c) in Equation 5-1a, the rigid end is on the left-hand side and the pin end is on the right-hand side.

*NOTE: in the matrices (Equations 5-1a, b, and c), released rotations, such as those encountered in pin ends, are expressed with zeros.*

$$(a) \quad k_a = \frac{EI}{L^3} \begin{bmatrix} 3 & 0 & -3 & 3 \\ 0 & 0 & 0 & 0 \\ & & 3 & -3 \\ \text{sym.} & & & 3 \end{bmatrix} \quad (\text{Eq. 5-1a})$$

$$(b) \quad k_b = \frac{EI}{L^3} \begin{bmatrix} 12 & 6L & -12 & 6L \\ & 4L^2 & -6L & 2L^2 \\ & & 12 & -6L \\ \text{sym.} & & & 4L^2 \end{bmatrix} \quad (\text{Eq. 5-1b})$$

$$(c) \quad k_c = \frac{EI}{L^3} \begin{bmatrix} 3 & 3 & -3 & 0 \\ & 3 & -3 & 0 \\ & & 3 & 0 \\ \text{sym.} & & & 0 \end{bmatrix} \quad (\text{Eq. 5-1c})$$

where: k: stiffness matrix  
subscripts: a: pin-rigid beam element  
                  b: rigid-rigid beam element  
                  c: rigid-pin beam element  
EI: stiffness of the beam element [Nm<sup>2</sup>]  
L: length of the beam – finite – element [m]

Consequently, the element types (a) and (c) are used for the beam elements adjacent to pin supports. Expressed in other words, they are accordingly chosen in order to meet the support conditions of the left-hand and right-hand sides respectively.

### 5.1.5 Derivation of the stiffness matrix of the girders and crossbeams

Using the concept of the matrix superposition and static condensation techniques, the stiffness matrix of the grillage system is built by vectorially superposing the fundamental stiffness matrix of the beam elements of the girders and crossbeams. This is mathematically expressed below:

$$K = \sum_{i=1}^n k_i \quad (\text{Eq. 5-2})$$

where:  $K$ : stiffness matrix of the girder or crossbeam members  
 $n$ : number of segments of the members (girders and crossbeams).

Merging of the beam elements is carried out by superposing the DOFs of the shared/common nodes of adjacent elements. This operation is illustrated in Figure 5-4.

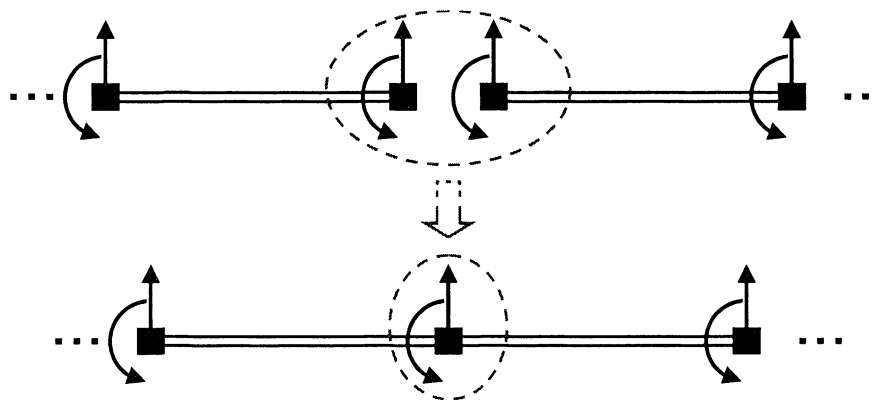


Figure 5-4: Merging of adjacent beam element → superposition of the node DOFs

Each rotational DOF of fundamental (element) stiffness matrix of the girders and crossbeams is condensed out, as shown in Figure 5-5.

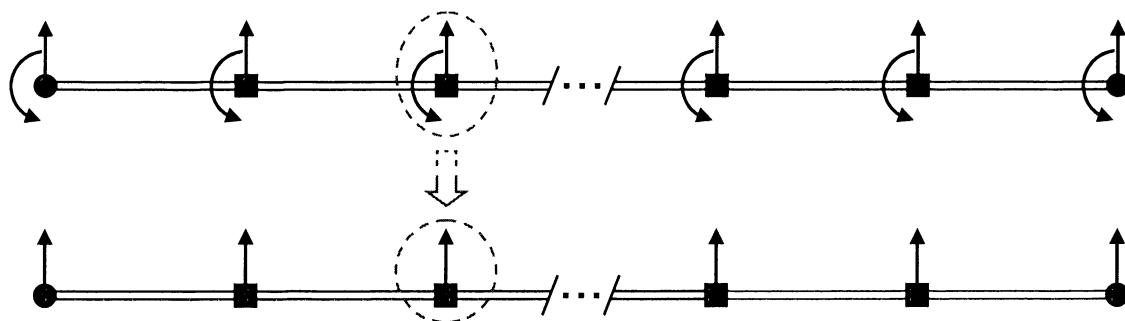


Figure 5-5: Condensation of DOF → node merging of girder members

The stiffness matrix  $K$  (Equation 5-2), representing the girder or cross-beam (Figure 5-5) is at this point partitioned into sub-matrices and labelled with subscript indexes  $v$  and  $\theta$  (Equation 5-3), where  $v$  and  $\theta$  are associated with the vertical and rotational DOF respectively.



$$K = \begin{bmatrix} k_{vv} & | & k_{v\theta} \\ \hline k_{\theta v} & | & k_{\theta\theta} \end{bmatrix} \quad (\text{Eq. 5-3})$$

in which:

$$k_{vv} = \sum_{i=1}^n (k_{vv})_i \quad (\text{Eq. 5-4a})$$

$$k_{v\theta} = \sum_{i=1}^n (k_{v\theta})_i \quad (\text{Eq. 5-4b})$$

$$k_{\theta v} = \sum_{i=1}^n (k_{\theta v})_i \quad (\text{Eq. 5-4c})$$

$$k_{\theta\theta} = \sum_{i=1}^n (k_{\theta\theta})_i \quad (\text{Eq. 5-4d})$$

where: v: vertical DOF [m]  
 θ: rotational DOF [RAD]

Equations 5-4a and 5-4d represent the stiffness matrix of the girder or crossbeam, which are associated with vertical and rotational DOFs respectively. Equations 5-4b and 5-4c are off-diagonal sub-matrices, which show the coupling action between the vertical and rotational DOFs.

### 5.1.6 Static condensation of the stiffness matrix of the girders and crossbeams

The static condensation is basically carried out to eliminate the coupling action of the rotational DOF from the vertical DOF of the static stiffness matrix of the girder and crossbeam. In this case, it is assumed that there is no external bending moment acting on the girders and the crossbeams. The static condensation process therefore corresponds to a matrix manipulation of the static equilibrium equations as demonstrated in Equation 5-5.

$$\begin{Bmatrix} P \\ M \end{Bmatrix} = \begin{bmatrix} k_{vv} & | & k_{v\theta} \\ \hline k_{\theta v} & | & k_{\theta\theta} \end{bmatrix} \begin{Bmatrix} v \\ \theta \end{Bmatrix} \quad (\text{Eq. 5-5})$$

where: P: force vector (normal load) [N]  
M: bending moment vector [Nm]

The condition of zero bending moment on the grillage members can be accommodated into Equation 5-5, as presented in Equation 5-6.

$$\begin{Bmatrix} P \\ 0 \end{Bmatrix} = \begin{bmatrix} k_{vv} & k_{v\theta} \\ k_{\theta v} & k_{\theta\theta} \end{bmatrix} \begin{Bmatrix} v \\ \theta \end{Bmatrix} \quad (\text{Eq. 5-6})$$

Equation 5-6 can be deployed into two equations, expressing the static equilibrium condition on the grillage model, that is, Equations 5-7a and b express the normal and flexural (zero) actions respectively.

$$P = k_{vv}v + k_{v\theta}\theta \quad (\text{Eq. 5-7a})$$

$$0 = k_{\theta v}v + k_{\theta\theta}\theta \quad (\text{Eq. 5-7b})$$

Equation 5-7a shows that the rotational DOF,  $\theta$ , can be expressed by the vertical DOF,  $v$ . Consequently, Equation 5-7a can be accommodated into Equation 5-7b. This operation is shown in Equation 5-8 after manipulation.

$$P = (k_{vv} - k_{v\theta}k_{\theta v}k_{\theta\theta})v \quad (\text{Eq. 5-8})$$

Furthermore, the stiffness matrices can be condensed into a single matrix, thus deriving the condensed stiffness matrix for the girders and crossbeams (Equation 5-9).

$$K^* = k_{vv} - k_{v\theta}k_{\theta v}k_{\theta\theta} \quad (\text{Eq. 5-9})$$

where:  $K^*$ : condensed stiffness matrix (girders and crossbeams).

### 5.1.7 Boundary condition of the grillage members

The vertical DOFs associated with the boundary conditions of the girder stiffness matrix can be simplified out because the deflection of these DOFs are commonly known. This simplification is performed on the equilibrium equation of the system (Equation 5-10), in which the condensed stiffness matrix is used. Furthermore, Equation 5-10 can be partitioned for “free” and “restrained” DOF. The restrained DOF, representing the boundary conditions, is used to account for the kinematic and/or static conditions of the supports.

$$\begin{Bmatrix} P_f \\ P_r \end{Bmatrix} = \begin{bmatrix} K_{ff}^* & K_{fr}^* \\ K_{rf}^* & K_{rr}^* \end{bmatrix} \begin{Bmatrix} v_f \\ v_r \end{Bmatrix} \quad (\text{Eq. 5-10})$$

subscripts: f: node with free DOF  
r: node with restrained DOF

The condensed stiffness matrix of the girder associated with a free DOF is subsequently superimposed to the condensed stiffness matrix of the crossbeam, resulting in the stiffness matrix of the grillage system with vertical DOFs. Because  $v_r$  is zero for pin support, Equation 5-10 can be rearranged to obtain the girder stiffness matrix for the free DOF (Equation 5-11).

$$P_f = K_{ff}^* v_f + K_{fr}^* v_r \quad (\text{Eq. 5-11a})$$

$$P_r = K_{rf}^* v_f + K_{rr}^* v_r \quad (\text{Eq. 5-11b})$$

Equation 5-11b represents a static equilibrium equation for boundary DOFs, while Equation 5-11a can be transformed to retain only free vertical DOFs, and thus also complies with the boundary conditions of the element ends. As indicated previously, the girder ends correspond to pin supports. Therefore, the vertical displacement is impeded, that is,  $v_r$  is considered equal to zero. As a result, Equation 5-11a can be re-written in a simplified form (Equation 5-12).

$$P_f = K_{ff}^* v_f \quad (\text{Eq. 5-12})$$

where:  $K_{ff}^*$ : static condensed stiffness matrix of the girder.

Consequently to this line of argument, the girders can be completed, that is, the boundary conditions are applied to the grillage elements. Figure 5–6 depicts the implementation of the boundary conditions to the girder members. The vertical (kinematic) DOF in the pin ends correspond to the support deflections, thus can be removed. The support forces, thus support reactions, can be computed back using Equation 5-11b.

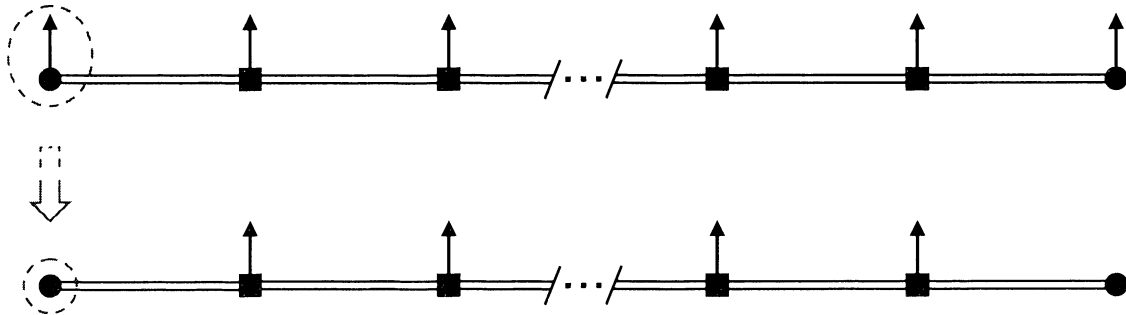


**Figure 5–6: Boundary conditions of the girders**

On the other hand, the crossbeams have no boundary conditions as such, because the end nodes coincide with interior free nodes of the girder members. The crossbeams correspond to the element models of “single” beam elements with rigid ends. Thus, the nodal vertical DOFs at the interface nodes to the girders must be retained to comply with the compatibility condition at the interface nodes. Figure 5–7 depicts the end node conditions of the crossbeams.



**Figure 5–7: Boundary conditions of the crossbeams**

### 5.1.8 Superposition technique – stiffness matrix of the grillage structure

Superposition is the process of nodal merging and vectorial addition performed on all girders and crossbeams at the interface nodes. It is mathematically expressed in Equation 5-13 and pictorially shown in Figure 5–8.

$$K_s = \sum_{gi=1}^{gm} K_{gi}^* + \sum_{cj=1}^{cn} K_{cj}^* \quad (\text{Eq. 5-13})$$

where:  $K_s$ : condensed stiffness matrix of the grillage structure (floor system)  
 subscripts:  $gi$ : girder sequence ( $gi = 1, 2, \dots, gm$ )  
 $cj$ : crossbeam sequence ( $cj = 1, 2, \dots, cn$ )

The condensed stiffness matrix of the grillage structure is associated with the vertical DOF only. Figure 5–8 depicts the assemblage of the crossbeam elements between the girder members. The end nodes of the crossbeam elements and the interior nodes of the girder members are merged and the nodal DOFs are superimposed at the interface nodes.

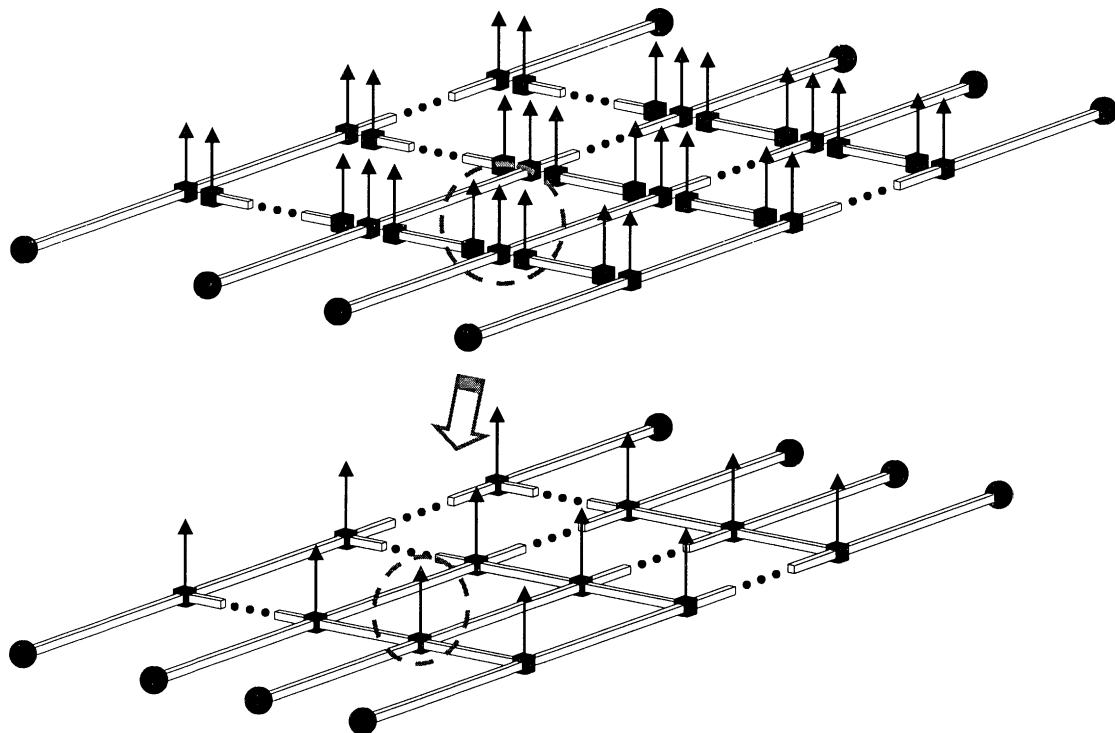


Figure 5–8: Merging the shared nodes of the girders and crossbeams → superposition of the node DOF

## 5.2 DEFINITION OF THE ATTRIBUTES OF THE GRILLAGE MODEL

Each member of the grillage model corresponds to a composite section, for example, box-section SSP systems are subdivided into C (exterior joist) and I (interior girder) composite girders and a box crossbeam. Consequently, the section properties of each member are calculated using the transformed-section method (refer to Chapter 4 in Part 1), whereby the longitudinal modulus of elasticity (MOE) of the I-joist flange – MOE parallel to the grain – is used for characterising the section properties of each member. Furthermore, the grillage calls upon the apparent stiffness of the members, which includes the effects of flexural deformation and shear distortion into a single value (refer to Sections 5.2.1 and 5.2.2). This practice allows reduction of the computation for the solution of the model.

### 5.2.1 Apparent stiffness of the girders

The apparent stiffness of the girders, which characterises the (longitudinal) stiffness properties of the grillage, accommodates the flexural stiffness and shear rigidity. Expressed in other words, the apparent stiffness of the girders defines the capability of resisting flexural and shear deformation. As identified previously (refer to Chapter 4 in Part 2), the magnitude of the shear deformation strongly affects the specimen behaviours because of the use of I-joists.

The composite girders, which “form” the specimen, correspond to L- and T-sections and to C- and I-sections for open- and box-section specimens respectively. It is widely accepted that the flanges of L-, T-, C- and I-sections experience normal stresses (induced by the flexural state of the beam), while the web takes the shear forces (Gere & Timoshenko 1997). This approach is taken into account for the consideration of the shear deformation experienced by the specimen. Therefore, for the theoretical approximation of the shear deformation, the cross-section coefficient – Kappa coefficient – is calculated by equating the “shear” area – area of the web – and the whole area of the SSP section. The “original” assumption of the shear area is similar to that of Trus Joist’s<sup>TM</sup> technical documents for I-joist designs (Trus Joist<sup>TM</sup> a Weyerhaeuser Business 2002b), that is, as per Figure 5–9 (coloured areas). However, the analysis of the testing program data has demonstrated that, with this approach, the effects of shear distortion are underestimated (refer to Chapter 4 in Part 2). This analysis

has identified that a calibration coefficient of 1.4 should be applied on the cross-section coefficient in order to replicate the shear distortion accurately.

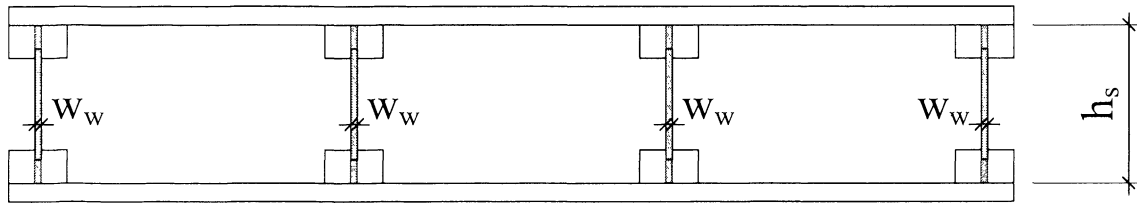


**Figure 5-9: Shear area of box-section SSP specimen**

The apparent stiffness of the girders is expressed in Equation 5-14, in which the aspects of the flexural and shear deformation have been accommodated.

$$EI_{gi,app} \in EI_{gi,true} \wedge GA_{gi,true} \quad (\text{Eq. 5-14})$$

where: EI: flexural stiffness of the girders [Nm<sup>2</sup>]  
 GA: shear modulus of the grillage elements [Nm<sup>2</sup>]  
 subscripts: g: (longitudinal) girder  
                   i: girder sequence (i = 1, 2, ... , m)  
                   app: apparent (flexural and shear effects included)  
                   true: actual

### 5.2.2 Apparent stiffness of the crossbeams

The use of crossbeams enables the load distribution to occur orthogonally to the girders, thus simulating the so-called “two-way” action. Expressed in other words, the magnitude of the load distribution is “modulated” by the mechanical properties of the crossbeam; hereafter described as the “apparent stiffness” of the crossbeam. The apparent stiffness of the crossbeam has a very significant role, which consists of regulating the magnitude of the loading captured by each girder; for example, considering a concentrated point load, the crossbeam properties determine the portion of loading eased away from the girder under load. On the other hand, this ability may have fewer relevancies with uniformly distributed load arrangements, where each girder captures equal or nearly equal magnitudes of load.

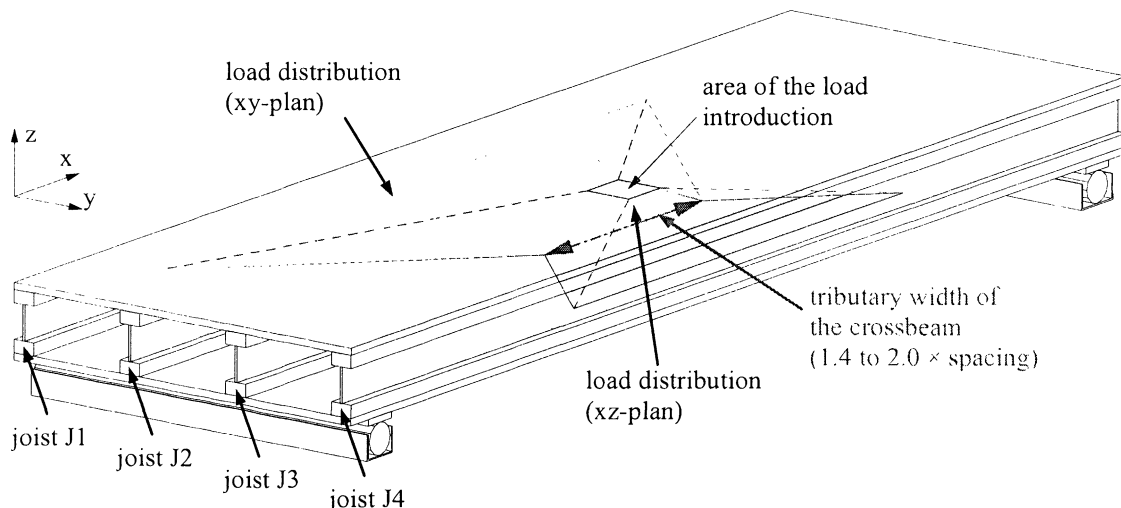
The flexural stiffness of the crossbeam and the torsional rigidity of the SSP assembly represent the major influential parameters that contribute to resisting point

loads. Therefore, the apparent stiffness of the crossbeam can be assumed to accommodate these aspects (Equation 5-15).

$$EI_{cj,app} \in EI_{cj,true} \wedge GA_{cj,true} \wedge GJ_d \quad (\text{Eq. 5-15})$$

where: EI: flexural stiffness of the girders [Nm<sup>2</sup>]  
 GA: shear modulus of the grillage elements [Nm<sup>2</sup>]  
 GJ: torsional rigidity of the deck [Nm<sup>2</sup>]  
 subscripts: c: (orthogonal) crossbeam  
 j: crossbeam segment (j = 1, 2, ... n)  
 d: deck unit  
 app: apparent (flexural and shear effects included)  
 true: actual

In order to estimate the flexural stiffness and the shear rigidity of the crossbeam, identification of its tributary width, which is anticipated to characterise the pattern of the load distribution in the SSP 3-Dimensional structure, is firstly required. However, approximating the crossbeam tributary width with the consideration of two dimensions essentially (*xy-plan*) – the parallel, *x-axis*, and orthogonal, *y-axis*, directions to the span (Figure 5–10) – corresponds to an acceptably accurate approach.



Note: point load is introduced on joist J3.

**Figure 5–10: Anticipated pattern of the load distribution**

Considering the distribution pattern along the axis parallel to the span (*x-axis*), the determination of the angle of the load distribution is arduous because of the heterogeneous and orthotropic properties of the material layers. Instead of such a



strenuous procedure, the effective width of the crossbeam, at the girder where the load is introduced, can be assumed to be equal to 1.4 to 2.0 times the girder spacing (Wilfred 2003). For the distribution pattern in the orthogonal direction to the span (*xy-plan*), the angle of the load distribution can be estimated using the “global” stiffness characteristics of the SSP deck. Respectively, it can be assumed that the stiffness properties of both the longitudinal – parallel to the span – and transversal – perpendicular to the span – exhibit a geometric relationship (Figure 5–11), which can be expressed as a fundamental trigonometric function (Equation 5-16).

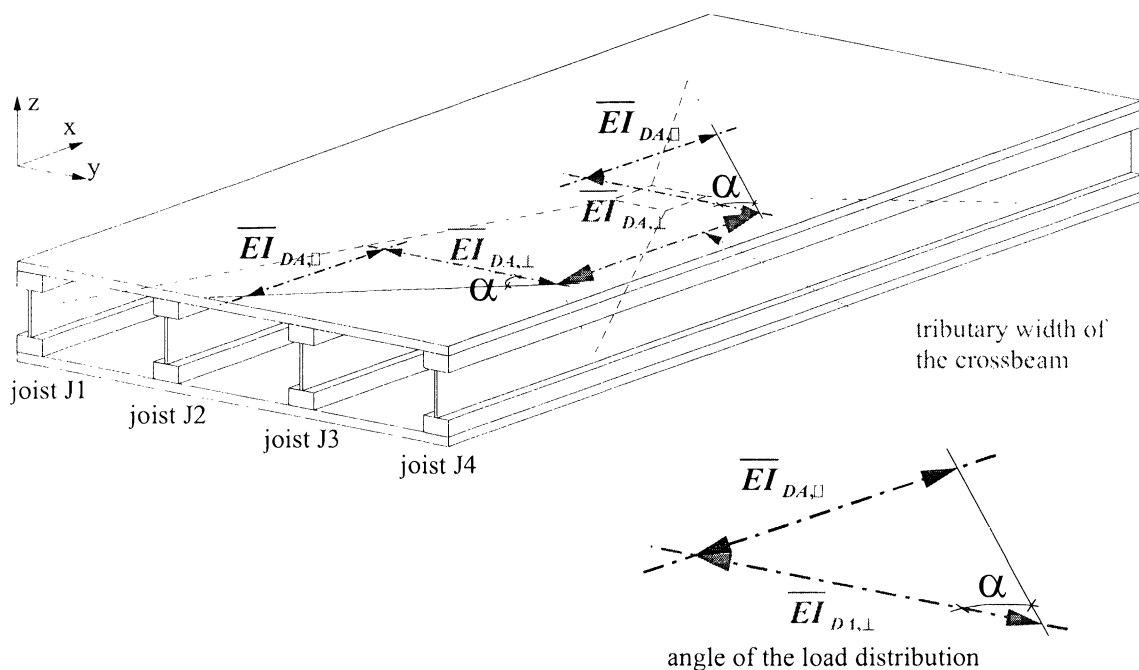


**Figure 5–11: Geometric characteristics of the anticipated load distribution pattern**

The approximation of angle of the load distribution,  $\alpha$  (in Equation 5-16), aims to include the “system” effect, which is created by the interaction between the girders and the skin(s). Therefore, Equation 5-16 considers the longitudinal (x-axis) and orthogonal (y-axis) stiffness properties of the deck. The member properties in Equation 5-16 are characterised by the apparent stiffness of the girders (numerator) and the sum of the apparent stiffness of the crossbeam and the torsional rigidity of the deck (denominator).

$$\tan \alpha = \frac{\overline{EI}_{DA,||}}{\overline{EI}_{DA,\perp}} = \frac{\sqrt{EI_{g,app} S EI_{S,app\_p.m.}}}{TW_{c,gi} \sqrt{(EI_{c,app\_p.m.} EI_{S\perp,app\_p.m.}) + GJ_d}} \quad (\text{Eq. 5-16})$$

in which:

$$\overline{EI}_{g,app} = \sqrt[n]{EI_{g1,app} EI_{g2,app} \dots EI_{gm,app}} \quad (\text{Eq. 5-17})$$

where: $\alpha$ :	angle of load distribution (Figure 5–11)	[ ° ]
$\overline{EI}$ :	characterised flexural stiffness properties	[Nm <sup>2</sup> ]
EI:	(local) flexural stiffness	[Nm <sup>2</sup> ]
GJ:	torsional rigidity	[Nm <sup>2</sup> ]
s:	spacing of the girders	[m]
TW:	tributary width of the crossbeam	[m]
subscripts: DA:	distribution angle	
	g:	(longitudinal) girder
	c:	(orthogonal) crossbeam
	s:	sheathing
	d:	deck unit
	app:	apparent (flexural and shear effects included)
	gi*:	number/position of the girder under load
	i:	girder sequence (i = 1, 2, ... , m)
	p.m.:	per metre width

*NOTE:  $EI_{S||,app}$  and  $EI_{S\perp,app}$  correspond to the apparent stiffnesses of the deck portions located between the joists, that is, only the contribution of the skin(s) is included. It is assumed that the properties of the skin(s) represent a significant aspect of the load distribution.*

The expression of the angle of the load distribution (Equation 5-16) indicates that the apparent stiffness of the crossbeam varies along the width of the floor structure. Therefore, the crossbeam properties should be correspondingly calculated at each girder location, that is, considering the tributary width that the crossbeam assumed at these locations.

Furthermore, the torsional rigidity, which is related to the construction of the SSP section, is considered constant for each girder. It is also logically accepted that open-section specimens exhibit lower torsional rigidity than that of box-section specimens. The consideration – background and principle – of the torsional rigidity in Equation 5-15 is explained/demonstrated in Chapter 5 in Part 2 and Appendix 5.

### 5.3 LOAD INTRODUCTION

The model is able to accommodate uniformly distributed and concentrated loads in the form of force vector at the structural nodes. Consequently, uniformly distributed (line and surface) loads are transformed into nodal forces at pro rata of the tributary area

around the nodes. Concentrated loads between two nodes cannot be processed by the model without their being transposed into nodal forces. The model construction can be adapted to the loading conditions, that is, the crossbeams are positioned in such way that they match the locations of the loading.

#### 5.4 SOLUTION OF THE GRILLAGE MODEL

The grillage model is capable of predicting the responses of SSP systems, which are the mid-span deflection, the mid-span flexural moment and the reactions in the supports. The solution of the model is conducted using the condensed stiffness matrix of the grillage structure, whereby the static equilibrium equation for the grillage system is expressed in Equation 5-18.

$$P_s = K_s v_s \quad (\text{Eq. 5-18})$$

where: P: force vector (normal load) [N]  
 K: condensed stiffness matrix of the grillage model (Equation 5-13)  
 v: displacement vector (deflection) [mm]  
 subscripts: s: grillage system

Rearranging Equation 5-18 and assuming that the load,  $P_s$ , is known, the deflection,  $v_s$ , can be estimated (Equation 5-19).

$$v_s = K_s^{-1} P_s \quad (\text{Eq. 5-19})$$

Consecutively to the determination of the vertical displacement (Equation 5-19), the reactions at the girder supports (Equation 5-20) can be estimated using the computed displacement vector (Equation 5-11b).

$$R_{g_i} = K_{r_f}^* v_s \quad (\text{Eq. 5-20})$$

where: R: reaction at the support [N]  
 K\*: condensed matrix of the grillage model (floor system)  
 subscripts: g: (longitudinal) girder  
 i: girder sequence ( $i = 1, 2, \dots, m$ )  
 r: node with restrained DOF  
 f: node with free DOF

The approximation of the bending moment of the girders requires the computation of the entire array of the rotational DOFs,  $\theta$ , that is, for each girder at beam level. This operation is carried out using Equation 5-7b. Consequently, the bending moment of the girder at member level can be computed with Equation 5-21, which is derived from Equation 5-5.

$$M_{ig} = k_{\theta v}v + k_{\theta\theta}\theta \quad (\text{Eq. 5-21})$$

where: M: bending moment of the girder [Nm]  
 k: stiffness matrix  
 $\theta$ : rotational DOF [RAD]  
 v: vertical DOF [m]

## 5.5 APPLICATION OF THE GRILLAGE MODEL TO THE SPECIMENS OF THE SUBJECT RESEARCH

### 5.5.1 Modelling principle – application to the specimens of the subject research

The models correspond to “flawless” or ideal representations of the actual structures, in which certain aspects and/or local phenomena are idealised. The girders and crossbeam exhibit full composite action characteristics (demonstrated in Chapter 6 in Part 2). The tributary width of the sheathing(s) to the I-joists – parallel direction to the span – is estimated according to EC5 guidelines (European Committee for Standardisation 1995) (demonstrated in Chapter 4 in Part 2), while Wilfred’s assumption (2003) is used for approximating the effective width of the crossbeam – orthogonal direction to the span. The girders and crossbeam properties (Table 5–1) are estimated using the material and product data provided either by the manufacturers’ technical documentation (Kronoply GmbH & Co. KG; Trus Joist™ a Weyerhaeuser Business 2002b) or available in Australian standards (Australian Standard™ 1997; Australian/New Zealand Standard™ 2004a, 2004b). Furthermore, the materials of the members are assumed to exhibit orthotropic and linear-elastic (demonstrated in Chapter 4 in Part 2) properties and their natural variability is ignored. The aspect of shear deformation of the I-joist is taken into account using a conjunction of the Trus Joist™ approach (Trus Joist™ a Weyerhaeuser Business 2002b) – shear stress taken by the I-joist web – and the calibration coefficient (1.4) identified the analysis of the results of the testing program (refer to Chapter 4 in

Part 2). On the other hand, the torsional distortion that the I-joist may suffer is not considered. The variability related to the manufacturing of the specimens is not accounted for either.

The actual boundary conditions are manipulated and introduced to the nodes of the model. Therefore, uniformly distributed line loads should be transposed into point loads and are applied to the nodes shared by the mid-span crossbeam and the girders. Concentrated loads are also idealised into point loads, that is, the area of the load application square block – 150-mm side length – is neglected. For this simulation, the model is treated as a simply supported structure, that is, with pin ends, while horizontal restraints are ignored because solely normal loads – vertical direction – are introduced on the model frame.

Studying the effect of discontinuities in the skin(s) can be conducted using minor manipulations, that is, a reduction coefficient is applied on the stiffness properties of girders. The magnitude of this reduction is reported in Table 5–3. More detailed information about the values of these coefficients is presented in Chapter 4 in Part 2.

#### a) Grillage model of 200-mm I-joist specimens

200-mm I-joist specimens were constructed with four 200-mm I-joists to which sheathing is nail-glued on either one or both sides. These specimens are consequently modelled with four (composite) girders and a (composite) crossbeam at mid-span (Figure 5–12). The developed model is assumed to be simply supported and subjected to (vertical) load arrangements.

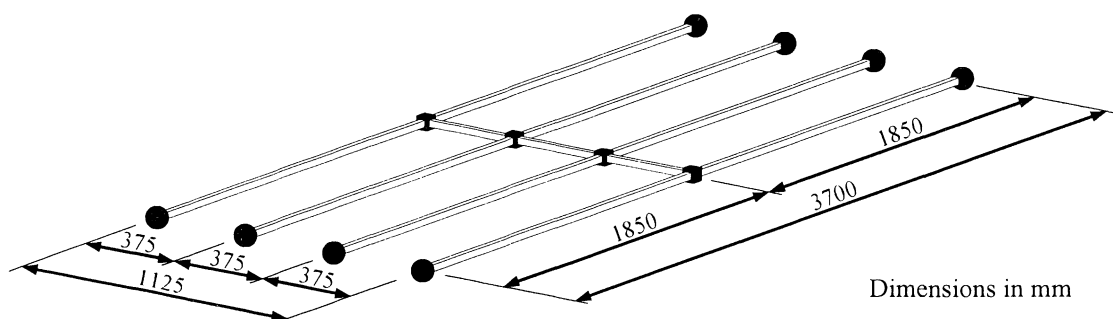


Figure 5–12: 200-mm I-joist grillage model

### b) Grillage model of 356-mm I-joist specimens

In accordance with the 356-mm I-joist specimens, which were constructed with 356-mm I-joist and sheathings compositely attached together, 356-mm I-joist grillage models consist of three (composite) girders and a single (composite) crossbeam located at mid-span (Figure 5–13). The grillage model is assumed to be simply supported and subjected to (vertical) load arrangements.

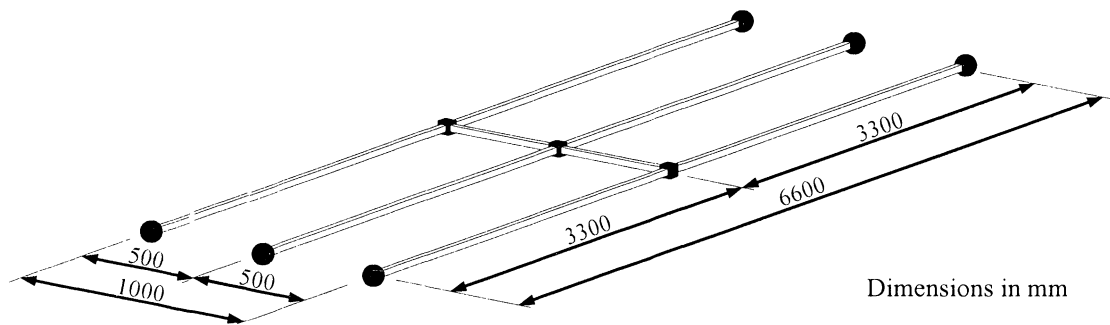


Figure 5–13: 356-mm I-joist grillage model

### 5.5.2 Material properties of the members of the grillage model

The material properties of grillage components are recapitulated in Table 5–1. This data is generally extracted from the codes and specialised literature. It is also derived from test data.

**Table 5–1: Material properties of the grillage components**

Description			Modulus of Elasticity	Shear modulus
			E	G
I-joist flange	solid wood <sup>A</sup>	MGP15	15200 MPa	1010 MPa
I-joist web	9-mm plywood <sup>+B</sup>	F11	1260 MPa	525 MPa
	12-mm plywood <sup>+B</sup>	F11	5040 MPa	525 MPa
Sheathing	15-mm plywood <sup>B</sup>	F11	10500 MPa	525 MPa
	19-mm particleboard <sup>C</sup>		3900 MPa	850 MPa
	22-mm oriented strand board <sup>D</sup>		8136 MPa	1000 MPa

<sup>\*</sup>200-mm I-joist web, <sup>†</sup>356-mm I-joist web.

**Source:** <sup>A</sup>in AS 1720.1–1997 (Australian Standard<sup>TM</sup> 1997) and specialised literature (Green, Winandy & Kretschmann 1999; Guitard 1987), <sup>B</sup>AS/NZS 2269:2004 (Australian/New Zealand Standard<sup>TM</sup> 2004a) and specialised literature (Finnish Forest Industries Federation 2002; Merz et al. 1998), <sup>C</sup>AS/NZS 1859.1:2004 (Australian/New Zealand Standard<sup>TM</sup> 2004b), specialised literature (Australian Wood Panels Association Incorporated 2004; Merz et al. 1998) and test data (in Appendix 8), <sup>D</sup>specialised literature (Kronoply GmbH & Co. KG; Merz et al. 1998) and test data (in Appendix 8).

## 5.6 COMPUTER SOLUTION ROUTINE

### 5.6.1 Concept

The development of a computer solution routine corresponds to the culminating point of the grillage model. The routine, which has been written in a MATLAB software environment (The MathWorks Inc. 2005) (refer to Appendix 10), conceptually adopts the uses of the matrix superposition method. This approach permits the computation to be kept to a minimum.

### 5.6.2 Working with the routine

The use of the computer solution routine is uncomplicated and permits computation of the deflection, the flexural moment and shear actions and the reactions at the supports of the girders. A computation session can be divided into three stages:

(1) **Pre-solution:** during this stage, the physical and mechanical properties of the grillage model are input. This includes, for example, the physical dimensions, the stiffness properties of the girders and crossbeam, and the loading.

(2) **Computation:** the routine is processed and the problem is solved.

(3) **Post-solution:** the results of the computation are displayed in the Matlab working space. Graphical plot depictions of the perpendicular profile of the mid-span deflection, along with tables, which can be imported in Excel (Microsoft Corporation 2003), are used for summarising the solutions of the procedure.

## 5.7 PARAMETERISATION OF THE GRILLAGE MODEL

### 5.7.1 Concept of the parameterisation

A mathematical model generally corresponds to an “idealisation” of the actual construction. In that perspective, a “parameterisation” may be viewed as the process of incorporating the “imperfections” of the actual decks and, to a lesser extent, of the testing set-up. To some extent, it is the pursuit of the best compromise because it aims at refining the model in order to enhance its predictive capability. For example, it aims at identifying and calibrating – in justified manners – the elements of the model in such a way that the predictive ability of the latter becomes more accurate, especially for concentrated point loads.

The parameterisation is carried out considering the parallel and orthogonal directions of the SSP deck. Therefore, it focuses on the definition of the member attributes – apparent stiffness – of the girders and crossbeams. The “best” magnitude of the tributary width of the crossbeam is also studied, the values proposed by Wilfred (2003) defining the boundaries. Thus, the tributary of the crossbeam is equal to 1.4 and 2.0 times the girder spacing (both values have been scrutinised). The examination of the crossbeam also includes quantifying the effective contribution of the torsional rigidity to the lateral distribution of point loads.

### 5.7.2 Benchmarks of the parameterisation

The benchmarks of the parameterisation are set by the test data – deflection responses at mid-span – collected on the physical specimens of C02-series<sup>a)</sup> and C08-series.<sup>b)</sup> Respectively, the data of the girder under direct loading are considered, that is, the responses of each girder in uniformly distributed line load situations and of the girder directly loaded with point load arrangements. These series are chosen because both are

---

<sup>a)</sup> C02-series specimens were built with 200-mm I-joists, on whose upper side 15-mm F11 plywood skin was attached by means of nail-gluing – using a one-component polyurethane adhesive – technique.

<sup>b)</sup> C08-series specimens were manufactured with 200-mm I-joists, on whose lower and upper sides 15-mm F11 plywood skins were nail-glued – using a one-component polyurethane adhesive.



entirely constructed with structural materials (wood members and interface adhesive), whose properties are thoroughly known. Because they have been spliced, the skins of the specimens of both series can be assumed as fully continuous. Furthermore, both series average the test results of three specimens.

The parameterisation of the longitudinal direction – parallel to the span – of the model is carried out using the test data of the uniformly distributed line loadings, while the orthogonal direction – perpendicular to the span – of the deck is calibrated to the test data of the concentrated point load arrangements. Furthermore, the data of the girder(s) under direct loading are considered as a priority because these responses are critical for the design safety of the SSP structures.

### 5.7.3 Key outcomes of the parameterisation

#### 5.7.3.1 Distribution of uniformly distributed line loads

The concept of the grillage model requires the loads to be introduced on the nodes. Consequently, areal/lineal loads are transformed in nodal loads. The analysis/interpretation of the test data of four- and three-point bending tests – uniformly distributed line loading<sup>c)</sup> – collected in the context of the subject research has identified that the specimens experience a (rather) uniform deflection pattern, indicating that the load distribution is governed by the stiffness of the girders (refer to Chapter 4 in Part 2). This load distribution principle, which is recapitulated in Equation 5-22, has been confirmed by the computations of the grillage model, that is, more accurate computed simulations are obtained when the load intensity – derived from uniformly distributed line loading – introduced on each node is determined pro rata of the apparent stiffness of the girder.

$$k_{gi} = \frac{EI_{gi,app}}{EI_{g1,app} + EI_{g2,app} + \dots + EI_{gm,app}} \quad (\text{Eq. 5-22})$$

where: k: load distribution coefficient [–]  
 EI: flexural stiffness [Nm<sup>2</sup>]  
 subscripts: g: (longitudinal) girder  
 i: girder sequence (i = 1, 2, ... , m)  
 m: number of girders

<sup>c)</sup> For both test arrangements, each line load is introduced by means of a stiff steel profile.

*NOTE: third-point loading principles – the four-point bending test principle (4PBT) – are accommodated into the grillage model by manipulating the intensity of the nodal load introduced on the mid-span crossbeam – the three-point bending test principle (3PBT). The modification, which is based on the deflection estimate, corresponds to:*

$$P_{3PBT} = 23/27P_{4PBT}.$$

### 5.7.3.2 Attribute of the crossbeam

Considering uniformly distributed line loads, the parameterisation phase exposes that with both tributary widths of the crossbeam, that is, 1.4 and 2.0 times the girder spacing (Wilfred 2003), no differences are noticeable in the model responses. This observation indicates that in the range of stiffness, as exhibited by the crossbeam of the specimens, increasing the tributary width of the crossbeam has no to little smoothing effect on the deflection. This observation confirms the conclusion of the previous section that the uniform deformed shape of the specimen is related to the load spreader instead of the orthogonal stiffness of the specimens.<sup>d)</sup>

Under the concentrated point load applied on an interior girder, the parameterisation enables identifying that the torsional rigidity of the deck should not be considered in the crossbeam properties, that is, the simulations of the model become more accurate when the torsional stiffness is ignored. Therefore, the equation of the apparent properties of the crossbeam (Equation 5-15) is manipulated in order to accommodate the flexural and shear deformation only. Equation 5-23 presents the crossbeam properties for concentrated point load on an interior girder.

$$EI_{c,j,app} \in EI_{c,j,true} \wedge GA_{c,j,true} \quad (\text{Eq. 5-23})$$

where: EI: “local” flexural stiffness of the crossbeam [Nm<sup>2</sup>]  
 GA: shear modulus of the grillage elements [Nm<sup>2</sup>]  
 subscripts: c: crossbeam  
 j: crossbeam segment (j = 1, 2, ... , n)  
 app: apparent  
 true: actual

<sup>d)</sup> It has been observed that the deflection of the girders can be smoothed – equal magnitude – with arbitrarily imposed extremely high stiffness.

On the other hand, it has been identified that under the concentrated point load applied on an exterior girder, the torsional rigidity of the deck represents a significant parameter of the crossbeam properties. However, its contribution should be modulated by a modification coefficient,  $K_{GJ}$ . This factor, which has been derived empirically, enables modulation of the intensity of the torsional rigidity to the location of the girder with regard to the location of the concentrated point load. Equation 5-24 depicts the crossbeam properties for concentrated point load on an exterior girder.

$$EI_{cj,app} \in EI_{cj,true} \wedge GA_{cj,true} \wedge K_{GJ} GJ_d \quad (\text{Eq. 5-24})$$

where:  $GJ_d$ : torsional rigidity of the deck [Nm<sup>2</sup>]  
 $K_{GJ}$ : modification coefficient [ - ]

The modification coefficient of the torsional rigidity,  $K_{GJ}$ , accounts for the longitudinal and perpendicular stiffness properties and the torsional rigidity of the deck (Equation 5-25).  $K_{GJ}$  is calculated at each girder location.

$$K_{GJ} = \frac{\log\left(\frac{h_{cj}}{h_g}\right)}{\log\left(\frac{h_d}{h_g}\right)} \quad (\text{Eq. 5-25})$$

in which:

$$h_{cj} = \frac{EI_{cj,app}}{s^3} = \frac{TW_{cj} EI_{S\perp,app\_p.m.}}{s^3} \quad (\text{Eq. 5-26a})$$

$$h_d = \frac{GJ_d}{L_r^3} \quad (\text{Eq. 5-26b})$$

$$h_g = \frac{\overline{EI}_g}{L^3} = \frac{\sqrt[m]{EI_{g1,app} EI_{g2,app} \dots EI_{gm,app}}}{L^3} \quad (\text{Eq. 5-26c})$$

where:  $K_{GJ}$ : modification coefficient  
 $h_{cj}$ : crossbeam (stiffness) [m<sup>-1</sup>]  
 $h_d$ : deck (torsional rigidity) [m<sup>-1</sup>]  
 $h_g$ : girder (stiffness) [m<sup>-1</sup>]  
 $EI$ : (local) flexural stiffness [Nm<sup>2</sup>]  
 $GJ$ : torsional rigidity [Nm<sup>2</sup>]  
 $\overline{EI}$ : characterised flexural stiffness properties [Nm<sup>2</sup>]

s:	spacing of the girders	[m]
TW:	tributary width of the crossbeam	[m]
$L_T$ :	eccentricity distance	[m]
L:	span (of the girders/deck)	[m]
subscripts: g:	(longitudinal) girder girder sequence (1, 2, ... , m)	
c:	(orthogonal) crossbeam	
j:	crossbeam segment ( $j = 1, 2, \dots, n$ )	
s:	sheathing	
d:	deck unit	
app:	apparent (flexural and shear effects included)	
p.m.:	per metre width	

## **5.8 EVALUATION OF THE CAPABILITY OF THE GRILLAGE MODEL**

In order to evaluate the predictive capability of the grillage model, a comparison between the calculated – grillage model computations – and the measured – test results – deflections is carried out. The evaluation focuses on two aspects: (1) the approximation of the deflection of the girder onto whose mid-span node a load is introduced (Figure 5–14), and (2) the prediction of the deformed shape, which is characterised by the mid-span deflection of the girders. The acceptability of the predictions – an acceptable variation between the model computations and the test results – is set at  $\pm 10\%$ . Such a range is reasonable considering the natural variability of structural timber and engineered wood products.

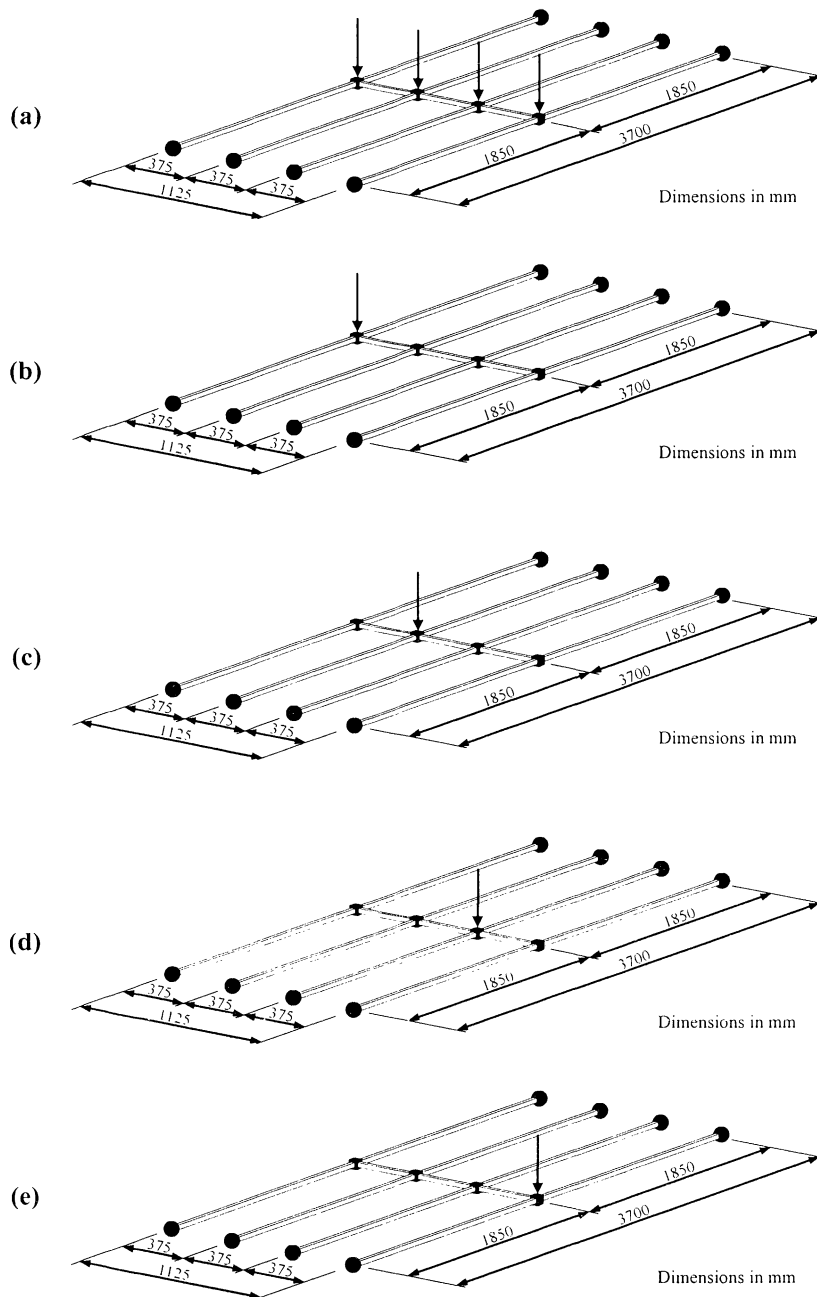


**Figure 5–14: Locations of the nodal loads – 200-mm grillage model**

The population of specimens tested in course of the subject research is used for this evaluation. The comparison is carried out on the mid-span deflections per unit load ( $\Sigma F = 1.0$  kN). Looking at the uniformly distributed line loadings, the comparison indicates that the model is capable of calculating the deflection acceptably (Table 5–2). Furthermore, there is only minimal difference – no identifiable difference – between the model computations considering either crossbeam tributary width, that is, 1.4 or 2.0 times the girder spacing. This is illustrated by the graphical plots of the comparison of the model computations and the measured data (Figure 5–15 (a)). In addition to this, for

both crossbeam tributary widths, the variations are within  $\pm 10\%$ , that is, of 60 computed results, 49 (82%) are within  $\pm 5\%$  of the test data, while the last 11 (18%) are within  $\pm 10\%$ . Such good agreements also suggest that the model assessment of the orthogonal profile of deflection is correct. They also permit the conclusion that the grillage model is capable of accurately predicting the responses of SSP system under both third- and centre-point loading – uniformly distributed line load(s) – arrangements.

As for concentrated point load arrangements, the model estimates of the behaviour of the girder directly under load are generally acceptable (Table 5–2). With such loading arrangements, the magnitude of the crossbeam tributary width becomes a parameter that needs to be considered. The analysis of the variations between the model computations and the test data suggests that assigning a crossbeam tributary width corresponding to 1.4 times the girder spacing (1.4-spacing) permits (slightly) more accurate computations of the model behaviour than those received with 2.0 times (2.0-spacing). Considering the 1.4-spacing crossbeam, of 30 computed deflections, 16 (53%) are within  $\pm 10\%$  of the test data, another 7 (23%) are within  $\pm 15\%$ , another 6 (20%) are within  $\pm 20\%$ , while the last one (4%) is within  $\pm 25\%$ . Looking at the 2.0-spacing crossbeam, of 30 computed deflections, 9 (30%) are within  $\pm 10\%$  of the test data, another 15 (50%) are within  $\pm 15\%$ , another 5 (17%) are within  $\pm 20\%$ , while the last one (3%) is within  $\pm 25\%$ . The graphical plots – comparison between the model computations and the measured data – illustrate this difference (Figure 5–15 (b)). On the other hand, with both crossbeam tributary widths, significant variations can be observed with the adjacent girders (girders not under load) (Table 5–2). This indicates that the model approximation of the orthogonal profile of deflection is less accurate. However, it is still acceptable. The outcomes of this evaluation of the SSP systems under point load have verified that the grillage provides acceptable computations of the specimen behaviours. It can therefore be concluded that the grillage model is also capable of successfully computing the situations of point loading.

The outcomes of the comparison between the computed (numerical) and measured (experimental) responses are reported in Table 5–2. The deflections are expressed per unit load ( $\Sigma F = 1.0 \text{ kN}$ ).

**Table 5-2: Comparison between the calculated – grillage model – and the measured – test results – deflections**

	deflection per 1.0-kN load ( $\Sigma F = 1.0$ kN)											
	joist J1			joist J2			joist J3			joist J4		
	model	test	VAR	model	test	VAR	model	test	VAR	model	test	VAR
	mm/kN			mm/kN			mm/kN			mm/kN		
<b>C02-series</b> (open-section specimen: 200-mm I-joist, F11 plywood (upper skin))												
<b>where the crossbeam tributary width is: 1.4-spacing (of the girder)</b>												
* udl (TPL)	0.49	0.49	1.58%	0.49	0.51	-2.34%	0.49	0.51	-2.64%	0.49	0.50	-0.21%
† udl (CPL)	0.57	0.52	9.86%	0.57	0.63	-9.25%	0.57	0.62	-8.39%	0.57	0.57	0.69%
‡ PL (J1)	1.94	1.83	6.00%	0.58	0.66	-12%	0.04	0.05	-28%	-0.23	-0.14	42%
PL (J2)	0.42	0.48	-15%	1.49	1.36	8.74%	0.32	0.52	-64%	0.04	-0.04	204%
PL (J3)	0.04	-0.14	434%	0.32	0.49	-57%	1.49	1.43	3.45%	0.42	0.52	-25%
PL (J4)	-0.23	-0.13	44%	0.04	0.09	-130%	0.58	0.76	-31%	1.94	2.00	-2.98%
<b>where the crossbeam tributary width is: 2.0-spacing (of the girder)</b>												
udl (TPL)	0.49	0.49	1.58%	0.49	0.51	-2.34%	0.49	0.51	-2.64%	0.49	0.50	-0.21%
udl (CPL)	0.57	0.52	9.86%	0.57	0.63	-9.25%	0.57	0.62	-8.39%	0.57	0.57	0.69%
PL (J1)	1.90	1.83	3.96%	0.64	0.66	-3%	0.05	0.05	2%	-0.26	-0.14	48%
PL (J2)	0.52	0.48	8%	1.30	1.36	-4.25%	0.39	0.52	-33%	0.05	-0.04	181%
PL (J3)	0.05	-0.14	359%	0.39	0.49	-26%	1.30	1.43	-10.29%	0.52	0.52	0%
PL (J4)	-0.26	-0.13	50%	0.05	0.09	-76%	0.64	0.76	-20%	1.90	2.00	-5.22%
<b>C08-series</b> (box-section specimen: 200-mm I-joist, F11 plywood (upper & lower skins))												
<b>where the crossbeam tributary width is: 1.4-spacing (of the girder)</b>												
udl (TPL)	0.37	0.38	-2.36%	0.37	0.36	1.89%	0.37	0.37	-1.13%	0.37	0.38	-2.60%
udl (CPL)	0.42	0.44	-4.01%	0.42	0.43	-1.76%	0.42	0.43	-1.58%	0.42	0.44	-2.51%
PL (J1)	1.35	1.22	9.53%	0.57	0.56	1%	0.08	0.13	-68%	-0.27	-0.16	40%
PL (J2)	0.49	0.55	-12%	0.82	0.85	-3.65%	0.27	0.35	-33%	0.09	0.15	-58%
PL (J3)	0.09	0.16	-66%	0.27	0.34	-29%	0.82	0.83	-1.09%	0.49	0.55	-12%
PL (J4)	-0.27	-0.21	24%	0.08	0.08	-10%	0.57	0.57	0%	1.35	1.28	4.78%
<b>where the crossbeam tributary width is: 2.0-spacing (of the girder)</b>												
udl (TPL)	0.37	0.38	-2.36%	0.37	0.36	1.89%	0.37	0.37	-1.13%	0.37	0.38	-2.60%
udl (CPL)	0.42	0.44	-4.01%	0.42	0.43	-1.76%	0.42	0.43	-1.58%	0.42	0.44	-2.51%
PL (J1)	1.33	1.22	8.11%	0.59	0.56	5%	0.09	0.13	-48%	-0.28	-0.16	43%
PL (J2)	0.55	0.55	1%	0.73	0.85	-17.28%	0.29	0.35	-20%	0.11	0.15	-36%
PL (J3)	0.11	0.16	-43%	0.29	0.34	-17%	0.73	0.83	-14.38%	0.55	0.55	0%
PL (J4)	-0.28	-0.21	28%	0.09	0.08	3%	0.59	0.57	4%	1.33	1.28	3.29%

/..



**Table 5–2: Comparison between the calculated – grillage model – and the measured – test results – deflections (cont.)**

	deflection per 1.0-kN load ( $\Sigma F = 1.0$ kN)											
	joist J1			joist J2			joist J3			joist J4		
	model	test	VAR	model	test	VAR	model	test	VAR	model	test	VAR
	mm/kN			mm/kN			mm/kN			mm/kN		
<b>C05-series</b> (open-section specimen: 200-mm I-joist, particleboard (upper skin))												
<b>where the crossbeam tributary width is: 1.4-spacing (of the girder)</b>												
* udl (TPL)	0.49	0.50	-1.60%	0.49	0.50	-2.41%	0.49	0.48	1.95%	0.49	0.48	2.29%
† udl (CPL)	0.56	0.59	-5.98%	0.56	0.61	-9.82%	0.56	0.57	-1.84%	0.56	0.53	5.33%
‡ PL (J1)	1.85	1.59	14.22%	0.61	0.90	-46%	0.05	0.19	-276%	-0.25	-0.18	29%
PL (J2)	0.51	0.80	-57%	1.26	1.21	3.74%	0.37	0.56	-53%	0.06	0.04	39%
PL (J3)	0.06	0.00	109%	0.37	0.57	-55%	1.26	1.23	2.81%	0.51	0.65	-29%
PL (J4)	-0.25	-0.22	14%	0.05	0.21	-317%	0.61	0.88	-43%	1.85	1.53	17.50%
<b>where the crossbeam tributary width is: 2.0-spacing (of the girder)</b>												
udl (TPL)	0.49	0.50	-1.60%	0.49	0.50	-2.41%	0.49	0.48	1.95%	0.49	0.48	2.29%
udl (CPL)	0.56	0.59	-5.98%	0.56	0.61	-9.82%	0.56	0.57	-1.84%	0.56	0.53	5.33%
PL (J1)	1.81	1.59	12.10%	0.67	0.90	-34%	0.07	0.19	-181%	-0.28	-0.18	37%
PL (J2)	0.60	0.80	-32%	1.10	1.21	-10.59%	0.43	0.56	-32%	0.07	0.04	52%
PL (J3)	0.07	0.00	107%	0.43	0.57	-34%	1.10	1.23	-11.67%	0.60	0.65	-9%
PL (J4)	-0.28	-0.22	23%	0.07	0.21	-212%	0.67	0.88	-31%	1.81	1.53	15.46%
<b>C13-series</b> (box-section specimen: 200-mm I-joist, particleboard (upper skin), F11 plywood (lower skin))												
<b>where the crossbeam tributary width is: 1.4-spacing (of the girder)</b>												
udl (TPL)	0.37	0.38	-3.49%	0.37	0.37	-1.26%	0.37	0.35	3.26%	0.37	0.37	-1.04%
udl (CPL)	0.41	0.45	-8.93%	0.41	0.44	-7.93%	0.41	0.41	-0.21%	0.41	0.42	-2.18%
PL (J1)	1.28	1.14	10.25%	0.59	0.65	-10%	0.09	0.17	-87%	-0.29	-0.09	69%
PL (J2)	0.51	0.59	-15%	0.73	0.81	-9.97%	0.28	0.37	-32%	0.10	0.17	-69%
PL (J3)	0.10	0.18	-82%	0.28	0.38	-36%	0.73	0.78	-5.87%	0.51	0.54	-6%
PL (J4)	-0.29	-0.09	69%	0.09	0.16	-76%	0.59	0.60	-1%	1.28	1.12	12.18%
<b>where the crossbeam tributary width is: 2.0-spacing (of the girder)</b>												
udl (TPL)	0.37	0.38	-3.49%	0.37	0.37	-1.26%	0.37	0.35	3.26%	0.37	0.37	-1.04%
udl (CPL)	0.41	0.45	-8.93%	0.41	0.44	-7.93%	0.41	0.41	-0.21%	0.41	0.42	-2.18%
PL (J1)	1.26	1.14	9.31%	0.60	0.65	-8%	0.10	0.17	-74%	-0.30	-0.09	70%
PL (J2)	0.56	0.59	-5%	0.66	0.81	-22.46%	0.30	0.37	-23%	0.11	0.17	-49%
PL (J3)	0.11	0.18	-60%	0.30	0.38	-27%	0.66	0.78	-17.89%	0.56	0.54	3%
PL (J4)	-0.30	-0.09	70%	0.10	0.16	-64%	0.60	0.60	1%	1.26	1.12	11.26%

/..

**Table 5–2: Comparison between the calculated – grillage model – and the measured – test results – deflections (cont.)**

	deflection per 1.0-kN load ( $\Sigma F = 1.0$ kN)											
	joist J1			joist J2			joist J3			joist J4		
	model	test	VAR	model	test	VAR	model	test	VAR	model	test	VAR
	mm/kN			mm/kN			mm/kN			mm/kN		
<b>C03&amp;04-family</b> (open-section specimen: 200-mm I-joist, oriented strand board (upper skin))												
<b>where the crossbeam tributary width is: 1.4-spacing (of the girder)</b>												
* udl (TPL)	0.43	0.41	4.13%	0.43	0.43	-0.74%	0.43	0.43	-0.64%	0.43	0.44	-1.39%
† udl (CPL)	0.49	0.49	-0.96%	0.49	0.52	-6.78%	0.49	0.52	-6.58%	0.49	0.49	-0.63%
* PL (J1)	1.65	1.35	18.32%	0.49	0.82	-66%	0.03	0.20	-475%	-0.20	-0.13	35%
PL (J2)	0.44	0.63	-45%	1.12	1.04	7.64%	0.29	0.52	-79%	0.06	0.06	3%
PL (J3)	0.06	0.08	-23%	0.29	0.52	-79%	1.12	1.02	9.59%	0.44	0.63	-44%
PL (J4)	-0.20	-0.13	35%	0.03	0.18	-432%	0.49	0.78	-59%	1.65	1.37	16.93%
<b>where the crossbeam tributary width is: 2.0-spacing (of the girder)</b>												
udl (TPL)	0.43	0.41	4.13%	0.43	0.43	-0.74%	0.43	0.43	-0.64%	0.43	0.44	-1.39%
udl (CPL)	0.49	0.49	-0.96%	0.49	0.52	-6.78%	0.49	0.52	-6.58%	0.49	0.49	-0.63%
PL (J1)	1.60	1.35	15.75%	0.55	0.82	-48%	0.05	0.20	-292%	-0.23	-0.13	44%
PL (J2)	0.53	0.63	-20%	0.97	1.04	-7.48%	0.35	0.52	-50%	0.08	0.06	23%
PL (J3)	0.08	0.08	2%	0.35	0.52	-50%	0.97	1.02	-5.21%	0.53	0.63	-19%
PL (J4)	-0.23	-0.13	45%	0.05	0.18	-262%	0.55	0.78	-41%	1.60	1.37	14.32%
<b>C10&amp;11-family</b> (box-section specimen: 200-mm I-joist, oriented strand board (upper skin), F11 plywood (lower skin))												
<b>where the crossbeam tributary width is: 1.4-spacing (of the girder)</b>												
udl (TPL)	0.33	0.34	-1.33%	0.33	0.33	1.85%	0.33	0.33	1.69%	0.33	0.34	-3.29%
udl (CPL)	0.38	0.40	-5.75%	0.38	0.39	-3.16%	0.38	0.39	-2.75%	0.38	0.39	-3.93%
PL (J1)	1.18	1.00	14.77%	0.53	0.57	-6%	0.08	0.16	-93%	-0.26	-0.09	64%
PL (J2)	0.46	0.52	-15%	0.69	0.69	0.30%	0.25	0.36	-46%	0.09	0.17	-89%
PL (J3)	0.09	0.16	-84%	0.25	0.35	-42%	0.69	0.69	-0.15%	0.46	0.51	-11%
PL (J4)	-0.26	-0.19	29%	0.08	0.10	-21%	0.53	0.56	-6%	1.18	1.01	14.44%
<b>where the crossbeam tributary width is: 2.0-spacing (of the girder)</b>												
udl (TPL)	0.33	0.34	-1.33%	0.33	0.33	1.85%	0.33	0.33	1.69%	0.33	0.34	-3.29%
udl (CPL)	0.38	0.40	-5.75%	0.38	0.39	-3.16%	0.38	0.39	-2.75%	0.38	0.39	-3.93%
PL (J1)	1.16	1.00	13.83%	0.55	0.57	-4%	0.09	0.16	-79%	-0.27	-0.09	66%
PL (J2)	0.51	0.52	-4%	0.62	0.69	-11.51%	0.27	0.36	-35%	0.10	0.17	-66%
PL (J3)	0.10	0.16	-61%	0.27	0.35	-31%	0.62	0.69	-12.01%	0.51	0.51	-1%
PL (J4)	-0.27	-0.19	31%	0.09	0.10	-12%	0.55	0.56	-3%	1.16	1.01	13.50%

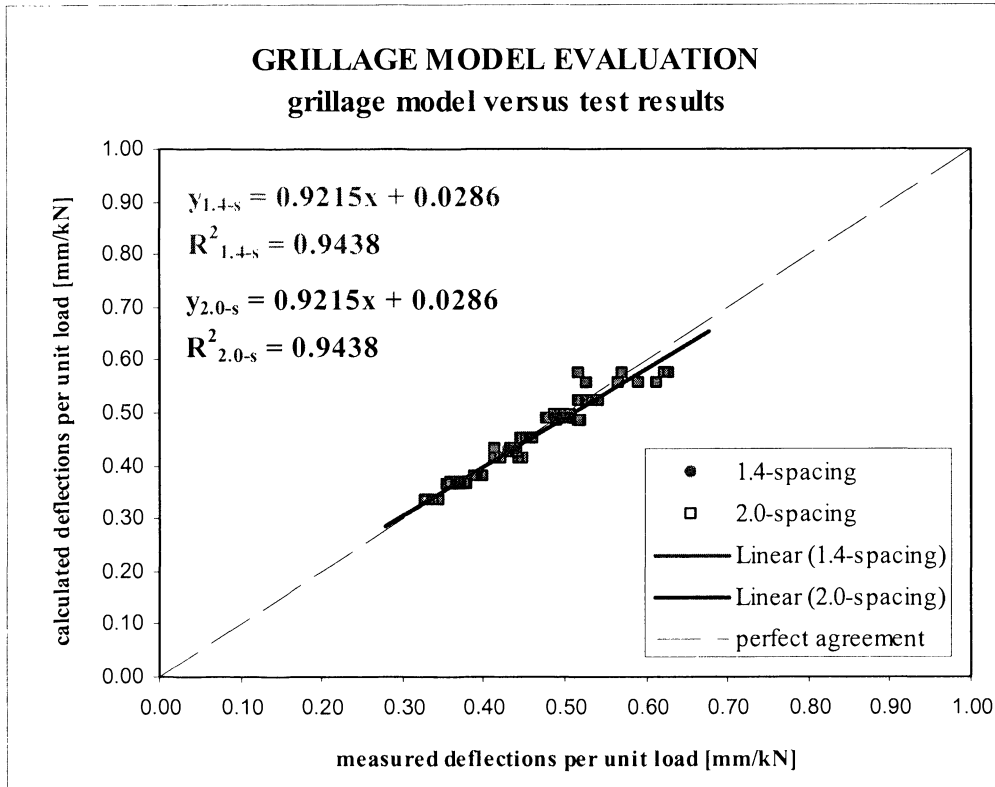
/..

**Table 5–2: Comparison between the calculated – grillage model – and the measured – test results – deflections (cont.)**

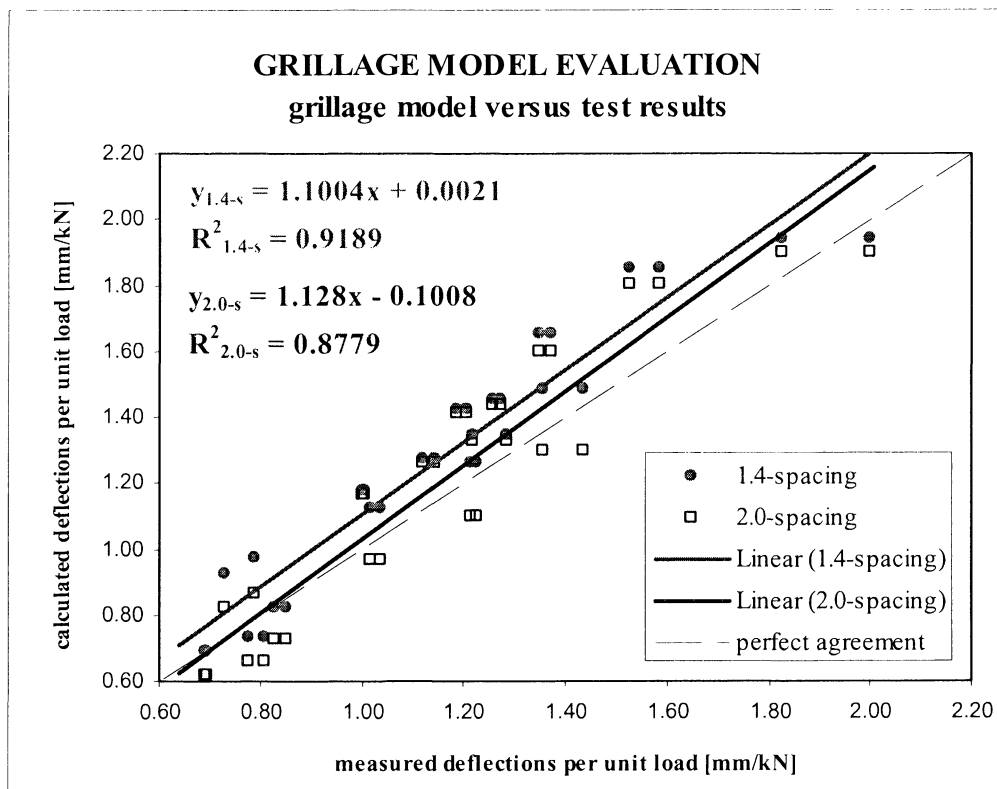
	deflection per 1.0-kN load ( $\Sigma F = 1.0$ kN)											
	joist J1			joist J2			joist J3			joist J4		
	model	test	VAR	model	test	VAR	model	test	VAR	model	test	VAR
	mm/kN			mm/kN			mm/kN			mm/kN		
<b>C09-series</b> (box-section specimen: 356-mm I-joist, F11 plywood (upper & lower skins))												
<b>where the crossbeam tributary width is: 1.4-spacing (of the girder)</b>												
* udl (TPL)	0.45	0.45	0.58%	0.45	0.45	-0.38%	0.45	0.45	-0.54%			
† udl (CPL)	0.52	0.53	-0.86%	0.52	0.53	-0.78%	0.52	0.53	-2.05%			
‡ PL (J1)	1.45	1.28	12.13%	0.32	0.39	-23%	-0.18	-0.07	59%			
PL (J2)	0.27	0.43	-58%	0.98	0.79	18.92%	0.27	0.45	-64%			
PL (J3)	-0.18	-0.10	46%	0.32	0.42	-31%	1.45	1.26	13.31%			
<b>where the crossbeam tributary width is: 2.0-spacing (of the girder)</b>												
udl (TPL)	0.45	0.45	0.58%	0.45	0.45	-0.38%	0.45	0.45	-0.54%			
udl (CPL)	0.52	0.53	-0.86%	0.52	0.53	-0.78%	0.52	0.53	-2.05%			
PL (J1)	1.44	1.28	11.21%	0.35	0.39	-14%	-0.19	-0.07	62%			
PL (J2)	0.33	0.43	-30%	0.87	0.79	8.78%	0.33	0.45	-34%			
PL (J3)	-0.19	-0.10	50%	0.35	0.42	-21%	1.44	1.26	12.41%			
<b>C12-series</b> (box-section specimen: 356-mm I-joist, oriented strand board (upper skin), F11 plywood (lower skin))												
<b>where the crossbeam tributary width is: 1.4-spacing (of the girder)</b>												
udl (TPL)	0.45	0.45	1.12%	0.45	0.46	-1.91%	0.45	0.45	0.53%			
udl (CPL)	0.52	0.52	1.14%	0.52	0.54	-3.82%	0.52	0.53	-1.21%			
PL (J1)	1.43	1.19	16.70%	0.36	0.45	-22%	-0.20	-0.05	75%			
PL (J2)	0.30	0.47	-56%	0.92	0.73	21.02%	0.30	0.48	-60%			
PL (J3)	-0.20	-0.06	71%	0.36	0.45	-24%	1.43	1.21	15.44%			
<b>where the crossbeam tributary width is: 2.0-spacing (of the girder)</b>												
udl (TPL)	0.45	0.45	1.12%	0.45	0.46	-1.91%	0.45	0.45	0.53%			
udl (CPL)	0.52	0.52	1.14%	0.52	0.54	-3.82%	0.52	0.53	-1.21%			
PL (J1)	1.41	1.19	16.04%	0.38	0.45	-16%	-0.21	-0.05	77%			
PL (J2)	0.36	0.47	-31%	0.82	0.73	11.40%	0.36	0.48	-35%			
PL (J3)	-0.21	-0.06	73%	0.38	0.45	-18%	1.41	1.21	14.77%			

\*third-point loading – two uniformly distributed line loads, †centre-point loading – one uniformly distributed line load, ‡centre-point loading – concentrated point load on joist J1 (successively on J2, J3 and J4).

The evaluation of the grillage model capability is further depicted in Figure 5–15. In both plots, each data point depicts the value of a composite girder in a particular loading situation, that is, each girder appears several times on the plot. Furthermore, the vertical and horizontal axes respectively indicate the calculated – grillage model computations – and the measured – test results – deflections per unit load ( $\Sigma F = 1.0$  kN), while the dashed line symbolises the perfect agreement between the calculated measured deflections. In graph (a), the comparison focuses on the uniformly distributed (line) loading. It shows that the grillage performs satisfactorily. It also verifies that both 1.4-spacing and 2.0-spacing give similar computed results. Considering the performance of the grillage model with point load situations, the graph (b) indicates that the 1.4-spacing regression is stronger than that of 2.0-spacing, the coefficient of determination of the first population ( $R^2_{1.4-s}$ ) is closer to 1.0. The slopes of the regressions also suggest that computations with 1.4-spacing are more accurate than 2.0-spacing, that is, the first one exhibits less variation to 1.0. This graph also indicates that, with 1.4-spacing, the grillage computations are consistently larger than the test measurements.



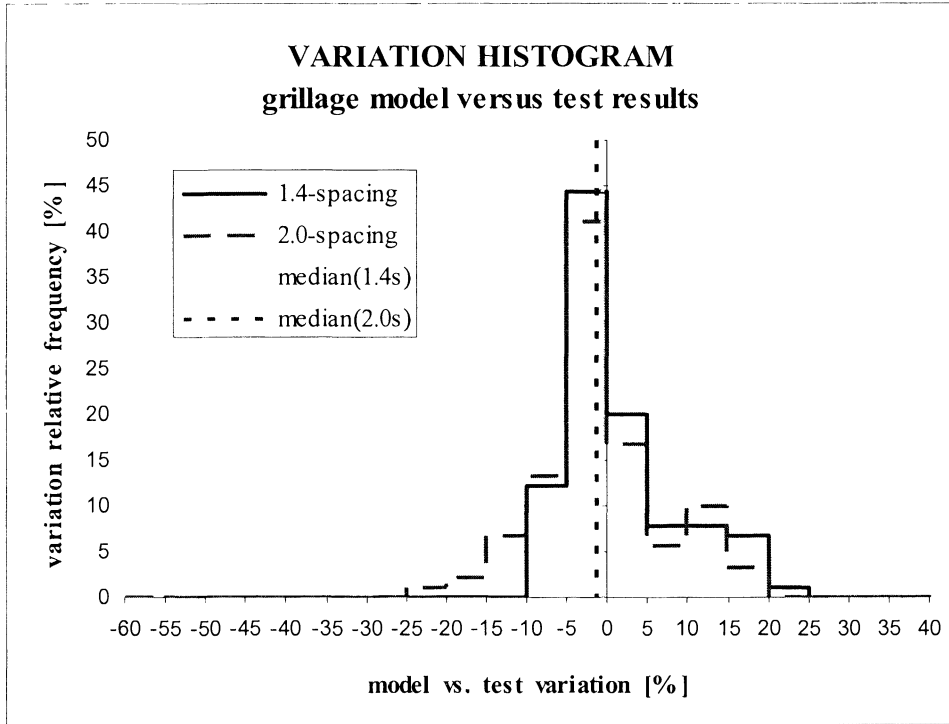
(a)



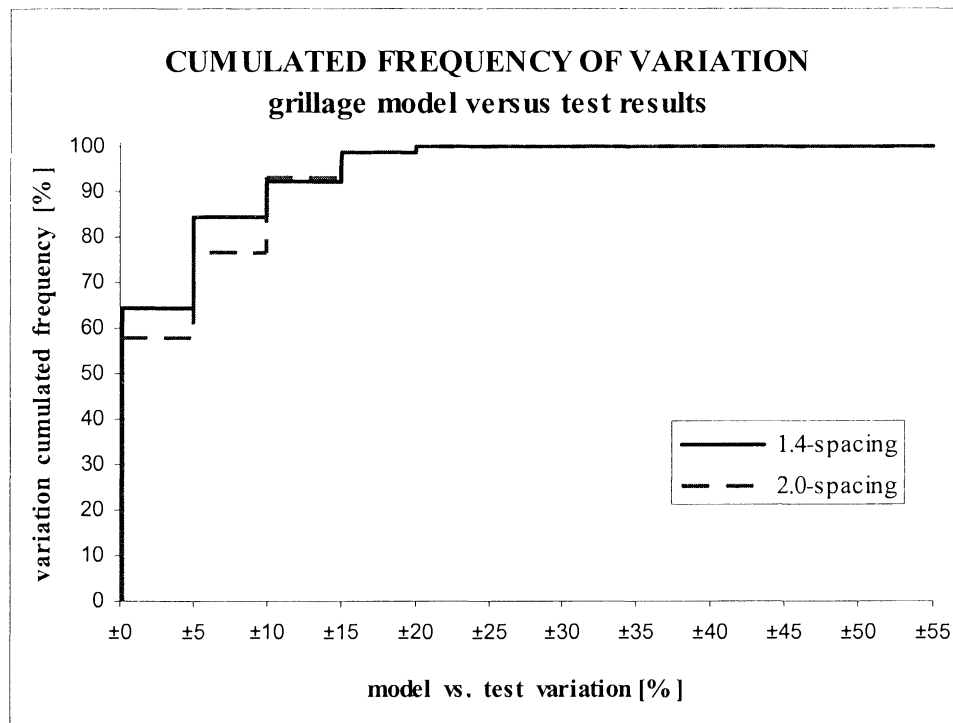
(b)

Figure 5–15: Comparison of the calculated – grillage model – and measured – test results – deflection per unit load (all load positions)

In Figure 5–16, the study of the variation between the model estimates and the test results are depicted. The continuous and dashed lines respectively demonstrate the variations of both the 1.4-spacing and 2.0-spacing tributary widths of the crossbeam, considering the girders onto which node a load vector is introduced. The histogram (a) shows that the location of both medians is very close to zero, indicating that about half of the model estimates are, for both tributary widths, either too large or too small. However, with 1.4-spacing, the deviations of the overestimated results are higher than those of the underestimated deflections. No such trend can be so clearly observed with 2.0-spacing. Furthermore, the cumulated frequency (b) indicates that about 70% of the model estimates, whose crossbeam tributary width corresponds to 1.4-spacing, are within  $\pm 10\%$  of the test results. With the crossbeam tributary width equal to 2.0-spacing, this proportion of estimates in that range reaches about 55%. The outcomes of the variation analysis are confirmation of the high capability of the model in estimating the responses of SSP specimens.



(a)



(b)

Figure 5-16: Histogram of the calculated – grillage model – and measured – test results – deflection per unit load

The grillage's good capability has been demonstrated by the evaluation and variation analyses. It can be identified in Table 5–2 and observed in Figures 5–15 to 5–16. The variations between the estimates of the grillage model and the laboratory observations are acceptable considering the natural variability of structural timber and wood-based materials. It is therefore concluded that the assumptions of the grillage, in particular the properties of the members and the tributary width of the crossbeam, and the interaction between the members are correct.

The graphical depictions (perpendicular profiles of deflection at mid-span) of three series – C05-series, C08-series and C09-series<sup>e</sup>, – are presented in Figures 5–17 to 5–19. These three series have been chosen to illustrate the capability of the grillage model, because they exemplify the performance that the latter can achieve well. The C05-series represents an example of the estimates that the grillage model can accomplish for open-section 200-mm I-joist specimens. Both the C08-series and C09-series depict the achievement of the grillage model in calculating the deflection of box-section specimens with 200-mm and 356-mm I-joists respectively.

*NOTE: these three series are representative of the performance of the grillage model, that is, the remaining specimen series and families exhibit perpendicular profiles of deflection with similar pattern to these three series (refer to Appendix 9).*

---

<sup>e</sup> C05-series: open-section specimen, 200-mm I-joist, particleboard (upper skin); C08-series: box-section specimen, 200-mm I-joist, F11 plywood (upper and lower skins); C09-series: box-section specimen, 356-mm I-joist, F11 plywood (upper and lower skins).



The C02-series depictions show that, for open-section SSP systems, the grillage model generally achieves respectable estimates of both the deflection size and the orthogonal profile (Figure 5–17). Looking at uniformly distributed line loadings, (a) and (b), the model performs brilliantly. For point load situations, (c) to (f), the model estimates – deflection of the joist under load – are also satisfactory. For point loading applied on an exterior girder, it is identified that the model overestimates the deflection. However, the deviations – computed versus measured values – are still acceptable, that is, within  $\pm 15\%$  and  $\pm 20\%$  for crossbeam tributary widths equal to 1.4-spacing and 2.0-spacing respectively.

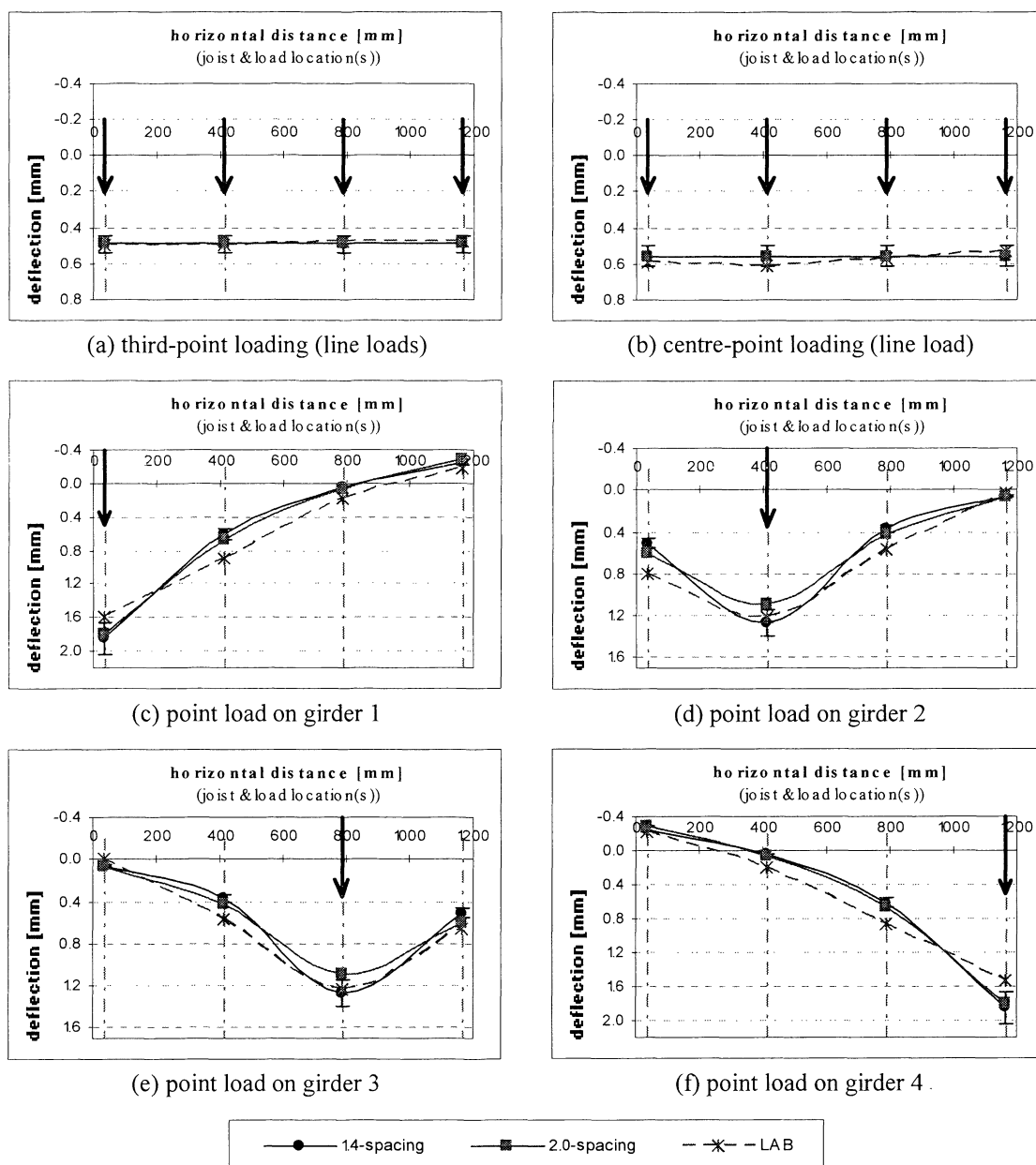


Figure 5–17: Grillage model computations – C05-series perpendicular profiles of deflection at mid-span (continuous skin)

In Figure 5–18, the depictions of C08-series indicate that, for a 200-mm I-joist box-section SSP deck, the grillage model is capable of estimating the deflection magnitude and orthogonal profile very accurately for all loading situations. It is also identified that the best estimates are generally achieved with a crossbeam tributary width equal to 1.4-spacing. With this crossbeam assumption, of 12 model estimates – deflection of the girder onto which a load vector is introduced, 11 (92%) are within  $\pm 5\%$  of the test results, while the remaining 1 (8%) is within  $\pm 10\%$ .

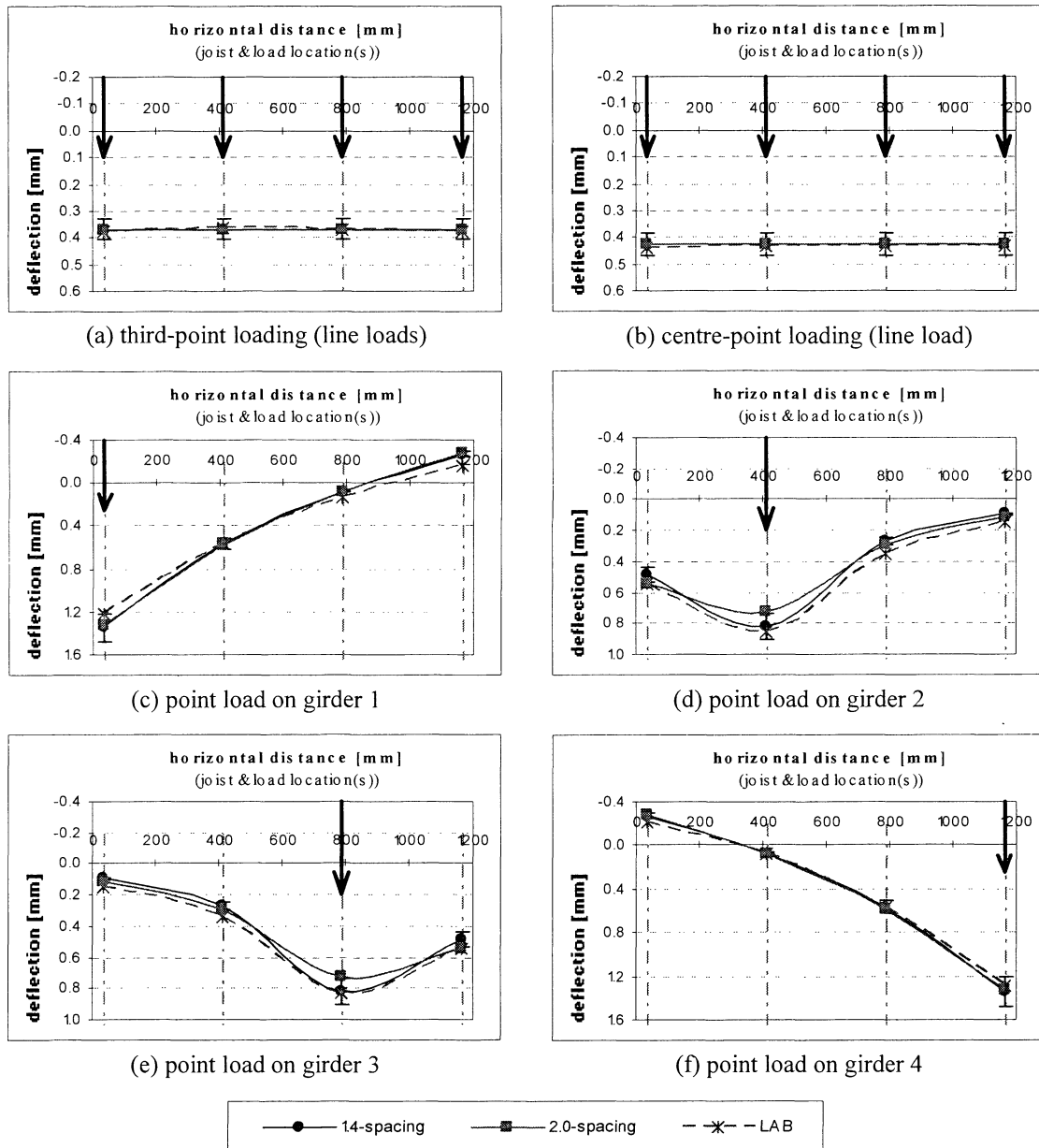


Figure 5–18: Grillage model computations – C08-series perpendicular profiles of deflection at mid-span (continuous skins)

Figure 5–19 presents depictions of the C09-series. It shows that the grillage model also performs well for 356-mm I-joist box-section SSP systems. It is generally capable of satisfactorily calculating both the deflection size and the orthogonal profile. Considering uniformly distributed line loadings, (a) and (b), the model is very accurate. For point load situations, (c) to (e), the model estimates – deflection of the joist under load – are also acceptable. The deviations – calculated versus measured results – are within  $\pm 20\%$  and  $\pm 15\%$  for crossbeam tributary widths equal to 1.4-spacing and 2.0-spacing respectively, the maximum variation occurring in the situation of point loading on the interior girder (d).

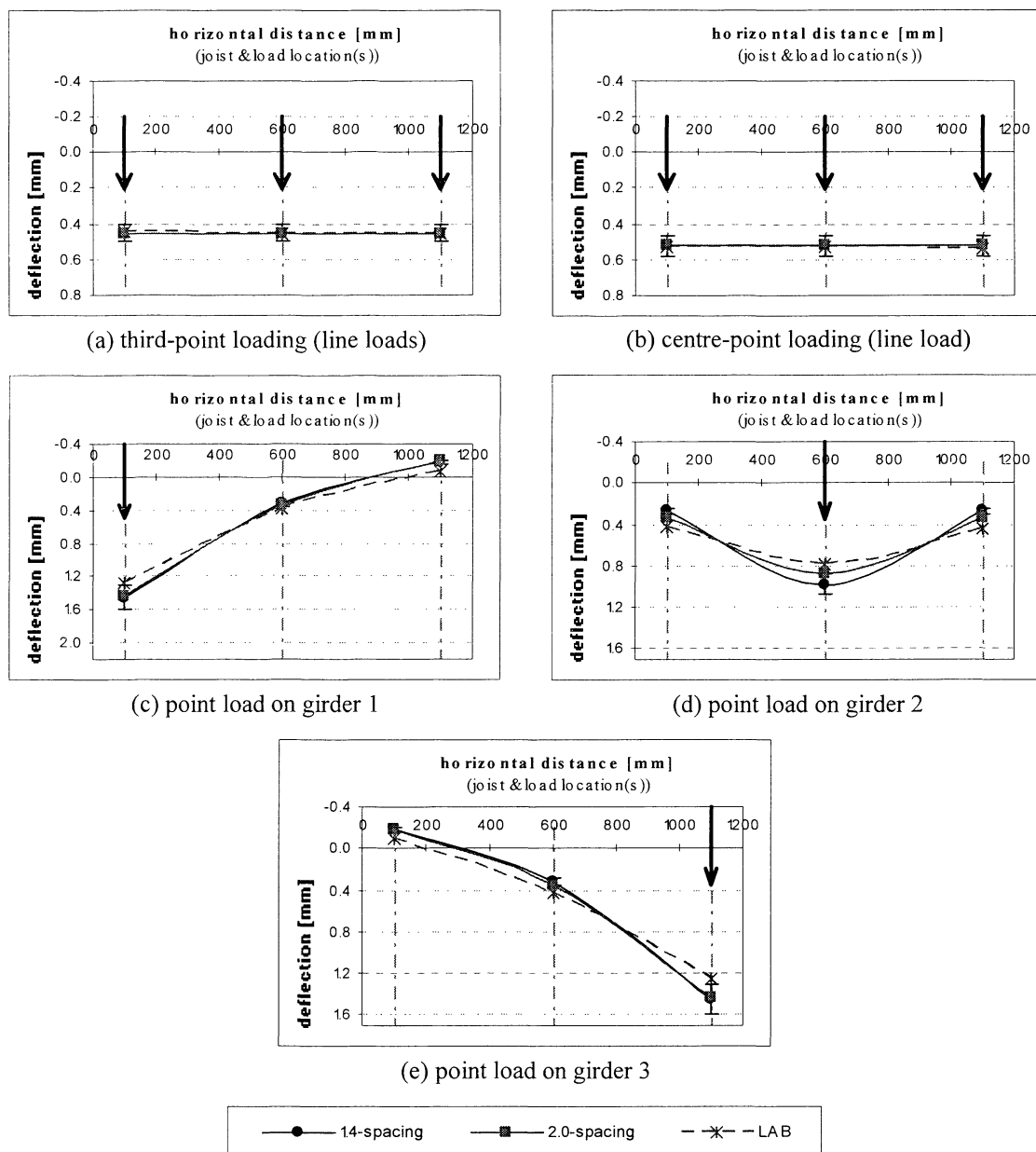


Figure 5–19: Grillage model computations – C09-series perpendicular profiles of deflection at mid-span (continuous skins)

## 5.9 INTRODUCING SKIN DISCONTINUITY(IES) IN THE GRILLAGE MODEL

Several researchers (Criswell 1981; Dawson 1974; Dawson & Goodman 1976; McCutcheon 1986; Sherwood & Moody 1989; Yang, Pham & Leicester 1994) have reported that discontinuing the sheathing of floor systems lowers their global stiffness, logically resulting in increased deflection. The analysis of the test results of the subject research has also identified this phenomenon (refer to Chapter 4 in Part 2). The present section discusses the capability of the grillage to accommodate the effect of discontinuing the skin(s). For this examination, the apparent stiffness of the girders is reduced to the extent quantified by the analysis of the test results. The reduction factors applied to the girders of the specimens considered in this analysis are summarised in Table 5–3. More detailed information about the determination of these factors is presented in Chapter 4 in Part 2.

**Table 5–3: Reduction factors (loss of global stiffness)**

sequence number	cross-section	*specimen global stiffness in Nm <sup>2</sup>		loss of local stiffness	reduction factor
		<sup>†</sup> EI <sub>cs</sub>	<sup>‡</sup> EI <sub>ds</sub>		
C02-03	200-mm I-joist open	1.8109E+06	1.6788E+06	-7.29%	0.927
C04-01		2.0588E+06	1.9089E+06	-7.27%	0.927
C05-01		1.8086E+06	1.7190E+06	-4.94%	0.951
C08-01	200-mm I-joist box	2.4126E+06	2.0807E+06	-13.76%	0.862
C11-01		2.6829E+06	2.3223E+06	-13.44%	0.866
C13-01		2.5430E+06	2.1050E+06	-17.23%	0.828
C09-01	356-mm I-joist box	1.0642E+07	9.7313E+06	-8.55%	0.914
C12-01		1.0752E+07	9.7671E+06	-9.13%	0.909

\* average of test data: 4- and 3-point bending tests (uniformly distributed line load), <sup>†</sup>continuous skin(s),

<sup>‡</sup>discontinuous skin(s).

The evaluation of the model's capability of taking into account skin discontinuities is compared to the test data of single specimens, that is, only one member among the population of each series and family has been investigated in the "damaged" state.<sup>f)</sup> The comparison is carried out similarly to the manner used for the previous evaluation of the model. Therefore, this analysis considers the mid-span deflections per unit load ( $\Sigma F =$

<sup>f)</sup> Skin discontinuities have been applied to the laboratory specimens by inflicting cuts within the zone of the maximum bending moment – 150 mm away from the mid-span.

1.0 kN). The outcomes of the evaluation, which are reported in Table 5–4, indicate that the reduction factors generally result in deflection overestimates by the grillage model. Compared to the evaluation previously completed in order to determine the capability of the grillage (refer to Section 5.8), it can be observed that the model has become less accurate. For example, considering the deviations between the grillage model computations and the test results – deflection of the girders onto which a load is introduced, of 90 computed deflections, 38 (42%) are within  $\pm 10\%$  of the measured deflections, another 24 (27%) are within  $\pm 15\%$ , another 18 (20%) are within  $\pm 20\%$ , while the last 10 (11%) are within  $\pm 25\%$ .<sup>g)</sup> The outcomes of the evaluation suggest that discontinuing the skin(s) of the physical specimens may result in modifying some interaction in the specimen, which may not be replicable by the model. However, it is difficult to single out a unique cause for the model’s loss of predictive capability/accuracy. For example, discontinuing the skin(s) may introduce some non-linearity in the behaviour of the specimen. In addition to this, for the present evaluation, the model responses are compared to the test data of single specimens.<sup>h)</sup> Arguably, such a small scope of experimental references may be more heterogeneous and thus accentuate the deviations with model estimates.

---

<sup>g)</sup> The performance of the grillage model for the specimen in the “healthy” state are recapitulated hereafter: of 90 computed deflections, 69 (77%) are within  $\pm 10\%$  of the test results, another 15 (17%) are within  $\pm 15\%$ , another 5 (5%) are within  $\pm 20\%$ , and the last one (1%) is within  $\pm 25\%$ .

<sup>h)</sup> The identification of the magnitude of the specimen loss of stiffness – determination of the reduction factor – relies on the test data of single specimens as well. Considering the natural variability of wood based products, some deviation with the average data of the test series and families upon which the “healthy” grillage model has been calibrated can be anticipated.

**Table 5-4: Comparison between the calculated – grillage model – and the measured – test results – deflections (discontinuous skin(s))**

		deflection per 1.0-kN load ( $\Sigma F = 1.0$ kN) — variation report										
		joist J1	joist J2	joist J3	joist J4	joist J1	joist J2	joist J3	joist J4	joist J1	joist J2	joist J3
		<b>C02-03</b>				<b>C08-01</b>				<b>C09-01</b>		
1.4-spacing	* udl (TPL)	12.1%	3.2%	3.2%	7.6%	16.3%	15.9%	9.4%	11.4%	5.6%	13.7%	5.2%
	† udl (CPL)	14.6%	-3.2%	3.4%	7.6%	11.6%	14.3%	8.4%	13.5%	3.9%	11.2%	6.6%
	‡ PL (J1)	17.0%	-35%	-267%	73%	12.4%	-3%	-117%	57%	11.5%	-45%	100%
	PL (J2)	-27%	10.2%	-75%	-13%	-11%	0.1%	-43%	-91%	-76%	10.7%	-74%
	PL (J3)	167%	-71%	1.0%	-32%	-89%	-40%	0.7%	-17%	94%	-50%	14.0%
	PL (J4)	58%	-304%	-53%	13.9%	32%	-54%	-6%	8.3%			
2.0-spacing	udl (TPL)	12.1%	3.2%	3.2%	7.6%	16.3%	15.9%	9.4%	11.4%	5.6%	13.7%	5.2%
	udl (CPL)	14.6%	-3.2%	3.4%	7.6%	11.6%	14.3%	8.4%	13.5%	3.9%	11.2%	6.6%
	PL (J1)	15.1%	-23%	-179%	76%	11.0%	1%	-92%	59%	10.5%	-32%	100%
	PL (J2)	-2%	-2.7%	-41%	12%	1%	-13.0%	-30%	-65%	-44%	-0.8%	-42%
	PL (J3)	152%	-39%	-13.2%	-6%	-63%	-27%	-12.3%	-4%	94%	-37%	13.1%
	PL (J4)	62%	-207%	-40%	11.9%	36%	-36%	-2%	6.9%			
		<b>C04-01</b>				<b>C11-01</b>				<b>C12-01</b>		
1.4-spacing	udl (TPL)	12.1%	6.8%	9.4%	1.9%	10.7%	12.7%	14.4%	15.3%	8.4%	12.2%	5.9%
	udl (CPL)	7.8%	3.6%	0.4%	3.5%	6.5%	8.5%	10.5%	14.9%	8.1%	8.8%	6.5%
	PL (J1)	16.9%	-74%	-492%	34%	17.1%	-9%	-134%	83%	16.5%	-34%	89%
	PL (J2)	-50%	8.4%	-79%	-21%	-16%	2.5%	-50%	-98%	-71%	17.1%	-71%
	PL (J3)	-54%	-81%	12.3%	-47%	-110%	-45%	4.3%	-7%	86%	-30%	15.3%
	PL (J4)	41%	-477%	-59%	15.6%	68%	-80%	-4%	22.9%			
2.0-spacing	udl (TPL)	12.1%	6.8%	9.4%	1.9%	10.7%	12.7%	14.4%	15.3%	8.4%	12.2%	5.9%
	udl (CPL)	7.8%	3.6%	0.4%	3.5%	6.5%	8.5%	10.5%	14.9%	8.1%	8.8%	6.5%
	PL (J1)	14.3%	-54%	-301%	44%	16.2%	-6%	-117%	83%	15.9%	-27%	90%
	PL (J2)	-23%	-6.7%	-50%	4%	-5%	-9.0%	-39%	-74%	-45%	7.0%	-44%
	PL (J3)	-22%	-52%	-2.2%	-21%	-84%	-34%	-7.0%	3%	87%	-23%	14.7%
	PL (J4)	50%	-291%	-41%	12.9%	70%	-66%	-1%	22.1%			
		<b>C05-01</b>				<b>C13-01</b>						
1.4-spacing	udl (TPL)	10.7%	-3.9%	3.6%	10.6%	15.3%	17.6%	17.7%	16.6%			
	udl (CPL)	10.6%	-10.1%	-1.9%	10.3%	11.5%	12.0%	15.9%	13.9%			
	PL (J1)	17.1%	-44%	-293%	8%	21.4%	0%	-114%	85%			
	PL (J2)	-44%	6.0%	-55%	42%	-9%	-0.4%	-33%	-79%			
	PL (J3)	-16%	-73%	0.2%	-37%	-103%	-40%	-0.3%	-1%			
	PL (J4)	32%	-409%	-49%	15.1%	89%	-127%	1%	17.4%			
2.0-spacing	udl (TPL)	10.7%	-3.9%	3.6%	10.6%	15.3%	17.6%	17.7%	16.6%			
	udl (CPL)	10.6%	-10.1%	-1.9%	10.3%	11.5%	12.0%	15.9%	13.9%			
	PL (J1)	15.0%	-32%	-194%	19%	20.6%	2%	-99%	86%			
	PL (J2)	-22%	-8.0%	-34%	55%	0%	-11.8%	-24%	-58%			
	PL (J3)	9%	-49%	-14.7%	-15%	-80%	-31%	-11.7%	8%			
	PL (J4)	39%	-280%	-37%	13.0%	90%	-111%	3%	16.5%			

\* third-point loading – two uniformly distributed line loads, † centre-point loading – one uniformly distributed line load, ‡ centre-point loading – concentrated point load on joist J1 (successively on J2, J3 and J4).

Figure 5–20 presents the general trend of the model computations (vertical axis) compared to the test results (horizontal axis). The thick coloured continuous lines correspond to the linear regression of both data series, while the dashed line symbolises the ideal situation – an exact match between the calculated and measured values. The graph shows that the slope of the regressions deviates from 1.0 quite notably, confirming that the reduction magnitude of the girder stiffness, as identified by the analysis of the test results, does not allow the model to calculate the deflection accurately. The coefficients of determination indicate that the strength of the regressions is acceptable.

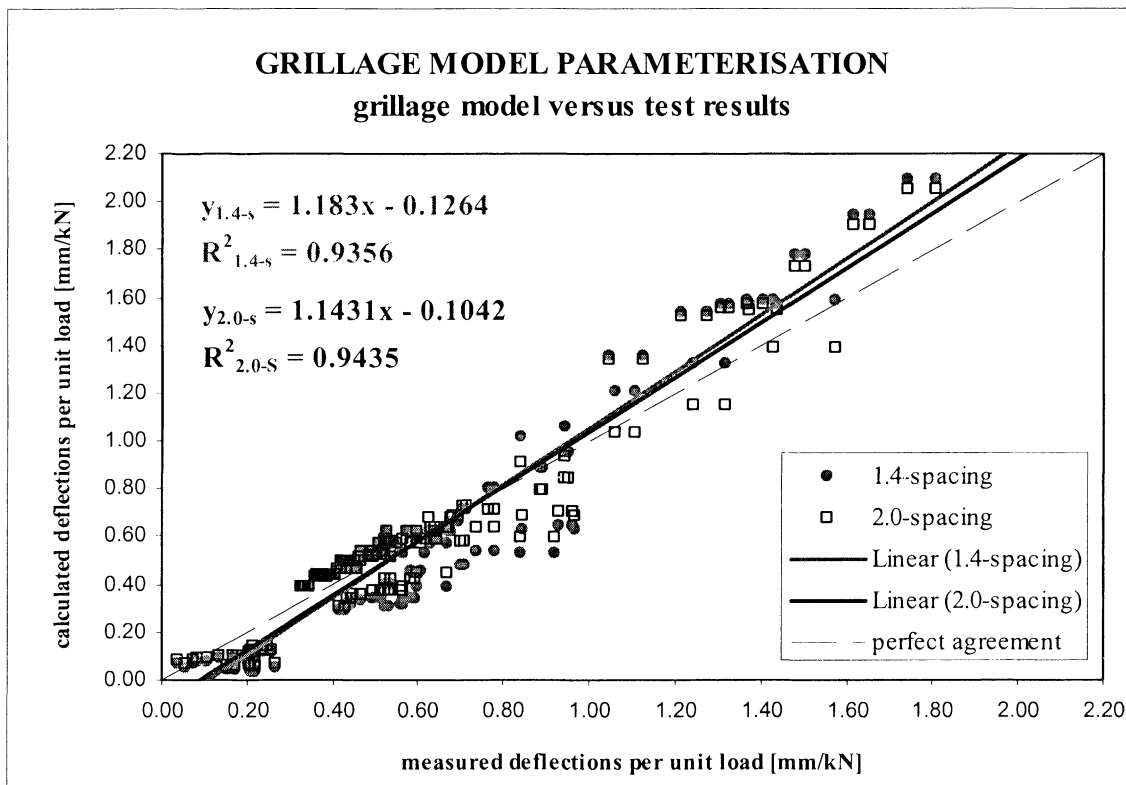
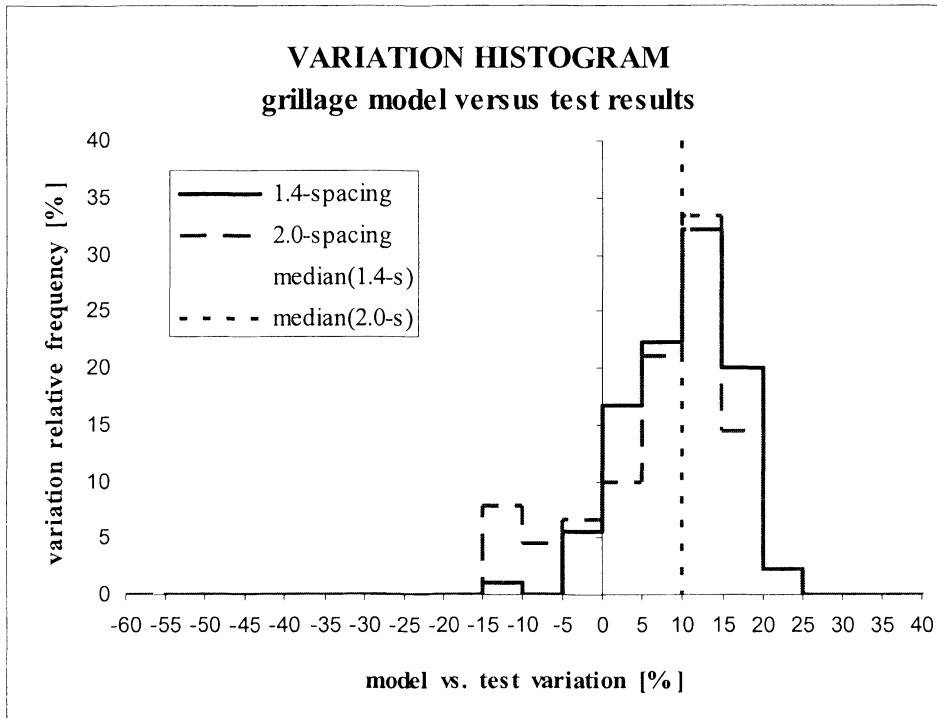


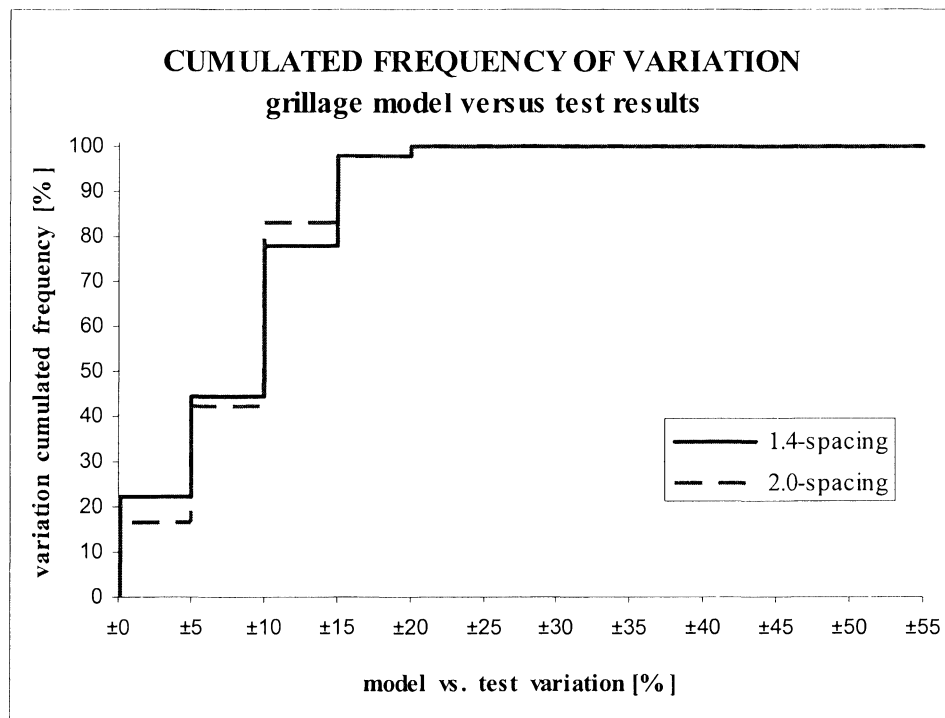
**Figure 5–20: Comparison of the calculated – grillage model – and measured – test results – deflection per unit load (discontinuous skin(s))**

The study of the deviation between the model computations and the test results is depicted in Figure 5–21. The histogram (a) permits identifying the tendency of the model to overestimate the mid-span deflection of the girders. These drifts are demonstrated by the medians, which are markedly located in the positive zone of the x-axis for both crossbeam tributary widths, that is, 1.4-spacing and 2.0-spacing. The cumulated frequency (b) is a confirmation of the loss of accuracy experienced by the

model. For both crossbeam tributary widths, only about 45% of the model estimates are within  $\pm 10\%$  of the test results.



(a)



(b)

Figure 5–21: Histogram of the calculated – grillage model – and measured – test results – deflection per unit load (discontinuous skin(s))



The analysis of the introduction of skin discontinuities into the grillage model has demonstrated that the model is capable of accommodating such parameter (Table 5–4 and Figures 5–20 and 5–21). However, it has identified that the value of the modification factor, as identified with physical specimens (refer to Chapter 4 in Part 2), fails to modify the behaviour of the grillage model adequately.

The C08-01<sup>i)</sup> specimen has been chosen to graphically exemplify the performance of the grillage model for specimens with discontinuous skin(s). Figure 5–22 depicts the patterns of changes – tendencies – that are exhibited by the C08-01 specimen as a consequence of discontinuing its skins. The depictions confirm that the size of the computed and measured deflections – considering the girder onto which a load vector is introduced – deviate quite significantly. On the other hand, the orthogonal profiles of deflection remain qualitatively acceptable.

*NOTE: the C08-01 specimen is representative of the performance of the grillage model for the specimens, whose skin(s) has(have) been discontinued, that is, these specimens exhibit perpendicular profiles of deflection with similar pattern to the C08-01 specimen (refer to Appendix 9).*

---

<sup>i)</sup> C08-series: box-section specimen, 200-mm I-joist, F11 plywood (upper and lower skins).

The C08-01 depictions show that the grillage model generally overestimates the size of the deflection (joist under direct loading) but achieves respectable approximation of the orthogonal profiles of deflection (Figure 5–22). The plots also indicate that the best estimates are generally achieved with a crossbeam tributary width equal to 1.4-spacing for all load situations. Considering this crossbeam tributary width, the evaluation of the model capability can be summarised as follows: of 12 estimated deflections, 5 (42%) are within  $\pm 10\%$  of the test results, another 5 (42%) are within  $\pm 15\%$ , while the last 2 (16%) are within  $\pm 20\%$ .

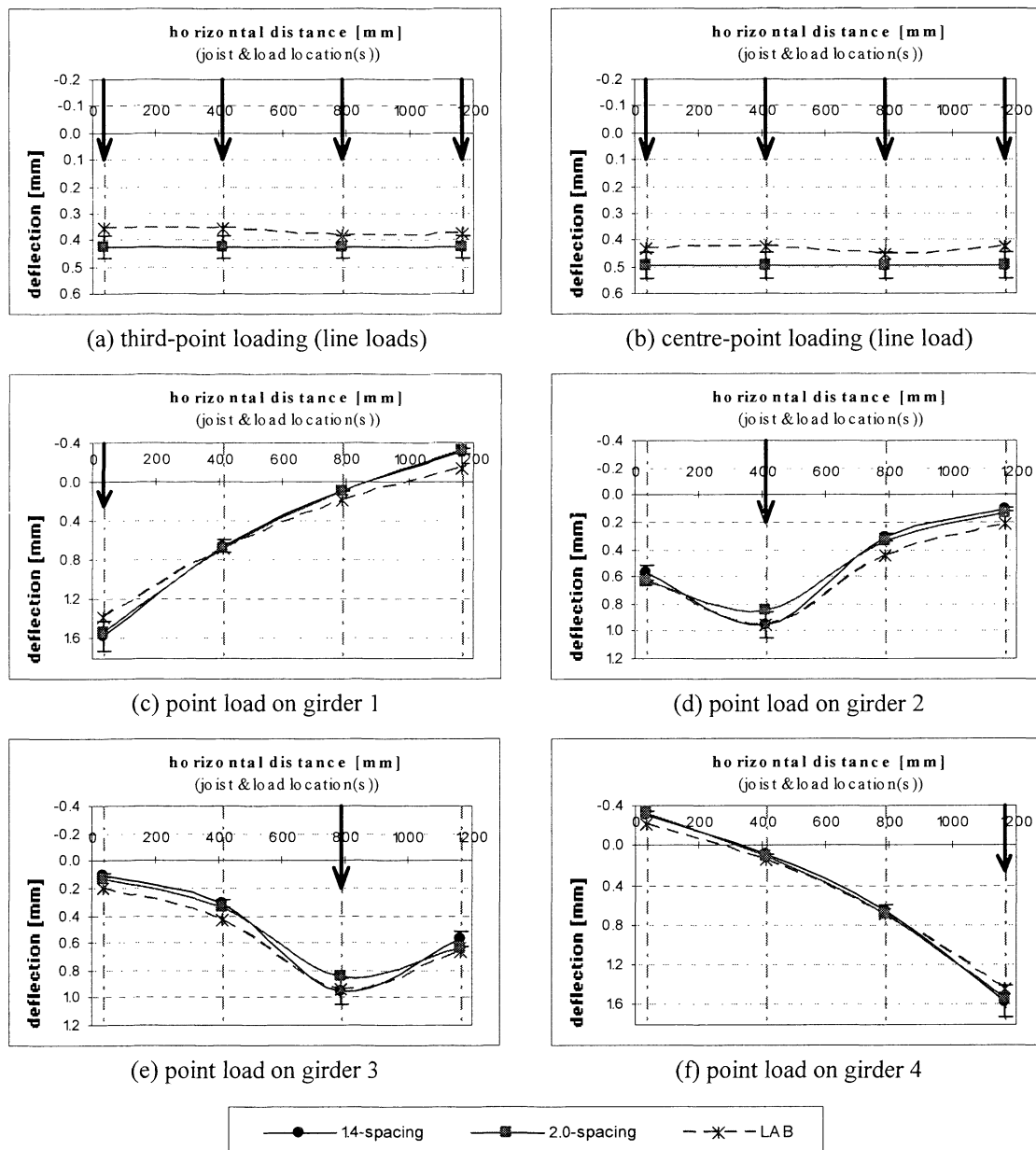


Figure 5–22: Grillage model computations – C08-01 perpendicular profiles of deflection at mid-span (discontinuous skins)

## 5.10 CONCLUDING SUMMARY

This chapter has presented a grillage model capable of computing the deflection of SSP systems under uniformly distributed (line) loading and concentrated point load arrangements. Expressed in other words, this model can satisfactorily calculate the quantitative and qualitative responses. Furthermore, the grillage model performs equivalently well for the specimens in healthy and damaged states.

Mathematical modelling involves idealising aspects of the physical structure to some extent. In that respect, characterising the two-way action ability in the grillage model has been successful. For uniformly distributed load arrangements, the significance of the crossbeam ability is not decisive, because arguably each girder captures a (quasi) equivalent intensity of load. Thus, the orthogonal profile of the deflection is homogenous. For the concentrated point load, the properties of the crossbeam become influential because they determine the ability in the model to laterally distribute/bridge a point loading action. For the grillage model to perform accurately, a series of measures are necessitated:

1. The section properties of each member should be estimated with reference to a single modulus of elasticity (MOE) – for the determination of every modular ratio. In the subject research, this MOE corresponds to that of the I-joist flange (direction parallel to the wood grain), that is, 15'200 MPa (Table 5–1).

2. The global stiffness of the grillage girders should accommodate the flexural stiffness (EI) and shear rigidity (GA) (Equation 5-14).

3. Under distributed (line) load arrangements (third-point and centre-point loadings), the grillage crossbeam should incorporate the flexural stiffness (EI) and shear rigidity (GA) (Equation 5-23). It has also been observed that the smoothing effect of the girder deflection is moderate under distributed (line) loading, that is, the (common property and dimension) sheathings, used in the subject research (Table 5–1), facilitate limited load (re)distribution among the girders.

4. In situations of concentrated point loading introduced on an interior girder, the grillage crossbeam should incorporate the flexural stiffness (EI) and shear rigidity (GA) (Equation 5-23). For such a load arrangement, there are indeed indications that the load distribution is dominantly governed by the apparent flexural stiffness of the crossbeam.

5. In situations where the concentrated point load is applied on an exterior girder, it has been observed that the crossbeam should also account for the torsional rigidity of

the SSP deck. The grillage crossbeam should consequently integrate the flexural stiffness (EI), shear rigidity (GA) and the torsional rigidity (GJ) (Equation 5-24).

6. The distribution pattern of the concentrated point loads inside the deck unit is characterised by the apparent global stiffness of the girders (deck unit) and the global stiffness and torsional properties of the crossbeam at the location of the load introduction (Equation 5-16). This angle is subsequently used for determining the crossbeam properties at each adjacent girder. Therefore, in the grillage model, each segment of the crossbeam is attributed varying properties.

The comparison with physical tests – specimens in the healthy state – has demonstrated that in most loading situations, the model performs, that is, the variations between both data populations are in general within  $\pm 10\%$ . Such deviation is acceptable considering the natural variability of structural timber and wood-based products.

The evaluation of the grillage model has also demonstrated that the grillage model can accommodate the effect of discontinuities – “damage” – in the skins. This is performed by applying a modification factor on the axial stiffness of the girders. These factors, which have been identified with the analysis of the test data (refer to Chapter 4 in Part 2), correspond to 0.9 and 0.8 for open- and box-section SSP systems respectively. The evaluation of the “damaged” model indicates that the predictions of the model are satisfactory in most situations, that is, generally within the  $\pm 10\%$  range.

The grillage model presented in this chapter has been developed focusing on the specimens of the subject research. It therefore counts either four or three girders, and a single crossbeam. The development of the model has been limited to this couple of constructions because of the changing properties of the crossbeam. The grillage model is, however, not limited to these two SSP systems. In the author’s opinion, this grillage model is capable of accommodating larger numbers of girders and/or crossbeams. It is also anticipated that it can be fitted into a general solution routine. The author suggests that this development should be given serious consideration and be the subject of future work.

Chapter 6 in Part 1 presents an alternative numerical procedure to the grillage model. This procedure corresponds to finite element model, which is assembled using ANSYS software. Chapter 6 discusses the development, parameterisation and validation of this model.



<b>6</b>	<b>FINITE ELEMENT MODEL AND ANALYSIS.....</b>	<b>156</b>
<b>6.1</b>	<b>Construction platform and fundamentals of the finite element model.....</b>	<b>157</b>
<b>6.2</b>	<b>Concept and development of the finite element model.....</b>	<b>159</b>
6.2.1	Schematic plan of the finite element analysis.....	160
6.2.2	Assisting tools.....	162
6.2.3	First prototype of the finite element model.....	163
6.2.4	The finite element model (FEM).....	165
6.2.5	Element types of the finite element model.....	165
6.2.6	Real constants of the finite element model.....	169
6.2.7	Material properties of the members of the finite element model.....	170
6.2.8	Characterising the I-joists.....	173
<b>6.3</b>	<b>Parameterisation of THE finite element model.....</b>	<b>175</b>
6.3.1	Concept of the parameterisation.....	175
6.3.2	Benchmarks of the parameterisation.....	176
6.3.3	Findings/outcomes of the parameterisation.....	176
<b>6.4</b>	<b>Evaluation of the finite element model's capability.....</b>	<b>179</b>
<b>6.5</b>	<b>Introducing skin discontinuity(ies) in the grillage model.....</b>	<b>188</b>
<b>6.6</b>	<b>Concluding summary.....</b>	<b>194</b>

## 6 FINITE ELEMENT MODEL AND ANALYSIS

SSP systems are highly complex, orthotropic, statically indeterminate and multi-layer assemblies. Furthermore, each member of the SSP system – joist and panel – exhibits orthotropic and viscoelastic properties, and non-linear behaviour under certain conditions. In addition to this, structural timber – such as that of the flange of the I-joist used in the subject research – is randomly affected by natural growth characteristics which can be described as “defects” in terms of uniform structural performance, that is, they can cause notable variability of the mechanical properties. Several researchers, for example, Polensek et al. (1972) and Vanderbilt et al. (1974), in describing wood joist systems, acknowledged that such systems are emphatically complex because of the material properties on the one hand, and the intricate interactions between the floor members on the other hand. Therefore, accommodating SSP systems into a finite element model is an arduous task, which is rendered even more complex by the use of I-joists for the centre part – web – of the SSP specimens tested in the subject research, and inevitably represents an idealisation of the actual systems.

This chapter introduces and discusses the concept, development and capability of a finite element model (FEM). The latter has been developed using the ANSYS software package (ANSYS Inc. 2003, 2004, 2005), which corresponds to a general-purpose finite element computer program, thus imposing restrictions on the choice, definition and control of the element attributes and solution. For example, the glued interlayers – connection between the I-joists and the skin(s) – are modelled with contact element technology, to which ANSYS offers restricted access for characterising the properties

and controlling the solution's *modus operandi*. The finite element analysis (FEA) focuses on the range of working load. It therefore focuses on simulating/replicating the linear-elastic behaviour of the specimen (refer to Chapter 4 in Part 2). The load arrangements and specimen boundary conditions of the non-destructive laboratory tests also define the scope of the FEA (refer to Chapter 3 in Part 2).

## 6.1 CONSTRUCTION PLATFORM AND FUNDAMENTALS OF THE FINITE ELEMENT MODEL

The finite element analysis (FEA) is carried out in the environment of the ANSYS software package (ANSYS Inc. 2003, 2004, 2005). In ANSYS, the construction of the finite element model (FEM) begins with the definition of the “physical” aspects of the elements, such as the element type (attribute of the elements), the real constant of the element (geometric parameters of the elements), and the material properties of the element (Modulus of Elasticity, Poisson's ratio). The main features of these aspects are concisely summarised hereafter. More detailed information about each aspect is available in ANSYS documentation (ANSYS Inc. 2005).

- **Element type**

The element type determines fundamental characteristics of the element, such as the field of analysis (structural, thermal, etc.) and the degree of freedom of the nodes. Therefore, it indicates whether the element lies in 2-D or 3-D space. Furthermore, the element type defines the number of nodes of the model; as such, 512000 nodes represent the number of nodes authorised by the licence conditions of The University of Technology, Sydney.

- **Real constant**

The element's real constants are the properties that characterise the element type. For example, they define the cross-sectional properties (shell thickness), or the stiffness matrix of the element.

- **Material properties**

Material properties characterise the behaviour/responses of the elements to loading action. The current research requires defining the matrices of orthotropic materials – materials with distinctive properties in three mutually orthogonal directions – for the engineered wood panels. Solid wood has been idealised as a bi-dimensional orthotropic material, that is, showing identical properties for the radial and tangential directions.



Material properties of the elements are derived from Australian standards (Australian Standard<sup>TM</sup> 1997; Australian/New Zealand Standard<sup>TM</sup> 2004a, 2004b), technical documentation published by associations or by the manufacturers (Kronoply GmbH & Co. KG; Trus Joist<sup>TM</sup> a Weyerhaeuser Business 2002b) and other sources (APA – The Engineered Wood Association 2005; Australian Wood Panels Association Incorporated 2004; Finnish Forest Industries Federation 2002; Merz et al. 1998, 2000). However, appropriate wood material data is not readily available at present, and defining the material properties of the model members proved more challenging, and a series of laboratory tests have been conducted by the author (refer to Appendix 8). Ultimately, in order to complete the material matrices, reasonable assumptions have been made for the “missing” material data.

In ANSYS, the orthotropic properties of the materials are defined with elasticity matrices that comprise three Moduli of Elasticity ( $E_x$ ,  $E_y$ ,  $E_z$ ), three Poisson’s ratios ( $\nu_{xy}$ ,  $\nu_{yz}$ ,  $\nu_{xz}$ ) and three shear moduli ( $G_{xy}$ ,  $G_{yz}$ ,  $G_{xz}$ ), whereby the compatibility of the material matrix is verified by Equation 6-1. The material data implemented in FEM are listed in Tables 6–1 and 6–2.

$$1.0 - \nu_{xy}^2 \frac{E_y}{E_x} - \nu_{yz}^2 \frac{E_z}{E_y} - \nu_{xz}^2 \frac{E_z}{E_x} - 2.0 \nu_{xy} \nu_{yz} \nu_{xz} \frac{E_z}{E_x} > 0 \quad (\text{Eq. 6-1})$$

where: E: modulus of elasticity [Pa]  
 G: shear modulus [Pa]  
 v: Poisson’s ratio [–]  
 subscripts: x, y & z: local axis of the elements

The pre-solution phase of the model construction continues with the entry of the physical properties of the FEM, which includes the geometry and dimension of the members, and the definition and generation of the mesh. In the subject research, mapped meshing has been chosen as opposed to free meshing. Using mapped meshing enables greater control over the dimensions and shape of the mesh, the number of elements and the transition and connectivity between the elements. Defining the boundary conditions (support conditions) and introducing the loading complete the FEA pre-solution phase.

## 6.2 CONCEPT AND DEVELOPMENT OF THE FINITE ELEMENT MODEL

ANSYS (ANSYS Inc. 2005) is a general-purpose finite element computer program. It imposes restrictions on the choice, definition and control of the element attributes. The finite element model (FEM) needs to comply with ANSYS rules and principles, for example, the compatibility requirements imposed on the elements. All the elements of the model have been chosen from the ANSYS library and characterised accordingly. Thus, no element development has been carried out in the subject research.

Modelling with computer software inherently represents an idealisation as well as a compromise of the “real” systems. However, to some extent, FEM succeeds in accounting for the complexity of the specimens – composite assemblies of I-joists and engineered wood product sheathing(s) – of the subject research, that is, to some extent it duplicates the complex characteristics and properties of the actual specimens. However, the high level of sophistication of SSP systems and, incidentally, of FEM, has pushed toward an evolving development. This approach also suits the fact that the FEM needs to consider several cross-section constructions (open and box sections), dimensions (200-mm and 356-mm I-joist specimens), and two specimen states (“healthy” and “damaged”<sup>a)</sup>).

The use of I-joists has imposed an intermediary phase on FEM development, in which the I-joists have been investigated and calibrated in single beam conditions (refer to Section 6.2.8). On the other hand, modelling the skin(s) is fairly straightforward and is carried out using shell elements, to which orthotropic mechanical properties are attributed. The concept of the interfaces happens in two distinct stages; while the interlayers of the first FEM prototype are modelled with pins (MATRIX27 elements (refer to Section 6.2.3)), the final FEM uses the contact element technology (CONTA173 and TARGE170 elements (refer to Section 6.2.4)). The evolution of the interlayer modelling has been dictated by the mitigated results achieved with the pinned solution.

In ANSYS (ANSYS Inc. 2005), many possibilities are given for the input of the boundary conditions. However, for the solution, ANSYS transposes each boundary condition into a nodal condition. This practice has necessitated introducing the

---

<sup>a)</sup> In the “healthy” state, the specimen have continuous skin(s); while in “damaged” state, the skin(s) has(have) been discontinued by inflicting it (them) a cut within the maximum bending moment zone – 150 mm away from mid-span.

boundary conditions directly onto the nodes. For example, nodal loads are entered instead of surface or line loads.

### 6.2.1 Schematic plan of the finite element analysis

The protocol of the finite element analysis (FEA) includes three major phases; firstly the pre-solution in which the model is assembled, secondly the analysis in which the model is solved under a defined loading situation, and thirdly the post-solution in which the output reports are put together. The FEA protocol aims at replicating the scope of the laboratory investigation. This implies that the last two phases are repeated for each load arrangement relevant to the SSP specimen under analysis (refer to Chapter 3 in Part 2).

The schematic plan of FEA corresponds to a network of files. It has been developed in order to accommodate the physical aspects of the specimens, such as open and box sections, material mix, “healthy” and “damaged” states, etc., the loading program, in the form of series of uniformly distributed line loads and concentrated point loads, and the analysis report, which include tables of data, pictures and animations. The main features/functions of the FEA files are briefly described hereafter (these files in extention can be found in Appendix 11):

1. The FEA protocol is controlled by the **central master** file. In the latter, the physical parameters and features of the finite element model (FEM) are selected/activated. The analysis is launched from the central master file respectively by means of the central master file, and any other file of the FEA protocol is subordinated to it.

2. The **model master** file contains the physical parameters (dimensions, mesh size) and material properties of the model members. It also includes modelling data such as the element types and real constants. The model master has a series of subordinate files, whose loading is compulsory (boundary conditions) or optional (pinned interlayers) for the completion of the analysis.

3. The analysis is launched with the **load master** file, which contains the solution protocol, the load case being uploaded from a subordinate file. The load master file also controls the assembling of the analysis reports. Because the information included in the reports is load-case related, so too are the load master files.

The structure of the FEA protocol is schematically depicted in Figure 6–1. It shows the links between the master files and subordinate files. It also indicates that until the full completion of the analysis – analysis of the  $n$ th load arrangement – the FEA protocol repeats the solution routine for each load master respectively, that is, after the completion of each load case, the FEA protocol resumes with reloading the pre-solved model.

*NOTE: after the protocol of a file is finished, the procedure returns to the directly superior file (red discontinuous lines (Figure 6–1)).*

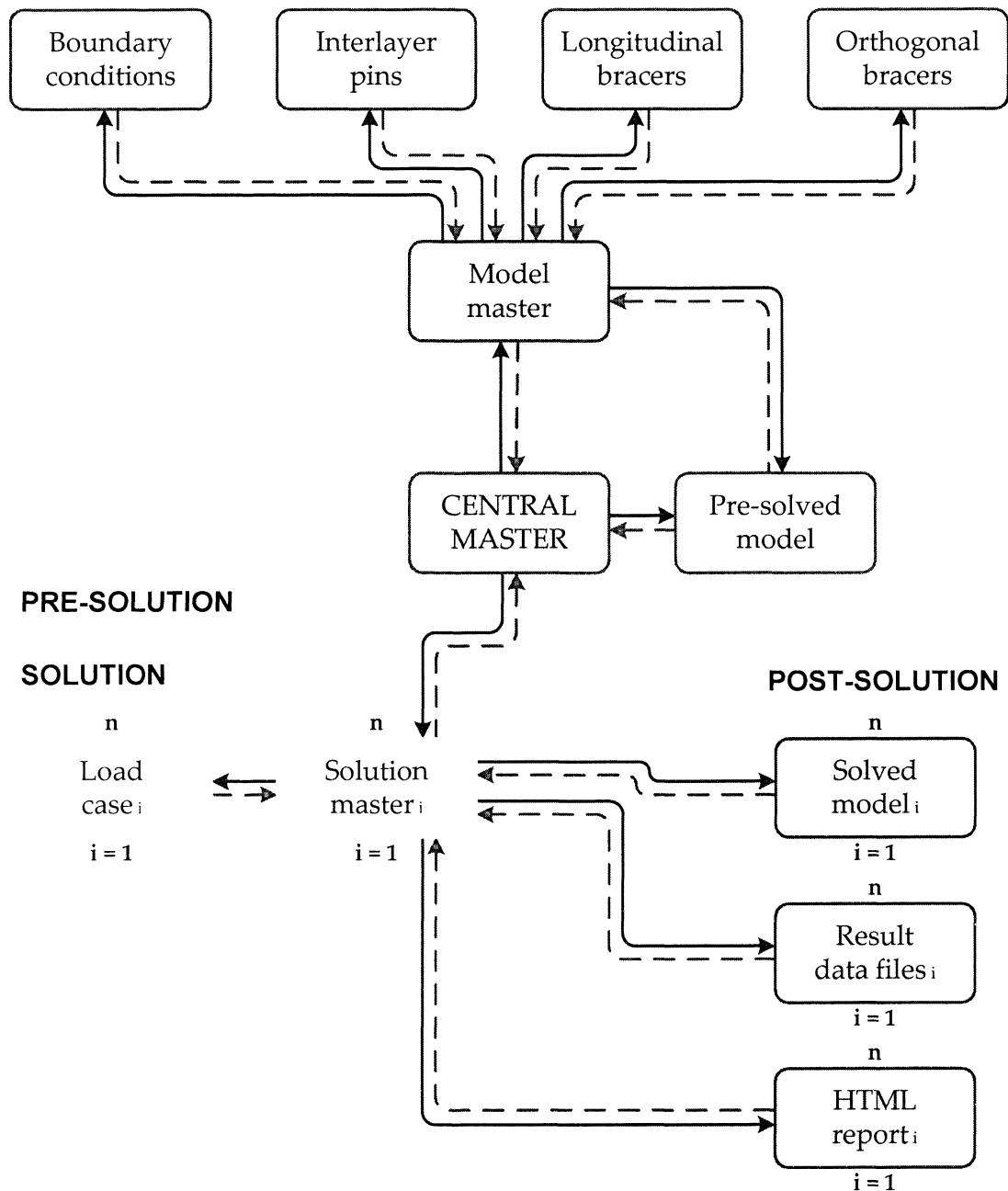


Figure 6–1: Schematic plan of the FEA protocol

### 6.2.2 Assisting tools

In ANSYS (ANSYS Inc. 2005), a considerable amount of data, for example, model attributes, output data, etc., is introduced on the nodes. In some instances, like positioning the elements used for modelling the interlayers, the numbers of nodes to identify and of elements to position are very high and it becomes time-consuming to carry out this task manually. For this reason, a series of Visual Basic programs

(Microsoft Corporation 2000) have been assembled to generate the files that necessitate identifying the node numbers. Thus, the same approach is repeated for identifying the nodes that are needed for assembling the analysis reports. Appendix 11 presents the program used to model the interlayers.

### 6.2.3 First prototype of the finite element model

The first development and trial of the finite element modelling focus on minimising the complexity of the model. As a consequence to this approach, the first model “prototype” – Alpha-FEM – is constructed with element types that permit proceeding with the linear solution mode. In Alpha-FEM, the I-joist flanges and web are modelled with SOLID186, while SHELL93 is chosen for the skin(s) (Figure 6–2). The flanges and web of the I-joist are connected by merging the nodes that they “share”, that is, the pair of superposed nodes (each node exhibiting identical coordinates – one belongs to the flange element and the other one to the web element) are merged together. Thus, the I-joist members are rigidly assembled, that is, the connections yield no slip. The interlayers – interfaces between the I-joists and the skin(s) – are built with several arrays of MATRIX27 elements (Figure 6–2), thus linking the nodes of the skin(s) and extreme fibres of the I-joist flanges. Because the nodes on the flanges exhibit “insufficient” constraints (SOLID186 nodes permits free rotation), they are arranged like small triangulated “frames”. Thus, these three-dimensional triangulations, in particular the diagonals – perpendicular (b) and longitudinal (c) bracers (Figure 6–2) – characterise the shear strength and slip modulus of the interfaces. As a consequence of the use of SOLID186, SHELL93 and MATRIX27 elements, the computation time is reasonably short (20 to 30 minutes per load arrangement<sup>b)</sup>). More detailed information about the elements used in Alpha-FEM is published in ANSYS documentation (ANSYS Inc. 2005).

---

<sup>b)</sup> The computation time is indicative for solving the model in the Graphical User Interface (GUI) environment and assembling the solution files and reports (Figure 6–1). It can vary depending on the processor and RAM capacity of the computer. Solving the model in Batch Mode, which permits speeding up the analysis in comparison to the GUI mode, is not possible because of the encounter of small pivot terms that terminate the analysis. In the GUI mode, ANSYS (ANSYS Inc. 2005) has a protocol to overcome these pivot terms.

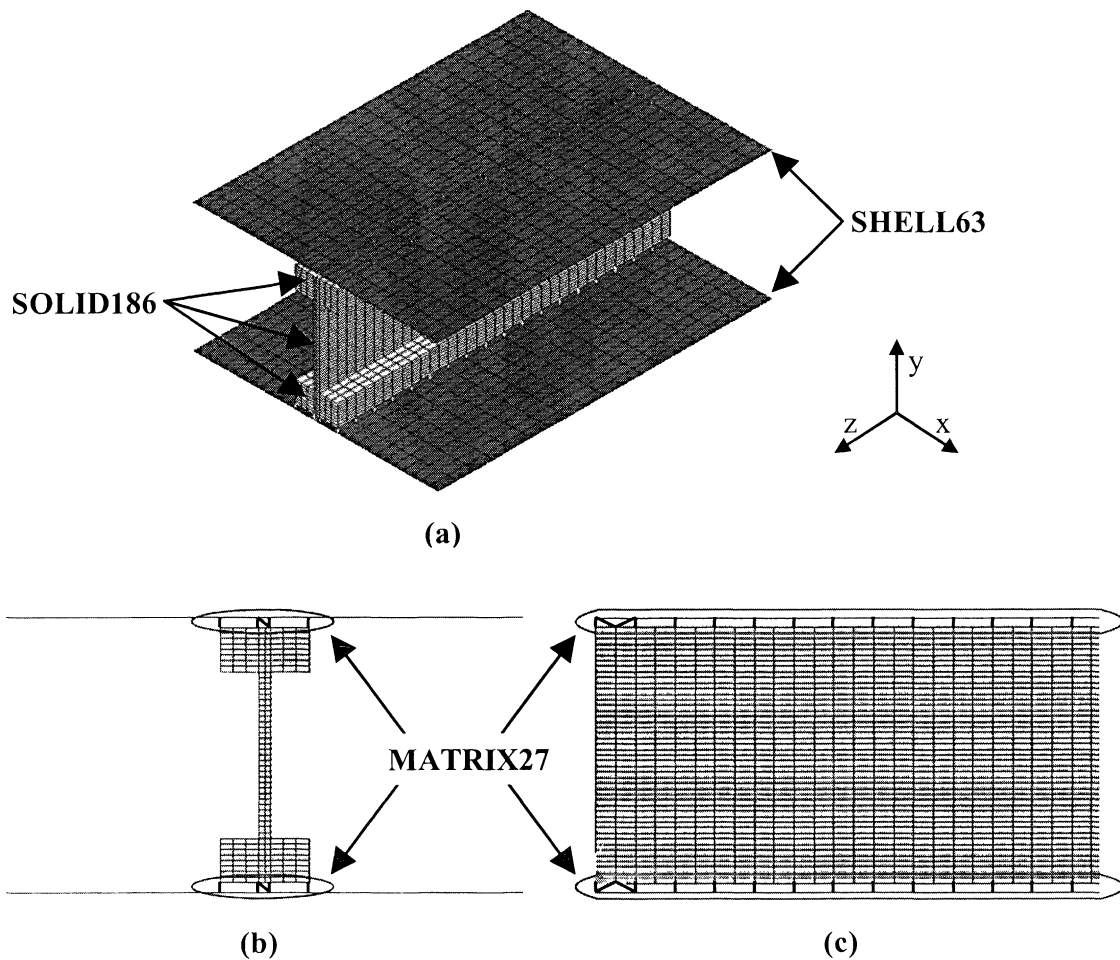


Figure 6–2: Element attributes of Alpha-FEM<sup>c)</sup>

The performance of Alpha-FEM has been evaluated by comparing the simulated deflection to that measured on the laboratory specimens.<sup>d)</sup> The Alpha-FEM simulations generally prove to be unacceptable. These unfavourable results are related to the difficulties in controlling the behaviour of the interlayer with the longitudinal bracers. The complete deactivation of the latter results in the FEM significantly overestimating the specimen deflection, while modulating their “strength” fails to achieve satisfactory simulations. For example, if the longitudinal bracers are calibrated toward the test data of the four-point bending tests (two uniformly distributed line loads), significant variations are identifiable between the simulated and measured values of the three-point bending tests (single uniformly distributed line load), and vice-versa. Furthermore,

<sup>c)</sup> More detailed information about elements SOLID186, SHELL93 and MATRIX27 is found in Release 10.0 Documentation for ANSYS (ANSYS Inc. 2005).

<sup>d)</sup> For the development phase, the evaluation is conducted considering the test data of C08-series (box-section specimen: 200-mm I-joist, 15-mm F11 plywood (upper & lower skins)).

Alpha-FEM is not capable of assessing the behaviour of the specimen acceptably under concentrated point load situations.

*NOTA BENE: During the early stage of the model development – precisely the modelling of the I-joist, it has been demonstrated that the meshing corresponds to a major aspect of the finite element model. It has indeed been identified that the size rather than the number of the finite elements must be approximately equal in order to obtain coherent/consistent simulated results with both I-joist dimensions. This aspect is particularly significant for the longitudinal – parallel to the span – direction (refer to Section 6.2.8).*

#### **6.2.4 The finite element model (FEM)**

The mixed successes of Alpha-FEM necessitate seeking alternatives in order to achieve more accurate and (possibly) more controllable finite element simulations. Simultaneously, the selection of the elements is also reviewed. The “new” or “second-generation” finite element model (FEM) shares some of the fundamentals of Alpha-FEM. The foremost difference corresponds to that, in FEM, the interlayers are modelled with contact elements. Using the contact element technology requires more computer power and time because the model is solved with a non-linear solution mode. However, because in this case FEM can be solved in Batch Mode (ANSYS Inc. 2005), the computation time is still reasonable for 200-mm I-joist models, that is, the solution of each load arrangement takes 60 to 90 minutes. On the other hand, some 4.5 hours are needed for solving each load cases of 356-mm I-joist model.<sup>o)</sup>

#### **6.2.5 Element types of the finite element model**

FEM associates five different element types: SOLID185, SOLSH190, SHELL43, CONTA173 and TARGE170 (Figure 6–3). These elements are available in the ANSYS library (ANSYS Inc. 2005). Compared to Alpha-FEM, this FEM is constructed with solid (SOLID185) and shell (SHELL43) elements, which are simpler, that is, they count fewer nodes, the nodes upholding the same degrees of freedom. Therefore, the quality of the information of the analysis is preserved. FEM also makes use of the “latest” element developed of ANSYS (state-of-the-art ANSYS Release 9.0 (ANSYS Inc.

---

<sup>o)</sup> These computation times are indicative for solving the model in Batch Mode and assembling the solution files and reports (Figure 6–1). They can vary, depending on the processor and RAM capacity of the computer.



2004)), using the SOLSH190 element for the web of the I-joists.<sup>f)</sup> Reducing/optimising the number of the nodes per element allows refining of the mesh. Consequently, FEM counts about as many nodes as Alpha-FEM does, that is, up to 500'803 in the 356-mm I-joist FEM with discontinuous skins, but has a finer mesh.

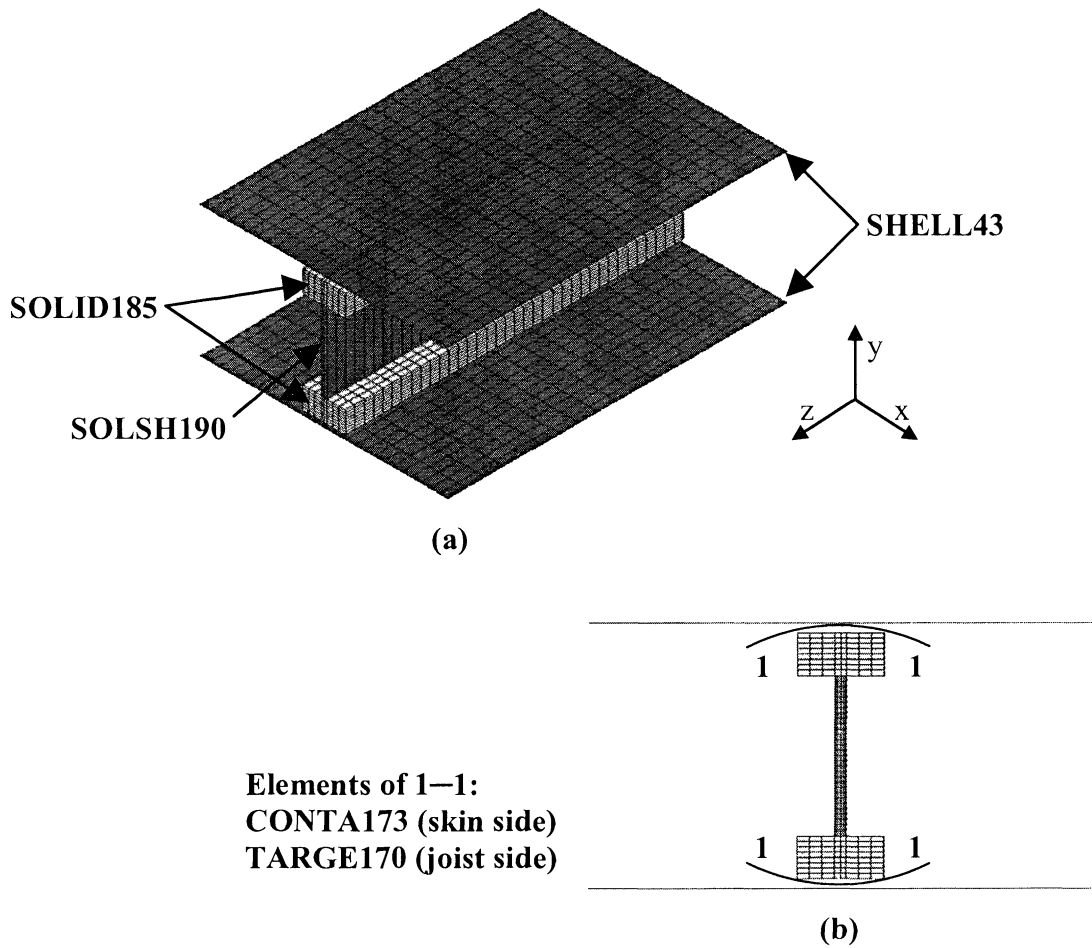


**Figure 6-3: Element attributes of the FEM**

<sup>f)</sup> The use SOLSH190 is rendered possible because of the change to SOLID185 for the I-joist flanges. SOLSH190 and SOLID186 are indeed incompatible, that is, they cannot be associated.

Hereafter, the elements used in FEM are recapitulated and briefly described:

- **SOLID185 (Figure 6–4)**

This element has been chosen to model the flanges of the I-joists. SOLID185 corresponds to an 8-node solid element, whose nodes have three degrees of freedom (x, y & z translations). SOLID185 supports large deflections and strains.

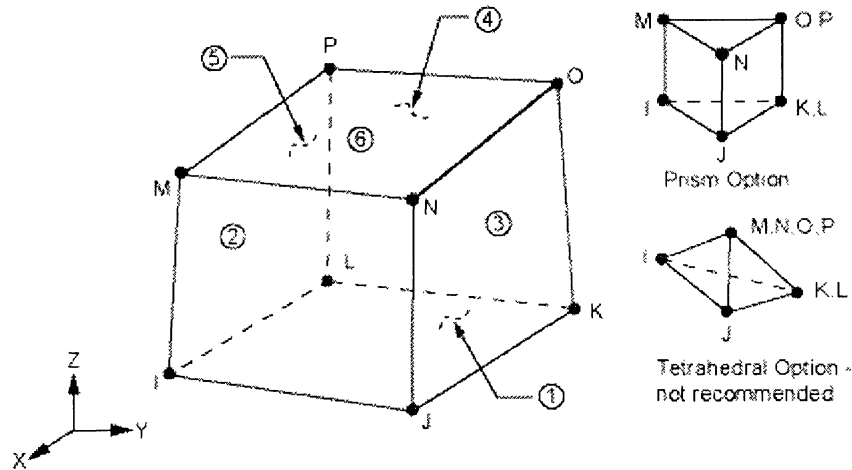


Figure 6–4: SOLID185 geometry (ANSYS Inc. 2005)

- **SOLSH190 (Figure 6–5)**

SOLSH190 has been chosen for modelling the webs of the I-joists. SOLSH190 is an 8-node layered solid shell element. This element can simulate shell structures, whereas the element possesses the topology and connectivity of a solid element. It is therefore recommended for modelling a “thin” volume, especially when an association with a solid element, for example SOLID185, is sought. SOLSH190 has a large deflection and large strain capabilities.

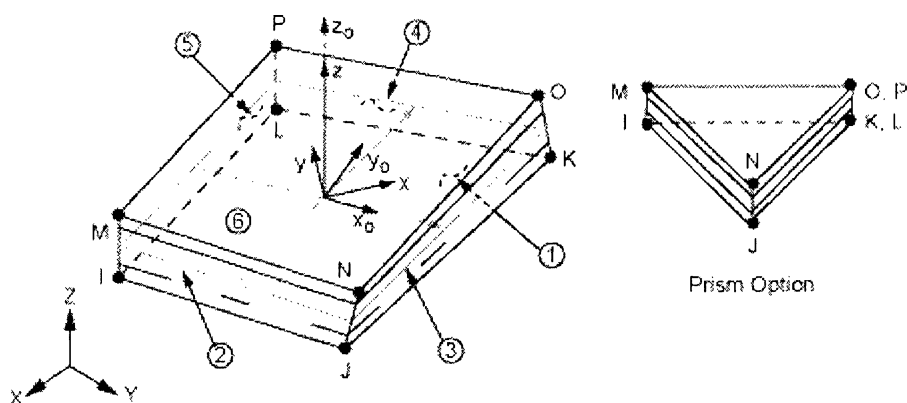


Figure 6–5: SOLSH190 geometry (ANSYS Inc. 2005)

- **SHELL43 (Figure 6–6)**

SHELL43 corresponds to a 4-node shell element. It is used for modelling the skin(s). SHELL43 nodes have six degrees of freedom, that is, three translation (x, y & z) and three rotations (about x, y & z axes). It has a large deflection and large strain capabilities.

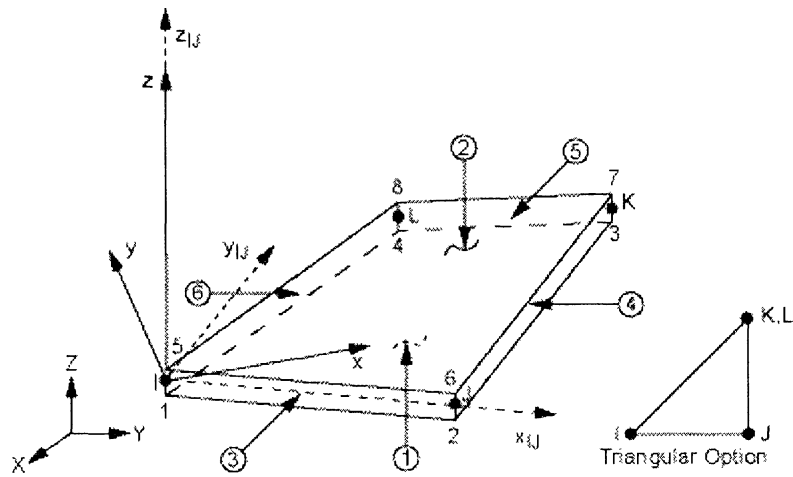


Figure 6–6: SHELL43 geometry (ANSYS Inc. 2005)

- **CONTA173 (Figure 6–7)**

CONTA173 has been chosen for modelling “one side” of the interlayers – CONTA173 is assigned to the skin portion superimposed to the joists. It is used to characterise the contact (adhesion and cohesion) and sliding (slip modulus) between two surfaces. It corresponds to a 4-node surface-to-surface contact element, thus it is compatible with both SOLID185 and SHELL43.

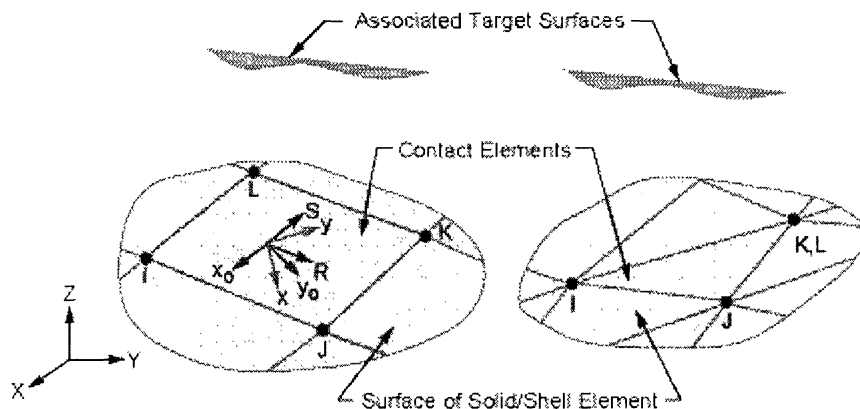


Figure 6–7: CONTA173 geometry (ANSYS Inc. 2005)

- **TARGE170 (Figure 6–8)**

The target segment TARGE170 is the counterpart to the contact element CONTA173, that is, both elements need to be associated for the simulation of the interlayers. The TARGE170 segment is overlaid on the face of the solid elements (SOLID185) located at the I-joist's extreme fibres (facing the skin).

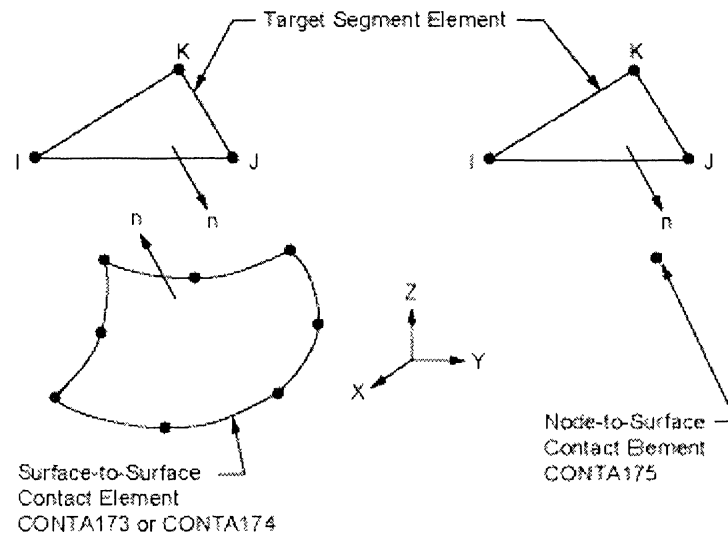


Figure 6–8: TARGE170 geometry (ANSYS Inc. 2005)

## 6.2.6 Real constants of the finite element model

SHELL43, CONTA173 and TARGE170 require real constant entries in order to complete the definition of their physical properties. In contrast, SOLID185 and SOLSH190 only need a real constant to comply with the ANSYS solution modulus operandi (ANSYS Inc. 2005). The real constants of the elements are listed and described hereafter.

- **Real constant of SOLID185**

No real constant has been defined for SOLID185 in particular. However, in order to meet the conditions of the ANSYS solution procedure, it is attributed with the real constant of SHELL43. The properties of the real constant have no effect on the behaviour/responses of SOLID185 elements.

- **Real constant of SOLSH190**

Ditto to SOLID185.

- **Real constant of SHELL43**

The real constant of SHELL43 defines the thickness of the sheathing. Each sheathing is therefore associated with an individual real constant.

- **Real constant of CONTA173**

The CONTA173 real constant enables definition of the interlayers' properties, such as the strength and slip modulus. Further parameters, peculiar to the ANSYS solution modus operandi, such as the “pinball” region, the superelement – sheathing – thickness and the target circle radius are also defined in the CONTA173 real constant.

- **Real constant of TARGE170**

The real constant of TARGE170 allows definition of the superelement's thickness and the target circle's radius. The other parameters are defined through their association with CONTA173.

### **6.2.7 Material properties of the members of the finite element model**

Generally, structural timber and wood-based panels are considered to exhibit orthotropic characteristics. Therefore, sets of orthotropic matrices are entered for the I-joists and sheathings. As mentioned previously, solid wood lengths are treated like bi-dimensional orthotropic materials.

- **Material properties of SOLID185 and SOLSH190**

The material properties of the I-joist flanges (SOLID185) and web (SOLSH190) are defined with one and two entries of orthotropic materials respectively. The material data of the I-joists are reported in Table 6–1.

**Table 6–1: Material properties of the I-joist flange (SOLID185) and web (SOLSH190)**

Description	*global axes	I-joist flange <sup>A</sup>	I-joist web <sup>B</sup>	
		MGP15	9-mm plywood <sup>†</sup>	12-mm plywood <sup>‡</sup>
Modulus of Elasticity	E <sub>x</sub>	955E6 Pa	955E6 Pa	955E6 Pa
	E <sub>y</sub>	955E6 Pa	5775E6 Pa	9135E6 Pa
	E <sub>z</sub>	15200E6 Pa	1260E6 Pa	5040E6 Pa
Poisson's ratio	v <sub>xy</sub>	0.569	0.05	0.05
	v <sub>yz</sub>	0.029	0.02	0.02
	v <sub>xz</sub>	0.029	0.30	0.30
Shear modulus	G <sub>xy</sub>	100E6 Pa	525E6 Pa	525E6 Pa
	G <sub>yz</sub>	940E6 Pa	52.5E6 Pa	52.5E6 Pa
	G <sub>xz</sub>	940E6 Pa	52.5E6 Pa	52.5E6 Pa

\*ANSYS global axes (x: orthogonal, y, vertical & z: longitudinal (in Figure 6–3)), <sup>†</sup>200-mm I-joist web, <sup>‡</sup>356-mm I-joist web.

**Source:** <sup>A</sup>AS 1720.1–1997 (Australian Standard<sup>TM</sup> 1997) and specialised literature (Green, Winandy & Kretschmann 1999; Guitard 1987). <sup>B</sup>AS/NZS 2269:2004 (Australian/New Zealand Standard<sup>TM</sup> 2004a) and specialised literature (Finnish Forest Industries Federation 2002; Merz et al. 1998).

- **Material properties of SHELL43**

The material properties of the sheathings are defined with three sets of orthotropic materials. Table 6–2 lists the material data of the sheathings.

**Table 6–2: Material properties of the sheathing (SHELL43)**

Description	* global axes	15-mm F11 plywood <sup>A</sup>	19-mm particleboard <sup>B</sup>	22-mm oriented strand board <sup>C</sup>
Modulus of Elasticity	E <sub>x</sub>	3150E6 Pa	3350E6 Pa	4719E6 Pa
	E <sub>y</sub>	8500E6 Pa	2054E6 Pa	4000E6 Pa
	E <sub>z</sub>	10500E6 Pa	3900E6 Pa	8136E6 Pa
Poisson's ratio	v <sub>xy</sub>	0.1	0.3	0.1
	v <sub>yz</sub>	0.3	0.35	0.2
	v <sub>xz</sub>	0.5	0.35	0.5
Shear modulus	G <sub>xy</sub>	52.5E6 Pa	85E6 Pa	100E6 Pa
	G <sub>yz</sub>	525E6 Pa	850E6 Pa	1000E6 Pa
	G <sub>xz</sub>	52.5E6 Pa	85E6 Pa	100E6 Pa

\*ANSYS global axes (x: orthogonal, y, vertical & z: longitudinal (in Figure 6–3)).

*Source:* <sup>A</sup>AS/NZS 2269:2004 (Australian/New Zealand Standard<sup>TM</sup> 2004a) and specialised literature (Finnish Forest Industries Federation 2002; Merz et al. 1998), <sup>B</sup>AS/NZS 1859.1:2004 (Australian/New Zealand Standard<sup>TM</sup> 2004b), specialised literature (Australian Wood Panels Association Incorporated 2004; Merz et al. 1998) and test data (Appendix 8), <sup>C</sup>specialised literature (Kronoply GmbH & Co. KG; Merz et al. 1998) and test data (Appendix 8).

*Note:* SHELL material properties must be input in local coordinates (ANSYS Inc. 2005).

- **Material properties of CONTA173**

For simulating bonded assemblies, the “material” properties of CONTA173 correspond to the friction, in other words, the shear strength – adhesion and cohesion – of the interfaces. Instead of entering values, ANSYS permits defining the type of the connection with the help of key options. One of these permits switching on the “always-bonded” mode. This assumption is acceptable because this finite element analysis focuses on the range of service load, within which it is anticipated that the interfaces of the SSP assembly would not suffer any damage. This agrees with the observations and outcomes of the analysis conducted on the full-scale laboratory specimens (refer to Chapters 4 to 6 in Part 2).

- **Material properties of TARGE170**

The TARGE170 element has no material data, respectively it is derived with the data of the CONTA173 element, to which it is associated.

## 6.2.8 Characterising the I-joists

The use of I-joists for the “web” of the specimens increases the complexity of the model. Therefore, characterising the I-joist corresponds to an intermediary, though important, phase of the FEM development. I-joists are themselves composite sections, whose members exhibit heterogeneous material properties and interact together complexly. For example, it has been identified that the shear deformation is a significant element of the deflection of I-joist because the tongue-and-groove connection of the web and flange has limited strength and is prone to distortion. This suggests therefore that modelling the I-joist, that is, identifying and characterising the behaviour of the I-joists, is necessary before actually developing the FEM of the floor assembly.

This investigation on the I-joist is carried out by studying the mid-span deflection of a single simply supported (pin and roller) joist under centre-point loading (three-point bending). The benchmark – deflection at mid-span – of the I-joist finite element model (IJ-FEM) is mathematically calculated using the transformed-section method (Gere & Timoshenko 1999) to estimate the section properties, because it is acceptable to assume that the I-joists comply with the requirements of fully composite cross-sections, that is, linear strain distribution in the cross-section (Amana & Booth 1967). As such, this has been demonstrated in Chapter 6 in Part 2. Determining the portion of the shear deformation has been conducted in agreement with the practice embraced by the I-joist manufacturer (Trus Joist<sup>TM</sup> a Weyerhaeuser Business 2002b). Trus Joist’s<sup>TM</sup> technical documentation is also used as a control tool for verifying the estimate of the I-joist section properties.

The I-joist is modelled with the element types, real constants and material data presented in Sections 6.2.5 to 6.2.7. Consequently, SOLID185 and SOLSH190 elements are used for the flanges and web of the I-joist respectively. The superposed nodes of the flanges and web, that is, nodes with identical coordinates, are merged together. This action gives fully rigid characteristics to the tongue-and-groove connections. It is anticipated that this action and the idealisation of the finite element environment – boundary conditions and material properties (no variability) – could result in the model overestimating the global stiffness of the I-joist. Because of the modelling of the tongue-and-groove connection, the parameterisation therefore consists of adjusting the material properties of the web of IJ-FEM. Expressed in other words, shear distortion is



imposed on the I-joist web through modulating its mechanical properties. The calibration task is conducted simultaneously on the 200-mm and 356-mm I-joist. It aims at identifying a single correction/calibration coefficient applicable for both I-joist dimensions.

A first run, in which the “original” material data are used (Table 6–1), demonstrates that the I-joist exhibits excessive stiffness. The IJ-FEM global stiffness exceeds that of the mathematical estimates by 67% and 71%, considering the 200-mm and 356-mm I-joist respectively, verifying that the anticipated behaviour of the model has been correct, that is, overestimating of the global stiffness of the physical I-joist. This also indicates that there is a need to “calibrate” the behaviour of the simulated I-joist.

The investigation has eventually identified that successful finite element simulations could be achieved with both the 200-mm and 356-mm I-joists, with a single calibration coefficient ( $awfac^g$ ) = 0.218351). The deviation between the finite element values and the mathematical estimates is less than  $\pm 0.5\%$  for both I-joist dimensions. Some extent of this deviation may be generated by the minimal difference of the mesh size – “physical” dimensions of the elements – between the 200-mm and 356-mm I-joists.<sup>h)</sup> In view of this incremental/negligible deviation, it is concluded that the objective of the I-joist characterisation has been successfully achieved, that is, a single calibration coefficient applicable to both I-joist dimensions has been identified.

---

<sup>g)</sup>  $awfac$  corresponds to the abbreviated denomination of the calibration coefficient, and as such is used in the finite element program (in Appendix 11).

<sup>h)</sup> It has been observed in the very early stage of the finite element work that, when keeping the mesh distribution – division of the volume – constant, the behaviours of the 200-mm and 356-mm I-joists deviate significantly. On the other hand, maintaining the size of the mesh constant in both I-joist types brings more stability and consistency to and between both models.

A plot of the I-joist characterisation is depicted in Figure 6–9. This depiction corresponds to a “close-up” of the final value of the calibration coefficient ( $awfac = 0.218351$ ). It demonstrates the minimal deviations between the IJ-FEM values and the mathematical estimates of both I-joist dimensions, that is, within  $\pm 0.5\%$ . Figure 6–9 also indicates that using individual calibration coefficients for the 200-mm and 356-mm I-joists permits IJ-FEM to achieve “perfect” simulations.

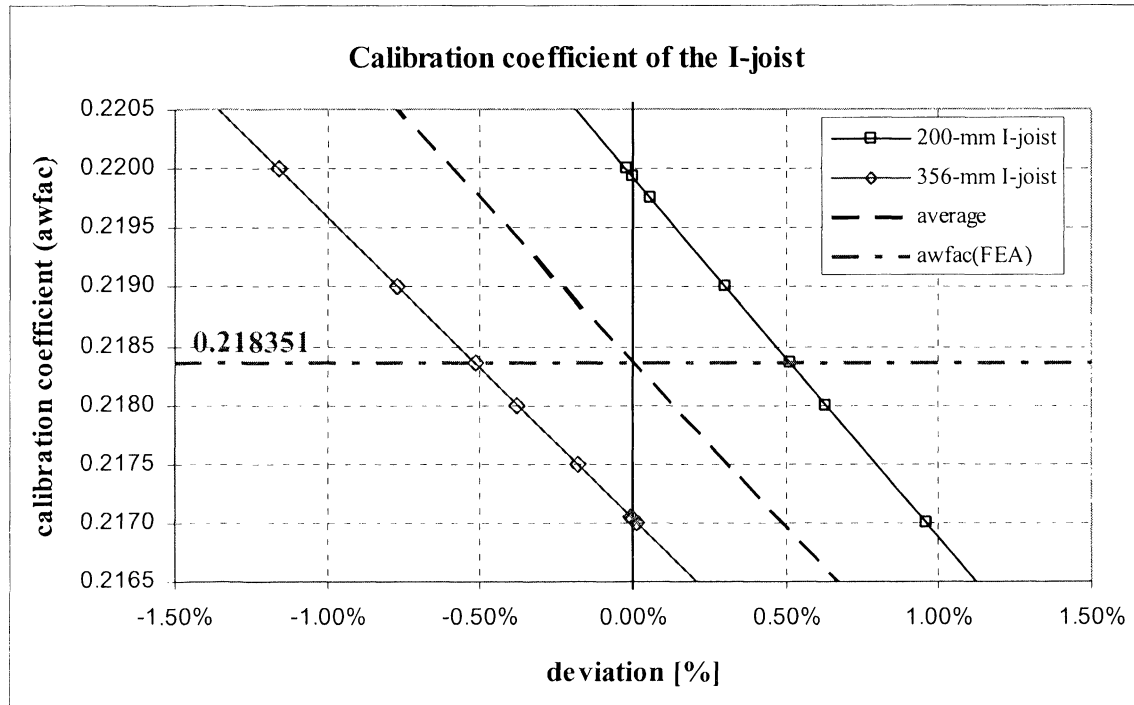


Figure 6–9: Calibration coefficient of the I-joist

## 6.3 PARAMETERISATION OF THE FINITE ELEMENT MODEL

### 6.3.1 Concept of the parameterisation

A finite element model (FEM) generally represents an “ideal” duplicate of the physical construction. The “parameterisation” can therefore be viewed as the operation with which the “imperfections” of the physical decks and, to a lesser extent, of the testing set-up are introduced into the model. It corresponds to a quest for the best calibration coefficients in order to improve and/or refine the predictive/simulative capability of the model. For example, it aims at identifying and calibrating – in justified manners – aspects/parameters of the model in such way that the latter becomes capable of more accurate simulations.

The parameterisation is carried out considering the parallel and orthogonal directions of the SSP deck. Therefore, it is carried out focusing on the mechanical properties of the I-joists, the skin(s) and the interlayers. For example, the two-way action properties of the deck are modulated by means of a modification factor on the mechanical properties – orthogonal direction – of the skin(s).

### 6.3.2 Benchmarks of the parameterisation

The benchmarks of the parameterisation are set by the non-destructive experimental data – mid-span deflection responses to service loading action – collected on the specimens of C02-series<sup>i)</sup>, C08-series<sup>j)</sup> and C09-series.<sup>k)</sup> Respectively, the data of the girder under direct loading are considered, that is, the responses of each girder in uniformly distributed line load situations and of the girder directly loaded with point load arrangements. These series are chosen because both are entirely constructed with structural materials (wood members and adhesive), whose properties are thoroughly known. The skins of the specimens of both series can be assumed continuous because they have been spliced longitudinally. These specimens also exhibit adequate proportions. Furthermore, both C02 and C08 series average the test results of three specimens, meanwhile the C09-series counted four individuals.

The test data of the uniformly distributed line loadings are used for parameterising the longitudinal direction – parallel to the span – of the model, while the calibration of the orthogonal direction – perpendicular to the span – of the deck is performed considering the test data of the concentrated point load arrangements. Furthermore, the references of the parameterisation are set by the girder(s) under direct load action. It is indeed anticipated that these girders are critical for the design safety. Thus, it is important the model is capable of accurately assessing the behaviours of these girders.

### 6.3.3 Findings/outcomes of the parameterisation

#### a) Global stiffness of the model – longitudinal direction

Considering the characterised I-joist for the construction of the deck's finite element model (FEM), initial analyses have demonstrated that the FEM exhibits a tendency to overestimate the deflection in comparison to the experimental measurements –

<sup>i)</sup> C02-series: open-section specimen, 200-mm I-joist, 15-mm F11 plywood (upper skin).

<sup>j)</sup> C08-series: box-section specimen, 200-mm I-joist, 15-mm F11 plywood (upper and lower skins).

<sup>k)</sup> C09-series: box-section specimen, 356-mm I-joist, 15-mm F11 plywood (upper and lower skins).

deflection of the specimens under uniformly distributed line loads (third- and centre-point loadings). Therefore, as observed elsewhere in the subject research (refer to Chapter 5 in Part 1), there are indications that, in the finite element simulations as well, the I-joists behave differently when implemented in single-beam or in SSP-system web situation. This phenomenon could be related to a re-distribution and/or intensification of the shear action in the I-joists. Consequently, adjusting the web factor of the I-joist (*awfac*) in relation to the construction of the specimen – open and box section – and to the depth of the joist is necessary in order to achieve acceptable/accurate results with the finite element analysis (FEA). Unfortunately, this operation results in preventing the use of a single modification coefficient. As a further consequence of this observation, the parameterisation needs to be performed considering the whole specimen population.

Table 6–3 summarises the calibration coefficients – applicable on the mechanical properties of the I-joist web – that have been identified for the specimens. It shows that the calibration coefficient of the 200-mm I-joist open-section specimens is incrementally close to that previously identified for the single I-joist. Meanwhile, the deviation is moderate and marked considering the 200-mm and 356-mm I-joist box-section specimens respectively. Further modification factors, for example, on the longitudinal properties of either the I-joist flanges or the skin(s), are not necessary, that is, the finite element simulations are acceptable with *awfac* “only”.

**Table 6–3 : Calibration coefficients of the I-joist (*awfac*)**

I-joist type	Single beam	SSP system	
		Open section	Box section
200 mm	0.218351	0.220	0.255
356 mm		–	0.339

These simulation results indicate that ANSYS (ANSYS Inc. 2005) fails to simulate the assembly interaction/features of SSP systems to some extent. The variation of the modification factor in relation to the construction and dimensions of the SSP systems curtails the potential of FEM, that is, extending the application of FEM to other SSP constructions requires the modification factor to be determined first.

### b) Global stiffness of the model – orthogonal direction

Initial FEAs have indicated that, for concentrated point load arrangements, the simulated deflections are significantly less than those measured on the laboratory specimens, suggesting that the orthogonal stiffness of FEM is excessive. These FEM results confirm that ANSYS (ANSYS Inc. 2005) lacks the capability to simulate the assembly interaction/features of SSP systems. In the orthogonal direction, the overestimating of the stiffness may be related to the idealisation of the tongue-and-groove connection between the I-joist web and flanges (node merging). In reality, this connection is weak and deformable, thus it is anticipated to experience some rotation, particularly under eccentric point load arrangements.

In order to improve the quality of FEM simulations (orthogonal direction), it has been chosen to impose a modification factor on the orthogonal mechanical properties of the skin(s). Consequently, calibration coefficients have been identified for each panel material (Table 6–4). The values of these calibration coefficients indicate that the modification is severe. In FEM, the orthogonal properties of the skin(s) are indeed reduced to fractions of the actual properties of the panels.

In order to improve the quality of FEM simulations, “freeing” the torsional distortion of the I-joists has been attempted by lowering the orthogonal mechanical properties of the edge elements of the I-joist web, that is, the arrays of elements, which are located at both the lower and upper fibres of the I-joist web. However, this operation fails to produce the expected effects. Consequently, it has been chosen to impose a modification factor on the orthogonal mechanical properties of the skin(s). Consequently, calibration coefficients have been identified for each panel material (Table 6–4). The values of these calibration coefficients indicate that the modification is severe. In FEM, the orthogonal properties of the skin(s) are indeed reduced to fractions of the actual properties of the panels.

**Table 6–4 : Calibration coefficients of the sheathing (epfac)**

<b>F11 plywood</b>	0.0157
<b>Particleboard</b>	0.0880
<b>Oriented strand board</b>	0.0700

NOTE: epfac is material related, that is, it is similar for 200-mm I-joist open and box, and 356-mm I-joist box specimens.

## 6.4 EVALUATION OF THE FINITE ELEMENT MODEL'S CAPABILITY

After parameterisation, the simulation capability of FEM is evaluated by comparing the FEM estimates of the deflection at mid-span to those measured on the laboratory specimens. The evaluation focuses on two aspects: (1) the approximation of the deflection of the girder onto which a load is applied, and (2) the prediction of the deformed shape, which is characterised by the mid-span deflection of the girders. The acceptability of the simulations – acceptable variation between the model estimates and the test results – is set at  $\pm 10\%$ , which corresponds to a reasonable range, considering the natural variability of structural timber and wood-based products.

The population of specimens tested in the course of the subject research is used for this evaluation. The comparison is carried out on the deflections per unit load ( $\Sigma F = 1.0$  kN). Looking at uniformly distributed line-loadings (third- and centre-point loadings), the comparison indicates that the FEM simulations are generally acceptable. Of 60 simulated results, 54 (90%) are within  $\pm 10\%$  of the test data, another 4 (7%) are within  $\pm 15\%$ , while the last 2 (3%) are within  $\pm 20\%$ . The good quality of the agreement also suggests that the simulation of the deformed shape is correct. It is therefore concluded that the FEA is capable of providing accurate estimates of the deflection magnitude and the specimen deformed shape for both third- and centre-point loading – uniformly distributed line load(s) – arrangements.

Considering the situations of concentrated point loading, the FEM simulations of the deflection responses of the girder directly under load are generally acceptable. Of 30 computed results, 25 (83%) are within  $\pm 10\%$  of the test data, another 4 (13%) are within  $\pm 20\%$ , while the last one (4%) is within  $\pm 25\%$ . On the other hand, while most of the other (unloaded) girders exhibit acceptable variations, significant deviations can also be observed among these girders. The most extreme deviations are, however, observable with girders that experience marginal deflection. These variations are thus not critical. Presumably, an FEM ideal environment prevents simulating the physical support conditions – FEM prohibits uplifts – and the apparent torsional rigidity of the specimens. This segment of the evaluation has demonstrated that FEA also permits the simulation of the specimen responses (deflection) to point load action.

The outcomes of the comparison between the simulated (FEA) and measured (test data) responses – deflection per unit load ( $\Sigma F = 1.0$  kN) – are reported in Table 6–5.

**Table 6-5 : Comparison between the simulated – finite element model – and the measured – test results – deflections**

	deflection per 1.0-kN load ( $\Sigma F = 1.0$ kN)											
	joist J1			joist J2			joist J3			joist J4		
	model	test	VAR	model	test	VAR	model	test	VAR	model	test	VAR
	mm/kN			mm/kN			mm/kN			mm/kN		
<b>C02-series</b> (open section specimen: 200-mm I-joist, F11 plywood (upper skin))												
* udl (TPL)	0.48	0.49	-0.80%	0.48	0.51	-5.40%	0.48	0.51	-5.71%	0.48	0.50	-2.64%
† udl (CPL)	0.59	0.52	11.52%	0.58	0.63	-7.92%	0.58	0.62	-7.06%	0.59	0.57	2.51%
‡ PL (J1)	1.93	1.83	5.50%	0.46	0.66	-44%	0.04	0.05	-27%	-0.04	-0.14	-216%
PL (J2)	0.46	0.48	-5%	1.38	1.36	1.97%	0.41	0.52	-27%	0.04	-0.04	210%
PL (J3)	0.04	-0.14	451%	0.41	0.49	-21%	1.38	1.43	-3.71%	0.46	0.52	-14%
PL (J4)	-0.04	-0.13	-204%	0.04	0.09	-127%	0.46	0.76	-67%	1.93	2.00	-3.54%
<b>C08-series</b> (box section specimen: 200-mm I-joist, F11 plywood (upper & lower skins))												
udl (TPL)	0.35	0.38	-6.41%	0.36	0.36	-0.61%	0.36	0.37	-3.71%	0.35	0.38	-6.66%
udl (CPL)	0.43	0.44	-3.15%	0.43	0.43	0.29%	0.43	0.43	0.46%	0.43	0.44	-1.67%
PL (J1)	1.25	1.22	2.26%	0.43	0.56	-30%	0.12	0.13	-8%	-0.04	-0.16	-269%
PL (J2)	0.43	0.55	-27%	0.84	0.85	-1.28%	0.31	0.35	-15%	0.12	0.15	-25%
PL (J3)	0.12	0.16	-31%	0.31	0.34	-12%	0.84	0.83	1.23%	0.43	0.55	-27%
PL (J4)	-0.04	-0.21	-367%	0.12	0.08	29%	0.43	0.57	-32%	1.25	1.28	-2.87%
<b>C05-series</b> (open section specimen: 200-mm I-joist, particleboard (upper skin))												
udl (TPL)	0.52	0.50	4.24%	0.52	0.50	3.07%	0.52	0.48	7.20%	0.52	0.48	7.91%
udl (CPL)	0.63	0.59	6.48%	0.63	0.61	2.60%	0.63	0.57	9.68%	0.63	0.53	16.46%
PL (J1)	1.89	1.59	15.95%	0.65	0.90	-38%	0.10	0.19	-92%	-0.07	-0.18	-153%
PL (J2)	0.65	0.80	-23%	1.18	1.21	-3.37%	0.56	0.56	0%	0.10	0.04	63%
PL (J3)	0.10	0.00	105%	0.56	0.57	-2%	1.18	1.23	-4.38%	0.65	0.65	-1%
PL (J4)	-0.07	-0.22	-208%	0.10	0.21	-114%	0.65	0.88	-35%	1.89	1.53	19.17%
<b>C13-series</b> (box section specimen: 200-mm I-joist, particleboard (upper skin), F11 plywood (lower skin))												
udl (TPL)	0.38	0.38	-0.71%	0.38	0.37	2.37%	0.38	0.35	6.72%	0.38	0.37	1.67%
udl (CPL)	0.46	0.45	1.60%	0.46	0.44	3.35%	0.46	0.41	10.27%	0.46	0.42	7.70%
PL (J1)	1.20	1.14	4.53%	0.52	0.65	-25%	0.17	0.17	-2%	-0.03	-0.09	-174%
PL (J2)	0.52	0.59	-14%	0.75	0.81	-7.59%	0.37	0.37	1%	0.17	0.17	2%
PL (J3)	0.17	0.18	-5%	0.37	0.38	-1%	0.75	0.78	-3.58%	0.52	0.54	-5%
PL (J4)	-0.03	-0.09	-177%	0.17	0.16	4%	0.52	0.60	-16%	1.20	1.12	6.59%

/..

**Table 6-5 : Comparison between the simulated – finite element model – and the measured – test results – deflections (cont.)**

	deflection per 1.0-kN load ( $\Sigma F = 1.0$ kN)											
	joist J1			joist J2			joist J3			joist J4		
	model	test	VAR	model	test	VAR	model	test	VAR	model	test	VAR
	mm/kN			mm/kN			mm/kN			mm/kN		
<b>C03&amp;04-family</b> (open section specimen: 200-mm I-joist, oriented strand board (upper skin))												
* udl (TPL)	0.48	0.41	13.27%	0.47	0.43	6.91%	0.47	0.43	7.00%	0.48	0.44	8.27%
† udl (CPL)	0.58	0.49	14.94%	0.56	0.52	8.01%	0.56	0.52	8.19%	0.58	0.49	15.21%
‡ PL (J1)	1.69	1.35	20.15%	0.64	0.82	-27%	0.11	0.20	-75%	-0.10	-0.13	-33%
PL (J2)	0.64	0.63	2%	0.94	1.04	-9.92%	0.53	0.52	1%	0.11	0.06	45%
PL (J3)	0.11	0.08	30%	0.53	0.52	1%	0.94	1.02	-7.60%	0.64	0.63	2%
PL (J4)	-0.10	-0.13	-31%	0.11	0.18	-61%	0.64	0.78	-21%	1.69	1.37	18.80%
<b>C10&amp;11-family</b> (box section specimen: 200-mm I-joist, oriented strand board (upper skin), F11 plywood (lower skin))												
udl (TPL)	0.35	0.34	3.50%	0.35	0.33	6.39%	0.35	0.33	6.23%	0.35	0.34	1.63%
udl (CPL)	0.42	0.40	5.87%	0.42	0.39	7.89%	0.42	0.39	8.25%	0.42	0.39	7.49%
PL (J1)	1.09	1.00	8.41%	0.50	0.57	-13%	0.17	0.16	4%	-0.04	-0.09	-141%
PL (J2)	0.50	0.52	-5%	0.64	0.69	-7.30%	0.36	0.36	-1%	0.17	0.17	-1%
PL (J3)	0.17	0.16	1%	0.36	0.35	2%	0.64	0.69	-7.79%	0.50	0.51	-1%
PL (J4)	-0.04	-0.19	-383%	0.17	0.10	40%	0.50	0.56	-12%	1.09	1.01	8.06%
<b>C09-series</b> (box section specimen: 356-mm I-joist, F11 plywood (upper & lower skins))												
udl (TPL)	0.43	0.45	-4.95%	0.44	0.45	-2.84%	0.43	0.45	-6.13%			
udl (CPL)	0.55	0.53	4.13%	0.57	0.53	7.34%	0.55	0.53	2.99%			
PL (J1)	1.30	1.28	1.93%	0.35	0.39	-11%	0.02	-0.07	463%			
PL (J2)	0.35	0.43	-21%	0.95	0.79	16.87%	0.35	0.45	-26%			
PL (J3)	0.02	-0.10	576%	0.35	0.42	-18%	1.30	1.26	3.25%			
<b>C12-series</b> (box section specimen: 356-mm I-joist, oriented strand board (upper skin), F11 plywood (lower skin))												
udl (TPL)	0.43	0.45	-4.01%	0.43	0.46	-6.48%	0.43	0.45	-4.64%			
udl (CPL)	0.55	0.52	6.29%	0.56	0.54	2.53%	0.55	0.53	4.06%			
PL (J1)	1.14	1.19	-4.40%	0.46	0.45	3%	0.07	-0.05	173%			
PL (J2)	0.46	0.47	-1%	0.73	0.73	0.05%	0.46	0.48	-4%			
PL (J3)	0.07	-0.06	185%	0.46	0.45	2%	1.14	1.21	-5.99%			

\*third-point loading – two uniformly distributed line loads, †centre-point loading – one uniformly distributed line load, ‡centre-point loading – concentrated point load on joist J1 (successively on J2, J3 & J4).



A further depiction of the FEM evaluation is plotted in Figure 6–10. The graph gives a general trend – depicted on the graphs by means of the linear regressions of the data-point series (thick red continuous lines) – of the FEM estimates. Each data point depicts the value of a girder in a particular loading situation, that is, each girder appears several times on the plot. In the graph, the vertical and horizontal axes respectively indicate the simulated – FEM – and the measured – test results – deflections per unit load ( $\Sigma F = 1.0 \text{ kN}$ ). The dashed line corresponds to the ideal situation, that is, the theoretical value matches the experimental one. It can be observed that the FEM values tally the test results well. Furthermore, the slope of the regression is close to 1.0, thus deviating about 1.5% from the perfect-agreement line. The coefficient of determination also indicates that the correlation in the regressions is reasonably strong.

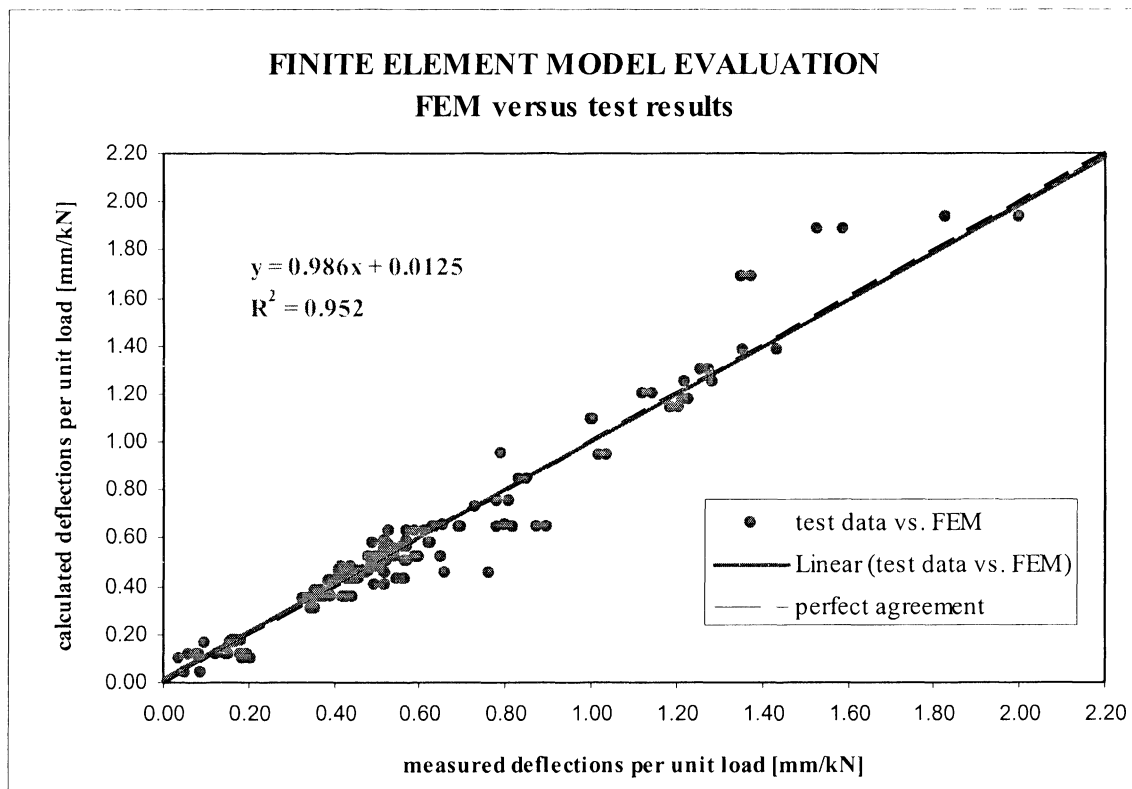
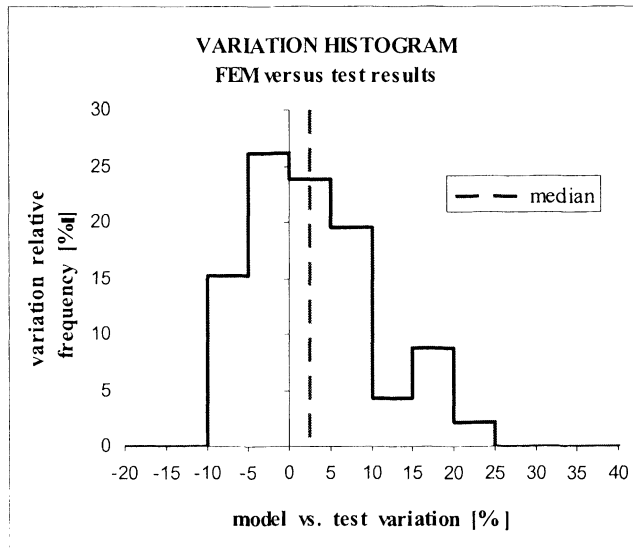


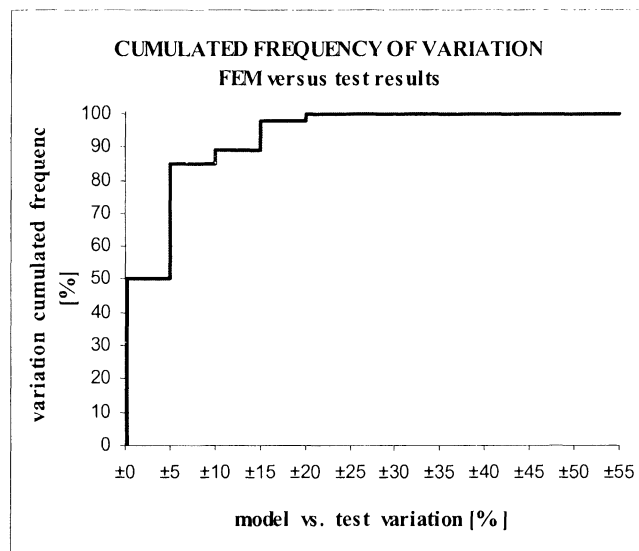
**Figure 6–10: Comparison of the calculated – finite element model – and measured – test results – deflection per unit load**

Further depictions of the FEM evaluation – results of the girders onto which a load is applied – are presented in Figure 6–11. The histogram (a) shows a minor tendency by the FEM to overestimate the deflection. This is manifested by the median (thick red dashed line), which is narrowly located in the positive zone of the x-axis. The

cumulated frequency (b) demonstrates that 83% of FEM simulations are within  $\pm 10\%$  of the test results. The outcomes of the variation analysis confirm that FEM performs acceptably in estimating the deflection of the SSP specimens.



(a)



(b)

**Figure 6–11: Histogram of the calculated – finite element model – and measured – test results – deflection per unit load**

The evaluation and variation analyses of the finite element model (FEM) have demonstrated the good capability of FEM in simulating the behaviour – deflection responses – of the SSP specimens. It can be identified in Table 6–5 and observed in Figures 6–10 and 6–11 that the FEM estimates and the laboratory measurements agree well; in about 83% of the situations, the deviations are within  $\pm 10\%$ . It is therefore concluded that the FEM assumptions/calibration coefficients are correct.

In Figures 6–12, 6–13 and 6–14, graphical depictions (perpendicular profiles of deflection at mid-span) of one family – C03&04-family<sup>l)</sup> – and two series – C13-series<sup>m)</sup> and C12-series<sup>n)</sup> – are presented in order to illustrate the performance of the FEM. The depictions of the family and series exemplify well the simulations achieved by FEM<sup>o)</sup>; the C03&04-family gives an example of the performance of FEM with open-section 200-mm I-joist specimens, while the C13-series and C12-series instance the outcomes of box-section specimens with 200-mm and 356-mm I-joists respectively.

*NOTE 1: the other specimen series and families exhibit perpendicular profiles of deflection with similar patterns to the three series discussed hereafter. They are presented in Appendix 9.*

*NOTE: ANSYS (ANSYS Inc. 2005) permits summarising the essential outcomes of FEA in HTML reports. The latter have been assembled at the end of each load case analysis. They contain, for example, pictorial presentations of the FEM in deformed status (refer to Appendix 11).*

---

<sup>l)</sup> C03&04-family: open-section specimen, 200-mm I-joist, 22-mm oriented strand board (upper skin).

<sup>m)</sup> C13-series: box-section specimen, 200-mm I-joist, 19-mm particleboard (upper skin), 15-mm F11 plywood (lower skin).

<sup>n)</sup> C12-series: box-section specimen, 356-mm I-joist, 22-mm oriented strand board (upper skin), 15-mm F11 plywood (lower skin).

<sup>o)</sup> The test family and series exhibit representative plot depictions of the test data and performance/capability of FEM, that is, the other specimen series and families exhibit perpendicular profiles of deflection with similar patterns (in Appendix 9).

In Figure 6–12, the depictions of the C03&04-family exemplify that, for open-section SSP assembly, FEM achieves respectable simulations; for most loading situations, the deflection magnitude and orthogonal profile are reasonably accurate. Considering eccentric point loads, (c) & (f), the deviation between the model simulation and the test data reaches about 20% – overestimation by the FEM. On the other hand, when the point load is introduced on an interior joist, FEM tends to underestimate the deflection of that particular joist marginally. This indicates that FEM to some extent fails to simulate the orthogonal properties of the specimens of the C03&04-family.

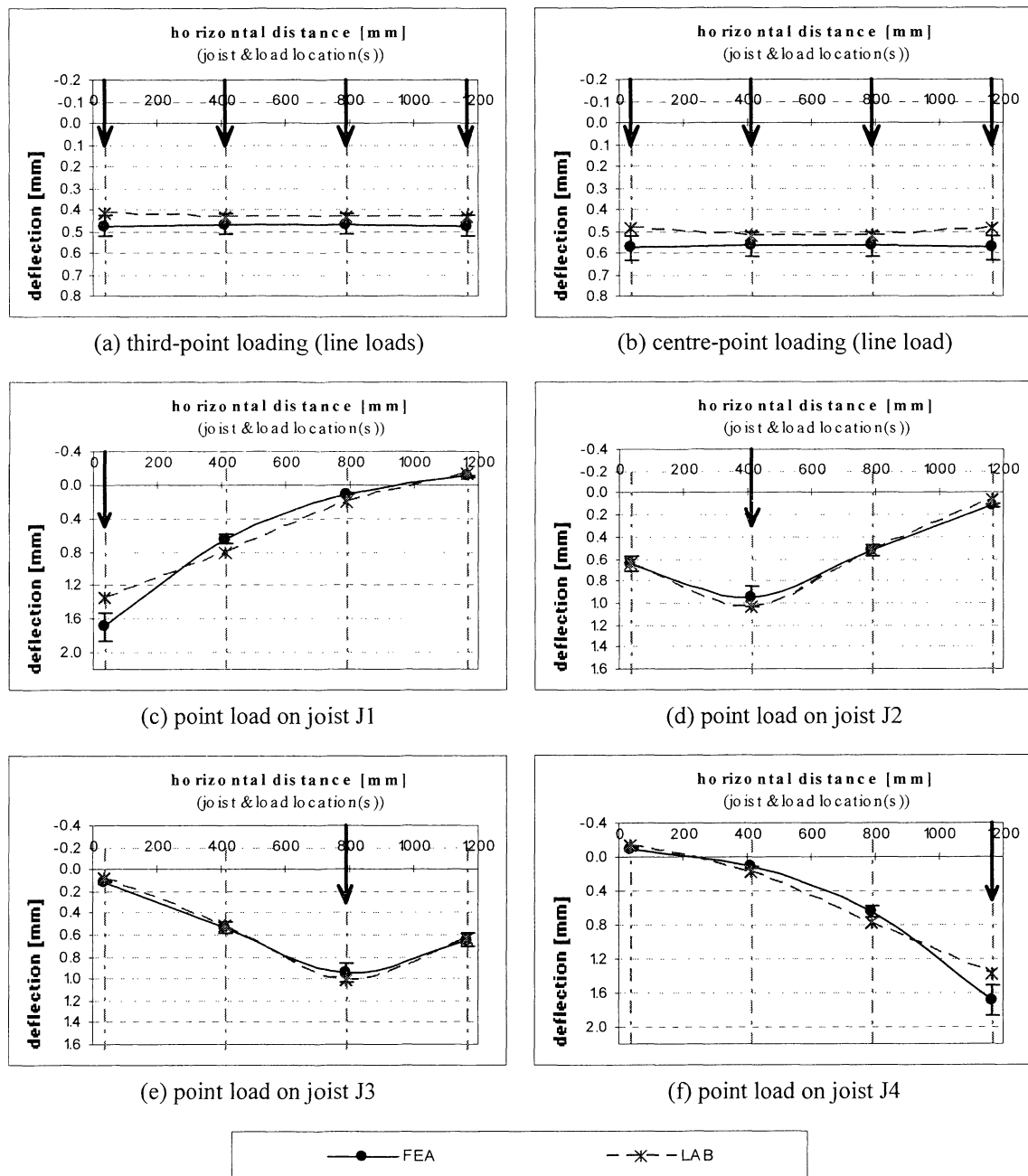


Figure 6–12: Finite element simulations – C03&04-family perpendicular profiles of deflection at mid-span

The C13-series depictions demonstrate that, for 200-mm I-joist box-section SSP systems, FEM achieves very accurate simulations of both the deflection magnitude and the deformed shape (Figure 6–13). This observation is valid for uniformly distributed line load situations (third- and centre-point loading) and point load arrangements.

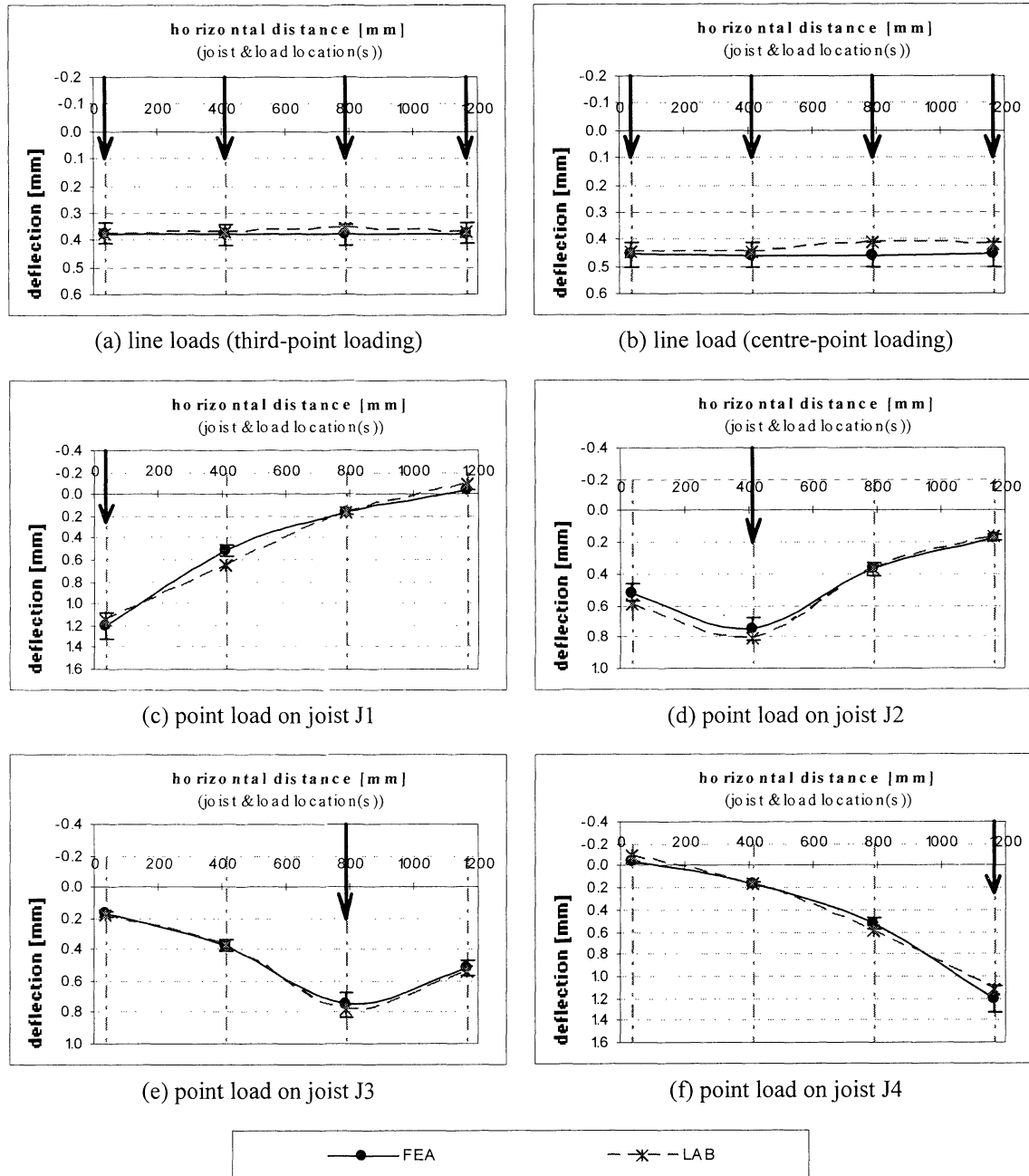


Figure 6–13: Finite element simulations – C13-series perpendicular profiles of deflection at mid-span

The C12-series depictions of the FEM simulations versus the laboratory measurements are presented in Figure 6–14. They demonstrate that the FEM and experimental results tally acceptably for 356-mm I-joist box-section specimens as well. Both the deflection magnitude and the orthogonal profile are accurately simulated by FEM for all loading situations, that is, uniformly distributed line and point load arrangements.

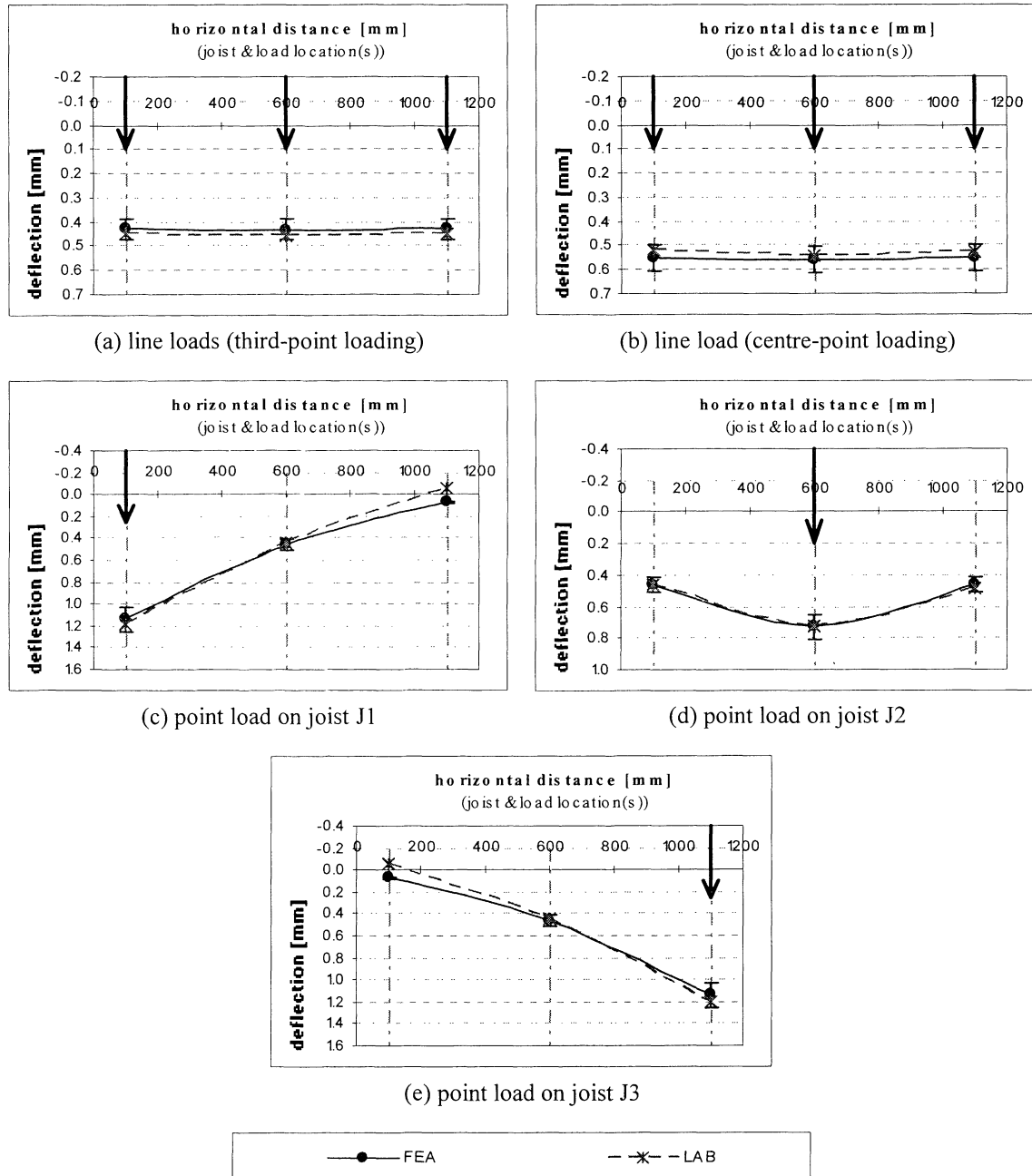


Figure 6–14: Finite element simulations – C12-series perpendicular profiles of deflection at mid-span

## 6.5 INTRODUCING SKIN DISCONTINUITY(IES) IN THE GRILLAGE MODEL

Discontinuing the sheathing of floor systems decreases their global stiffness (Criswell 1981; Dawson 1974; Dawson & Goodman 1976; McCutcheon 1986; Sherwood & Moody 1989; Yang, Pham & Leicester 1994). Consequently, the deflection becomes larger. This phenomenon has also been identified by the analysis of the test results of the subject research (refer to Chapter 4 in Part 2). The present section discusses the capability of the finite element model (FEM) to accommodate the skin discontinuities, that is, to simulate their effects.

For laboratory investigations of the effects of skin discontinuities, the latter have been introduced by inflicting cuts within the zone of the maximum bending moment – 150 mm away from mid-span. In order to replicate a similar feature with FEM, each skin is modelled by means of separate areas, whereby the latter areas meet at approximately 150 mm away from the mid-span. Continuous skins are created by merging the nodes that these areas share at this location (nodes with identical coordinates). Thus, a skin discontinuity can be created by keeping these nodes unmerged. With the ANSYS software package (ANSYS Inc. 2005), there is no need to create a physical gap because the ANSYS regular solution mode permits “interpenetration” of the elements. Indeed, unless it is expressly specified in the protocol of the finite element analysis, that is, apposition of contact elements on the surfaces of the elements, ANSYS considers that the surfaces of the elements have no resistance. For example, the compression resistance that would be anticipated in actual gaps as they close is ignored.

The evaluation of the FEM’s capability in accounting for skin discontinuities is carried out by comparing the FEM simulations to the test data of single specimens. Indeed, among the members of each series and families, generally one individual has been investigated with discontinuous skin(s). The comparison is performed in a similar manner to that used for the previous evaluation of the model, that is, the mid-span deflections per unit load ( $\Sigma F = 1.0 \text{ kN}$ ) are examined. The outcomes of the evaluation are summarised in Table 6–6. The simulative performance of FEM is not as accurate for the specimens with discontinuous skin(s) – damaged state – as for the specimens with continuous skin(s) – healthy state, however, FEM is still moderately successful in accommodating skin discontinuities. For example, looking at the uniformly distributed

line loadings (third- and centre-point loadings), the simulations generally deviate excessively – more than  $\pm 10\%$  – from the measured values. Nevertheless, in view of the scale of the deviations, the overall performance of FEM is in general satisfactory, that is, of 90 computed deflections, 38 (42%) are within  $\pm 10\%$  of the measured deflections, another 24 (27%) are within  $\pm 15\%$ , another 18 (20%) are within  $\pm 20\%$ , while the last 10 (11%) are within  $\pm 25\%$ .

**Table 6-6 : Comparison between the simulated – finite element model – and the measured – test results – deflections (discontinuous skin(s))**

	deflection per 1.0-kN load ( $\Sigma F = 1.0$ kN) — variation summary											
	joist J1	joist J2	joist J3	joist J4	joist J1	joist J2	joist J3	joist J4	joist J1	joist J2	joist J3	
	<b>C02-03</b> (open section specimen: 200-mm I-joist, F11 plywood (upper skin))				<b>C08-01</b> (box section specimen: 200-mm I-joist, F11 plywood (upper & lower skins))				<b>C09-01</b> (box section specimen: 356-mm I-joist, F11 plywood (upper & lower skins))			
* udl (TPL)	5.4%	2.8%	2.5%	3.7%	5.7%	12.2%	9.4%	5.4%	0.7%	3.3%	-0.4%	
† udl (CPL)	18.1%	2.1%	2.9%	9.7%	10.6%	15.1%	15.3%	11.9%	11.8%	15.4%	10.8%	
‡ PL (J1)	10.4%	-25%	13%	-175%	10.5%	-8%	22%	-514%	7.2%	2%	274%	
PL (J2)	9%	8.2%	-12%	175%	-6%	9.4%	6%	9%	-7%	22.3%	-11%	
PL (J3)	341%	-7%	2.9%	1%	5%	9%	11.6%	-6%	328%	-4%	8.5%	
PL (J4)	-165%	-56%	-45%	1.9%	-678%	49%	-10%	5.8%				
	<b>C04-01</b> (open section specimen: 200-mm I-joist, oriented strand board (upper skin))				<b>C11-01</b> (box section specimen: 200-mm I-joist, oriented strand board (upper skin), F11 plywood (lower skin))				<b>C12-01</b> (box section specimen: 356-mm I-joist, oriented strand board (upper skin), F11 plywood (lower skin))			
udl (TPL)	18.8%	13.9%	14.0%	14.1%	14.3%	18.0%	17.9%	12.6%	1.8%	0.0%	1.2%	
udl (CPL)	21.2%	16.2%	16.3%	21.5%	18.1%	21.2%	21.5%	19.5%	13.7%	10.9%	11.6%	
PL (J1)	24.1%	-15%	-44%	-31%	16.0%	2%	26%	-683%	1.1%	12%	150%	
PL (J2)	10%	-1.1%	11%	55%	10%	5.5%	15%	22%	8%	7.8%	5%	
PL (J3)	42%	11%	1.0%	11%	24%	18%	5.1%	12%	159%	11%	-0.4%	
PL (J4)	-30%	-33%	-10%	22.8%	-1470%	54%	3%	15.7%				
	<b>C05-01</b> (open section specimen: 200-mm I-joist, particleboard (upper skin))				<b>C13-01</b> (box section specimen: 200-mm I-joist, particleboard (upper skin), F11 plywood (lower skin))							
udl (TPL)	8.2%	8.0%	12.0%	11.7%	9.0%	12.8%	16.7%	11.2%				
udl (CPL)	11.0%	8.6%	15.3%	20.5%	12.9%	15.5%	21.6%	18.3%				
PL (J1)	18.7%	-29%	-62%	-156%	11.2%	-10%	20%	-1160%				
PL (J2)	-15%	1.6%	6%	69%	0%	2.9%	16%	23%				
PL (J3)	104%	5%	0.6%	6%	17%	13%	6.5%	8%				
PL (J4)	-212%	-80%	-26%	21.8%	-1176%	24%	-1%	13.1%				

\* third-point loading – two uniformly distributed line loads, † centre-point loading – one uniformly distributed line load, ‡ centre-point loading – concentrated point load on joist J1 (successively on J2, J3 & J4).



Figure 6–15 presents the general trend of the FEM estimates (vertical axis) versus the test results (horizontal axis). The comparison considers the deflection per unit load ( $\Sigma F = 1.0 \text{ kN}$ ) of the girders. Respectively, each data point depicts the value of a girder in a particular loading situation, each girder therefore appearing several times on the plot. The thick red continuous line corresponds to the linear regression of the data points. The dashed line symbolises the ideal situation – perfect agreement between the simulated and measured values. The plot indicates that the FEM estimates and the test results tally well. This is confirmed by the slope of the linear regression, whose deviation from the perfect-agreement line is equal to about 3%. Furthermore, the coefficient of determination demonstrates that the regression parameters – FEM values to test data – are strongly correlated.

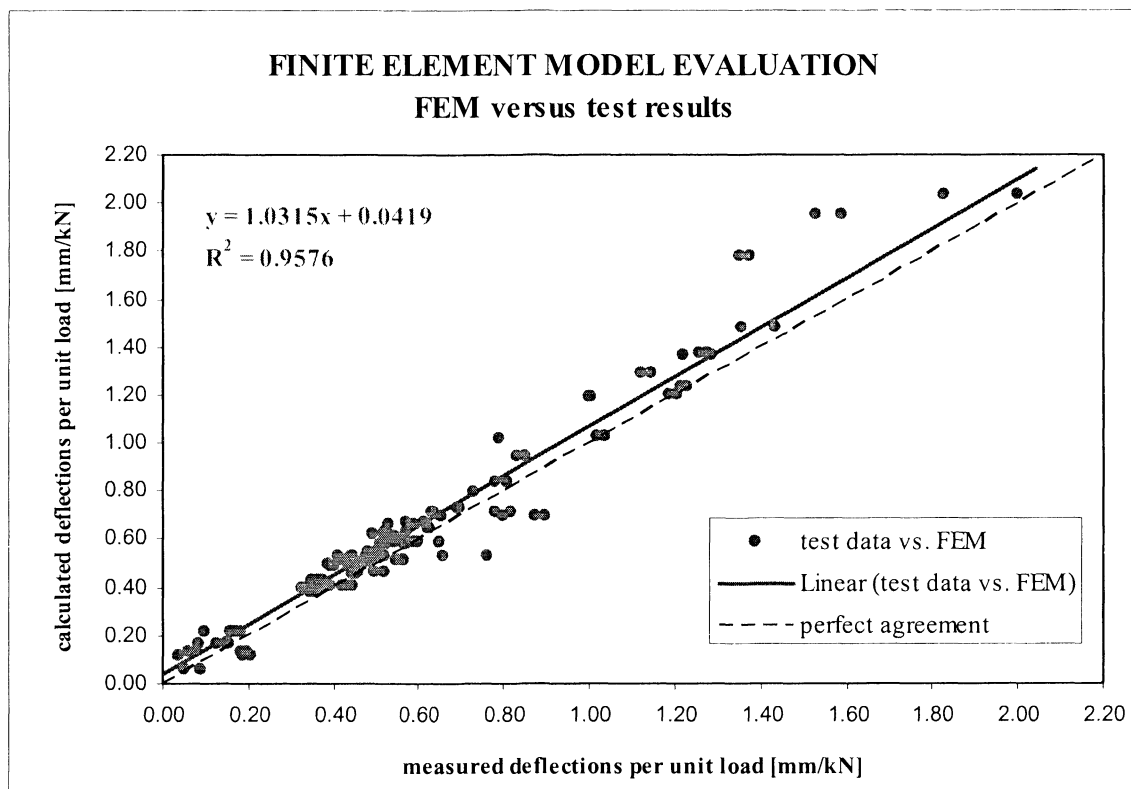
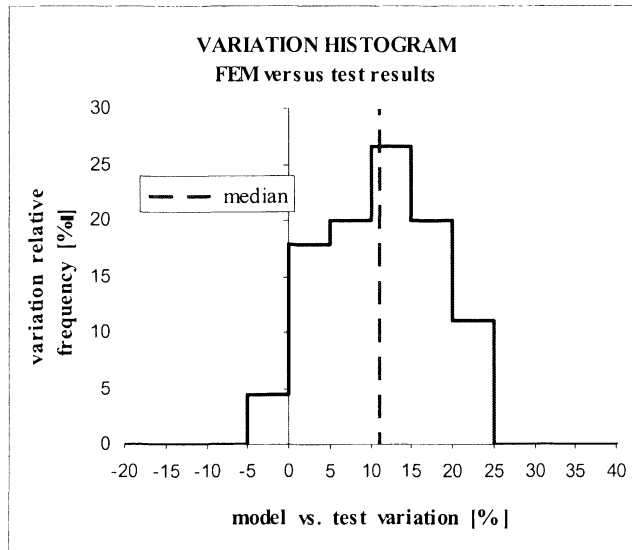


**Figure 6–15: Comparison of the simulated – finite element model – and measured – test results – deflection per unit load (discontinuous skin(s))**

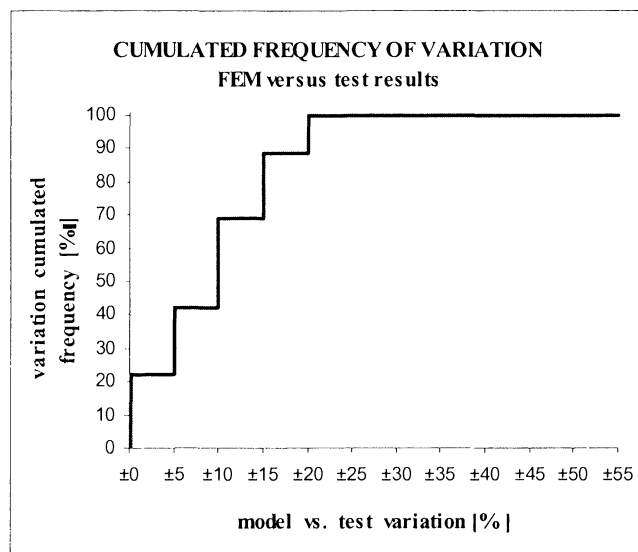
The deviation between the model simulations and the test results is further depicted in Figure 6–16. The histogram (a) shows that the model tends to overestimate the mid-span deflection of the specimens. This is demonstrated by the median (thick red dashed line), whose location is notably on the positive side of the x-axis. The cumulated

frequency depicted in (b) confirms that some 40% of FEM simulations are within  $\pm 10\%$  of the test results, about another 30% are within  $\pm 15\%$  and the remainder (about 20%) are within  $\pm 20\%$ . The outcomes of the variation analysis thus confirm that FEM is acceptably successful in accommodating skin discontinuities. Thus, it is capable of satisfactorily simulating the behavioural responses of the specimens in the damaged state.

The analysis of the introduction of skin discontinuities into FEM has demonstrated that the model is capable of accommodating this change of the specimen's integrity with some success. The FEM simulations and the test results exhibit acceptable agreement (Table 6-6 and Figures 6-15 and 6-16). Thus, the deviation between both sets of data is generally satisfactory. It is therefore concluded that the practice used for the introduction of the discontinuities in the skin(s) is suitable.



(a)



(b)

**Figure 6–16: Histogram of the simulated – finite element model – and measured – test results – deflection per unit load (discontinuous skin(s))**

Plot depictions of the C13-01<sup>p)</sup> specimen have been chosen to graphically exemplify<sup>q)</sup> the ability of FEM to accommodate skin discontinuities (Figure 6–17). As identified previously, the plots of the uniformly distributed line loads – third-point (a) and centre-point (b) loadings – for example, confirm that the FEM simulates deflections

<sup>p)</sup> C13-01: box-section specimen, 200-mm I-joist, 19-mm particleboard (upper skin), 15-mm F11 plywood (lower skin).

<sup>q)</sup> This specimen exhibits representative plot depictions of the test data – specimens in the damaged state (with discontinued skin(s)) – and the performance/capability of FEM with skin discontinuity(ies), that is, the other specimens, whose skin(s) has(have) discontinued, exhibit perpendicular profiles of deflection with similar patterns (in Appendix 9)

exceedingly well. On the other hand, FEM is capable of accurately approximating the behaviour of the deck under concentrated point load. The latter plots also demonstrate that FEM manages to simulate a respectable qualitative approximation of the orthogonal profiles of deflection.

*NOTE: ANSYS (ANSYS Inc. 2005) permits summarising the essential outcomes of FEA in HTML reports. The latter have been assembled at the end of each load case analysis. They contain, for example, pictorial presentations of the FEM in the deformed status (refer to Appendix 11).*

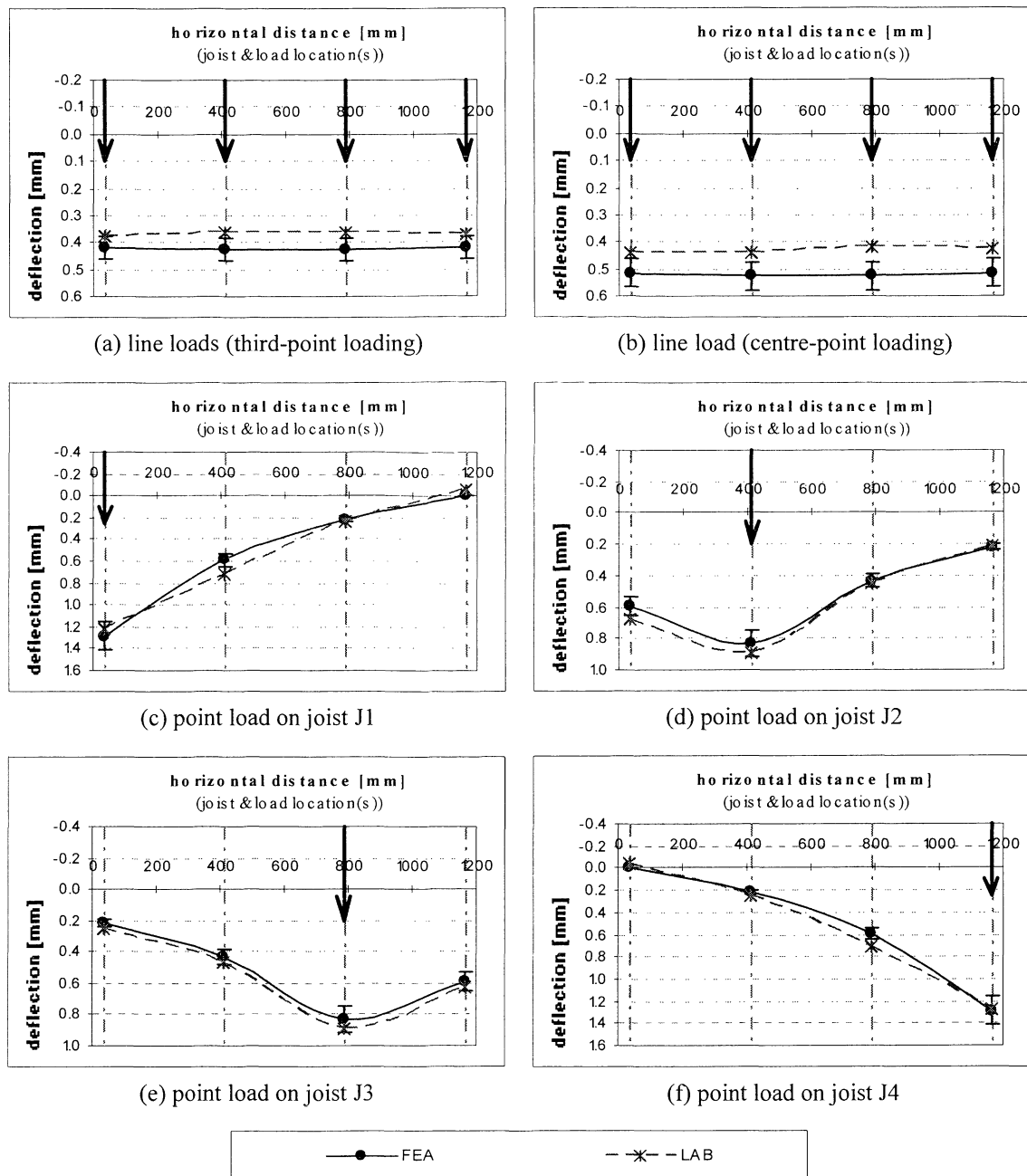


Figure 6-17: Finite element simulations – C13-01 perpendicular profiles of deflection at mid-span (discontinuous skin(s))

## 6.6 CONCLUDING SUMMARY

In this chapter, a finite element model (FEM) has been presented. FEM has been developed on the ANSYS platform (ANSYS Inc. 2005). It is capable of performing satisfactory simulations of the behavioural responses of SSP systems – the magnitude of the deflection (quantitative) and the orthogonal profile of the mid-span deflection (qualitative) – under uniformly distributed loading and concentrated point load arrangements, and for the specimens in healthy and damaged states.

Developing a model in a computer environment, such as the ANSYS package (ANSYS Inc. 2005), implies constructing an ideal replica of the physical structure. Consequently, in FEM, the interlayers/connections are infinitely rigid, the variability of structural timber and wood-based products is ignored and the boundary conditions are idealised (ignoring the specimen's irregular sitting on the testing frame supports and blocking of uplifts). Therefore, in order to achieve accurate simulations, the development of FEM is accompanied by a series of measures, whose aims are to introduce the “imperfections” of the physical specimen and/or testing environment into the FEM:

1. The size of the mesh should be as consistent as possible, especially in the longitudinal – parallel to the span – direction, for the different models. For example, the sizes of the longitudinal dimension of the skin element are equal to 30.83 mm and 30.56 mm in 200-mm and 356-mm I-joist FEMs respectively.

2. The modelling of the I-joists – rigid connection (merged nodes) between the flanges and web – results in simulations with excessive stiffness. In order to “correct” this, a modification factor (*awfac*) is imposed on the material properties of the web. An *awfac* of 0.218351 has been identified for the I-joists in single-beam situations (similar for both 200-mm and 356-mm I-joists) (Table 6–3). However, I-joists as members – webs – of SSP assemblies exhibit behavioural differences from those identified in single-beam situations. Therefore, the deck model requires three modification coefficients, that is, for 200-mm I-joist open-section FEM, *awfac* = 0.220; for 200-mm I-joist box-section FEM, *awfac* = 0.255; and for the 356-mm I-joist box-section FEM, *awfac* 0.339 (Table 6–3).

3. The ideal FEM also requires modifying/adjusting the orthogonal global stiffness of the deck unit in order to account for the distortion occurring in the latter.

This is incorporated into the model with the assistance of a modification factor (epfac) applied on the orthogonal material properties of the skin(s), that is, a modification coefficient has been identified for each type of sheathing material: epfac = 0.0157 for 15-mm F11 plywood, epfac = 0.0880 for 19-mm particleboard, and epfac = 0.0700 for 22-mm oriented strand board (Table 6–4).

The consideration of these recommendations/observations characterises the boundaries of FEM applicability/transposability to other SSP constructions. Within these boundaries, it is anticipated that FEM can accommodate and simulate any load situations, thus providing a helpful and accurate tool that can assist in acquiring a better understanding of the structure. Outside these boundaries, FEM has, from the strict point of view of the qualitative performance, the capability of simulating the behaviour of a wider population of SSP systems. On the other hand, the quantitative performance is limited to a much narrower application range because of the specific values of awfac and epfac.

The evaluation of FEM has demonstrated that there is a good agreement between the FEM simulations and measurements of the laboratory tests (specimens in the healthy state). Considering the uniformly distributed line and point load arrangements, FEM estimates of the deflection magnitude at mid-span – the joist onto which a load is applied – are generally within  $\pm 10\%$  of the test data, which is acceptable in view of the natural variability of structural timber and wood-based materials. Furthermore, the orthogonal profiles of deflection simulated by FEM are also accurate.

It has also been demonstrated that FEM can successfully accommodate the effect of discontinuities – “damage” – in the skins. The deviations between FEM estimates of the deflection magnitude at mid-span – the joist onto which a load is applied – agree generally well with the laboratory measurements, about 90% of the simulated values being within  $\pm 20\%$  of the test data. FEM qualitative simulations of the orthogonal profiles of deflection are also acceptable.

The performance of the FEM developed in the subject research has demonstrated that, albeit having to be assembled according to a strict/limitative set of rules, the FEM can provide a helpful and accurate tool for acquiring a better understanding of SSP systems. The availability of efficient simulative aids can contribute towards saving costly experiments, that is, optimising/reducing the number of physical specimens. Indeed, experimental study with many repetitions is only appropriate to determine the

material properties of single lengths, becoming unsuitable and expensive for structural assemblies, because of the expense it involves. From this perspective, accurate simulative aids provide the investigation and development ground while the laboratory investigation becomes the validating aspect of the investigation.

In Chapters 5 and 6 in Part 1, two numerical procedures are presented. Both the grillage and finite element models are capable of adequately and accurately predicting the behaviour of SSP structures. These models and the experimental work, which is presented in Part 2 of this thesis, enables to enhanced the understanding of SSP systems. This knowledge also contributes to the outline of the design procedure and recommendations, which are presented in Chapter 7 in Part 1.

<b>7</b>	<b>DESIGN PROCEDURE AND RECOMMENDATIONS .....</b>	<b>198</b>
<b>7.1</b>	<b>Background summary .....</b>	<b>199</b>
<b>7.2</b>	<b>Recapitulation of the key outcomes .....</b>	<b>200</b>
<b>7.3</b>	<b>Design recommendations.....</b>	<b>200</b>
7.3.1	Introduction and concept of the design recommendations.....	200
7.3.2	Outline of the design procedure of stressed-skin panels.....	202
<b>7.4</b>	<b>Concluding summary.....</b>	<b>212</b>



## 7 DESIGN PROCEDURE AND RECOMMENDATIONS

In Australia the current code edition of timber design, AS 1720.1–1997 (Australian Standard™ 1997), contains only minimal requirements for the design of SSP systems, such as directives for determinations of stresses in the sheathing and interlayers. On the other hand, it includes no guideline for estimating the tributary width of the panel. However, the latter represents an essential aspect of SSP systems because it governs the section properties of the floors, thus the strength and serviceability of the structures.

In Section 7.3.2, an amendment proposal to Section 5 of AS 1720.1–1997 (Australian Standard™ 1997) is outlined. It corresponds to a thorough design procedure for SSP constructions. It has been written and detailed in a form that could be submitted to the Code Committee. The proposed guidelines address the composite properties of SSP constructions – composite action and tributary width of the sheathing – and the stress determinations in the SSP cross-sections. They are based on the findings of the subject research and are related to EC5 (European Committee for Standardisation 1995). Furthermore, to complement the design procedure, assessment methods of the load distribution are also proposed in the form of two equations (Equations 7-9 and 7-11). These equations, which are capable of approximating the distribution of concentrated point loads, permit the taking into account of the two-way action ability of SSP structures.

Further recommendations derived from the findings of the subject research are also proposed in this chapter. In connection to the consideration of skin discontinuities, reduction coefficients, which are applied to the apparent stiffness of the composite section of the SSP assemblies, are suggested. As for accounting for the type of joists –

composite I-joists – used for building the specimens of the subject research, a modification coefficient, which aims at calibrating the actual shear distortion experienced by the I-joists, is proposed.

## **7.1 BACKGROUND SUMMARY**

In SSP systems, the joists and sheathing interact both by composite and two-way actions (Vanderbilt et al. 1974). Thus, the sheathing acts compositely with the joists and forms continuous beams crossing the joists. Therefore, SSP floors cannot be accurately designed solely on the mechanical properties of the composite joists and sheathings considered as series of individual bare elements, because such an approach results in using the material strength properties of the SSP components inefficiently. Furthermore, it ignores the systems' composite and two-way actions. The first one primarily “controls” the performance of the girders, while the lateral load distribution is regulated by the second one. This suggests that both actions attain maximum intensity when the strength axis of the sheathing coincides with that of the action. Therefore, optimising the composite and two-way actions is antagonistic, because the composite action is maximised when the joist orientation and the strength axis of the sheathing concur, whereas the optimum two-way action is obtained when the joist's longitudinal axis and the strength axis of the sheathing cross orthogonally.

In Australia the current code edition for timber structures, AS 1720.1–1997 (Australian Standard<sup>TM</sup> 1997), widely ignores the interactions present in SSP systems. It provides only minimal recommendations about the design of SSP structures. For example, it provides some directives for the determination of stresses in the sheathing and interlayers but includes no guideline to characterise the composite properties of the SSP cross-section. These are the composite action and the tributary width of the panel. In comparison, in Europe, more comprehensive guidelines are available in several national codes (British Standard 2004; DIN Deutsches Institut für Normung e. V. 2004; Société Suisse des Ingénieurs et Architectes 2003).<sup>a)</sup> In these standards, clear instructions are provided for estimating the contribution of the sheathing(s) and for verifying the stresses. On the other hand, no consideration is given to the two-way action ability, for example, assessing the distribution of concentrated point loads. Indeed, these codes consider SSP assemblies as series of composite beams formed by

---

<sup>a)</sup> These national codes have been revised in recent times and have, on the particular topic of SSP systems, accommodated the design guidelines of EC5 (European Committee for Standardisation 1995).

the joists and portions of the sheathing(s) with no connectivity/interaction between them, whereas, AS 1720.1–1997 (Australian Standard™ 1997) admits some load-sharing capability in repetitive parallel member constructions, to which SSP systems belong.

## 7.2 RECAPITULATION OF THE KEY OUTCOMES

The design recommendations presented in Section 7.3 are based on a series of observations/parameters, which have been identified with the laboratory investigation conducted on full-scale SSP specimens. Precisely, the analyses/interpretations of this investigation have permitted understanding and identifying key behavioural responses of SSP systems, the latter being incorporated into the design recommendations. These key outcomes are summarily recapitulated hereafter:

- linear-elastic behaviour of SSP systems; this includes the determination of the limit of the linear-elastic domain and the global stiffness (refer to Chapter 4 in Part 2)
- two-way action; this includes the quantification/characterisation of the lateral load distribution capability of SSP systems (refer to Chapter 5 in Part 2)
- composite characteristics; this includes the identification of the degree of the composite action and the contribution of the skin(s) – tributary width – (refer to Chapter 6 in Part 2).

*NOTE: detailed information on the laboratory investigation, for example, the concept, research plan and loading regime, is presented in Chapter 3 in Part 2.*

## 7.3 DESIGN RECOMMENDATIONS

### 7.3.1 Introduction and concept of the design recommendations

The following section of this chapter outlines an amendment proposal for Section 5 of the present edition of the Australian code for timber design, AS 1720.1–1997 (Australian Standard™ 1997). It aims to provide a thorough design procedure for SSP systems for Australian engineers. For example, it presents guidelines for the approximation of the tributary width of the sheathing. As mentioned previously, this aspect is not dealt with by AS 1720.1–1997. Furthermore, this procedure recommends a series of stress verifications, which agree with the pattern of stress distribution observed

in test specimens (refer to Chapter 6 in Part 2). To some extent, the stress analysis required by AS 1720.1–1997 disagrees with the actual stress pattern experienced by the skin(s).

Conceptually, the design recommendations proposed hereafter are related to EC5 (European Committee for Standardisation 1995). They are also influenced by the concept of the British (British Standard 2004) and Swiss (Société Suisse des Ingénieurs et Architectes 2003) design codes. Therefore, some aspects of these codes' structure and sequence are recognisable, and as such have been referenced in footnotes. The design recommendations also capitalise on the observations and findings of the subject research.

The procedure of EC5 has been chosen for the platform of these design recommendations, because it is accessible and provides a safe design for SSP floors with the most common dimensions. The capability of this EC5 approach has been demonstrated in the subject research (refer to Chapter 4 in Part 2), that is, the deviations between the estimated ( $EI_{T,deck2}$ ) and measured ( $EI_{T,LAB}$ ) stiffness – derived from the experimental results – is generally within  $\pm 10\%$ . Furthermore, EC5 estimates of the tributary width call upon simple formulae, which consider the material of the sheathing and the span of the floor and account for shear lag and/or plate buckling. Furthermore, EC5, by imposing normal stress verifications on the sheathing, considers a stress pattern, which reflects SSP behaviour more accurately.

In the next section, the design procedure attempts to follow a layout that permits a step-by-step progress. Consideration of its compatibility with AS1720 has also been given. Therefore, arrangements to accommodate Australian specificities such as references to related or relevant Australian codes have been made and detailed in footnotes. Complementary information, such as comments and references, is also presented in footnotes.

### 7.3.2 Outline of the design procedure of stressed-skin panels

#### A) General design considerations

(1) This design procedure assumes that the stressed-skin panel exhibits the following characteristics:

- (a) Linear variation of strain over the depth of the stressed-skin panel<sup>b)</sup>
- (b) Glued splicing of the skins, ensuring continuous skins.

Therefore, the section properties of the stressed-skin panel can be calculated with the transformed-section method.<sup>b)</sup>

(2) If condition (a), refer to (1), is not fulfilled, a more detailed calculation of the section properties of the stressed-skin panel must be made.

(3) If condition (b), refer to (1), is not fulfilled – skins of the stressed-skin panels are constructed without glued splices – the skins should be considered discontinuous and the section properties of the stressed-skin panel should be reduced by 10% for one-sided and 20%<sup>c)</sup> for two-sided stressed-skin panels.

(4) The glued interfaces of the stressed-skin panel, which must exhibit structural properties, require the implementation of structural adhesive such as those described in AS/NZS 4364:1996.<sup>d)</sup>

---

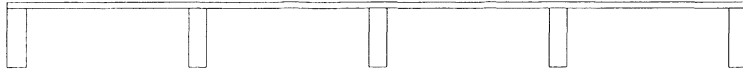
<sup>b)</sup> This prerequisite is expressly recommended in BS EN 1995-1-1:2004 (British Standard 2004). As a result of the linear distribution of the strain, stressed-skin panel structures comply with the requirements of the simple beam theory (Amana & Booth 1967). Furthermore, the section properties of the composite beams can be calculated with the transformed-section method (Gere & Timoshenko 1999).

<sup>c)</sup> The intensity of these retrenchments corresponds to the outcomes identified by the analysis of the laboratory testing data, that is, the analysis conducted on the global stiffness of the specimens of the subject research has identified that discontinuing the skin(s) generate global stiffness losses of about 10% and 20% in one- and two sided specimens respectively (in Chapter 4 in Part 2).

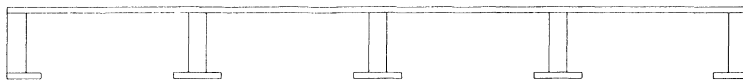
<sup>d)</sup> Australian code for bonded assemblies in load-bearing timber structures (Australian/New Zealand Standard<sup>TM</sup> 1996).

(5) Stressed-skin panels can be sheathed on one or two sides and should be considered as a number of composite girders, the sections of which are described in Figure 7-1:

**One-sided stressed-skin panels (assembly of L-beams and T-beams)**



**One-sided stressed-skin panels with reinforcement of the tensile side of the webs<sup>e)</sup>**



**Two-sided stressed-skin panels (assembly of C-beams and I-beams)**



**Figure 7-1: Construction of stressed-skin panels**

(6) The influence of the non-uniform distribution of the stresses in the skins due to shear lag and buckling (refer to Figure 7-2) must be accounted for.<sup>f)</sup> Unless a more detailed calculation is carried out, the tributary width of the flange(s) is calculated according to Table 7-1.

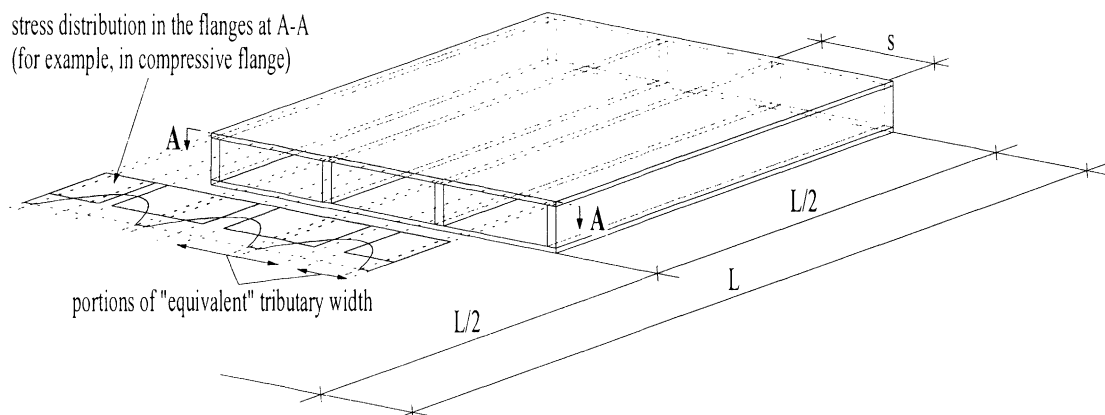


**Figure 7-2: Stress distribution and tributary width of the skin under flexural action**

<sup>e)</sup> McLain (1999) and Desler (2002) described this construction of stressed-skin panels as a "T-flange".

<sup>f)</sup> Under flexural action, the skins mostly experience normal stresses (Foschi 1969b; Ozelton & Baird 2002), whose distribution is not uniform in the section of the cantilevered — unsupported — portion of the skin(s) because of the occurrence of shear deformation (Raadschelders & Blass 1995), and whose maximum intensity is exhibited on the webs (Foschi 1969b; Ozelton & Baird 2002).

(7) The magnitude of the tributary width of the skin(s) (refer to Figure 7-3) – when more detailed calculations are not required – is calculated as follows:

- For T-beam and I-beams

$$b_{ef} = b_w + b_{c,ef} \quad (\text{or } b_w + b_{t,ef}) \quad (\text{Eq. 7-1})$$

- For L-beam and C-beams

$$b_{ef} = b_w + 0.5b_{c,ef} \quad (\text{or } b_w + 0.5b_{t,ef}) \quad (\text{Eq. 7-2})$$

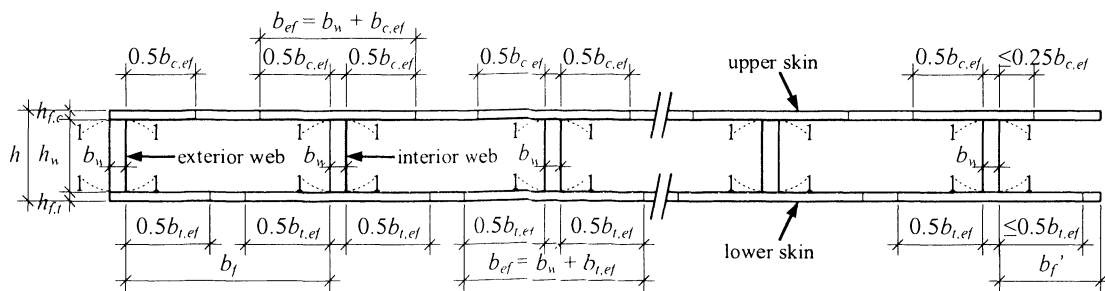


**Figure 7-3: Tributary width of the skins under flexural action (two-sided stressed-skin panel)<sup>g)</sup>**

The values of  $b_{c,ef}$  and  $b_{t,ef}$  should not exceed the maximum value calculated for shear lag from Table 7–1. In addition to this, the value of  $b_{c,ef}$  should not exceed the maximum value for plate buckling from Table 7–1.<sup>h)</sup>

(8) The maximum effective contribution of the skin(s) – unsupported portions of the skin(s) – governed by shear lag and plate buckling should be calculated according to Table 7–1, where  $L$  corresponds to the span of the composite girder and  $h_{f,c}$  corresponds to the thickness of the compressive skin.

**Table 7–1: Maximum effective contribution of the skins due to the effects of shear lag and plate buckling<sup>i)</sup>**

Skin material	Shear lag <sup>1)</sup>	Plate buckling <sup>2) 3)</sup>
---------------	-------------------------	---------------------------------

<sup>g)</sup> The symbolic representation of the tributary width – grey shading – corresponds to that of SIA 265 (Société Suisse des Ingénieurs et Architectes 2003).

<sup>h)</sup> This statement agrees with that of BS EN 1995-1-1:2004 (British Standard 2004).

<sup>i)</sup> Further research on the value of these coefficients might be beneficial in order to verify that they suit the panel products available on the Australian market and to make optimum use of the panel's mechanical properties, particularly that of the group of structural plywood panels (Australian/New Zealand Standard<sup>TM</sup> 2004a).

	(tensile and compressive skins)	(boundary conditions: ●————●)
Plywood, with the grain direction of the outer plies:		
– Parallel to the webs	$0.1 L$	$20 h_{f,c}$
– Perpendicular to the webs	$0.1 L$	$25 h_{f,c}$
Oriented strand board	$0.15 L$	$25 h_{f,c}$
Particleboard or fibreboard with random fibre orientation	$0.2 L$	$30 h_{f,c}$

- <sup>1)</sup> Values for simply supported systems with single span  $L$ , respectively for systems with multiple spans where  $L$  = distance between null flexural moment. Over the support region of the multi-span systems, the effective contribution of the skin should be halved.
- <sup>2)</sup> For an unrestrained skin edge (refer to Figure 7-3), the effective contribution of the skin should be equal to a quarter of the value, due to plate buckling.
- <sup>3)</sup> The unsupported portion of the skin – clear distance between the webs  $b_f$  (refer to Figure 7-3) – should not be greater than twice the effective contribution of the skin, due to plate buckling.



## B) Design capacity

(9) The critical stresses of stressed-skin panels – identified as such in Figure 7-4 – should be verified, whereby a linear variation of strain over the depth of the stressed-skin panel is assumed.

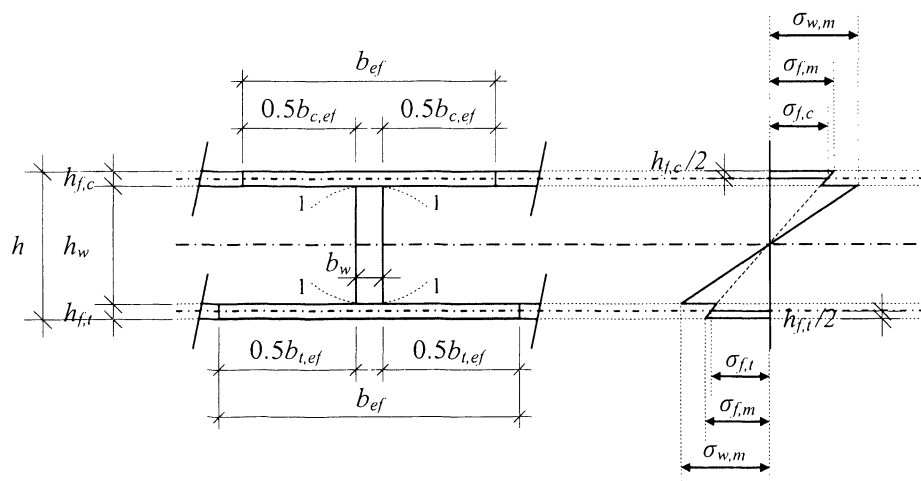


**Figure 7-4: Critical stresses of the stressed-skin panel under flexural action (two-sided stressed-skin panel)**

(10) The skins are assumed to experience flexural and axial stresses. Therefore, both stresses, based on the relevant effective tributary width of the skins, should satisfy the following conditions<sup>l)</sup>:

- The flexural strength at the extreme – exterior – fibre of the skins should satisfy (refer to Clause 3.2<sup>k)</sup>):

$$(\phi M) \geq M^* \quad (\text{Eq. 7-3})$$

where:

- $M^*$  is the design action effect in bending (refer to Clause 1.5.2.2<sup>l)</sup>)
- $\phi$  is the capacity factor (refer to Clause 2.3<sup>m)</sup>).

<sup>l)</sup> The design requirements of the axial – compression and tension – strengths are similarly identified and qualified in BS EN 1995-1-1:2004 (British Standard 2004) and SIA265 (Société Suisse des Ingénieurs et Architectes 2003). The conditions for verifying the flexural stresses are also described under another section of both codes, that is, “Glued thin-web beams”. While flexural stresses are generally not decisive for SSP systems with common dimensions (domestic housing), they might circumstantially become critical.

<sup>k)</sup> Reference to Clause 3.2 of AS 1720.1–1997 (Australian Standard<sup>TM</sup> 1997).

<sup>l)</sup> Reference to Clause 1.5.2.2 of AS 1720.1–1997 (Australian Standard<sup>TM</sup> 1997).

<sup>m)</sup> Reference to Clause 2.3 of AS 1720.1–1997 (Australian Standard<sup>TM</sup> 1997).

- The compression and tensile – axial – strength at the centre fibre of the skins should satisfy (refer to Clause 3.3<sup>n)</sup> and 3.4<sup>o)</sup>):

$$(\phi N_c) \geq N_c^* \quad (\text{Eq. 7-4})$$

where:

$N_c^*$  is the design action effect in compression (refer to Clause 1.5.2.2<sup>p)</sup>)

$\phi$  is the capacity factor (refer to Clause 2.3<sup>q)</sup>)

*Note: the stability factor,  $k_{12}$ , will be equal to 1.0 (refer to Clause 3.3.3<sup>r)</sup>)*

$$(\phi N_t) \geq N_t^* \quad (\text{Eq. 7-5})$$

where:

$N_t^*$  is the design action effect in tension (refer to Clause 1.5.2.2<sup>p)</sup>)

$\phi$  is the capacity factor (refer to Clause 2.3<sup>q)</sup>).

Unless it is assumed that the skins are discontinuous, the glued splices of the skins should satisfy the strength requirements of the axial strength of the skins.

(11) Unless the glued splices of the skins satisfy the strength requirements of the axial strength of the skins, the skins will be considered discontinuous and the strength of the stressed skins panel will be reduced according to paragraph (3).

---

<sup>n)</sup> Reference to Clause 3.3 of AS 1720.1–1997 (Australian Standard<sup>TM</sup> 1997).

<sup>o)</sup> Reference to Clause 3.4 of AS 1720.1–1997 (Australian Standard<sup>TM</sup> 1997).

<sup>p)</sup> Reference to Clause 1.5.2.2 of AS 1720.1–1997 (Australian Standard<sup>TM</sup> 1997).

<sup>q)</sup> Reference to Clause 2.3 of AS 1720.1–1997 (Australian Standard<sup>TM</sup> 1997).

<sup>r)</sup> Reference to Clause 3.3.3 of AS 1720.1–1997 (Australian Standard<sup>TM</sup> 1997).

(12) The webs are assumed to experience flexural and shear stresses.<sup>s)</sup> Therefore, the flexural strength at the extreme fibre of webs should satisfy Equation 7-3, and the shear strength at the location of the maximum shear – neutral axis of the stressed-skin panel – should satisfy Equation 7-6 (refer to Clause 3.3<sup>l)</sup>):

$$(\phi V) \geq V^* \quad (\text{Eq. 7-6})$$

where:

$V^*$  is the design action effect in shear (refer to Clause 1.5.2.2<sup>u)</sup>)

$\phi$  is the capacity factor (refer to Clause 2.3<sup>v)</sup>).

(13) The shear stress in the glued interfaces – sections 1–1 (refer to Figure 7-3) – should satisfy Equation 7-7a (refer to Clause 5.6<sup>w)</sup>) and Equation 7-7a<sup>x)</sup>:

$$(\phi V_{sj}) \geq V_{sj}^* \quad \text{for } b_w \leq 8h_f \quad (\text{Eq. 7-7a})$$

$$(\phi V_{sj}) \left( \frac{8h_f}{b_w} \right)^{0.8} \geq V_{sj}^* \quad \text{for } b_w > 8h_f \quad (\text{Eq. 7-7b})$$

where:

$V_{sj}^*$  is the design action effect for shear at the glued interfaces (refer to Clause 1.5.2.2<sup>u)</sup>)

$\phi$  is the capacity factor (refer to Clause 2.3<sup>v)</sup>)

$h_f$  &  $b_w$  refer to Figure 7-3.

For L-shaped and C-shaped cross-sections, the same expression (Equation 7-7) should be verified, but with  $8h_f$  substituted by  $4h_f$ . The values of  $b_{c,ef}$  and  $b_{t,ef}$  should not exceed the maximum value calculated for shear lag from Table 7–1. In addition, the value of  $b_{c,ef}$  should not exceed the maximum value for plate buckling from Table 7–1.

<sup>s)</sup> It is widely supported that the skins of SSP systems for the most part resist flexural stresses – in the form of axial stresses – and the joists experience shear stress predominantly and flexural stress to a lesser extent (APA – The Engineered Wood Association 1990; Desler 2002; McLain 1999; Moody, Hernandez & Liu 1999).

<sup>l)</sup> Reference to Clause 3.2.5 of AS 1720.1–1997 (Australian Standard<sup>TM</sup> 1997).

<sup>u)</sup> Reference to Clause 1.5.2.2 of AS 1720.1–1997 (Australian Standard<sup>TM</sup> 1997).

<sup>v)</sup> Reference to Clause 2.3 of AS 1720.1–1997 (Australian Standard<sup>TM</sup> 1997).

<sup>w)</sup> Reference to Clause 5.6.2 of AS 1720.1–1997 (Australian Standard<sup>TM</sup> 1997).

<sup>x)</sup> It is proposed in BS EN 1995-1-1:2004 (British Standard 2004) that the permissible strength of the glued interfaces should be limited whenever the stressed-skin panel exhibits “out of proportion” physical dimensions, for example, thin skin(s) and/or (very) wide webs.

(14) The serviceability of the stressed-skin panel should satisfy the requirements of the service limit state – deformation and vibration – such as imposed by AS/NZS 1170 series (Australian/New Zealand Standard<sup>TM</sup> 2002b).

(15) Unless the skins satisfy the requirements of continuity, the skins will be considered discontinuous and the apparent stiffness<sup>y)</sup> of the stressed skins panel will be reduced according to paragraph (3).

### C) Two-way action assessment

(16) This section of the design procedure provides a method for the assessment of the lateral load distribution of concentrated loading action. The strength-sharing factor,  $k_g$  (refer to Clause 2.4.5.3<sup>z)</sup>), may be taken in combination with the lateral distribution effects.<sup>aa)</sup>

(17) For a point load,  $P^*$ , applied onto a girder (refer to Figures 7-5 and 7-6), the maximum bending moment and shear design load effects, and also the maximum deflection should be taken to be equal to that of an isolated girder subjected to a reduced point load,  $P_{eff}^*$  (refer to Equation 7-8).<sup>bb)</sup>

$$P_{eff}^* = CT_{gi} P^* \quad (\text{Eq. 7-8})$$

where:

$P_{eff}^*$ : effective specified design point load

$P^*$ : specified design point load

CT: coupling term for the load introduction on a girder

subscripts: g: girder

i: 1, 2, 3 ... n

*NOTE: the two-way action assessment presented hereafter in Equations 7-9 and 7-11 should be restricted to SSP systems, whose spacing/depth > 1.6.<sup>cc)</sup> The SSP structures should also count at least four girders.<sup>dd)</sup>*

<sup>y)</sup> The apparent stiffness accounts for the effects of the flexural and shear deformations.

<sup>z)</sup> Reference to Clause 2.4.5.3 of AS 1720.1–1997 (Australian Standard<sup>TM</sup> 1997).

<sup>aa)</sup> This consideration agrees with that of Appendix E8, AS 1720.1–1997 (Australian Standard<sup>TM</sup> 1997).

<sup>bb)</sup> This approach accords with that presented in Appendix E8, AS 1720.1–1997 (Australian Standard<sup>TM</sup> 1997).

<sup>cc)</sup> This ratio corresponds to that of SSP systems with common dimensions/proportions such as those exhibited by floors in domestic housing, for example, the dimensions/proportions of 356-mm I-joist specimens are arguably not common; ratio = 1.3.

**C1) Concentrated loading action on interior girder**

(18) For a point load,  $P^*$ , applied onto an interior girder (refer to Figure 7-5), the coupling term,  $CT_{gi}$ , should be approximated with Equation 7-9. The width of the crossbeam should be equal to 1.4 times the web spacing (refer to Figure 7-5).

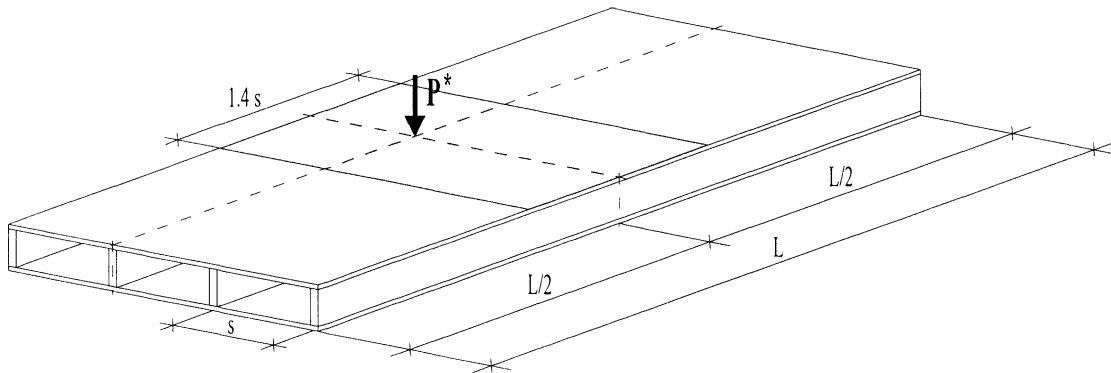


**Figure 7-5: Point load location – interior girder**

$$CT_{gi} = 0.698n_s - 0.339 \log \left( \frac{h_c}{h_{gi}} + 0.35 \right) \quad (\text{Eq. 7-9})$$

in which:

$$h_{gi} = \frac{EI_{gi,app}}{L^3} \quad (\text{Eq. 7-10a})$$

$$h_c = \frac{EI_{c,app}}{s^3} \quad (\text{Eq. 7-10b})$$

where:

- CT: coupling term for the load introduction on a girder
- $h_{gi}$ : interior girder-related expression (associated with the longitudinal stiffness of SSP system)
- $h_c$ : crossbeam-related expression (associated with the perpendicular stiffness of SSP system)
- $n_s$ : number of skin(s)

<sup>dd)</sup> This number of girders represents the minimum that SSP systems should count (in Chapter 5 in Part 2).

*NOTE: Both Equations 7-9 and 7-11 have been calibrated/verified using the specimens of the subject research. It is therefore necessary to investigate/verify Equations 7-9 and 7-11 before generalising/authorising them. Consequently, further research is required in order to determine/finalise the scope of both equations. This scope should at least include the physical dimensions and the number of girders (in Chapter 5 in Part 2). Furthermore, introducing a security coefficient in order to account for the natural variability of structural timber and wood-based products also represents a sound and safe practice.*

EI:      apparent flexural stiffness  
subscripts: g: girder  
              i: 1, 2, 3 ... n  
              c: crossbeam  
              app: apparent<sup>ee)</sup>  
L:        span (of the girder)  
s:        spacing of the girders

## C2) Concentrated loading action on an exterior joist

(19) For a point load,  $P^*$ , applied onto an exterior girder (refer to Figure 7-6), the coupling term,  $CT_{gi}$ , should be approximated with Equation 7-11. The width of the crossbeam should be equal to 1.4 times the web spacing (refer to Figure 7-6).

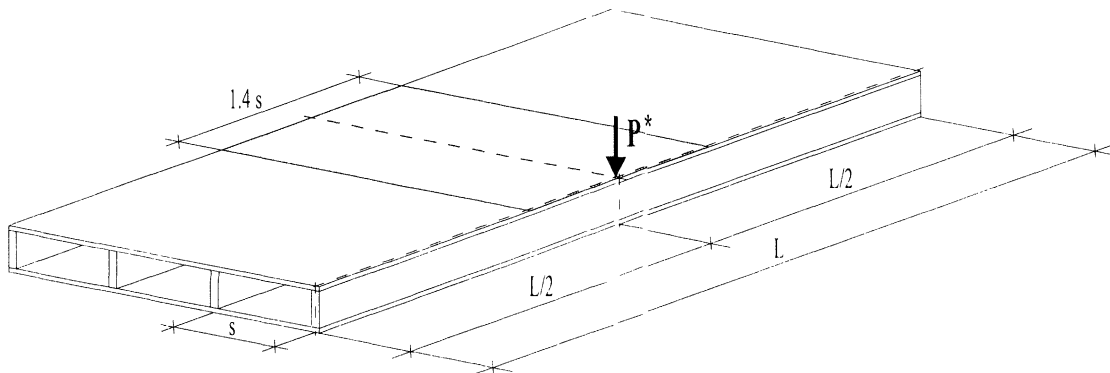


Figure 7-6: Point load location – interior girder

$$CT_{gi} = 0.969n_s - 0.479 \left[ \log \left( \frac{h_c}{h_{gi}} + 0.35 \right) \log \left( \frac{h_d}{h_{gi}} + 0.35 \right) \right]^{0.5} \quad (\text{Eq. 7-11})$$

in which:

$$h_{gi} = \frac{EI_{g,app}}{L^3} \quad (\text{Eq. 7-12a})$$

$$h_c = \frac{EI_{c,app}}{s^3} \quad (\text{Eq. 7-12b})$$

$$h_d = \frac{GJ_d}{L_T^3} \quad (\text{Eq. 7-12c})$$

<sup>ee)</sup> The apparent stiffness of the member indicates that the stiffness implemented in Equations 7-10a and b accounts for the effect of the flexural and shear deformation.

where:

- CT: coupling term for the load introduction on a girder
- $h_g$ : interior girder-related expression (associated with the longitudinal stiffness of SSP system)
- $h_c$ : crossbeam-related expression (associated with the perpendicular stiffness of SSP system)
- $h_d$ : deck-related factor (associated with the torsional stiffness of nS:  
number of skin(s))
- EI: apparent flexural stiffness
- GJ: torsional stiffness
- subscripts: g: girder  
i: 1, 2, 3 ... n  
c: crossbeam  
d: deck  
app: apparent<sup>ff)</sup>
- L: span (of the girder)
- s: spacing of the girders
- LT: eccentricity distance

#### D) Particular design considerations

(20) The use of composite member for the web of the stressed-skin panel should be investigated for shear distortion in particular.<sup>gg)</sup>

- (a) 1.4 is the modification factor that should be conjoined to the section coefficient.
- (b) *Further recommendation.*<sup>hh)</sup>

## 7.4 CONCLUDING SUMMARY

The subject research has demonstrated that, in SSP systems, the sheathing and joists act compositely together (refer to Chapter 6 in Part 2). Therefore, the design procedure should take account of the system interactions, that is, the composite characters –

---

<sup>ff)</sup> The apparent stiffness of the member indicates that the stiffness implemented in Equations 7-12a and b accounts for the effect of the flexural and shear deformation.

<sup>gg)</sup> The laboratory investigation into SSP specimens has identified that, in SSP systems built with I-joists, complex interactions may generate increased shear distortion in the joists in comparison to that approximated with the section coefficient, *Kappa*, approach (refer to Trus Joist's<sup>TM</sup> specifier (Trus Joist<sup>TM</sup> a Weyerhaeuser Business 2002b)). The *Kappa* coefficient should therefore be factorised – modification factor equal to 1.40 – in order to accurately account for the shear distortion experienced by the joists.

<sup>hh)</sup> The author recommends that future work examines this phenomenon of shear distortion in other I-joist sections and other engineered composite joists.

composite action and tributary width of the skin(s) – of SSP structures. In this chapter, an amendment to Section 5 of the current edition of the Australian code for timber design, AS 1720.1–1997 (Australian Standard™ 1997), which only provides minimal guidelines for the design of SSP structures, has been outlined (refer to Section 7.3.2). This proposal, which corresponds to a thorough design procedure for SSP systems, has been influenced by the design guidelines of EC5 – EC5 code-based literature such as BS EN 1995-1-1:2004 (British Standard 2004) and SIA265 (Société Suisse des Ingénieurs et Architectes 2003).

The design procedure introduced in this chapter is uncomplicated and presents a safe design for SSP floors with the most common dimensions. The tributary width is estimated with simple formulae, which consider the material of the sheathing and the span of the floor. It accounts for shear lag and/or plate buckling. The design procedure also gives directives for thorough verification of the stress. For example, it imposes normal stress verifications on the sheathing, considering therefore a stress distribution, which reflects SSP behaviour accurately (refer to Chapter 6 in Part 2).

The effects of discontinuing the skin(s) is also accounted for in the design procedure. It is introduced by means of a modification factor, which reduces the properties of the SSP cross-section, that is, the properties of the structure with continuous skin(s) are reduced. As indicated in Section 7.3.2, it is recommended that the reduction should be as much as –10% and –20% for open- and box-section SSP systems respectively (refer to Chapter 4 in Part 2).

This design procedure outline also contains directives – in form of two equations (Equations 7-9 and 7-11) – for the assessment of the two-way action, that is, the lateral distribution of concentrated point loads. Both equations permit accurate approximations of the two-way action ability of SSP systems (refer to Chapter 5 in Part 2), thus achieving an efficient design, which avoids conservative and non-economic structures. However, because Equations 7-9 and 7-11 have only been calibrated to the behavioural responses of the full-scale specimens of the subject research, further investigation may be recommended before making both equations valid for a broader population of SSP systems. Furthermore, the application/enforcement of a security coefficient, which accounts for the natural variability of structural timber and wood-based products, can contribute to achieving a safer design.



In this design procedure, the influence of using engineered composite joists, such as I-joists, for the web is also accounted for. It has indeed been identified that the behaviour of such joists can be altered when they are components of SSP systems.

Furthermore, the design procedure recommends that using engineered composite joists for the web of the SSP constructions demands a thorough analysis of the shear deformation. It has indeed been identified that the behaviour of composite joists can be altered when they are components of SSP systems. For example, the analysis of the laboratory investigation of the subject research has demonstrated that I-joists experience increased shear deformation (refer to Chapter 4 in Part 2). This phenomenon can mathematically be accounted for using a modification coefficient applied in conjunction with the section coefficient *Kappa* (refer to Chapter 4 in Part 1 and Chapter 3 in Part 2).

<b>8</b>	<b>CONCLUSIONS .....</b>	<b>216</b>
<b>8.1</b>	<b>Literature review.....</b>	<b>216</b>
<b>8.2</b>	<b>Modelling of SSP systems .....</b>	<b>217</b>
8.2.1	Numerical (grillage) model.....	218
8.2.2	Finite element model.....	218
<b>8.3</b>	<b>Design recommendations.....</b>	<b>219</b>
<b>8.4</b>	<b>Final comments .....</b>	<b>220</b>

## 8 CONCLUSIONS

This PhD project involved numerical modelling – Part 1: Review, modelling and design – and laboratory investigation – Part 2: Experimental work. The objectives of Part 1 included developing predictive numerical models, which are capable of simulating the behavioural responses of SSP systems within the range of working load, and outlining a procedure for the design of SSP systems in Australia. Elsewhere in Part 2, a study and assessment of the behavioural responses and of the aspects of the composite action of SSP systems are reported. In meeting the objectives presented in Part 1, a number of critical outcomes have been achieved. These are summarised in the remainder of this chapter.

### 8.1 LITERATURE REVIEW

The context for the PhD project has been introduced in Chapter 2 in Part 1. The latter presents a detailed review of the development and research of wood joist floors, with particular reference to the work on stressed-skin panels (SSP). It discusses ways of representing/approaching the construction of the lightweight floor systems, and key aspects of these systems, such as the interlayers and skin (dis)continuity.

Chapter 3 in Part 1 has presented a review of the concept and development of wood joist floors. It identifies the position of SSP constructions within the family of lightweight floors. It also presents the advantages of SSP technology over conventional wood joist systems, which are, for example, higher structural performance, diaphragm capability, architectural advantages and prefabrication.

A comprehensive review of design procedures is presented in Chapter 4 in Part 1. The composite properties of SSP systems have been discussed. In particular, different approaches for the approximation of the tributary have been scrutinised, exposing minimal variation between these approaches.

These reviews have indicated the need for further laboratory investigation, specifically in areas of the composite properties of SSP systems, such as the composite action and the distribution of concentrated point loads. Understanding the composite properties/mechanism, which characterise the structural performance, and quantifying the load-sharing capability, which characterises the load intensity received by each joist, is essential for designing SSP structures safely, reliably and efficiently. Furthermore, this review has also identified that the current Australian for timber design, AS 1720.1–1997 (Australian Standard™ 1997), proposes incomplete guidelines for the design of SSP systems.

## 8.2 MODELLING OF SSP SYSTEMS

The interpretative analysis of the experimental results presented in Chapters 4 to 6 in Part 2 forms the references for the predictive models described in Chapters 5 (grillage model) and 6 (finite element model) in Part 1. Both models have been developed and characterised to the physicality of the full-scale SSP specimens of the subject research. The author envisages future development aiming to generalise both models, that is, expand the models to the whole population of SSP systems. Furthermore, efforts to simplify both model procedures will also be made.

The models have been verified through comparative analysis with the experimental data (refer to Chapters 4 to 6 in Part 2). The predictions of the grillage have been demonstrated to be internally consistent and to have accuracy within  $\pm 10\%$  of the measured values, both quantitatively (magnitude of the mid-span deflection) and qualitatively (orthogonal profile of the mid-span deflection) for the specimens in healthy and damaged<sup>a)</sup> states (in Chapter 5 in Part 1). Meanwhile, the finite element model performance has been identified to be within  $\pm 10\%$  for the specimens in the healthy state and  $\pm 20\%$  for the specimens in the damaged state (in Chapter 6 in Part 1).

---

<sup>a)</sup> A specimen in the damaged state corresponds to an individual into whose skin(s), discontinuity has been introduced by inflicting a cut (single cut per skin) within the zone of the maximum bending moment — 150 mm away from the mid-span.

In a normal design situation, SSP systems will have inherent variability, which in general exceeds or equals that identified in the models.

### 8.2.1 Numerical (grillage) model

Mathematical modelling involves idealising aspects of the physical structure to some extent. In that respect, characterising the two-way action ability in the grillage model has been successful. For the grillage model to perform consistently and accurately, a series of measures are necessitated:

1. The section properties of each member of the model should be estimated with reference to a single modulus of elasticity (determination of every modular ratio).
2. The global stiffness of the grillage girders should accommodate the flexural stiffness ( $EI$ ) and shear rigidity ( $GA$ ).
3. The global stiffness of the crossbeam should incorporate:
  - For **uniformly distributed loading**, the flexural stiffness ( $EI$ ) and shear rigidity ( $GA$ )
  - For **concentrated point loading on an exterior girder**, the flexural stiffness ( $EI$ ), shear rigidity ( $GA$ ) and torsional rigidity ( $GJ$ )
  - For **concentrated point loading on an interior girder**, the flexural stiffness ( $EI$ ), and shear rigidity ( $GA$ ).
4. The tributary width of the crossbeam (at each girder) is derived by means of the distribution pattern inside the deck unit. This pattern is characterised by the apparent global stiffness of the girders (deck unit) and the global stiffness and torsional properties of the crossbeam at the location of the load introduction.

### 8.2.2 Finite element model

Developing a model in a computer environment corresponds to constructing an “ideal” replica of the physical structure. The achievement of consistent and accurate simulations by finite element model (FEM) imposes a set of measures. Among them, some are analogous to calibration factors, whose aims are to introduce the “imperfections” of the physical specimen and/or testing environment into the FEM:

1. The size of the mesh should be as consistent as possible, especially in the longitudinal – parallel to the span – direction, in order to minimise the variation between FEMs, whose physical dimensions are different.

2. The modelling of the I-joist – rigid connection (merged nodes) between the flanges and web – requires a calibration factor to be applied on the material properties of the web. In the subject research, these factors have been identified:

- 0.220 for **200-mm I-joist open-section specimen**.
- 0.255 for **200-mm I-joist box-section specimen**.
- 0.339 for **356-mm I-joist box-section specimen**.

3. The orthogonal global stiffness of the deck unit needs to be calibrated as well:

- 0.0157 for **15-mm F11 plywood**.
- 0.0880 for **19-mm particleboard**.
- 0.0700 for **22-mm oriented strand board**.

### 8.3 DESIGN RECOMMENDATIONS

The subject research has demonstrated that, in SSP systems, the sheathing and joists act compositely together (refer to Chapter 6 in Part 2). Therefore, the design procedure should take account of the composite characters – composite action and tributary width of the skin(s) – of SSP structures. In Chapter 7 in Part 1, an amendment to Section 5 of the present edition of the Australian code for timber design, AS 1720.1–1997 (Australian Standard™ 1997), which provides incomplete guidelines for the design of SSP structures, is presented.

Skin discontinuity(ies) can be accounted for in the design of SSP structures by means of a modification factor, which reduces the properties of the SSP cross-section approximated for a structure with continuous skin(s). In the subject research, these factors have been identified (refer to Chapter 4 in Part 2):

- 0.9 for **open-section SSP construction**
- 0.8 for **box-section SSP construction**.

A practice for the load distribution – uniformly distributed and concentrated point loads – has also been identified. Two equations have been developed for evaluating the

distribution of point load on an interior (Equation 7–9 in Chapter 7 in Part 1) and exterior (Equation 7–11 in Chapter 7 in Part 1) girder respectively.

The use of composite engineered wood products, for example I-joist, for the webs of SSP systems should be subjected to thorough analysis of the (shear) distortion. It has been identified in the subject research that I-joists in SSP systems presumably experience intensified shear deformation. Thus, they need to be calibrated (refer to Chapter 4 in Part 2).

#### **8.4 FINAL COMMENTS**

The author's comprehensive investigation on wooden SSP systems has resulted in a better understanding of the serviceability and ultimate performance, and of the composite characteristics of SSP systems (refer to Part 2: Experimental work). This PhD project has also resulted in the development of numerical procedures that predict the behavioural responses of SSP elements. A mathematical procedure has been derived from the grillage theory (Chapter 5 in Part 1) and a finite element model has been developed (Chapter 6 in Part 1). In addition, comprehensive design recommendations have been proposed, culminating in an outline of a design procedure for AS 1720 (Chapter 7 in Part 1).

Whilst there is a need to undertake further work to generalise/expand the application field of the grillage and finite element models, the objectives of the numerical procedures have been achieved. Both the grillage and finite element models are capable of accurately predicting the serviceability responses of SSP structures. With regard to the design directive, the objectives of the latter have also been achieved. The design procedure is both useable and straightforward to implement. It is also comprehensive and satisfies the requirements of structural safety and comfortable serviceability. However, future work on the design procedure should consider the generalisation of the two-way action equations and of the composite-joist modification factor. Further investigation should also assess the effects of creep on the structural safety and of vibration on the serviceability.